AD NUMBER

AD442757

NEW LIMITATION CHANGE

TO

Approved for public release, distribution unlimited

FROM

Distribution authorized to U.S. Gov't. agencies and their contractors; Administrative/Operational Use; Jul 1963. Other requests shall be referred to Army Ballistic Research Lab, Aberdeen Proving Ground, MD 21005-5066.

AUTHORITY

USAARDC ltr, 22 Jan 1971

BRL R 1216

BRL

REPORT NO. 1216

FREE FLIGHT MOTION OF SYMMETRIC MISSILES

by

Charles H. Murphy

July 1963

U. S. ARMY MATERIEL COMMAND
BALLISTIC RESEARCH LABORATORIES
ABERDEEN PROVING GROUND, MARYLAND

B A L L I S T I C R E S E A R C H L A B O R A T O R I E S

REPORT NO. 1216

JULY 1963

FREE FLIGHT MOTION OF SYMMETRIC MISSILES

Charles H. Murphy

Exterior Ballistics Laboratory

RDT & E Project No. 1M010501A005

A B E R D E E N P R O V I N G G R O U N D, M A R Y L A N D

B A L L I S T I C R E S E A R C H L A B O R A T O R I E S

REPORT NO. 1216

CHMurphy/bj/idk
Aberdeen Proving Ground, Md.
July 1963

FREE FLIGHT MOTION OF SYMMETRIC MISSILES

ABSTRACT

The linearized angular motion of a symmetric missile is developed in some detail with some consideration of the rolling motion, drag, aerodynamic jump and the effect of varying coefficients. The tricyclic motion of a missile with misaligned control surfaces is briefly considered. This linear theory is, then, applied to the analysis of ballistic range data.

Next, simple cubic nonlinearities in static moment and Magnus moment are treated by a quasi-linear analysis and these cubic coefficients obtained from ballistic range flight data. More generalized relations for arbitrary symmetric nonlinear terms are derived and their use in the construction of "amplitude" planes indicated. These amplitude planes have proven to be quite useful for the prediction of missile flight performance. Finally, the influence of strongly nonlinear static moments is determined by a perturbation method which makes use of two quasi-constants of the motion -- total energy and angular momentum.

PREFACE

The material of this report was prepared in the form of five chapters of a book, The Theory and Application of Ballistic Ranges, which is being written under the joint authorship of G. V. Bull and C. H. Murphy for publication by Prentice-Hall. These chapters were written by C. H. Murphy and form a complete treatment of the angular motion of symmetric missiles acted on by both linear and nonlinear forces and moments with an emphasis on the analysis of ballistic range data. Although most of the results have appeared in various BRL publications, this unified form is felt to be sufficiently useful for separate publication as a BRL Report.

Each section is numbered by a decimal which indicates its chapter and position in that chapter. Thus section 6.2 is the second section of Chapter VI. Each equation could then be identified by its section and position in that section. Equation (6.2.4) is the fourth equation in section 6.2. For simplicity, however, the number identifying the chapter has been omitted from all equation numbers except when a reference is made to an equation in a different chapter.

TABLE OF CONTENTS

TABLE OF CONTENTS (Cont'd)

CHAPTER V

DRAG AND ROLLING MOTION

5.1 Introduction

Historically, the first interest of the ballistician was the drag force exerted on his projectile by the air. Thus, the first measurements made on ballistic ranges were drag measurements. These measurements also have the attractive characteristic of being direct and conceptually very simple. Since the rolling motion has a similar data analysis, it will also be considered in this chapter.

5.2 The Drag Equation

The drag force, D, is usually expressed in terms of a drag coefficient by means of the following definition.

$$D = (1/2)\rho V^2 S C_D \tag{2.1}$$

where ρ is air density
V is velocity
S is reference area and
C_D is the drag coefficient

The velocity of the missile must then satisfy the equation

$$m\dot{V} = - (1/2)\rho V^2 S C_D \tag{2.2}$$

In most ballistic range work, distance is a more convenient independent variable than time. For pitching and yawing motion, it also introduces an important simplification in the equations of motion (see Chapter VI). If ℓ is used to denote a characteristic length, a dimensionless arclength may be defined by the relation

$$s = \frac{1}{\ell} \int_{t_o}^{t} V \, dt \tag{2.3}$$

In most cases, the reference area is taken to be the maximum body cross sectional area and the reference length the maximum body diameter. For this new variable, Equation (2.2) transforms to

$$(\ell n V)' = \frac{V'}{V} = - \left(\frac{\rho S \ell}{2m}\right) C_D \equiv - C_D^* \tag{2.4}$$

where prime denotes derivative with respect to s.

The factor, $\frac{\rho S \ell}{2m}$, will appear a number of times in later chapters. Since the volume of the missile usually varies from $(2/3)S\ell$ for a sphere to $10S\ell$ for a missile with high fineness ratio, the inverse of this factor is a measure of the model mean density relative to that of air. The relative density of plastic is 10^3 and that of steel is 8×10^3. Thus this relative density factor has a maximum of 10^{-3} for a plastic sphere and is usually of the order of 10^{-4}.

For constant C_D, Equation (2.4) has a solution of

$$V = V_o e^{-C_D^* s} \tag{2.5}$$

Integrating Equation (2.5), a distance-time relation results

$$t = t_o + \frac{\ell(e^{C_D^* s} - 1)}{V_o C_D^*} \tag{2.6}$$

$$= t_o + \left(\frac{\ell}{V_o}\right) s + \left(\frac{\ell C_D^*}{2V_o}\right) s^2 + \ldots$$

It is important to note that in any data analysis the origin for s must be selected as the midpoint of the timing stations so that the linear and the quadratic coefficients are related to well determined velocities and retardations.

There are two approaches to the data analysis problem. One is that of the engineer[5-3] and the other is that of the mathematician[5-1]. Fortunately, the results of the two methods are practically identical. In the first method, the engineer makes use of his love for plotting data and exercising his personal opinion as to the best fit. This is done by use of Equation (2.4). He plots the logarithm of the average velocity between a pair of timing points versus the location of the midpoint of the interval. He then draws a straight line through the points and computes the drag coefficient from its slope.

The mathematician displays his characteristic fear of plotted data and human decision making. He fits his time-position data by a cubic least squares process. For the usual flat trajectories, s can be well approximated by x_1/ℓ where x_1 is distance measured downrange.

$$t = t_o + a_1 x_1 + a_2 x_1^2 + a_3 x_1^3 \tag{2.7}$$

where

$$a_1 = V_o^{-1}$$

$$a_2 = \frac{\rho S}{4mV_o} C_D$$

$$\therefore C_D = \left(\frac{4m}{\rho S}\right) \left(\frac{a_2}{a_1}\right) \tag{2.8}$$

The cubic coefficient absorbs any Mach number variation in C_D as well as errors in the expansion of the exponential in Equation (2.6). In those cases where the cubic fits well, the resulting C_D differs very little from that obtained from the first approach.

The accuracy of a measured drag coefficient may be estimated statistically when a least squares reduction has been performed or determined by the physical size of the drag "disturbance". Since the velocity is so much better determined than the deceleration, the error in C_D is directly proportional to the error in a_2 alone. This error may be estimated from the corresponding diagonal term of the inverse matrix formed from the least squares normal equations.

$$\frac{\epsilon_{C_D}}{C_D} = \frac{\sqrt{A_{33}}}{a_2} \epsilon \tag{2.9}$$

where $\epsilon = \sqrt{\frac{\Sigma(\Delta t)^2}{n - 4}}$

Δt = $t_{calc.} - t_{measured}$

n = number of measurements and

A_{33} is the diagonal element corresponding to a_2 of the inverse matrix of the normal equations.

The use of the size of the measurable effect of drag introduces physical insight into this error analysis which is sadly lacking in the above cold statistical formula. If drag were not present, the missile would travel at constant velocity indefinitely. The drag changes the time of passage of the model at the various observation points. The maximum drag-induced time decrement with respect to constant velocity flight at the average velocity, V_o, occurs at the ends of the range. If V_o is measured at the midpoint of the range* and the range length is ℓL, the endpoints are located at $s = \pm (L/2)$. Maximum time decrement may then be computed for Equation (2.6)

$$d_t = \frac{\ell(e^{C_D^* s} - 1)}{V_o C_D^*} - \frac{\ell s}{V_o}$$

$$\doteq \frac{\ell C_D^* s^2}{2V_o}$$

$$= \frac{\rho S \ell^2}{16 m V_o} C_D L^2 \qquad (2.10)$$

The engineer can now make the reasonable assumption that the percentage error in C_D is given by the ratio of measurement error to the maximum time decrement, ϵ/d_t. Usually, the time measurements are less accurate than distance measurements and maximum estimated error in time can be used. Should the range survey be the limiting factor, the distance error can be converted to an equivalent time error by division by V_o and the result compared with d_t.

The presence of length squared in the time decrement shows the value of long flight paths. Exploitation of this property is limited, however, by the presence of Mach number dependence in the drag coefficient. It is also

* The midpoint is not the point at which the actual velocity is exactly equal to the average velocity. A small correction can be employed to eliminate this minor difficulty[5-3].

interesting to note that higher velocity tends to degrade drag accuracy. In any event, it is the common experience that ballistic ranges with lengths of one thousand calibers can attain better than 1/2 percent accuracy in C_D at high supersonic velocities.

The question of an optimum distribution of timing stations for a given length can be easily answered. Since the drag appears in the quadratic term of a parabola, it is determined by the curvature of the time-distance curve with respect to the midrange point. Thus, one half of the observations should be at the center and one half at the ends. It can be shown theoretically[5-4] that this distribution of 1/4 - 1/2 - 1/4 will yield 15 - 20 percent less error in C_D than a symmetric distribution. Such a small improvement is of little interest for most drag measurements.

5.3 Effect of Pitching and Yawing Motion

If the angular motion is not small, variations in the drag coefficient are observed. Usually this functional dependence on angle is well represented by a quadratic function.

$$C_D = C_{D_o} + C_{D_{\delta^2}}\delta^2 \tag{3.1}$$

where

$\delta^2 = \alpha^2 + \beta^2$

α = angle of attack

β = angle of sideslip

As will be shown in the next chapter, the variation of δ^2 for a symmetric missile is described by the equation

$$\delta^2 = K_1^2 + K_2^2 + 2K_1K_2\cos\hat{\phi} \tag{3.2}$$

where $K_j = K_{j_o} e^{\lambda_j s}$

$\phi_j = \phi_{j_o} + \phi_j' s$

$\hat{\phi} = \phi_1 - \phi_2$

and λ_j and ϕ_j' are constants.

For a quadratic drag coefficient, Equation (2.4) can be integrated once to yield

$$\ell n \frac{V}{V_o} = - \left(\frac{\rho S \ell}{2m}\right) \left(C_{D_o} s + C_{D_{\delta^2}} \int_o^s \delta^2 \, dr\right) \tag{3.3}$$

This can be expressed in exponential form, expanded in a power series, and integrated again

$$t = t_o + \frac{\ell}{V_o} s + \left(\frac{\rho S \ell^2 C_{D_o}}{4 V_o m}\right) s^2 + \frac{\rho S \ell^2 C_{D_{\delta^2}}}{2 V_o m} I(s) + \ldots$$

$$\text{where } I(s) = \int_o^s \int_o^q \delta^2 \, dr \, dq \tag{3.4}$$

The distance over which drag deceleration is measured is at least several times longer than the period of δ^2 amd, hence, the influence of the periodic part of δ^2 on I(s) can be neglected. If the effects of damping are also neglected, I(s) assumes the simple form

$$I(s) \doteq \frac{s^2}{2} (K_{10}^2 + K_{20}^2) \tag{3.5}$$

$$\text{and} \quad \left(\frac{4m}{\rho S}\right) \left(\frac{a_2}{a_1}\right) \doteq C_{D_o} + C_{D_{\delta^2}} (K_{10}^2 + K_{20}^2) \tag{3.6}$$

At first glance, it seems that Equation (3.6) could have been directly derived by replacing the constant C_D in Equation (2.8) by the average value of C_D, i.e.,

$$C_{D \text{ average}} = C_{D_o} + C_{D_{\delta^2}} \overline{\delta^2}$$

$$\text{where } \overline{\delta^2} = \frac{1}{L} \int_{-L/2}^{L/2} \delta^2 \, ds. \tag{3.7}$$

It seems intuitively obvious that fitting a cubic to the time-distance data should have this effect of "averaging" the drag coefficient in this way. It is clear that for the case of no damping this is correct. As we shall see, it is not correct for large damping.

The least squares process includes in a_2 the "best" quadratic approximation of I(s). Thus an average $\tilde{\delta}^2$ is defined by the requirement that

$$\int_{-L/2}^{L/2} \left[I(s) - \frac{s^2}{2} \tilde{\delta}^2 \right]^2 ds \text{ is a minimum.}$$

A relation for $\tilde{\delta}^2$ may be obtained by differentiating the above with respect to $\tilde{\delta}^2$, setting the result equal to zero, and solving for $\tilde{\delta}^2$.

$$\tilde{\delta}^2 = \frac{5}{(L/2)^5} \left\{ \int_{-L/2}^{L/2} s^2 I(s)\, ds \right\} \tag{3.8}$$

$$= K_{10}^2 + K_{20}^2 + \frac{5L^2}{84} (\lambda_1^2 K_{10}^2 + \lambda_2^2 K_{20}^2) + \ldots$$

The mean squared angle defined after Equation (3.7) has the expansion

$$\overline{\delta^2} = K_{10}^2 + K_{20}^2 + \frac{L^2}{6} (\lambda_1^2 K_{10}^2 + \lambda_2^2 K_{20}^2) + \ldots \tag{3.9}$$

Thus, the proper average value of δ^2 is not the same as $\overline{\delta^2}$ and the more precise form of Equation (3.6) is

$$\frac{4m}{\rho S} \left(\frac{a_2}{a_1} \right) \equiv C_{D_{range}} = C_{D_o} + C_{D_{\delta^2}} \tilde{\delta}^2 \tag{3.10}$$

According to Equation (3.10), the drag coefficient obtained from the range data reduction is a linear function of $\tilde{\delta}^2$. Thus, if $C_{D_{range}}$ is plotted versus $\delta^2 \doteq K_{10}^2 + K_{20}^2$ for different model tests at the same Mach number, the points

should fall on a straight line. This technique has been used for a number of years to determine C_{D_o} and $C_{D_{\delta^2}}$ for a large variety of symmetric configurations with complete success.

In Figure 5.1, the data for a large angle of attack program[5-5] is plotted as an illustration of this technique. In this program, a 20mm bullet was tested at angles up to 25° and a good linear correlation of C_D and $\tilde{\delta}^2$ was obtained. $C_{D_{\delta^2}}$ was determined from the slope of the line to be 4.63. This value agreed very well with a wind tunnel measurement of 4.71.

As can be seen from a comparison of Equations (3.8) and (3.9), the distinction in the proper average δ^2 is rather minor. The determination of the proper average δ^2 is much more important for other angle dependent aerodynamic coefficients. It is for this reason that the concept of $\tilde{\delta}^2$ was introduced here.

5.4 Experimental Results

The first systematic ballistic range drag measurements were of spheres. Charters and Thomas[5-6] tested 9/16" spheres at Mach numbers varying from 0.3 to 4.0 in the BRL Aerodynamics Range. By tests in the NOL Pressurized Ballistics Range, May and Witt[5-7] were able to vary the Reynolds number by more than a hundred for a fixed Mach number. The results of this program are shown in Figure 5.2, which is a contour plot of C_D on the Mach number - Reynolds number plane.

The presence of a saddle point in the vicinity of M = 2.0 and R_e = 30,000 is clearly shown in this figure. In passing along the line R_e = 30,000 a maximum is found near this point, while a minimum is encountered on the line M = 2.0.

The influence of wall temperature on the skin friction has been studied in a quite elegant manner by Sommer and Short[5-8]. The test vehicles were spin-stabilized hollow cylinders with fineness ratios of either 1.4 or 1.8. The nose contours were either a double wedge or a double circular arc. (See Figures 5.3 and 5.4) Similar cylinders with a fineness ratio of 0.4 were used

as tare models. The difference in drag coefficients of the test models and the tare models is, except for small corrections, a measure of the average skin friction drag of the added length of the test model. Boundary layer trips were used to ensure the presence of turbulent boundary layers.

The tests were made in the Ames Free Flight Wind Tunnel at Mach number of 2.8 and 3.9 in still air and 7.2 in a Mach number 2 air stream. Since the model flight time was less than .02 sec, its wall-temperature heat rise was less than 45°F. Thus, the ratio of wall-temperature to boundary-layer-edge temperature, T_W/T_1, was determined by the local temperature in the tunnel, i.e., 1.05 for still air and 1.3 or 1.7 for air flow. Since calculated recovery temperatures were two and a half to six times greater than the estimated wall temperatures, considerable heat transfer was in process. In Figure 5.5, the results of the program are plotted and compared with a curve based on zero heat transfer wind tunnel data. It can be seen that the presence of heat transfer can increase the skin friction by over 30 percent.

By a somewhat similar approach, base pressures have been extracted from ballistic range drag data. Charters and Turetsky[5-9] determined the base pressure for 20° cones and cone cylinders by computing head drag and skin friction drag and subtracting the results from the total drag. The base pressure may also be determined by a measurement of the wake angle from a spark photograph. The pressure outside the wake is computed by characteristics and assumed to be the same as at the base of the model. A comparison of ratio of base pressure to free stream pressure, P_B/P_1, as obtained from these two methods, is given in Table I.

TABLE I

P_B/P_1 for M = 1.84

Model	Fineness Ratio	Total Drag Method	Wake Angle Method
Cone	2.9	0.50	0.49
Cone-cylinder	3.2	0.53	0.50
Cone-cylinder	5.0	0.61	0.59

A final example of ballistic range drag data is shown in Figures 5.6 and 5.7. It can be seen that the separated flow over the nose spike of this fin-stabilized round can assume two different configurations. The model with the larger separated flow has one-third less drag than the identical shape with the smaller separated region! This low drag flow occurs when the initial launch angle is less than two or three degrees. For larger angles, the high drag flow is established and persists[5-10].

5.5 The Roll Equation

The aerodynamicist usually writes the roll moment due to control deflection and aerodynamic damping in the form

$$M_X = (1/2)\rho V^2 b \left[S_\delta C_{\ell_\delta} \delta_f + S_t C_{\ell_p} \frac{pb}{2V} \right] \tag{5.1}$$

where b is span

S_δ is profile area of deflected fins

S_t is total profile area of fins

δ_f fin deflection angle for pair of differentially canted fins

$p = \frac{d\phi}{dt}$ roll rate

Equation (5.1) has two reference areas and two reference lengths, b and b/2. If the test missile possesses surfaces with two different spans, the decision as to which is the reference length becomes quite difficult. In ballistic range work, it is quite convenient to use one reference area, S, and one reference length, ℓ. With this in mind, we can redefine the roll moment as

$$M_X = (1/2)\rho V^2 \ell S \left[\delta_f C_{\ell_\delta} + \frac{p\ell}{V} C_{\ell_p} \right] \tag{5.2}$$

Conversion relations for the aerodynamic coefficients may be obtained by a comparison of Equation (5.1) and (5.2). All ballistic range data should contain a specification of the reference area and reference length which were used.

The equation for rolling motion is

$$I_x\ddot{\phi} = (1/2)\rho V^2 \ell S \left[\delta_f C_{\ell_\delta} + \frac{\dot{\phi}\ell}{V} C_{\ell_p}\right] \tag{5.3}$$

If drag can not be neglected, Equation (5.3) is linear with variable coefficients. For a constant drag coefficient, transforming the independent variable from time to distance will provide us with a linear equation with constant coefficients. Since distance is the natural variable for ballistic ranges, this transformation is doubly attractive. We therefore introduce the variable s, which was defined by Equation (2.3).

$$\phi' \equiv \frac{d\phi}{ds} = \frac{d\phi}{dt}\frac{dt}{ds} = \frac{\ell}{V}\dot{\phi} \tag{5.4}$$

$$\phi'' \equiv \frac{d^2\phi}{ds^2} = \left(\frac{\ell}{V}\right)^2 \left[\ddot{\phi} + \frac{\rho S \ell}{2m} \frac{V}{\ell} C_D \dot{\phi}\right] \tag{5.5}$$

Substituting Equation (5.4 - 5.5) in Equation (5.3), we have the roll equation in the form

$$\phi'' + K_p\phi' - K_\delta = 0 \tag{5.6}$$

where $K_p = -\frac{\rho S \ell}{2m}\left[k_a^{-2} C_{\ell_p} + C_D\right]$

$$K_\delta = \frac{\rho S \ell^3}{2I_x}\delta_f C_{\ell_\delta}$$

$$k_a = \sqrt{\frac{I_x}{m\ell^2}} \quad \text{axial radius of gyration}$$

The solution to Equation (5.6) is

$$\phi = \phi_o + \phi'_s s + A(e^{-K_p s} - 1) \tag{5.7}$$

where $\phi_s' = \frac{K_\delta}{K_p}$ is the steady state roll.

$$A = (\phi_s' - \phi_o') K_p^{-1} = (K_\delta - \phi_o' K_p) K_p^{-2}$$

ϕ_o, ϕ_o' are the conditions at the middle of the observed flight.

If $K_p s$ is small enough, the exponential in Equation (5.7) can be expanded as a cubic

$$\phi = \phi_o + \phi_o' s + (AK_p^2) \left(\frac{s^2}{2} - \frac{K_p s^3}{6} \right) \tag{5.8}$$

Equation (5.8) can be fitted by the same least squares reduction that was used for the drag equation (Equation (2.7)). Unfortunately, in order to separate K_p and K_δ, the cubic coefficient in Equation (5.8) must be well determined. In other words, $K_p s$ can not be too small! At the Ames Free Flight Wind Tunnel, which has a test section of 15 feet, this determination has been found to be quite difficult[5-2].

This difficulty can be avoided by attempting to measure these quantities separately. K_p can be determined fairly well from the quadratic term when $K_\delta = 0$, i.e., for spinning bodies of revolution or missiles with uncanted fins. Next, the influence of K_p can be eliminated from the quadratic term by causing the model to reach zero rolling velocity near the center of the observed flight path.

$$\therefore AK_p^2 \doteq K_\delta \tag{5.9}$$

This can be done by properly prespinning the model in a direction opposite to steady state spin through the use of a rifled gun.

If $K_p s$ is large, the exponential character of Equation (5.7) is manifested and both K_p and K_δ can be determined. The usual least squares fitting process is handicapped by the fact that the parameter K_p appears in a nonlinear fashion. An iterative fitting process is, therefore, necessary.

A set of initial values of ϕ_o, ϕ'_s, A and K_p are required for this process. To obtain these values, we differentiate Equation (5.7) and combine the result with Equation (5.7) to eliminate the exponential term.

$$\phi' + K_p\phi \cdot (K_p\phi'_s)s + (K_pA - K_p\phi_o - \phi'_s) = 0 \qquad (5.10)$$

ϕ' can be computed by first differences and Equation (5.10) fitted by least squares since it is linear in the parameters K_p, $K_p\phi'_s$, and $K_pA - K_p\phi_o - \phi'_s$. Values of these parameters plus the measured value of ϕ_o provide the required set of initial numbers.

These values for ϕ_o, ϕ'_s, A, and K_p may be placed in Equation (5.7) and ϕ computed for each measurement point. The difference between these numbers and the actual measurements will be denoted by $\Delta\phi = \phi_{measured} - \phi_{observed}$. If the data is reasonably good, these residuals of fit, $\Delta\phi$'s, should be less than ten degrees (0.2 rad.). Assuming that they are due to small errors in ϕ_o, ϕ_s, A, and K_p, we differentiate Equation (5.7) with the result:

$$\Delta\phi \doteq \Delta\phi_o + s\Delta\phi'_s + (e^{-K_p s} - 1)\Delta A - Ase^{-K_p s}\Delta K_p \qquad (5.11)$$

Equation (5.11), for measured ϕ and s, are linear in the unknowns $\Delta\phi_o$, $\Delta\phi'_s$, ΔA, and ΔK_p. These equations may be solved by least squares and new parameters computed from the old by adding the corresponding changes, i.e., $\Delta\phi_o$, $\Delta\phi'_o$, etc. If the corresponding residuals are smaller, the process is successful and may be repeated until no further improvement is obtained. Probable errors in fit of less than 0.5^o are common.

5.6 Experimental Results

For a spinning body of revolution, Charters and Kent[5-11] have derived a simple relation between the roll damping moment C_{ℓ_p} and the skin friction drag coefficient $C_{D_{sf}}$. For a basically cylindrical body and a reference length which is the cylinder diameter, the relation is

$$C_{D_{sf}} = 4C_{\ell_p} \qquad (6.1)$$

The derivation may be summarized by the following steps:

(1) For a spinning body of revolution, the local velocity of the surface relative to free stream is

$$V_r = V\sqrt{1 + \left(\frac{pd}{2V}\right)^2} \tag{6.2}$$

where d is body diameter

(2) The local skin friction force has the direction of V_r and therefore is inclined at an angle of arccos $\frac{V}{V_r}$ to the axis of rotation.

(3) The skin friction drag coefficient and the roll damping moment may be written in terms of the integrals

$$(1/2)\rho V^2 S C_{D_{sf}} = (1/2)\int_0^{\ell} \rho V_r^2 \left(\frac{V}{V_r}\right) C_f(\pi d)dx \tag{6.3}$$

$$(1/2)\rho V^2 S\ell C_{\ell_p}\left(\frac{p\ell}{V}\right) = (1/2)\int_0^{\ell} \frac{d\rho V_r^2}{2}\left(\frac{\frac{pd}{2}}{V_r}\right) C_f(\pi d)dx \tag{6.4}$$

where C_f is the local skin friction coefficient.

(4) For constant d = ℓ, Equation (6.1) follows directly from Equations (6.3 - 6.4).

The roll damping moment has been measured for shell and other bodies of revolution. For these cases, $k_a^{-2} C_{\ell_p}$ is negative but one-third the size of the drag coefficient. Thus, for these shapes the roll per distance actually increases, ($K_p < 0$). C_{ℓ_p} can be measured to an accuracy of better than 10 percent and relation (6.1) has been verified by a number of investigators[5-12, 5-13].

The rolling motion of finned missiles was first studied on a ballistic range by Bolz and Nicolaides[5-14]. The test vehicle was a cone cylinder of fineness ratio ten with square-plane form cruciform fins. The fin chord to body diameter

was one. As can be seen from Figures 5.8 and 5.9, the experimental results verify the prediction of the linearized theory. In this program, C_{ℓ_p} and C_{ℓ_δ} were determined to an accuracy of better than 2 percent. (Reference area was body cross sectional area, $\frac{\pi d^2}{4}$ and reference length was body diameter, d.)

REFERENCES

5-1. McShane, E. J., Kelley, J. L. and Reno, F. V. Exterior Ballistics. University of Denver Press, 1953.

5-2. Seiff, A. A Free-Flight Wind Tunnel for Aerodynamic Testing at Hypersonic Speeds. NACA Report 1222, May 1955.

5-3. Seiff, A. A New Method for Computing Drag Coefficients from Ballistic Range Data. Jour. Aero. Sciences, Vol. 25, pp. 133-4, February 1958.

5-4. Karpov, B. G. The Accuracy of Drag Measurements as a Function of Number and Distribution of Timing Stations. BRL Report No. 658, February 1948.

5-5. Roecker, E. T. Large Yaw Firings of 20mm HEI, T282E1 Shell with Fuse T196 at Mach Number 2.3. BRL Memorandum Report No. 888, April 1955.

5-6. Charters, A. C. and Thomas, R. N. The Aerodynamic Performance of Small Spheres from Subsonic to High Supersonic Velocities. Jour. Aero. Sciences, Vol. 12, pp. 468-476, October 1945.

5-7. May, A. and Witt, W. R., Jr. Free-Flight Determination of the Drag Coefficients of Spheres. Jour. Aero Sciences, Vol. 20, pp. 635-638. September 1953. (Also published as NAVORD Report 2352, August 1952.)

5-8. Sommer, S. C. and Short, B. J. Free-Flight Measurements of Skin Friction of Turbulent Boundary Layers with High Rates of Heat Transfer at High Supersonic Speeds. Jour. Aero. Sciences, Vol. 23, pp. 536-542, June 1956. (Also published as NACA TN 3391, March 1955.)

5-9. Charters, A. C. and Turetsky, R. A. Determination of Base Pressure from Free-Flight Data. BRL Report No. 653, March 1948.

5-10. Karpov, B. G. and Piddington, M. J. Effect on Drag of Two Stable Flow Configurations over the Nose Spike of the 90mm T316 Projectile. BRL Technical Note No. 955, October 1954.

5-11. Charters, A. C. and Kent, R. H. The Relation Between the Skin Friction Drag and the Spin Reducing Torque. BRL Report No. 287, July 1942.

5-12. VanAllen, J. A. and Hitchcock, H. P. Loss of Spin of Projectiles. Jour. Aero. Sciences, Vol. 15, pp. 35-40, January 1948.

5-13. Murphy, C. H. and Schmidt, L. E. The Effect of Length on the Aerodynamic Characteristics of Bodies of Revolution in Supersonic Flight. BRL Report No. 876, August 1953.

5-14. Bolz, R. E. and Nicolaides, J. D. A Method of Determining Some Aerodynamic Coefficients from Supersonic Free-Flight Tests of a Rolling Missile. Jour. Aero. Sciences, Vol. 17, pp. 609-621, October 1950.

5-15. Chapman, D. R. and Kester, R. H. Turbulent Boundary-Layer and Skin-Friction Measurements in Axial Flow Along Cylinders at Mach Numbers Between 0.5 and 3.6. NACA TN 3097, 1954.

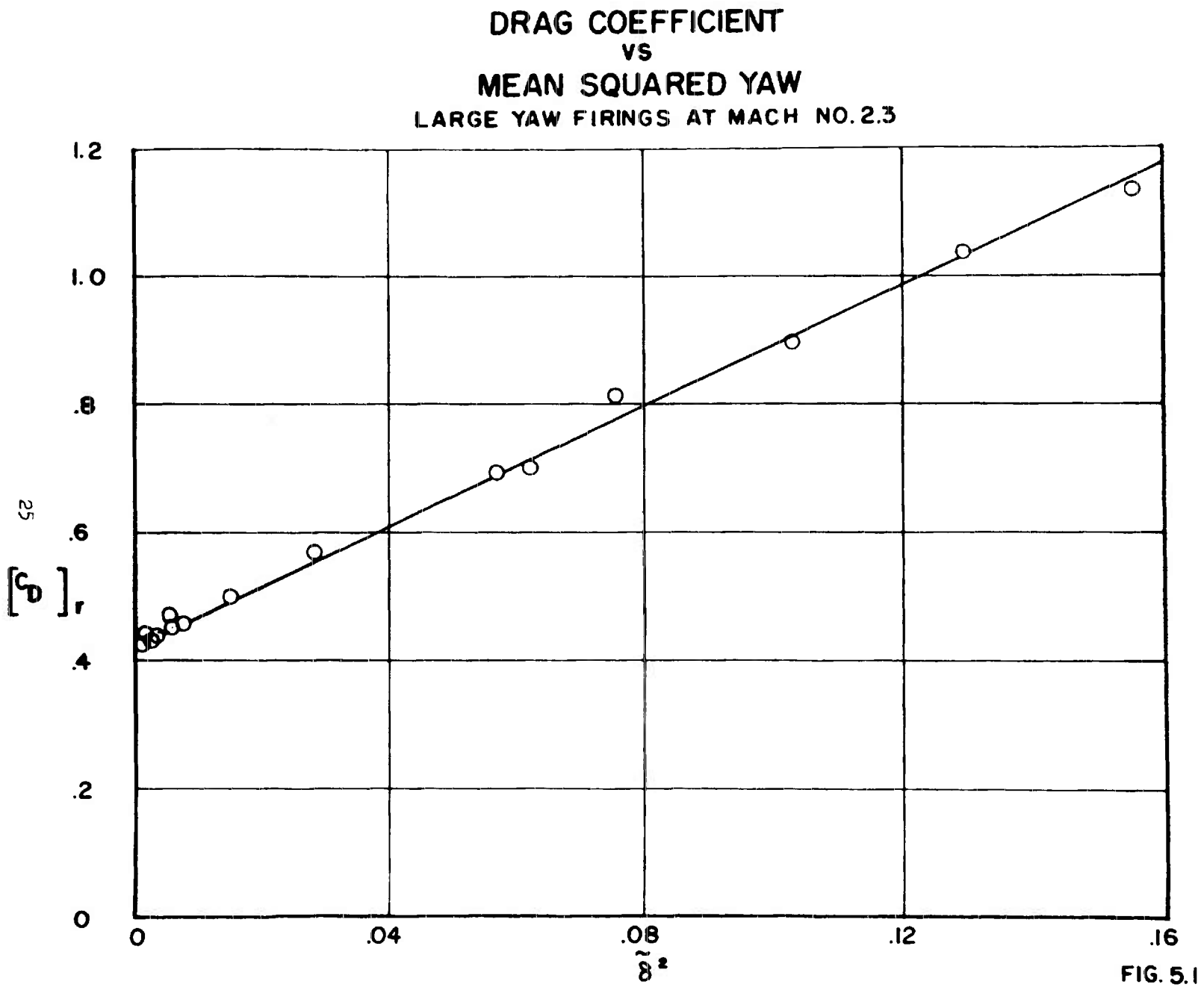
DRAG COEFFICIENT
VS
MEAN SQUARED YAW
LARGE YAW FIRINGS AT MACH NO. 2.3
1.2
1.0
.8
.6
.4
.2
0
$[C_D]_r$
0
.04
.08
.12
.16
$\tilde{\delta}^2$

FIG. 5.1

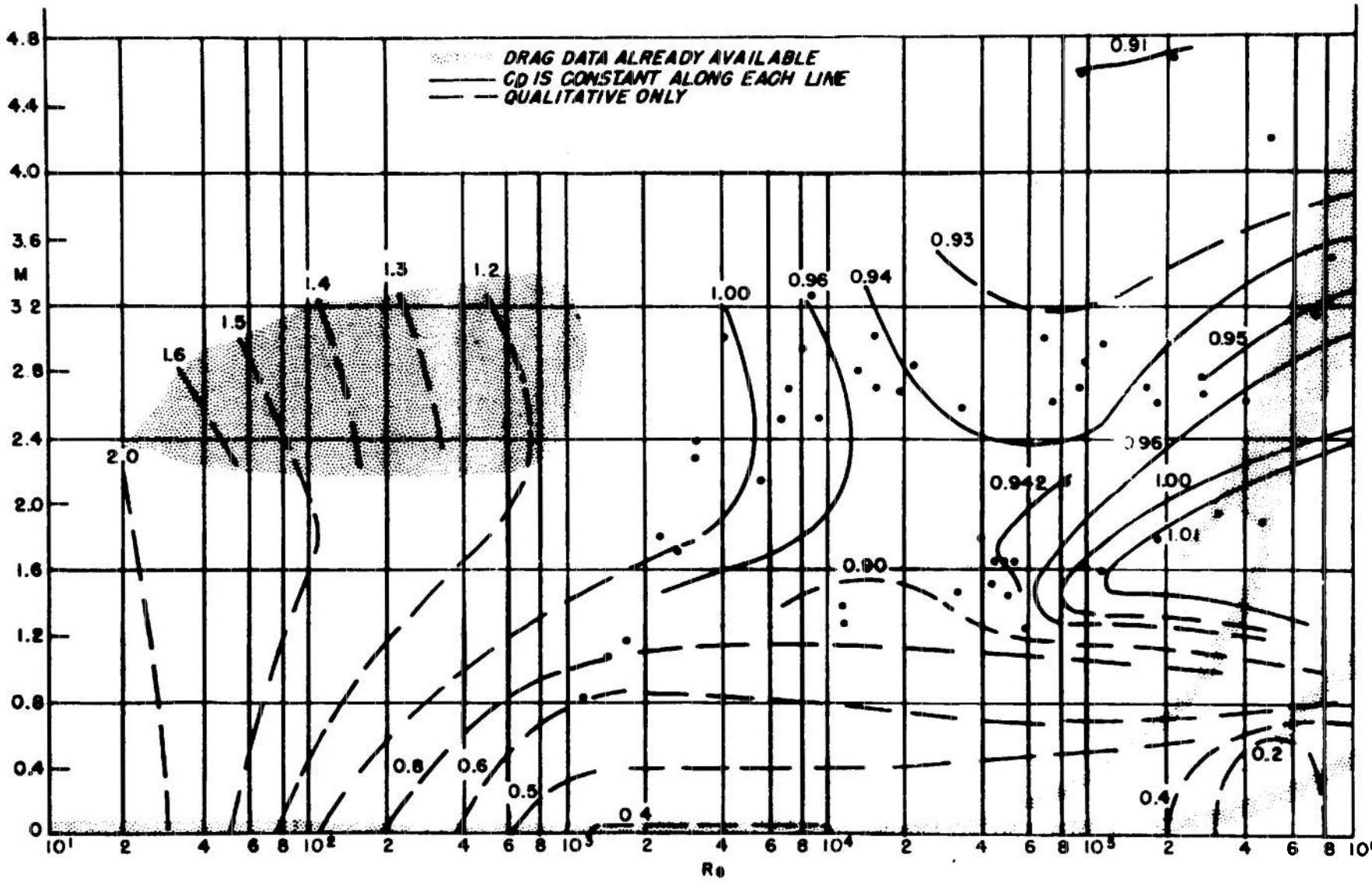

CONTOUR MAP OF DRAG COEFFICIENT AS A FUNCTION OF MACH NUMBER AND REYNOLDS NUMBER

COURTESY NAVAL ORDNANCE LABORATORY WHITE OAK, MD.

FIG. 5.2

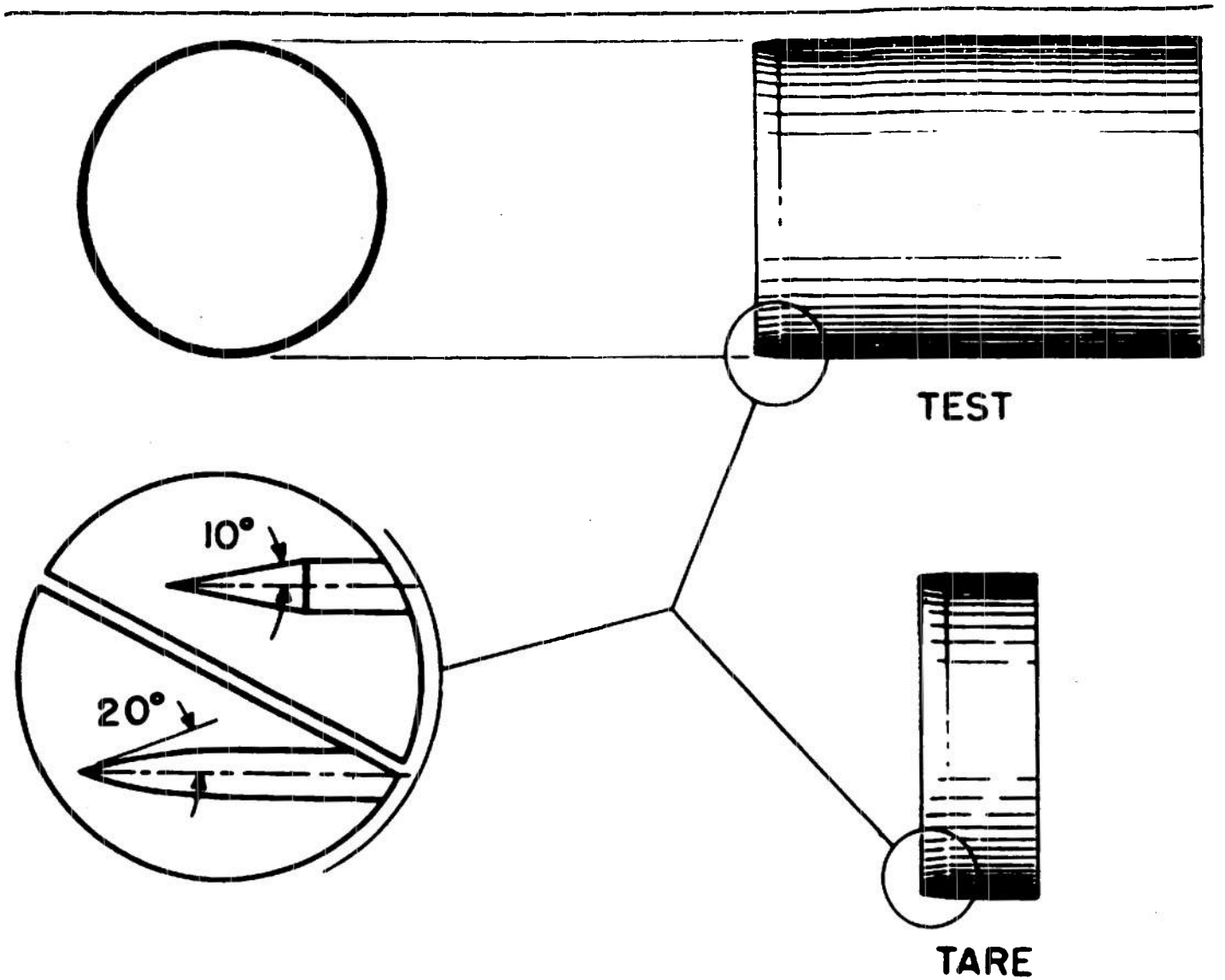

TYPICAL HOLLOW-CYLINDER MODELS

COURTESY AMES RESEARCH CENTER , NASA FIG. 5.3

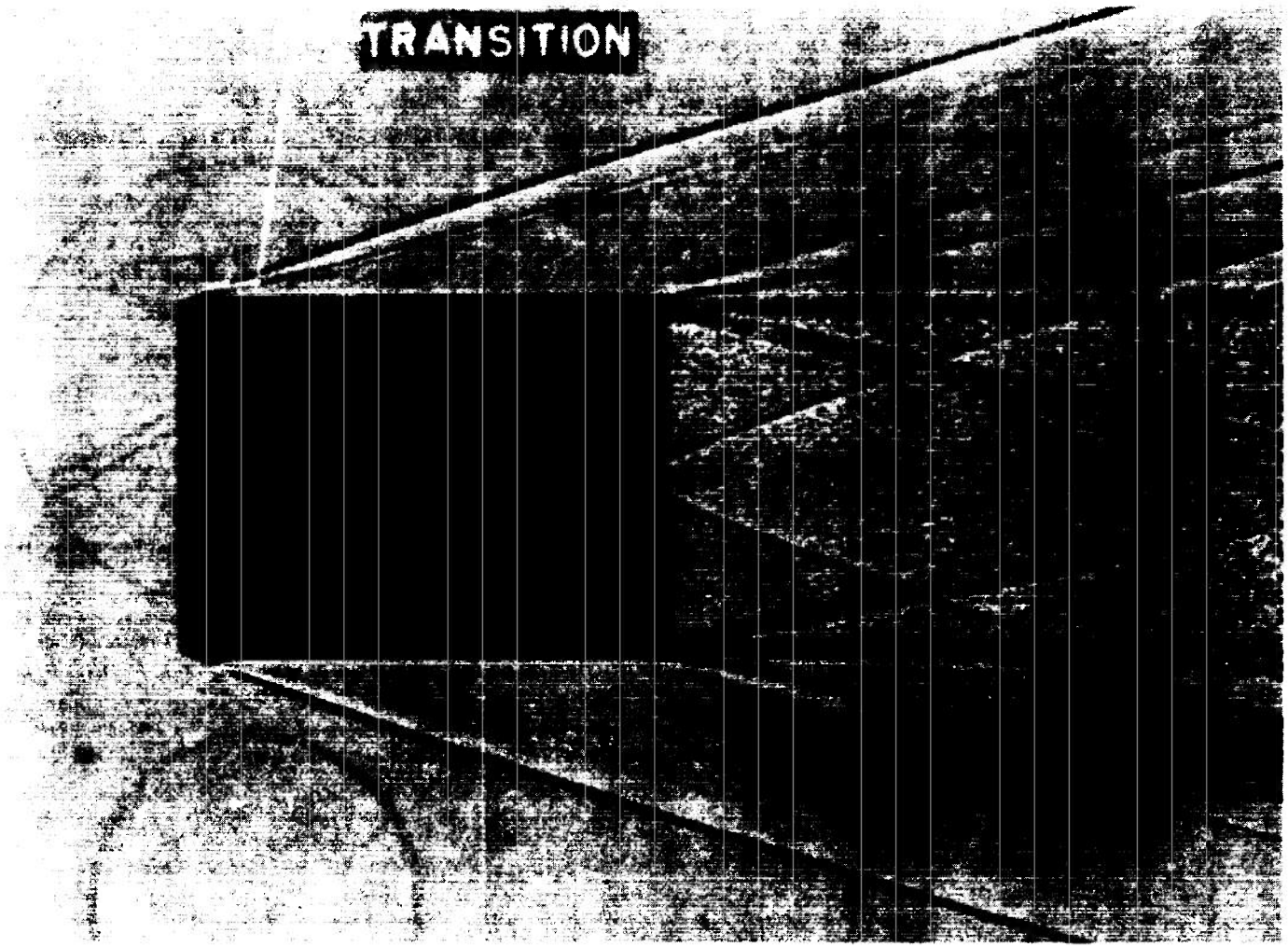

SHADOWGRAPH OF TEST MODEL WITH BOUNDARY-LAYER TRIP OF 0.003-IN-DEEP THREADS AT $M_0 = 3.9$

COURTESY AMES RESEARCH CENTER, NASA

FIG. 5.4

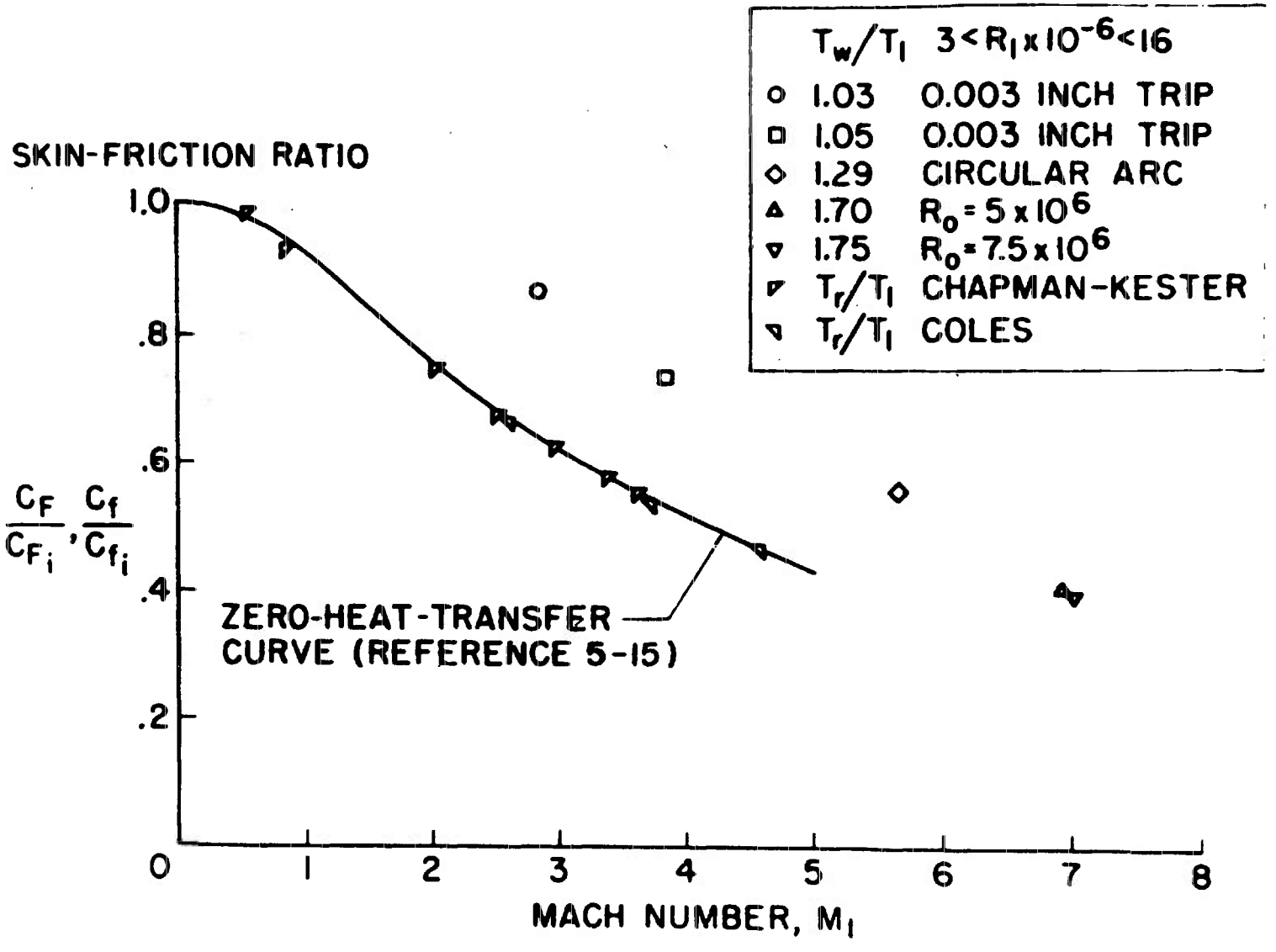

COURTESY AMES RESEARCH CENTER, NASA FIG. 5.5

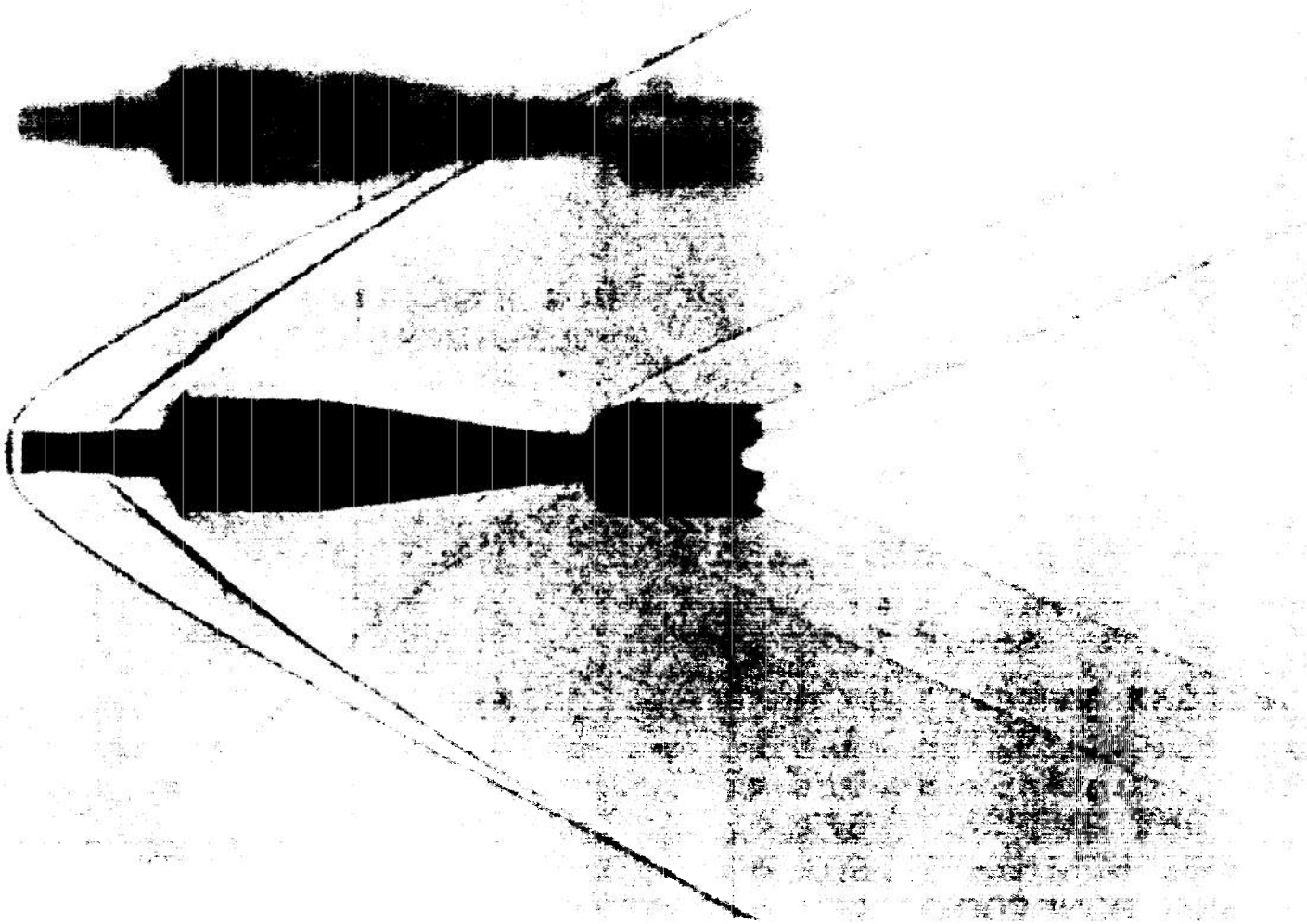

HIGH DRAG FLOW M=2.44 C_D= .782

FIG. 5.6

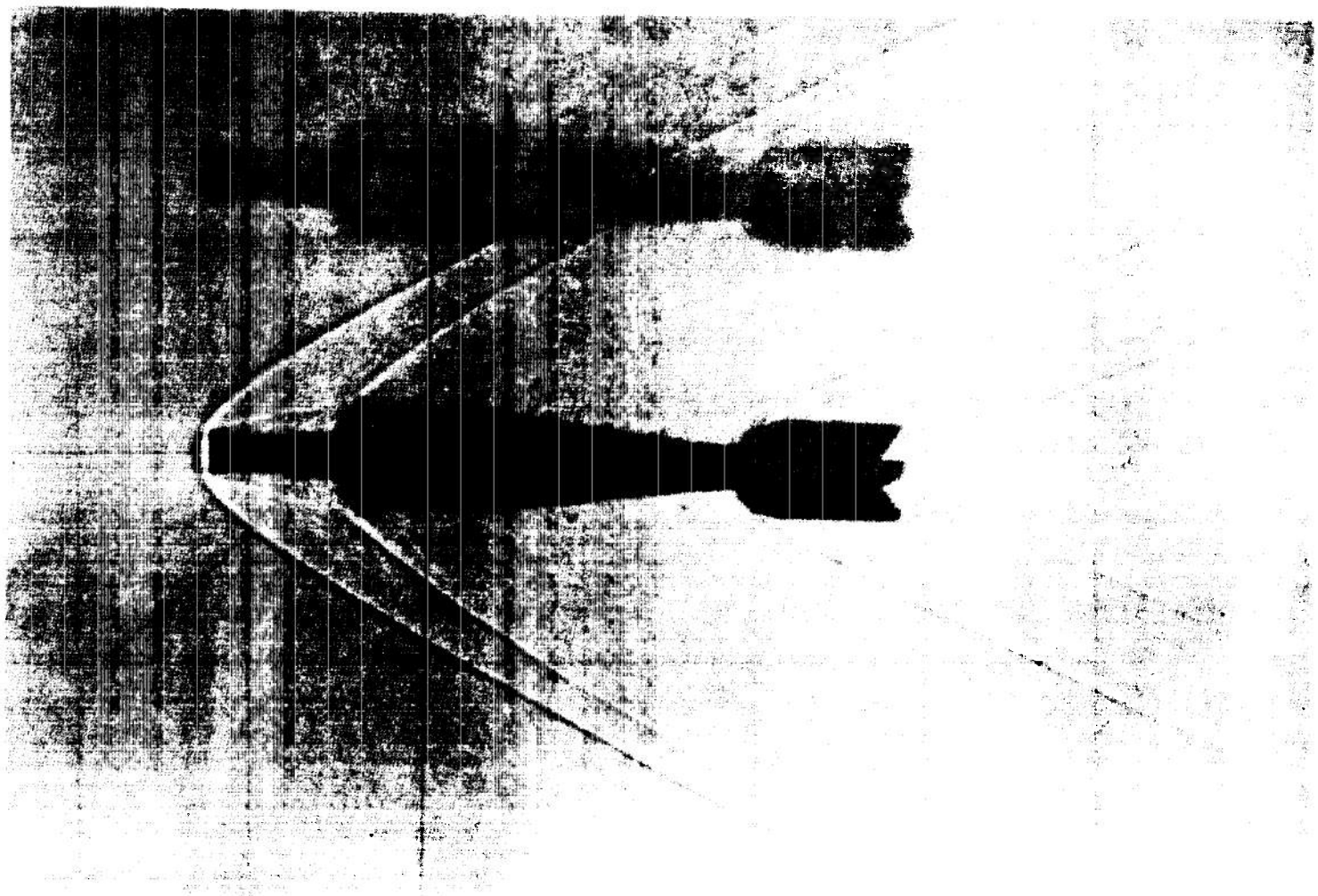

LOW DRAG FLOW M=2.43 C_D= .534

FIG. 5.7

COMPARISON OF THE EXPERIMENTAL VALUES OF C_{ℓ_p} WITH THE THEORETICAL CURVE

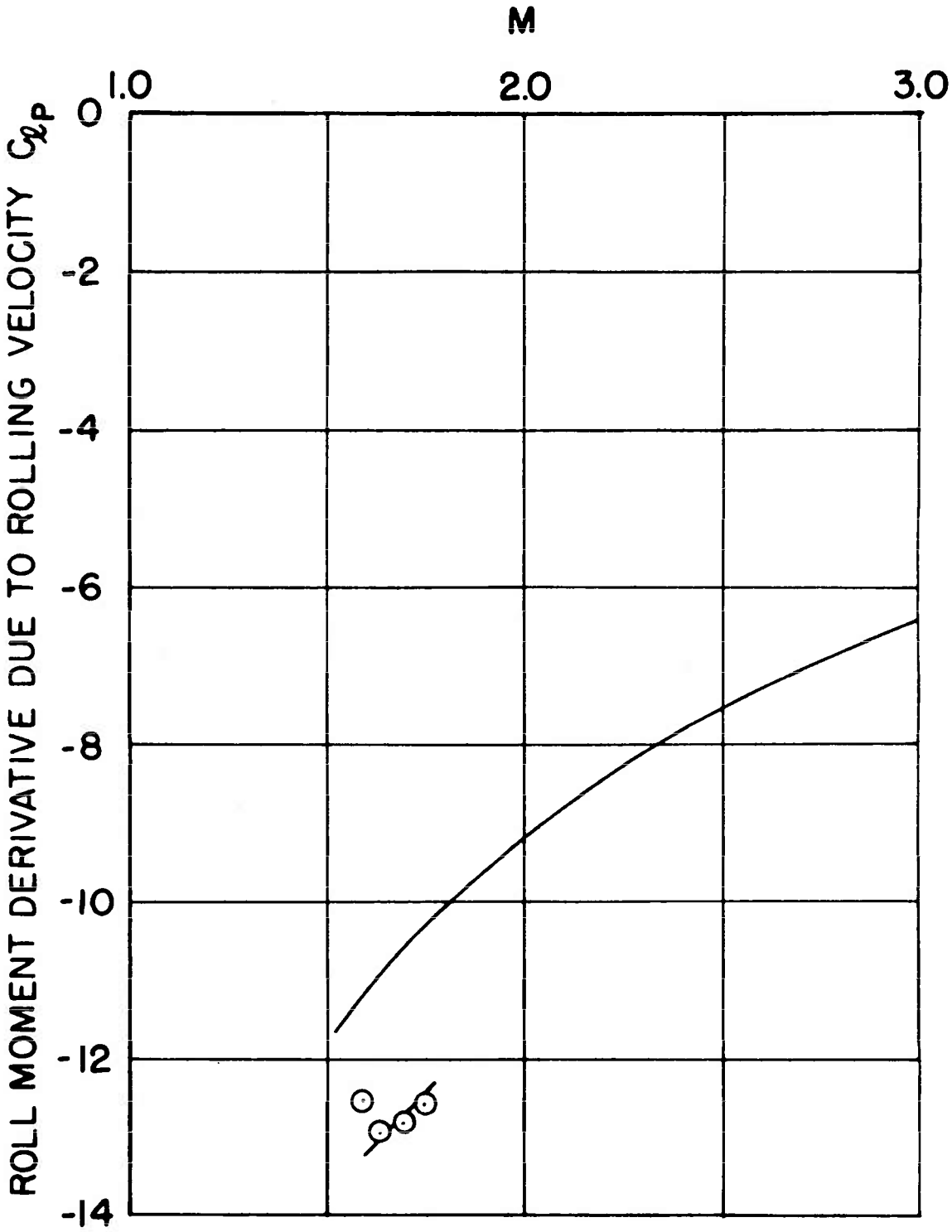

FIG. 5.8

COMPARISON OF THE EXPERIMENTAL VALUES OF C_{l_δ} WITH THE THEORETICAL CURVE

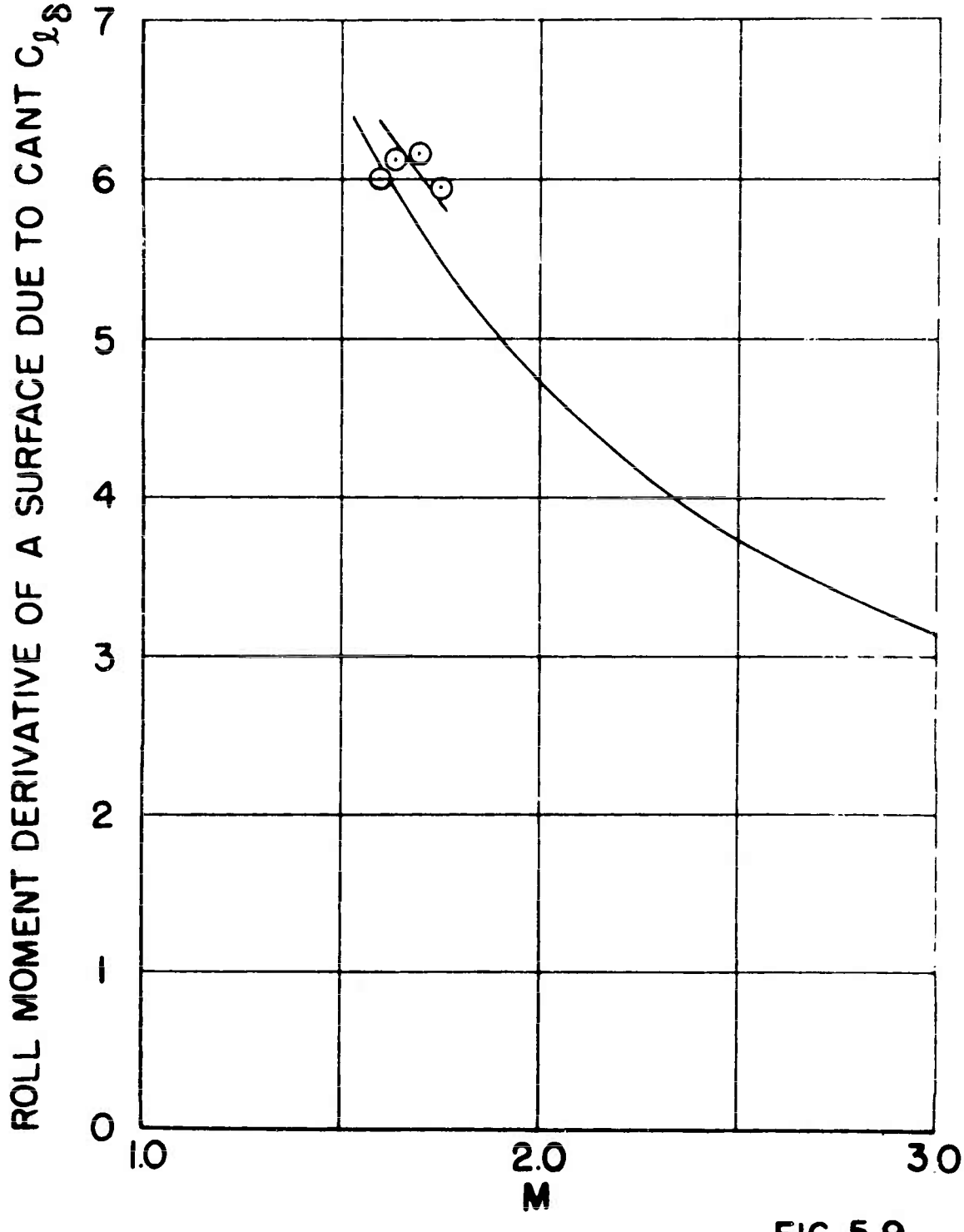

FIG. 5.9

CHAPTER VI

LINEARIZED THEORY OF MOTION OF SYMMETRIC MISSILES

6.1 Introduction

All the early stability tests on ballistic ranges involved spinning bodies of revolution which might be used as shell. In 1947, 57mm models of the General Electric Dragonfly missile were fired at the Ballistic Research Laboratories[6-1]. Since that time the number of nonspinning missiles tested has increased. Although static stability was initially obtained by the use of fins, in recent times statically stable bodies of revolution which could be used as ICBM nose cones have dominated this area of ballistic range testing. Traditionally, all stability tests have implied the assumption of linear moments, but this limitation also has been lifted in certain cases.

In this chapter we will reverse the historical development and consider the theoretically simpler case of a nonspinning missile. Next, nonzero spin and the associated gyroscopic and Magnus moments will be introduced. This work will not be linearized until very late in the development so that the results can be used in Chapter VIII on the analysis of nonlinear data.

6.2 Small Amplitude Pitching Motion of a Nonspinning Missile

For an airplane, the pitching motion is the angular motion of the airplane's thrust line in the vertical plane of symmetry. The yawing motion is then the motion of the thrust line perpendicular to this plane of symmetry. When a missile in free flight is considered, these definitions have to be altered. Since most missiles have rotationally symmetric bodies, the thrust line can be replaced by the axis of symmetry. Unfortunately, a missile can possess a number of planes of symmetry and none of them may be vertical. In this case, the selection of the plane of pitching motion is arbitrary.

We leave the definition of pitching motion for a missile without a plane of symmetry to the engineer who designed such an unusual configuration. If a basically symmetric missile is either accidentally deformed in some minor way or has intentional asymmetries due to control surfaces at a small angle of deflection, its pitching motion can, however, be defined in terms of its original symmetric shape. The influence of the asymmetries is incorporated into the total aerodynamic force and moment by the introduction of small constant force and moment terms.

Before concentrating on the simple problem of pure pitching motion we must first consider two coordinate systems: a missile-fixed system and an earth-fixed system. The missile-fixed coordinate axes, X, Y, and Z, are defined in the following way[6-2]: X - centerline of symmetrical body, positive forward; Y - perpendicular to plane of symmetry, positive to the right when looking forward*; Z - perpendicular to both the X and Y axes and directed according to the right hand rule, i.e., downward. In a similar manner, earth-fixed axes may be defined: X_e - perpendicular to the gravity vector; Y_e - perpendicular to X_e axis and the gravity vector, positive to the right when looking in the positive X_e direction; Z_e along the gravity vector, positive downward.

These two axis-systems are shown in Figure 6.1. The relative position of the axes can be described by the Eulerian angles Ψ, θ, ϕ. The velocity vector, V, is also shown in this figure. Its coordinates in the missile-fixed system are u, v, w and its orientation determined by the angle of attack, α, and the angle of sideslip, β. Notice that positive α and β are measured opposite to the positive directions of the Z and Y axes respectively.

The aerodynamic force acting on a missile in flight is usually expressed in the missile-fixed system with coordinates F_X, F_Y, F_Z. From these force components dimensionless coefficients can be obtained.

$$F_X = (1/2)\ \rho S V^2 C_X \tag{2.1}$$

$$F_Y = (1/2)\ \rho S V^2 C_Y \tag{2.2}$$

$$F_Z = (1/2)\ \rho S V^2 C_Z \tag{2.3}$$

The aerodynamic moment has components M_X, M_Y, M_Z. To distinguish the corresponding coefficients the subscripts ℓ, m, n are used. In conflict with aircraft design practice but in accordance with our remarks of Section 5.5 we will use only one reference length.

---

* If the plane of symmetry is not exactly vertical, it is possible to place yourself on the axis of symmetry in a forward facing position in the plane of symmetry so that your head is above your feet. Once this is done the selection of the positive direction of the Y axis is easy. If the missile is rolling, this selection must be made at some instant in time and the direction fixed with respect to the missile thereafter.

$$M_X = (1/2)\ \rho V^2 S \ell C_\ell \tag{2.4}$$

$$M_Y = (1/2)\ \rho V^2 S \ell C_m \tag{2.5}$$

$$M_Z = (1/2)\ \rho V^2 S \ell C_n \tag{2.6}$$

These quantities are shown in Figure 6.2. The angular velocity, which is not shown there, has components p, q, r with positive senses which are the same as those shown for C_ℓ, C_m, and C_n, respectively.

For a nonspinning missile undergoing pure pitching motion, the functional dependence of C_X, C_Z, and C_m must be stated. For small angles, C_X is essentially the negative of C_D. It is not unreasonable to expect the lateral force and pitch moment to depend on the actual motion in addition to the flow parameters, Mach number and Reynold's number. Although the motion can be described completely by α, q, and all their time derivatives at some given time, we will only consider α, q, and $\dot{\alpha}$. For small amplitude motion, a further assumption of linear dependence can be made and the explicit relations for C_Z and C_m follow.

$$C_Z = C_{Z_o} + C_{Z_\alpha}\alpha + C_{Z_q}\left(\frac{q\ell}{V}\right) + C_{Z_{\dot{\alpha}}}\left(\frac{\dot{\alpha}\ell}{V}\right) \tag{2.7}$$

$$C_m = C_{m_o} + C_{m_\alpha}\alpha + C_{m_q}\left(\frac{q\ell}{V}\right) + C_{m_{\dot{\alpha}}}\left(\frac{\dot{\alpha}\ell}{V}\right) \tag{2.8}$$

where C_{Z_o} and C_{m_o} are due to asymmetries.

The various important angles are shown in Figure 6.3. The equations of motion are the drag Equation (5.2.2), the force equation* along the inertial axis Z_e and the moment equation about the Y axis.

$$m\dot{V} = -D \sim F_X \tag{2.9}$$

$$m\ddot{z}_e = F_Z \cos\Theta - F_X \sin\Theta + mg \tag{2.10}$$

* This force equation neglects a small Coriolis force term due to the earth's rotation. This term will be introduced in the more complete analysis of Section 6.9.

$$I_y \ddot{\theta} = M_Y \tag{2.11}$$

where I_y is the moment of inertia about the Y axis.

From Figure 6.3 it is clear that

$$\dot{z}_e = - V \sin (\theta - \alpha) \tag{2.12}$$

This, together with the assumption of a small angle of attack and a flat trajectory ($\theta << 1$), allows us to revise Equation (2.10).

$$- m \left[V(\dot{\theta} - \dot{\alpha}) + \dot{V}(\theta - \alpha) \right] = F_Z - F_X \theta + mg \tag{2.13}$$

Equations (2.7, 9) and the relation $\dot{\theta} = q$ can now be used to simplify Equation (2.13).

$$\left[1 + C^*_{Z_q} \right] \frac{q\ell}{V} = \left[1 - C^*_{Z_{\dot{\alpha}}} \right] \frac{\dot{\alpha}\ell}{V} - (C^*_{Z_\alpha} + C^*_D) \alpha - C^*_{Z_o} - g\ell V^{-2} \tag{2.14}$$

where $C^*_{Z_i} = \frac{\rho S \ell}{2m} C_{Z_i}$

Since the density factor $\frac{\rho S \ell}{2m}$ is less than 10^{-3}, $C^*_{Z_q}$ and $C^*_{Z_{\dot{\alpha}}}$ can probably be neglected in comparison with unity and Equation (2.14) can be written in an even simpler form.

$$\frac{q\ell}{V} = \frac{\dot{\alpha}\ell}{V} - (C^*_{Z_\alpha} + C^*_D) \alpha - C^*_{Z_o} - g\ell V^{-2} \tag{2.15}$$

From this form we see that a good first approximation for q is $\dot{\alpha}$. The remaining terms in Equation (2.15) can have a measurable effect and so should be retained. Equation (2.15) is now used to eliminate $\ddot{\theta} = \dot{q}$ and q from Equation (2.11) with the result

$$\ddot{\alpha} + \hat{H}_1 \dot{\alpha} - \hat{M}_1 \alpha = \hat{A}_1 + \hat{G} \tag{2.16}$$

where $\hat{H}_1 = -\left[C^*_{Z_\alpha} + C^*_D + k_y^{-2}\,(C^*_{m_q} + C^*_{m_{\dot\alpha}})\right]\left(\frac{V}{\ell}\right)$

$$\hat{M}_1 = \left[k_y^{-2}\,C^*_{m_\alpha} - (C^*_{Z_\alpha} + C^*_D)\,(k_y^{-2}\,C^*_{m_q} + C^*_D)\right]\left(\frac{V}{\ell}\right)^2$$

$$\sim k_y^{-2}\,C^*_{m_\alpha}\left(\frac{V}{\ell}\right)^2$$

$$\hat{A}_1 = \left[k_y^{-2}\,C^*_{m_o} - C^*_{Z_o}\,(k_y^{-2}\,C^*_{m_q} + C^*_D)\right]\left(\frac{V}{\ell}\right)^2$$

$$\sim k_y^{-2}\,C^*_{m_o}\left(\frac{V}{\ell}\right)^2$$

$$\hat{G} = -\,(k_y^{-2}\,C^*_{m_q} - C^*_D)\left(\frac{g}{\ell}\right)$$

$k_y = \sqrt{\frac{I_y}{m\ell^2}}$ is radius of gyration about the Y-axis.

The starred aerodynamic coefficients contain the density factor and, hence, are quite small. Products of starred coefficients are omitted in comparison with a starred coefficient*.

Equation (2.16) is linear but with variable coefficients. This variation in the coefficients can be removed by replacing time by distance as the independent variable.

$$\therefore \alpha'' + H_1\alpha' - M_1\alpha = A_1 + G\left(\frac{V}{V_o}\right)^{-2} \qquad (2.17)$$

* The products of starred coefficients are important for the angular motion of lighter than air ships, submarines and topedoes. For these vehicles, $\hat{M}_1$ can be negative when C_{m_α} is positive! See Reference 6-10.

$$\text{where } H_1 = -\left[C^*_{Z_\alpha} + 2C^*_D + k_y^{-2}\left(C^*_{m_q} + C^*_{m_{\dot\alpha}}\right)\right]$$

$$M_1 = k_y^{-2} C^*_{m_\alpha}$$

$$A_1 = k_y^{-2} C^*_{m_o}$$

$$G = -\left(k_y^{-2} C^*_{m_q} - C^*_D\right)\left(g\ell V_o^{-2}\right)$$

The solution to this equation for a statically stable missile ($C_{m_\alpha} < 0$) is

$$\alpha = \alpha_a + \alpha_g \left(\frac{V}{V_o}\right)^{-2} + \alpha_o e^{-(1/2)H_1 s} \cos\left(\omega s + \phi_o\right) \qquad (2.18)$$

$$\text{where } \alpha_a = -\frac{C_{m_o}}{C_{m_\alpha}}$$

$$\alpha_g = \left[\frac{C_{m_q} - k_y^2 C_D}{C_{m_\alpha}}\right]\frac{g\ell}{V_o^2}$$

$$\omega^2 = -M_1 - \frac{H_1^2}{4} \sim -\frac{\rho S \ell^3}{2I_y} C_{m_\alpha}$$

α_o and ϕ_o are determined by initial conditions. By definition the influence of this initial disturbance will damp out if the missile is dynamically stable ($H_1 > 0$). For such a missile the angle of attack will eventually reach an equilibrium angle $\alpha_a + \alpha_g$. The aerodynamic part of this angle, α_a, can easily be interpreted as satisfying the requirement that the aerodynamic moment coefficient must vanish for equilibrium, i.e., $C_{m_\alpha}\alpha_a + C_{m_o} = 0$. A similar

interpretation for α_g is possible when it is noted from Equation (2.15) that $g\ell V^{-2}$ is the curvature of the trajectory due to gravity. This angular velocity has a moment whose magnitude is determined by $C_{m_q} g\ell V^{-2}$. In addition to this there is a change in the curvature due to decrease in velocity. This angular acceleration due to drag gives rise to the quantity $k_y^2 C_D g\ell V^{-2}$. For equilibrium the sum of these two terms must be matched by the moment coefficient $C_{m_\alpha} \alpha_g$. For models as big as 6 inches, $g\ell V^{-2}$ is always less than 6×10^{-5} and, hence, this gravity-induced, steady-state angle of attack is not directly measurable. The aerodynamic induced angle, α_a, can be quite large and is measurable.

The vertical motion of the missile can now be obtained from Equation (2.10). The usual change of independent variable is made to absorb the velocity variation, and small angles are assumed.

$$\frac{z_e''}{\ell} = C_{Z_o}^* + (C_{Z_\alpha}^* + C_D^*)\,\alpha + C_{Z_q}^* \left(\frac{q\ell}{V}\right) + C_{Z_{\dot\alpha}}^* \alpha' + g\ell V_o^{-2}\left(\frac{V}{V_o}\right)^{-2} \qquad (2.19)$$

According to Equation (2.15), $\frac{q\ell}{V}$ can be replaced by α' in Equation (2.19) since the remaining terms of Equation (2.15) yield products of starred coefficients after the substitution.

$$\therefore \frac{z_e}{\ell} = a_z + b_z s + \left[C_{Z_o}^* + (C_{Z_\alpha}^* + C_D^*)\,\alpha_a\right] \frac{s^2}{2}$$

$$+ (C_{Z_\alpha}^* + C_D^*)\,\alpha_o \int_0^s \int_0^{s_2} e^{-(H_1/2)s_1} \cos(\omega s_1 + \phi_o)\, ds_1 ds_2$$

$$+ (C_{Z_q}^* + C_{Z_{\dot\alpha}}^*) \int_0^s \alpha\, ds_1$$

$$+ \left[g\ell V_o^{-2} + (C_{Z_\alpha}^* + C_D^*)\,\alpha_g\right] \int_0^s \int_0^{s_2} e^{2C_D^* s_1}\, ds_1 ds_2 \qquad (2.20)$$

The first two integrals in Equation (2.20) yield linear functions plus damped cosines. The cosines do, however, differ in phase. The third integral can be approximated by $\frac{s^2}{2}$. Thus, the vertical motion is essentially a parabola in s plus damped cosines which arise from the pitching motion.

Equation (2.20) indicates a measurable influence of α_g. During firing-table tests of finned bombs during World War II, it was found that times of flight were higher than expected[6-3]. In fact, negative drag coefficients were required to fit the observations by a theory in which only the drag force is considered. The definition of α_g shows that it is positive for C_{m_q} negative and, hence, the missile will fly in an equilibrium position with its nose slightly above its flight path. For almost all missiles the aerodynamic force is in the direction of the angle of attack and, therefore, C_{Z_α} is negative. Thus $(C^*_{Z_\alpha} + C^*_D)\,\alpha_g$ opposes gravity and increases the flight time. For short flights in a ballistic range this effect is too small to measure. Gravity-induced equilibrium angles do, however, cause measurable effects for missiles with high spin rates. These effects are described in Section 7.2.

6.3 Combined Pitching and Yawing Motion of a Nonspinning Missile

Except for the absence of gravity the analysis for the yawing motion is almost identical to that for the pitching motion:

$$m\ddot{y}_e = F_Y \cos\Psi + F_X \sin\Psi \tag{3.1}$$

$$I_z\ddot{\Psi} = M_Z \tag{3.2}$$

$$\dot{y}_e = V \sin(\Psi + \beta) \tag{3.3}$$

$$C_Y = C_{Y_o} + C_{Y_\beta}\,\beta + C_{Y_r}\left(\frac{r\ell}{V}\right) + C_{Y_{\dot\beta}}\left(\frac{\dot\beta\ell}{V}\right) \tag{3.4}$$

$$C_n = C_{n_o} + C_{n_\beta}\,\beta + C_{n_r}\left(\frac{r\ell}{V}\right) + C_{n_{\dot\beta}}\left(\frac{\dot\beta\ell}{V}\right) \tag{3.5}$$

In Figure 6.4, the positive senses of Ψ and β are indicated and the correctness of Equations (3.1-3) directly verified. Note that the definition of β is consistent with that of α in that it is positive when the missile's nose is

away from the positive direction of the corresponding transverse axis. Normally, C_{Y_β} is negative like C_{Z_α}. The sense of Ψ is such that $\dot{\Psi}$ has a positive direction in accordance with the right hand rule. Thus for pure yawing motion, $\dot{\Psi} = r$.

The relation between r and $\dot{\beta}$ is quite similar to Equation (2.15)

$$\frac{r\ell}{V} = -\frac{\dot{\beta}\ell}{V} + (C^*_{Y_\beta} + C^*_D)\,\beta + C^*_{Y_o} \tag{3.6}$$

From this, an equation for yawing motion similar to Equation (2.17) can be written.

$$\beta'' + H_2\beta' - M_2\beta = A_2 \tag{3.7}$$

where $H_2 = -\left[C^*_{Y_\beta} + 2C^*_D + k_z^{-2}\,(C^*_{n_r} - C^*_{n_{\dot{\beta}}})\right]$

$$M_2 = -\,k_z^{-2}\,C^*_{n_\beta}$$

$$A_2 = -\,k_z^{-2}\,C^*_{n_o}$$

$k_z = \left[\frac{I_z}{m\ell^2}\right]^{1/2}$ is radius of gyration about Z-axis.

It follows immediately from the right-hand rule that for a positive C_{n_β}, a positive β induces a rotation in the negative β direction. Thus yawing motion is statically stable when C_{n_β} is positive.

With the exception of Chapter X, we will consider throughout this book basically symmetric bodies. This symmetry must apply to mass distribution as well as exterior shape, i.e., $I_y = I_z$. With the present restriction to zero spin and neglect of the small asymmetry terms ($C_{Z_o} = C_{Y_o} = C_{m_o} = C_{n_o} = 0$) it should not be possible to distinguish pitching or yawing motion. This slightly metaphysical argument will be replaced by a more explicit algebraic one in Section 6.5. For either approach, relations between various coefficients can be obtained.

$$- C_{N_\alpha} \equiv C_{Z_\alpha} = C_{Y_\beta} \qquad C_{M_q} \equiv C_{m_q} = C_{n_r}$$

$$C_{M_{\dot\alpha}} \equiv C_{m_{\dot\alpha}} = - C_{n_{\dot\beta}} \qquad C_{M_\alpha} \equiv C_{m_\alpha} = - C_{n_\beta} \tag{3.8}$$

The new symbols introduced above are used to indicate the coefficients of a symmetric body. Equations (2.17) and (3.7) can now be combined by the simple device of multiplying the first by i and adding to the second.

$$\xi'' + H\xi' - M\xi = iA + iG\left(\frac{V}{V_o}\right)^{-2} \tag{3.9}$$

where $\xi = \beta + i\alpha$

$H = H_1 = H_2$

$M = M_1 \equiv M_2$

$A = k_t^{-2}\left[C_{m_o}^* + iC_{n_o}^*\right]$

$k_t = k_z = k_y$ is transverse radius of gyration.

The solution to this simple equation in the complex variable ξ is

$$\xi = K_1 e^{i\phi_1} + K_2 e^{i\phi_2} + K_3 e^{i\phi_{30}} + \xi_g \tag{3.10}$$

where $K_j = K_{j0} e^{\lambda_j s} \qquad j = 1,2$

$\phi_j = \phi_{j0} + \phi_j' s$

$\lambda_1 = \lambda_2 = - (1/2)H$

$\phi_1' = - \phi_2' = \sqrt{- M}$

$$K_3 e^{i\phi_{30}} = \frac{-i(C_{m_o} + iC_{n_o})}{C_{M_\alpha}}$$

$$\xi_g = \frac{i(C_{M_q} - k_t^2 C_D) g\ell/V^2}{C_{M_\alpha}}$$

ϕ_{j0} and K_{j0} for $j = 1,2$ are determined by the initial angles and angular velocities.

The various terms in Equation (3.10) can represent two dimensional vectors in the $\alpha\beta$ plane. ξ, then, is the sum of these vectors (Figure 6.5). A sample motion, which is shown in Figure 6.6, is a damped elliptical motion; the semi-major axis of the ellipse is $K_1 + K_2$, its semi-minor axis is $|K_1 - K_2|$, and its center is located at $K_3 e^{i\phi_{30}} + \xi_g$. Equation (2.17) for the pitching motion can be obtained from the imaginary part of Equation (3.9). This use of the complex variable, which introduces a minor elegance in the problem of a nonspinning missile, forms an essential feature of the analysis of the motion of a spinning missile.

6.4 Exact Equations of Motion for a Spinning Missile

The motion of a rigid body may be described by a pair of vector equations

$$m\dot{\vec{V}} = \vec{F} + m\vec{g} \tag{4.1}$$

$$\dot{\vec{H}} = \vec{M} \tag{4.2}$$

where $\vec{V}$ is velocity of center of mass

$\vec{F}$ is aerodynamic force

$\vec{g}$ is acceleration due to gravity

$\vec{H}$ is angular momentum

$\vec{M}$ is aerodynamic moment.

The components of the vector derivatives in Equations (4.1-2) may be calculated by the well-known relation

$$(U_1, U_2, U_3)^{\cdot} = (\dot{U}_1, \dot{U}_2, \dot{U}_3) + \vec{\omega} \times (U_1, U_2, U_3) \tag{4.3}$$

where

U_1, U_2, U_3 are the components of the vector U and

$\vec{\omega}$ is the angular velocity vector of the coordinate system with respect to an inertia system.

For the missile-fixed axes previously defined, the vectors in the above equations may be given in component form

$$\vec{V} = (u, v, w) \tag{4.4}$$

$$\vec{F} = (F_X, F_Y, F_Z) \tag{4.5}$$

$$\vec{g} = (g \sin \theta, g \cos \theta \sin \phi, g \cos \theta \cos \phi) \tag{4.6}$$

$$\vec{H} = (I_x p + I_{xy} q + I_{xz} r, I_y q + I_{xy} p + I_{yz} r, I_z r + I_{xz} p + I_{yz} q) \tag{4.7}$$

$$\vec{M} = (M_X, M_Y, M_Z) \tag{4.8}$$

$$\vec{\omega} = (p, q, r) \tag{4.9}$$

where I_{xy}, I_{xz}, and I_{yz} are products of inertia.

If we assume that the plane of aerodynamic symmetry (the XZ plane) is also a plane of mass symmetry, two of the products of inertia vanish. ($I_{xy} = I_{yz} = 0$) and H reduces to the form applicable to an airplane ($I_x p + I_{xz} r$, $I_y q$, $I_z r + I_{xz} p$). For an aircraft the X-axis can be defined as the thrust line or the zero lift line. A third choice could be that direction for which I_{xz} vanishes (principal axis of inertia). If this is done and mass rotational symmetry assumed ($I_y = I_z$), the angular momentum vector has the simple component form ($I_x p$, $I_y q$, $I_y r$).

If the aerodynamic force and moment can be defined in terms of u, v, w, p, q, and r, and the effect of gravity neglected, Equations (4.1-2) yield a complete set of six first order differential equations in these six dependent variables. In those cases where gravity has a measurable effect, relations between the Eulerian angle defining the orientation of the missile-fixed axes and earth-fixed axes* and the components of angular velocity are

* In ballistic range work, the influence of the earth's rotation can normally be neglected and the distinction between earth-fixed axes and inertia axes thereby vanishes. One exception to this is the deflection of subsonic models due to Coriolis force. This effect is discussed in Section 6.9.

$$p = \dot{\phi} - \dot{\psi} \sin \theta \tag{4.10}$$

$$q = \dot{\theta} \cos \phi + \dot{\psi} \cos \theta \sin \phi \tag{4.11}$$

$$r = - \dot{\theta} \sin \phi + \dot{\psi} \cos \theta \cos \phi \tag{4.12}$$

Equations (4.10-12) now increase our set of differential equations to nine first order equations in nine dependent variables. Finally, if the location of the missile (x_e, y_e, z_e), which is indirectly present in the aerodynamic force and moment through air density, air temperature and wind structure, varies enough to cause measurable effects, then the velocities must be integrated and our set of equations becomes twelfth order.

Fortunately, in ballistic range tests, $\theta << 1$ so that Equations (4.10-12) can be linearized and absorbed into Equations (4.1-2) without increase in order. The axial angular velocity component of the roll equations can be solved independently of the other component equations and the rotational symmetry assumption reduces the system to a quite simple fourth order system. This simplicity is exploited through the use of a nonrolling coordinate system and complex variables.

For this nonrolling coordinate system, the missile's velocity vector is (u, $\tilde{v}$, $\tilde{w}$) and its angular velocity vector is (p, $\tilde{q}$, $\tilde{r}$) while the angular velocity of the coordinate system is $\vec{\omega} = (0, \tilde{q}, \tilde{r})$ where

$$\tilde{q} = q \cos \tilde{\phi} - r \sin \tilde{\phi}; \quad \tilde{v} = v \cos \tilde{\phi} - w \sin \tilde{\phi} \tag{4.13}$$

$$\tilde{r} = q \sin \tilde{\phi} + r \cos \tilde{\phi}; \quad \tilde{w} = v \sin \tilde{\phi} + w \cos \tilde{\phi} \tag{4.14}$$

$$\tilde{\phi} = \int_0^t p \, dt \tag{4.15}$$

The angular momentum vector has the simple form ($I_x p$, $I_y q$, $I_y r$); its transverse components transform in the same way as those of the velocity and angular velocity (Equations (4.13-14))

$$H_{\tilde{y}} = (I_y q) \cos \tilde{\phi} - (I_y r) \sin \tilde{\phi} = I_y \tilde{q} \tag{4.16}$$

$$H_{\tilde{z}} = (I_y q) \sin \tilde{\phi} + (I_y r) \cos \tilde{\phi} = I_y \tilde{r} \tag{4.17}$$

In the nonrolling coordinates, the angular momentum for a missile with mass symmetry retains its simple form while derivatives of vectors computed by Equation (4.3) are much simpler. For example, the angular momentum vector and its derivative are

$$\vec{H} = (I_x p,\ I_y \tilde{q},\ I_y \tilde{r}) \tag{4.18}$$

$$\dot{\vec{H}} = (I_x \dot{p},\ I_y \dot{\tilde{q}} + I_x p\tilde{r},\ I_y \dot{\tilde{r}} - I_x p\tilde{q}) \tag{4.19}$$

The simplicity of Equation (4.19) and the corresponding equation for the velocity vector makes the nonrolling system a very attractive one.

The four transverse component equations derived from Equations (4.1-2) reduce to

$$\dot{\tilde{v}} + u\tilde{r} = \left(\frac{\rho S V^2}{2m}\right) C_{\tilde{Y}} + g_{\tilde{y}} \tag{4.20}$$

$$\dot{\tilde{w}} - u\tilde{q} = \left(\frac{\rho S V^2}{2m}\right) C_{\tilde{Z}} + g_{\tilde{z}} \tag{4.21}$$

$$\dot{\tilde{q}} + \left(\frac{I_x}{I_y}\right) p\tilde{r} = \frac{\rho S V^2 \ell}{2I_y} C_{\tilde{m}} \tag{4.22}$$

$$\dot{\tilde{r}} - \left(\frac{I_x}{I_y}\right) p\tilde{q} = \frac{\rho S V^2 \ell}{2I_y} C_{\tilde{n}} \tag{4.23}$$

where tilde superscripts denote components in the nonrolling coordinates.

If the second equation of each pair is multiplied by i and added to the first, the independent variable changed to distance, and dimensionless variables introduced, Equations (4.20-23) assume the simple form

$$\tilde{\xi}' - C_D^* \tilde{\xi} - i\gamma\tilde{\mu} = C_{\tilde{Y}}^* + iC_{\tilde{Z}}^* + (g_{\tilde{y}} + ig_{\tilde{z}})\ell/V^2 \tag{4.24}$$

$$\tilde{\mu}' - C_D^* \tilde{\mu} - iP\tilde{\mu} = (C_{\tilde{m}}^* + iC_{\tilde{n}}^*)\, k_t^{-2} \tag{4.25}$$

where

$$\tilde{\xi} = \frac{\tilde{v} + i\tilde{w}}{V}$$

$$\tilde{\mu} = \frac{(\tilde{q} + i\tilde{r})\ell}{V}$$

$$\gamma = \frac{u}{V}$$

$$P = \frac{I_x}{I_y}\left(\frac{p\ell}{V}\right)$$

The complex variable $\tilde{\xi}$ locates the plane which contains the velocity vector and the missile's axis. Its magnitude is the sine of the angle between the velocity vector and the missile's axis and this angle will be called the resultant angle of attack, α_r. From this it is clear that γ is cos α_r. Since $P\tilde{\mu}$ is the gyroscopic moment, P is a measure of the gyroscopic effects. When the force and moment are specified in terms of $\tilde{\xi}$, $\tilde{\mu}$ and their derivatives, $\tilde{\mu}$ can be eliminated between Equations (4.24-25) and a second order equation in $\tilde{\xi}$ results.

6.5 Linear Force and Moment Expansion

The proper linear terms will first be derived in the more natural missile-fixed coordinates and then transformed to nonrolling coordinates. The variable $\xi = (v + iw)\, V^{-1}$ is quite similar to the angles of attack and sideslip. Indeed, for small angles $\xi \doteq \beta + i\alpha$. Coefficients of this variable will have the subscript α for this reason.

Our object is the most general linear expression in ξ, μ, ξ', μ' for the force and moment acting on a symmetric missile. In components form, Y-force expansion would be

$$C_Y = e_1(v/V) + e_2(w/V) + e_3(q\ell/V) + e_4(r\ell/V) + e_5(v/V)' + e_6(w/V)' + e_7(q\ell/V)' + e_8(r\ell/V)' \qquad (5.1)$$

A similar expansion would apply for C_Z. Since $v/V = (\xi + \bar{\xi})/2$ and $w/V = (\xi - \bar{\xi})/2i$ and similar relations exist for the other quantities in Equation (5.1), the force coefficient expansion can be written in terms of complex quantities.

$$C_Y + iC_Z = A_1\xi + A_2\mu + A_3\xi' + A_4\mu' + B_1\bar{\xi} + B_2\bar{\mu} + B_3\bar{\xi}' + B_4\bar{\mu}' \qquad (5.2)$$

If we now consider a new missile system which differs in roll angle, $\hat{\phi}$, from our original system and identify quantities in this system by a circumflex superscript, it is clear that

$$\hat{C}_Y + i\hat{C}_Z = (C_Y + iC_Z)e^{i\hat{\phi}} = A_1\hat{\xi} + A_2\hat{\mu} + A_3\hat{\xi}' + A_4\hat{\mu}' + (B_1\hat{\bar{\xi}} + B_2\hat{\bar{\mu}} + B_3\hat{\bar{\xi}}' + B_4\hat{\bar{\mu}}')e^{2i\hat{\phi}} \tag{5.3}$$

We now select $\hat{\phi}$ to be an angle of rotational symmetry. In other words, when the missile is rotated through the angle $\hat{\phi}$ its relative appearance to a fixed observer is unchanged. Its force expansion then should be unaffected. But the coefficients of the conjugate variables are multiplied by $e^{2i\hat{\phi}}$. We, therefore, have the important result that if a missile has an angle of rotational symmetry of 120° or less, the coefficients of the conjugate variables must be zero. In other words, the linear force expansion of a symmetric three-fin missile is the same as a body of revolution and terms which express their different nature must be second order or higher! The reasoning is identical for the moment.

For a rotationally symmetric missile

$$C_Y + iC_Z = A_1\xi + A_2\mu + A_3\xi' + A_4\mu' \tag{5.4}$$

$$C_m + iC_n = C_1\xi + C_2\mu + C_3\xi' + C_4\mu' \tag{5.5}$$

The coefficients in Equations (5.4-5) are complex quantities. The character of their real and imaginary parts can be determined by a consideration of their dependence on roll for a missile with a plane of mirror symmetry. If the XY-plane is taken to be the plane of symmetry and the coordinate system is transformed by a reversal of the Z-axis ($\hat{Z} = -Z$), a missile with mirror symmetry would be unaffected and so would be the form of its aerodynamic force and moment expansion. Under such a transformation the velocity and force vectors reverse their Z components but the angular velocity and moment vectors reverse their X and Y components. This is due to the fact that the sign of a component of angular velocity or moment is directly related to the right- or left-handedness of the coordinate system through their definitions as cross products. For example, a positive p rotation rotates the Y-axis toward the Z-axis, a positive q rotation rotates the Z-axis toward the X-axis and a positive r rotation rotates the X-axis toward the Y-axis. A reversal of the Z-axis then has the stated effect of changing the sign of p and q. The results of this transformation can be summarized.

$$\hat{V} = V, \qquad \hat{p} = - p \tag{5.6}$$

$$\hat{\xi} = \overline{\xi} \qquad \hat{\mu} = - \overline{\mu} \tag{5.7}$$

$$\hat{\xi}' = \overline{\xi}' \qquad \hat{\mu}' = - \overline{\mu}' \tag{5.8}$$

$$\hat{C}_Y + i\hat{C}_Z = C_Y - iC_Z = \overline{A}_1\hat{\xi} - \overline{A}_2\hat{\mu} + \overline{A}_3\hat{\xi}' - \overline{A}_4\hat{\mu}' \tag{5.9}$$

$$\hat{C}_m + i\hat{C}_n = - C_m + iC_n = - \overline{C}_1\hat{\xi} + \overline{C}_2\hat{\mu} - \overline{C}_3\hat{\xi}' + \overline{C}_4\hat{\mu}' \tag{5.10}$$

Since mirror symmetry requires that it be impossible to distinguish a change in the aerodynamic force and moment from this transformation, the coefficients in Equations (5.9-10) must equal those in Equations (5.4-5). If the coefficients are constants, this means that the imaginary parts of A_1, A_3, C_2, and C_4 and the real parts of A_2, A_4, C_1 and C_3 must be zero. The presence of non-zero roll should affect the force and moment, and so we make the assumption that the coefficients are functions of p. With this assumption the quantities which previously had to vanish must now change sign with p. This means that they are <u>odd</u> functions of p. (A power series expansion in p would contain only odd powers.) The remaining real and imaginary parts do not change sign and, therefore, are even functions of p. When p is zero, the odd functions are zero. In order to make this explicit, we will write these odd functions as products of p and even functions of p.

$$\begin{aligned} C_Y + iC_Z = &\left[a_1 + i\left(\frac{p\ell}{V}\right) b_1\right] \xi + \left[\left(\frac{p\ell}{V}\right) b_2 + ia_2\right] \mu \\ &+ \left[a_3 + i\left(\frac{p\ell}{V}\right) b_3\right] \xi' + \left[\left(\frac{p\ell}{V}\right) b_4 + ia_4\right] \mu' \end{aligned} \tag{5.11}$$

$$\begin{aligned} C_m + iC_n = &\left[\left(\frac{p\ell}{V}\right) d_1 + ic_1\right] \xi + \left[c_2 + i\left(\frac{p\ell}{V}\right) d_2\right] \mu \\ &+ \left[\left(\frac{p\ell}{V}\right) d_3 + ic_3\right] \xi' + \left[c_4 + i\left(\frac{p\ell}{V}\right) d_4\right] \mu' \end{aligned} \tag{5.12}$$

The b_j and d_j coefficients are called Magnus coefficients and denote interaction effects between spin and cross-flow induced by one of the four complex quantities. Simple examples of a Magnus effect are the curving of a baseball and the hooking or slicing of a golf ball[6-5].

Equations (5.11-12) are not in the proper form for use in the equations of motion. We need to convert to the nonrolling coordinates by multiplication by exp $i\phi$. This will transform the transverse force and moment variables ξ and μ properly but not ξ' and μ'.

$$e^{i\phi}\xi' = \tilde{\xi}' - i\left(\frac{p\ell}{V}\right)\tilde{\xi} \tag{5.13}$$

$$e^{i\phi}\mu' = \tilde{\mu}' - i\left(\frac{p\ell}{V}\right)\tilde{\mu} \tag{5.14}$$

This follows from the fact that derivatives of vectors in rotating systems do not transform in the same way as the vectors themselves. A second complication, which follows from this, is that a spinning missile flying at a constant angle of attack in the nonspinning system ($\tilde{\xi}' = 0$) has a non-zero ξ'. The non-Magnus coefficients of ξ' are usually taken to be non-steady damping force and moment coefficients - $C_{N_{\dot{\alpha}}}$ and $C_{M_{\dot{\alpha}}}$. For a body of revolution flying with constant $\tilde{\xi}$, it is very hard to see why a damping force or moment should be present[6-6] and it is difficult to explain such a force and moment for a symmetric finned missile. For this reason we will rearrange the terms in Equations (5.11-12) so that the variables are ξ, μ, and their derivatives in the nonrolling coordinates. The coefficients are then identified so that they reduce to the quantities as defined in Sections 6.2 and 6.3 for the case of zero roll and small angles.

$$\begin{aligned} C_Y + iC_Z = &- \left[C_{N_\alpha} + i\left(\frac{p\ell}{V}\right)C_{N_{p\alpha}}\right]\xi - \left[\left(\frac{p\ell}{V}\right)C_{N_{pq}} + iC_{N_q}\right]\mu \\ &- \left[C_{N_{\dot{\alpha}}} + i\left(\frac{p\ell}{V}\right)C_{N_{p\dot{\alpha}}}\right]\left[\xi' + i\left(\frac{p\ell}{V}\right)\xi\right] \\ &- \left[\left(\frac{p\ell}{V}\right)C_{N_{p\dot{q}}} + iC_{N_{\dot{q}}}\right]\left[\mu' + i\left(\frac{p\ell}{V}\right)\mu\right] \end{aligned} \tag{5.15}$$

$$C_m + iC_n = \left[\left(\frac{p\ell}{V}\right) C_{M_{p\alpha}} - iC_{M_\alpha}\right] \xi + \left[C_{M_q} - i\left(\frac{p\ell}{V}\right) C_{M_{pq}}\right] \mu$$

$$+ \left[\left(\frac{p\ell}{V}\right) C_{M_{p\dot{\alpha}}} - iC_{M_{\dot{\alpha}}}\right] \left[\xi' + i\left(\frac{p\ell}{V}\right) \xi\right]$$

$$+ \left[C_{M_{\dot{q}}} - i\left(\frac{p\ell}{V}\right) C_{M_{p\dot{q}}}\right] \left[\mu' + i\left(\frac{p\ell}{V}\right) \mu\right] \qquad (5.16)$$

One last task remains before returning to the equations of motion. This is the determination of the variation of the coefficients defined above with center of gravity location. To do this we will compare the force and moment for two models with identical motion but different center of mass locations. The difference in c.g. location will be denoted $s_{cg} = (\hat{x}_{cg} - x_{cg})\ell^{-1}$ where the circumflex superscript identifies quantities associated with the missile with the second c.g. location. Under our assumption that corresponding points have the same motion, the angular velocity is unchanged but the linear velocity, which is defined to be the velocity of the center of gravity, is affected.

$$\hat{\xi} = \xi - is_{cg}\mu \qquad \hat{\mu} = \mu \qquad (5.17)$$

$$\hat{\xi}' = \xi' - is_{cg}\hat{\mu}' \qquad \hat{\mu}' = \mu' \qquad (5.18)$$

In a similar fashion the force is unaffected but the moment, which is defined with respect to the c.g. location, does change. If we assume that the change in ξ is small enough to leave the total velocity, V, invariant, the relations for force and moment coefficients are the same as for the force and moment themselves. This means that the resulting c.g. relations are good for small angular velocities.

$$\hat{C}_Y + i\hat{C}_Z = C_Y + iC_Z \qquad (5.19)$$

$$\hat{C}_m + i\hat{C}_n = C_m + iC_n - is_{cg}(C_Y + iC_Z) \qquad (5.20)$$

Equations (5.15-18) are substituted in Equations (5.19-20) and the sought-for c.g. transformations are found. These are listed in Table 6-1.

This table reveals a number of interesting facts. Note that if $C_{N_{\dot{\alpha}}}$ and $C_{M_{\dot{\alpha}}}$ are not zero, then $C_{N_{\dot{q}}}$ and $C_{M_{\dot{q}}}$ must be non-zero for most c.g. positions. Thus the omission of these coefficients in previous articles would yield incomplete expansion under c.g. transformations. $C_{N_{\dot{q}}}$ and $C_{M_{\dot{q}}}$ have no measurable effect on missile motion and are omitted for this reason*. In a similar way $C_{N_{pq}}$ and $C_{M_{pq}}$ are needed for consistent c.g. transformation for non-zero $C_{N_{p\alpha}}$ and $C_{M_{p\alpha}}$ but have no measurable effect on motion. The Magnus coefficients involving $\dot{\alpha}$ and $\dot{q}$ also have no measurable effect, do not appear in c.g. relation for other coefficients, and, therefore, can be completely dropped at this time**. The final form of the linear force and moment expansion in nonrolling coordinates is, therefore,

$$\tilde{C}_Y + i\tilde{C}_Z = -\left[C_{N_\alpha} + i\left(\frac{p\ell}{V}\right)C_{N_{p\alpha}}\right]\tilde{\xi} - iC_{N_q}\tilde{\mu} - C_{N_{\dot{\alpha}}}\tilde{\xi}' \tag{5.21}$$

$$\tilde{C}_m + i\tilde{C}_n = \left[\left(\frac{p\ell}{V}\right)C_{M_{p\alpha}} - iC_{M_\alpha}\right]\tilde{\xi} + C_{M_q}\tilde{\mu} - iC_{M_{\dot{\alpha}}}\tilde{\xi}' \tag{5.22}$$

Equations (5.21-22) contain considerable information which is not immediately obvious due to the unfamiliar complex number notation. It should be noted that $\tilde{\xi} \doteq \tilde{\beta} + i\tilde{\alpha}$ has components whose algebraic sign is the reverse of the corresponding forces and moments. This can be seen from Figures 6.3 and 6.4.

---

* In wind tunnel measurements of damping in pitch derivatives by means of forced-oscillations the coefficient $C_{M_{\dot{q}}}$ can have a measurable effect quite similar to the static moment coefficient C_{M_α}.

** The various statements about certain coefficients having no measurable effect may be verified by retaining these quantities in the analysis of the next section. It would then develop that through the small size of the density factor $\frac{\rho S\ell}{2m}$ these coefficients would have little effect on the pitching and yawing motion or the c.g. transformation of coefficients which do influence that motion.

Thus, the normal force, $- C_{N_\alpha} \tilde{\xi}$, is a force proportional to the sine of the angle of attack and acting in the same direction as the angle of attack when C_{N_α} is positive. (With the exception of very low fineness ratio configuration C_{N_α} is always positive.)

The Magnus force for a spinning body of revolution is at right angles to the normal force and proportional in size to the product $P\,|\tilde{\xi}|$. Its usual direction can be inferred by consideration of the Magnus force which causes a baseball or golf ball to "hook" or "slip". (Figure 6.7) From the figure we can see that the circulation induced in the flow field about the ball by the spin and viscosity causes an asymmetric pressure distribution. This pressure distribution then gives rise to a side force. The same theoretical model may be used for a spinning body of revolution. For this purpose we assume that Figure 6.7 is a cross sectional view of the flow field. The cross flow is induced by the angle of attack and has a magnitude $V_o\,|\tilde{\xi}|$. This simple picture predicts a Magnus force with direction obtained by a 90^o rotation from the normal force against the spin. Since multiplication by ip yields a 90^o rotation in the direction of spin, the usual sign for $C_{N_{p\alpha}}$ is negative.

The interpretation of the damping force coefficients C_{N_q} and $C_{N_{\dot{\alpha}}}$ is somewhat more difficult. This is not unexpected since the coefficient C_{N_q} is a linear function of c.g. location. Indeed since both coefficients have not been directly measured and have only importance for their effect on the dependence of their moment coefficients on c.g. location, we will interpret them in terms of the c.g. transformation of the moment coefficients and move on to consider these coefficients.

The form of the moment expansion was obtained by multiplying the force coefficients by i and replacing the N subscripts by M's. This is justified by the convention the orientation of a moment is the axis about which it tends to cause rotation and this axis is perpendicular to the corresponding moment. As each coefficient is discussed its influence on stability will be explored.

The most important moment coefficient is that associated with the normal force, i.e., the static moment coefficient, C_{M_α}. This moment causes rotation about an axis at right angles to the angle of attack. Since a negative coefficient corresponds to a moment opposing the angle of attack, a negative coefficient is stabilizing.

The Magnus moment coefficient, $C_{M_{p\alpha}}$, has an axis of rotation in the plane of the angle of attack and, therefore, causes the missile's nose to rotate around the trajectory. For a positive $C_{M_{p\alpha}}$ this motion is in the direction of the spin. Its influence of stability depends on the interaction of this moment coefficient with the others and will be examined later.

The damping moment coefficients C_{M_q} and $C_{M_{\dot\alpha}}$ cause rotation about the same axes as the corresponding angular velocities $\tilde\mu$ and $\tilde\xi'$. Their moments both oppose their angular velocities when they are negative and, hence, negative values of these coefficients are stabilizing.

6.6 Pitching and Yawing Motion of Symmetric Missiles

With linear expansion of the force and moment defined, the derivation and solution of the equations for pitching and yawing motion can proceed. Equations (5.21-22) are substituted into Equations (4.24-25) and C^*'s neglected in comparison with one.

$$\tilde\xi' - i\gamma\tilde\mu = -\left(C^*_{N_\alpha} - C^*_D + i\left(\frac{p\ell}{V}\right) C^*_{N_{p\alpha}}\right)\tilde\xi + \left[g_{\tilde y} + ig_{\tilde z}\right]\ell V^{-2} \qquad (6.1)$$

$$\tilde\mu' - iP\tilde\mu = k_t^{-2}\left[\left(\frac{p\ell}{V}\right) C^*_{M_{p\alpha}} - iC^*_{M_\alpha}\right]\tilde\xi + \left(k_t^{-2} C^*_{M_q} + C^*_D\right)\tilde\mu - ik_t^{-2} C^*_{M_{\dot\alpha}}\tilde\xi' \qquad (6.2)$$

The expression, $C_{N_\alpha} - C_D$, has a special significance which we can derive here. Figure 6.8 shows the model at a fixed resultant angle of attack, α_r, and the resolution of the aerodynamic force into axial and normal components, F_X and F_N, as well as drag and lift components.

$$D = - \cos \alpha_r F_X + \sin \alpha_r F_N \tag{6.3}$$

$$L = \sin \alpha_r F_X + \cos \alpha_r F_N \tag{6.4}$$

where $\cos \alpha_r = \gamma$

$$\sin \alpha_r = |\xi| = \delta$$

The definitions of the corresponding aerodynamic coefficients can be inserted and common factors cancelled

$$C_D = - \gamma C_X + \delta^2 C_{N_\alpha} \tag{6.5}$$

$$C_{L_\alpha} = \gamma C_{N_\alpha} + C_X \tag{6.6}$$

C_X can be eliminated from Equation (6.5) by the use of Equation (6.6)

$$\therefore \gamma C_{L_\alpha} = C_{N_\alpha} - C_D \tag{6.7}$$

Thus, this combination, $C_{N_\alpha} - C_D$, is essentially the well known lift coefficient. Equation (6.5) also expresses the usual relations for induced drag. For constant C_X and C_{N_α} this yields $C_{D_{\delta^2}} = C_{N_\alpha} + (1/2)\, C_X \doteq C_{L_\alpha} + (1/2)\, C_{D_o}$.

Equations (6.1-2) can be combined to eliminate $\tilde{\mu}$ and $\tilde{\mu}'$.

$$\tilde{\xi}'' + \left(H - \frac{\gamma'}{\gamma} - iP\right) \tilde{\xi}' - (M + iPT)\, \tilde{\xi} = G \tag{6.8}$$

where $H = \gamma C^*_{L_\alpha} - C^*_D - k_t^{-2} \left(C^*_{M_q} + \gamma C^*_{M_{\dot\alpha}}\right)$

$$M = \gamma k_t^{-2} C^*_{M_\alpha} - \gamma \left(C^*_{L_\alpha}\right)'$$

$$T = \gamma \left[C^*_{L_\alpha} + k_a^{-2} C^*_{M_{p\alpha}}\right] - \left(\frac{I_y}{I_x}\right) \left(C^*_{N_{p\alpha}}\right)'$$

$$G = \left[\frac{(g_{\tilde{y}} + i g_{\tilde{z}})\, \ell}{V^2}\right]' - \left[k_t^{-2} C^*_{M_q} + C^*_D + iP\right] \left[\frac{(g_{\tilde{y}} + i g_{\tilde{z}})\, \ell}{V^2}\right]$$

Equation (6.8) is exact and has no linear approximations other than those which are implicit in the definition of the force and moment expansions. The retention of derivatives of the lift coefficient and the Magnus force coefficient allows these coefficients to be variables and, therefore, could represent a nonlinear force. Since the moment coefficients were not differentiated in the derivation their derivatives do not appear. They are not necessarily constants and can represent a nonlinear moment. This equation can and will be used in the chapter dealing with nonlinear forces and moments. In this chapter, however, Equation (6.8) will be linearized by the approximations

$$\gamma = 1,\ \gamma' = C'_{L_\alpha} = C'_{N_{p\alpha}} = 0 \tag{6.9}$$

$$g_{\tilde{y}} + ig_{\tilde{z}} = ig \text{ (flat trajectory)} \tag{6.10}$$

$$\therefore\ G = \left[P - i(k_t^{-2} C^*_{M_q} - C^*_D)\right] g\ell V^{-2} \tag{6.11}$$

For high spin rates P can be as large as .05. The imaginary part of G is the same as that given in Section 6.2 for no spin. Since it was found there that this term has no effect on the motion which can be measured during the relatively short flight in a ballistic range, it will be neglected and G approximated by $Pg\ell V^{-2}$.

$$\therefore\ \tilde{\xi}'' + (H - iP)\tilde{\xi}' - (M + iPT)\tilde{\xi} = G \tag{6.12}$$

$$\text{where } H = \left(\frac{\rho S\ell}{2m}\right)\left[C_{L_\alpha} - C_D - k_t^{-2}\left(C_{M_q} + C_{M_{\dot{\alpha}}}\right)\right]$$

$$M = \frac{\rho S\ell^3}{2I_y} C_{M_\alpha}$$

$$T = \left(\frac{\rho S\ell}{2m}\right)\left[C_{L_\alpha} + k_a^{-2} C_{M_{p\alpha}}\right]$$

$$G = Pg\ell V^{-2} \doteq Pg\ell V_o^{-2}$$

Although Equation (6.8) is a fourth order system in the variables v and w it is written as a simple second order system in the complex variable ζ-ξ. This symmetry allows us to express the solution as a constant plus two complex exponentials.

$$\tilde{\xi} = \tilde{\xi}_g + K_1 e^{i\phi_1} + K_2 e^{i\phi_2} \tag{6.13}$$

$$\text{where } \tilde{\xi}_g = \left[\frac{-P}{M + iPT}\right] g\ell V_o^{-2}$$

$$K_j = K_{jo} e^{\lambda_j s}$$

$$\phi_j = \phi_{jo} + \phi_j' s$$

$$\lambda_j + i\phi_j' = (1/2)\left[-H + iP \pm \sqrt{4M + H^2 - P^2 + 2iP(2T - H)}\right]$$

The actual size of $\tilde{\xi}_g$ is barely measurable but its influence on the trajectory can be measured for subsonic tests in ballistic ranges. Since M usually is much larger that PT and is positive, $\tilde{\xi}_g$ is a small negative real number. Thus this equilibrium angle due to gravity curvature of trajectory causes the missile to point to the right of its flight path. The lift force associated with this angle causes a drift to the right. This right deflection is characteristic for all artillery shell. For most supersonic tests, $\tilde{\xi}_g$ will be neglected in any consideration of Equation (6.13) but its associated drift will be computed when the swerving motion of the c.g. is discussed.

The other terms in Equation (6.13) describe the missile's response to initial conditions. The amplitudes of the disturbances due to initial conditions (K_{jo}) can either grow or decrease exponentially while the orientation changes at constant rates (ϕ_j'). The resulting motion is known as a damped epicycle. As has been shown previously a nonspinning statically stable missile ($P = 0$, $M < 0$) has a damped elliptical pitching and yawing motion when H is positive, and an undamped elliptical motion when it is negative. The damping rates are equal and the frequencies are negatives of each other. If the same missile is spun slowly, the frequencies shift a little and the elliptical motion starts to precess. This is shown in Figure (6.9a). At

higher spin rates the damping exponents change as well as the frequencies and more complicated motion with nodes is produced as shown in Figure (6.9b). Note that maximum angles occur when the modal vectors add $(K_1 + K_2)$ and minimum angles occur when they subtract $(|K_1 - K_2|)$.

For a statically unstable missile such as a rifle bullet the motion is quite different. If the missile is not spun, the modal frequencies are zero, one modal amplitude is strongly damped $\lambda_1 = \left[- H - \sqrt{4M + H^2} \right] /2$ where the other amplitude is strongly undamped $\lambda_2 = \left[- H + \sqrt{4M + H^2} \right] /2$. This motion is quite unstable.

For a spinning missile as well as a nonspinning missile the predominant aerodynamic effect is the static moment coefficient. If the other aerodynamic coefficients are neglected, the frequencies and damping exponents become

$$\lambda_j + i\phi_j' = (1/2) \left[iP \pm \sqrt{4M - P^2} \right] \tag{6.14}$$

The presence of spin in the square root indicates the possibility of stabilizing a statically unstable missile by spin. When spin is large enough, the right side of Equation (6.14) is a pure imaginary number. The damping exponents become zero, and the envelope of the motion will not grow. The necessary condition on the spin rate is the inequality

$$4M - P^2 < 0 \tag{6.15}$$

For a statically unstable missile, M is positive and Inequality (6.15) may be written in the form

$$\frac{P^2}{4M} > 1 \tag{6.16}$$

The ballistician has for many years made use of a gyroscopic stability factor s_g which is proportional to the ratio of squared gyroscopic spin to the static moment coefficient and is precisely $P^2/4M$. Thus s_g must be greater than unity for a statically unstable missile to perform periodic motion and not quickly tumble. This is the condition for a sleeping top.

Since the sign of M is not essential for Inequality (6.15), we will define a missile to be gyroscopically stable when that inequality is satisfied or equivalently

$$\frac{1}{s_g} < 1 \tag{6.17}$$

Thus a statically stable missile ($M < 0$) is always gyroscopically stable.

According to Equations (6.13, 6.14) the pitching and yawing motion of a gyroscopically stable missile with only a linear static moment acting, may be represented by the sum of two complex numbers with constant magnitude and rotating with constant angular velocity.

$$\phi'_j = 1/2 \left[P \pm \sqrt{P^2 - 4M} \right] \tag{6.18}$$

We will call these numbers modal vectors. If C_{M_α} is positive, they rotate in the same direction as the spin and the usual epicyclic motion associated with the motion of the axis of a top results. If C_{M_α} is negative, the square roots dominate in Equation (6.13) and these modal vectors rotate in opposite directions.

Gyroscopic stability like static stability is sufficient for oscillatory motion but does not guarantee that initial conditions will not grow. This requirement of dynamic stability which reduces to a need for positive H for a nonspinning missile is satisfied when the exponential coefficients are both negative. The pitching and yawing motion for a dynamically stable, gyroscopically stable, but statically unstable missile is shown in Figure 6.10. For a statically stable missile the frequencies differ in algebraic sign and the nodes are on the outside. For this case the frequencies have the same sign and the nodes are on the inside.

The initial orientation and amplitude of the modal vectors are functions of initial conditions. Equation (6.13) and its derivatives may be evaluated at $s = 0$ to yield $\tilde{\xi}_o$ and $\tilde{\xi}'_o$ in terms of these quantities.

$$\tilde{\xi}_o = K_{10} e^{i\phi_{10}} + K_{20} e^{i\phi_{20}} \tag{6.19}$$

$$\tilde{\xi}'_o = (\lambda_1 + i\phi'_1) K_{10} e^{i\phi_{10}} + (\lambda_2 + i\phi'_2) K_{20} e^{i\phi_{20}} \tag{6.20}$$

These relations determine $\tilde{\xi}_o$ and $\tilde{\xi}'_o$ in terms of quantities measurable from ballistic range tests. In design studies it is sometimes important to compute initial values of the modal vectors from specified values of $\tilde{\xi}_o$ and $\tilde{\xi}'_o$. This can be done by inverting Equations (6.19-20).

$$K_{10}e^{i\phi_{10}} = \frac{\tilde{\xi}'_o - (\lambda_2 + i\phi'_2)\,\tilde{\xi}_o}{\lambda_1 - \lambda_2 + i(\phi'_1 - \phi'_2)} \tag{6.21}$$

$$K_{20}e^{i\phi_{20}} = \frac{\tilde{\xi}'_o - (\lambda_1 + i\phi'_1)\,\tilde{\xi}_o}{\lambda_2 - \lambda_1 + i(\phi'_2 - \phi'_1)} \tag{6.22}$$

The amplitude of these disturbances due to initial conditions will grow exponentially for a dynamically unstable missile ($\lambda_1 > 0$ and/or $\lambda_2 > 0$).

The relations for $\lambda_j + i\phi'_j$ are convenient for computing the frequencies and exponential coefficients when the aerodynamic coefficients are known. In ballistic range work $\lambda_j + i\phi'_j$ is known from the data analysis and the aerodynamic coefficients are unknown. The necessary equations can be easily derived from the fact that in Equation (6.12) the coefficient of $\tilde{\xi}'$ is the negative sum of the roots of the characteristic equation $(\lambda_j + i\phi'_j)$ and the coefficient of $\tilde{\xi}$ is their product.

$$\therefore\ P = \phi'_1 + \phi'_2 \tag{6.23}$$

$$H = -\left[\lambda_1 + \lambda_2\right] \tag{6.24}$$

$$M = \phi'_1\,\phi'_2 - \lambda_1\lambda_2 \tag{6.25}$$

$$PT = -\left[\phi'_2\lambda_1 + \phi'_1\lambda_2\right] \tag{6.26}$$

6.7 Dynamic Stability Criteria

One of the primary uses of range data is the determination of proper dynamic stability for a proposed configuration. The usual dynamic stability requirement is that the damping exponents are nonpositive throughout the flight

of the missile. We will first consider a generalized version of this stringent requirement. Then the more moderate conditions of a realistic designer that the angular motion does not become excessively large will be analyzed. As we shall see, then, under this criterion the damping exponents may become positive for "short" portions of the flight.

Equations (6.24) and (6.26) may be solved explicitly for the damping exponents

$$\lambda_1 = \frac{-\left[\phi_1' H - PT\right]}{\phi_1' - \phi_2'} = \frac{-\left[\phi_1' H - PT\right]}{2\phi_1' - P} \tag{7.1}$$

$$\lambda_2 = \frac{-\left[\phi_2' H - PT\right]}{\phi_2' - \phi_1'} = \frac{-\left[\phi_2' H - PT\right]}{2\phi_2' - P} \tag{7.2}$$

The indicated divisions in Equations (7.1-2) may now be performed

$$\lambda_1 = -\left(\frac{1}{2}\right)\left[H - \frac{P(2T - H)}{2\phi_1' - P}\right] = -\left(\frac{1}{2}\right)\left[H - \frac{P(2T - H)}{\phi_1' - \phi_2'}\right] \tag{7.3}$$

$$\lambda_2 = -\left(\frac{1}{2}\right)\left[H - \frac{P(2T - H)}{2\phi_2' - P}\right] = -\left(\frac{1}{2}\right)\left[H + \frac{P(2T - H)}{\phi_1' - \phi_2'}\right] \tag{7.4}$$

According to Equations (7.3-4) the damping exponents for a nonspinning missile are both -H/2. If H - 2T is not zero, one of the damping exponents will be less than H/2 and the other greater than H/2. From Equation (6.18) which is a good approximation* for the frequencies we see that $P\left[\phi_1' - \phi_2'\right]^{-1}$ has a magnitude which is less than one for statically stable missiles and greater than one

* Although Equation (6.18) is exactly correct for H = T = 0, it is an excellent approximation when aerodynamic damping is present. Use of this equation is equivalent to the assumption that the product of the frequencies is much greater than the product of the damping exponents in Equation (6.25).

for statically unstable missiles. Thus, the H/2 in the second term of Equation (7.4) dominates the first term for a statically unstable missile and one damping exponent must be positive if the Magnus and lift coupling term T is zero.

We will now obtain precise stability conditions on T as a function of spin. The usual dynamic stability requirement is that the exponential coefficients, λ_j, be both negative. These conditions are somewhat more restrictive than necessary for a missile designer. His primary concern is that the initial conditions do not have an adverse effect during the flight. What constitutes an adverse effect depends on the mission and trajectory of the given missile. In some cases we would want initial angles to damp to half their values in 1,000 ft; in other cases if they doubled in 10,000 ft., the performance would be unaffected. To include this flexible criteria in our analysis, we will introduce a level of damping, λ, which is set by the designer and require that the damping exponents be less than this value. The resulting generalized criteria reduce to the conventional one when $\lambda = 0$. If the frequencies are approximated by Equation (6.18), this requirement of generalized dynamic stability assumes the form

$$\lambda_j - \lambda = \frac{-1}{2}\left[(H + 2\lambda) \pm \frac{P(2T - H)}{\sqrt{P^2 - 4M}}\right] \leqq 0 \tag{7.5}$$

Inequalities (7.5) are equivalent to the following inequalities

$$H + 2\lambda \geqq 0$$

$$|H + 2\lambda| \geqq \left| \frac{P(2T - H)}{\sqrt{P^2 - 4M}} \right| \tag{7.6}$$

The second inequality in (7.6) can be squared, solved for spin squared, and reduced to a simple form by the introduction of a generalized dynamic stability factor, s_d

$$\frac{4M}{P^2} = \frac{1}{s_g} \leqq s_d(2 - s_d) \tag{7.7}$$

where $s_d = \dfrac{2(T + \lambda)}{H + 2\lambda}$

The relation between the spin and the various types of stability are summarized in Figure 6.11. To these relations must be added the single inequality $H + 2\lambda \geq 0$. Three comments of great importance may be derived from an inspection of this figure.

(1) A dynamically stable missile must be gyroscopically stable.

(2) If s_d lies in the interval (0,2), a statically unstable missile may be stabilized by sufficiently high spin and a statically stable missile is always dynamically stable.

(3) If s_d lies outside this interval, a statically unstable missile cannot be spin-stabilized and statically stable missile may be made dynamically unstable by a sufficiently high spin.

Experimental values of the various coefficients for a variety of configurations will be given in the next chapter. From these data it can be shown that most of the ways a symmetric missile can theoretically become unstable have been observed.

The use of Figure 6.11 to determine lower bounds on spin for a statically unstable missile and upper bounds for statically stable missiles is based on the assumption that s_d is not a function of spin. The bounds on s_g indicated in the figure may then be converted into bounds on spin.

Frequently the spin variation of the Magnus moment can not be ignored. When this is the case s_d is a function of spin and Figure 6.11 can not be used to determine spin boundaries for dynamic stability for a given missile. Inequality (7.7), however, is still valid. The equality sign in (7.7) yields an equation in spin whose roots are endpoints of intervals of spin for which the missile is either dynamically stable or dynamically unstable. If the spin in a given interval satisfies Inequality (7.7) the missile will be dynamically stable for spin in that interval and conversely.

The requirement that the exponential coefficients be negative throughout the flight is much stronger than necessary in a number of applications. This can be seen by the following example. Consider the case of a specific shell whose exponential coefficients are strongly negative for $M \leq 2.0$ except for the

Mach number interval (0.9, 1.1) where both exponents are positive. Exact numerical integration showed that an initial maximum angle of attack of four degrees for the launch Mach number of two will decay to a tenth of a degree before the Mach number decreases to 1.1. The dynamic instability associated with the transonic velocities then will cause the maximum angle to grow to approximately one degree and then decrease a second time when subsonic stability is established. Thus the "dynamically unstable" shell has maintained a small angle of attack over the entire trajectory*.

The effect of slowly varying coefficients can be treated by means of the WKB method[6-3]. The exact algebra, however, will make considerable use of the epicyclic solution associated with constant coefficients. We will assume the solution for varying coefficients can be written in the form

$$\tilde{\xi} = K_1 e^{i\phi_1} + K_2 e^{i\phi_2} \tag{7.8}$$

where the ϕ_j' are not necessarily constants and the K_j are not necessarily exponential functions. Differentiating Equation (7.8) twice, we have

$$\tilde{\xi}' = (\lambda_1 + i\phi_1')K_1 e^{i\phi_1} + (\lambda_2 + i\phi_2')K_2 e^{i\phi_2} \tag{7.9}$$

$$\begin{aligned}\tilde{\xi}'' = &\left[\lambda_1' + \lambda_1^2 - (\phi_1')^2 + i(\phi_1'' + 2\lambda_1\phi_1')\right] K_1 e^{i\phi_1} \\ &+ \left[\lambda_2' + \lambda_2^2 - (\phi_2')^2 + i(\phi_2'' + 2\lambda_2\phi_2')\right] K_2 e^{i\phi_2}\end{aligned} \tag{7.10}$$

$$\text{where } \lambda_j = \left[\ell n(K_j/K_{jo})\right]' = \frac{K_j'}{K_j}$$

Equations (7.8-10) are now substituted in the homogeneous form of Equation (6.12) and the result grouped as to mode

---

* Precisely this behavior occurred during the development of an important shell. As a result of ballistic range tests the shell design was stated to be unsatisfactory by the experts. Fortunately, the project engineer who had not studied the mathematical theory of this chapter was able to get approval for full range firings. The shell gave one of the best dispersion patterns ever observed and the "experts" learned from bitter experience.

$$\left\{(\phi_1')^2 - P\phi_1' + M - \lambda_1(\lambda_1 + H) - \lambda_1' - i\left[(2\phi_1' - P)\lambda_1 + \phi_1'' + H\phi_1' - PT\right]\right\}$$

$$= -\left\{(\phi_2')^2 - P\phi_2' + M - \lambda_2(\lambda_2 + H) - \lambda_2'\right.$$

$$\left. -i\left[(2\phi_2' - P)\lambda_2 + \phi_2'' + H\phi_2' - PT\right]\right\} \quad (K_2/K_1)e^{-i\hat{\phi}} \tag{7.11}$$

where $\hat{\phi} = \phi_1 - \phi_2$

If λ_j and ϕ_j' vary slowly in a period of $\hat{\phi}$, Equation (7.11) can only be satisfied by both expressions in braces vanishing. Since the λ_j terms in the real part of each of these expressions is usually much smaller than $(\phi_j')^2$, the frequency equations for varying coefficients are essentially the same as those for constant coefficients.

$$\phi_j' = \frac{P}{2} \pm \sqrt{\frac{P^2}{4} - M} \tag{7.12}$$

The logarithmic derivatives, λ_j, are somewhat different as can be seen from the imaginary parts of the expressions in braces.

$$\lambda_j = -\frac{H\phi_j' - PT + \phi_j''}{2\phi_j' - P}$$

$$= \lambda_j^* - \frac{1}{2}\left[\ell n(\hat{\phi}_j'/\hat{\phi}_{jo}')\right]' - \frac{P'}{4\hat{\phi}_j'} \tag{7.13}$$

where $\hat{\phi}_j' = \phi_j' - \frac{P}{2}$

$$\lambda_j^* = -\frac{H\phi_j' - PT}{2\phi_j' - P}$$

For constant frequencies and spin-to velocity ratio, λ_j reduces to λ_j^*.

The definition of λ_j can be used to yield a prediction on the size of the modal amplitudes for slowly varying coefficients.

$$K_j/K_{jo} = \left[\frac{P_o^2 - 4M(0)}{P^2 - 4M(s)}\right]^{1/4} e^{\int_o^s (\lambda_j^* - \frac{P'}{4\hat{\phi}_j}) ds} \tag{7.14}$$

Since the major concern of a designer is the growth of initial disturbances, this can be controlled by a restriction on the ratios K_j/K_{jo}. The actual value of these ratios may be computed throughout flight and compared with the restriction. Clearly strict dynamic stability will satisfy this, but these considerations allow a certain amount of dynamic instability over part of the flight. Thus a much weaker type of stability has been formulated. This stability includes the necessity of gyroscopic stability throughout the flight.

An interesting application of these equations is that of a missile with constant aerodynamic coefficients and spin which is entering or leaving an exponential atmosphere*

$$\rho = \rho_o e^{-\sigma z} \tag{7.15}$$

where z is the altitude in feet.

If $\psi(s)$ is the angle the flight path makes with respect to the vertical, z can be related to our independent variable s by the equation

$$z = -\int_o^s \ell \cos \psi\,(s_1) ds_1 \tag{7.16}$$

where $0 < \psi < 90^\circ \rightarrow$ entering the atmosphere

$90^\circ < \psi < 180^\circ \rightarrow$ leaving the atmosphere

$$\therefore \quad \frac{\rho'}{\rho} = \sigma \ell \cos \psi = \tilde{\sigma} \tag{7.17}$$

For this case it is easy to show that

$$\lambda_j = \lambda_j^* - \frac{\tilde{\sigma}}{4(1 - s_g)} \tag{7.18}$$

where $s_g = \frac{P^2}{4M}$

* For the earth a good value for σ is $\frac{1}{22{,}000 \text{ ft.}}$.

As can be seen from Equation (7.18) an entering statically stable missile ($s_g < 0$) is stabilized by the density gradient while an entering statically unstable missile which is gyroscopically stable ($s_g > 1$) is destabilized by the density gradient. These predictions are only good at altitudes for which the changes in the coefficients are small in a period of $\hat{\phi}$, the nutational frequency.

6.8 Angular Motion of a Slightly Unsymmetric Missile

Since no actual missile is exactly symmetric, the study of the effect of slight asymmetries is very important for a missile designer. It is also quite possible that lifting surfaces may be slightly deflected so that they may induce a trim angle of attack. These aerodynamic asymmetries which may be either intentional or unintentional have the effect of introducing constant nonzero lift and moment when the angle of attack with respect to the basic symmetric missile's axis of symmetry is zero. This introduces a constant $C_{Y_o} + iC_{Z_o}$ into Equation (5.15) and a constant $C_{m_o} + iC_{n_o}$ into Equation (5.16).

The corresponding linear differential equation for the pitching and yawing motion is

$$\tilde{\xi}'' + (H - iP)\tilde{\xi}' - (M + iPT)\tilde{\xi} = iAe^{i\phi} \tag{8.1}$$

$$\text{where } A = \frac{\rho S \ell}{2m} \left[k_t^{-2}(C_{m_o} + iC_{n_o}) + \left(P\left(\frac{I_y}{I_x}\right) - 1 \right) (C_{Y_o} + iC_{Z_o}) \right]$$

$$\phi = \int_o^s \phi' ds_1 \quad \text{and}$$

$$\phi' = \frac{p\ell}{V}$$

For constant spin rate the aerodynamic asymmetry introduces an exponential forcing function. A particular solution to this inhomogeneous equation can be obtained by assuming a solution of the same form

$$\tilde{\xi} = K_3 e^{i\phi_3} \tag{8.2}$$

$$\text{where } \phi_3 = \phi_{30} + \phi$$

This particular solution can easily be found by direct substitution and the result added to the epicyclic solution to yield the general solution of Equation (8.1)

$$\tilde{\xi} = K_1 e^{i\phi_1} + K_2 e^{i\phi_2} + K_3 e^{i\phi_3} \qquad (8.3)$$

$$\text{where } K_3 e^{i\phi_{30}} = \frac{-iA}{(\phi')^2 - P\phi' + M - i(\phi' H - PT)}$$

The denominator of $K_3 e^{i\phi_{30}}$ is usually dominated by the real part. This real part is the quadratic expression for the epicyclic frequencies. Therefore it will become zero when the spin rate equals one of these frequencies. By definition the magnitude of the slow rate is less than $(I_x/I_y)|\phi'|$ and, hence, for most missiles this resonance phenomena occurs when the spin rate equals the fast rate. The usual value of I_x/I_y is less than a tenth and, thus, the $P\phi'$ term is much smaller than $(\phi')^2$ and the spin rate may be directly compared with the zero-spin pitch frequency, $\sqrt{-M}$, to determine whether concern about resonance is reasonable.

In most ballistic range tests for which asymmetries are present, the spin rate is usually not constant. If it is not near resonance Equation (8.3) is a good approximation but for roll rapidly varying through resonance it is definitely a very poor approximation. This special case can be handled by the method of variation of parameters.

If varying spin is assumed, Equation (8.1) is a linear equation with varying coefficients with a specified forcing function. Although the particular solution for this forcing function is quite sensitive to roll rates near resonance, the complimentary solution for the homogeneous equation is relatively insensitive. Indeed, for roll rates near resonance P is usually quite small. This means that we can either neglect P on the left side of Equation (8.1) or replace it by a constant average value. The problem is now to find the solution of an inhomogeneous linear equation with constant coefficients.

The basic approach of the method of variation of parameters is to assume the constants K_{jo}, ϕ_{jo} in Equation (6.13) to be functions of s. For convenience, the quantities $A_j = K_{jo} e^{i\phi_{jo}}$ are introduced

$$\tilde{\xi}_A = A_1 e^{(\lambda_1 + i\phi_1')s} + A_2 e^{(\lambda_2 + i\phi_2')s} \tag{8.4}$$

where A_j are complex functions of s and

$\tilde{\xi}_A$ is the particular solution due to asymmetry for zero initial conditions. ($\tilde{\xi}_{A_o} = \tilde{\xi}'_{A_o} = 0$)

Equation 8.4 is now differentiated.

$$\tilde{\xi}'_A = (\lambda_1 + i\phi_1')A_1 e^{(\lambda_1 + i\phi_1')s} + (\lambda_2 + i\phi_2')A_2 e^{(\lambda_2 + i\phi_2')s} + A_1' e^{(\lambda_1 + i\phi_1')s} + A_2' e^{(\lambda_2 + i\phi_2')s} \tag{8.5}$$

If the last two terms are set equal to zero

$$A_1' e^{(\lambda_1 + i\phi_1')s} + A_2' e^{(\lambda_2 + i\phi_2')s} = 0 \tag{8.6}$$

and

$$\tilde{\xi}'_A = (\lambda_1 + i\phi_1')A_1 e^{(\lambda_1 + i\phi_1')s} + (\lambda_2 + i\phi_2')A_2 e^{(\lambda_2 + i\phi_2')s} \tag{8.7}$$

Differentiating again we obtain the following:

$$\tilde{\xi}''_A = (\lambda_1 + i\phi_1')^2 A_1 e^{(\lambda_1 + i\phi_1')s} + (\lambda_2 + i\phi_2')^2 A_2 e^{(\lambda_2 + i\phi_2')s} + (\lambda_1 + i\phi_1')A_1' e^{(\lambda_1 + i\phi_1')s} + (\lambda_2 + i\phi_2')A_2' e^{(\lambda_2 + i\phi_2')s} \tag{8.8}$$

If Equations (8.4, 8.7-8) are substituted in Equation (8.1) and it is recalled that terms without A_j' come from the solution of the homogeneous equation and must cancel, the following equation can be obtained.

$$(\lambda_1 + i\phi_1')A_1' e^{(\lambda_1 + i\phi_1')s} + (\lambda_2 + i\phi_2')A_2' e^{(\lambda_2 + i\phi_2')s} = iAe^{i\phi} \tag{8.9}$$

Substituting Equation (8.6) in Equation (8.9)

$$A_1' = \frac{iA\, e^{-(\lambda_1 + i\phi_1')s + i\phi}}{\lambda_1 - \lambda_2 + i(\phi_1' - \phi_2')} \tag{8.10}$$

$$A_2' = \frac{iA\, e^{-(\lambda_2 + i\phi_2')s + i\phi}}{\lambda_2 - \lambda_1 + i(\phi_2' - \phi_1')} \tag{8.11}$$

Equations (8.10-11) may now be integrated, the integrals substituted in Equation (8.4), and the general solution for arbitrary rolling motion $\phi(s)$ derived

$$\tilde{\xi} = K_1 e^{i\phi_1} + K_2 e^{i\phi_2} + \tilde{\xi}_A \tag{8.12}$$

where

$$\tilde{\xi}_A = \frac{iA \int_0^s \left[e^{(\lambda_1 + i\phi_1')(s - s_1)} - e^{(\lambda_2 + i\phi_2')(s - s_1)} \right] e^{i\phi(s_1)}\, ds_1}{\lambda_1 - \lambda_2 + i(\phi_1' - \phi_2')}$$

As was noted in the definition of $\tilde{\xi}_A$, its initial values are zero and, hence, the relations between the initial values of the modal vectors and the angle and angular velocity are precisely those of Equations (6.21-22). Since the tricycle mode ($K_3 e^{i\phi_3}$) in Equation (8.3) does not have this property, the initial values of the modal vectors in this equation do not have the same relationship with the initial angles and angular velocity. The correct relations, however, may be quickly derived if necessary.

6.9 Swerving Motion

Once the pitching and yawing motion is known and the linear aerodynamic force is determined, the motion of the center of mass may be computed. A first approximation to the actual trajectory is the so called particle trajectory. This is the trajectory determined by gravity and zero-lift drag and is followed by a missile which maintains zero angle of attack. The motion of the center of mass of a missile perpendicular to this trajectory is called the swerving motion. This motion is quite important in ballistic range work since direct determination of the aerodynamic force is possible from measurements of this motion.

For most ballistic range tests, the observed trajectory is well approximated by a horizontal straight line. Thus the swerving motion is primarily the projection of the three-dimensional motion on a plane perpendicular to this line. If the X_e - axis of the earth fixed coordinate is directed along this line, the variation of the Y_e and Z_e coordinates of the center of motion provide us with the swerving motion. The differential equation controlling these quantities is

$$m(\ddot{y}_e + i\ddot{z}_e) = F_{Y_e} + iF_{Z_e} + img + ma_c \tag{9.1}$$

a_c, the transverse component of the Coriolis acceleration induced by the earth's rotation, can be specified in terms of the latitude of the range, θ_ℓ, and the azimuth of the line of fire*, θ_a,

$$a_c = \frac{VV_o}{\ell}\ \hat{a}_c$$

$$= -\frac{VV_o}{\ell}\left[2\ \frac{\Omega\ell}{V_o}\quad (\sin\theta_\ell + i\cos\theta_\ell \sin\theta_a)\right] \tag{9.2}$$

where $\Omega = 2\pi$ radians per day

$= 7.3 \times 10^{-5}$ rad/sec

The force components along the Y_e and Z_e axes are given by Equations (2.10) and (3.1). For small angles these equations may be combined with Equations (2.12) and (3.3) to yield:

$$F_{Y_e} + iF_{Z_e} = F_Y + iF_Z - F_X\left(\tilde{\xi} - \frac{\dot{y}_e + i\dot{z}_e}{V}\right) \tag{9.3}$$

For a slightly unsymmetric missile with a linear aerodynamic force, then,

---

* The BRL Aerodynamics Range, for example, is located at Aberdeen Proving Ground, Maryland and fires due East. For this range $\theta_\ell = 39^\circ\ 26'$ and $\theta_a = 90^\circ$.

$$F_X = -(1/2)(\rho V^2) S\, C_D \tag{9.4}$$

$$F_Y + iF_Z = -(1/2)\,\rho V^2 S \left\{ \left[C_{N_\alpha} + i\left(\frac{p\ell}{V}\right) C_{N_{p\alpha}} \right] \tilde{\xi} \right. \tag{9.5}$$

$$\left. + iC_{N_q} \tilde{\mu} + C_{N_{\dot{\alpha}}} \tilde{\xi}' - (C_{Y_o} + iC_{Z_o}) e^{i\phi} \right\}$$

Equation (4.24) may be used to eliminate $\tilde{\mu}$ in Equation (9.5) with the usual neglect of squared density terms. The derivatives with respect to time may be replaced by derivatives with respect to arclength by the relation

$$y_e'' + iz_e'' = (\ddot{y}_e + i\ddot{z}_e)\left(\frac{\ell}{V}\right)^2 - (\dot{y}_e + i\dot{z}_e)\left(\frac{\dot{V}\ell^2}{V^3}\right)$$

$$= (\ddot{y}_e + i\ddot{z}_e)\left(\frac{\ell}{V}\right)^2 + (\dot{y}_e + i\dot{z}_e)\left(\frac{\ell}{V}\right) C_D^* \tag{9.6}$$

These equations may now be used to write Equation (9.1) in a much more convenient form

$$\frac{y_e'' + iz_e''}{\ell} = -\left[C_{L_\alpha}^* + i\left(\frac{p\ell}{V}\right) C_{N_{p\alpha}}^* \right] \tilde{\xi} \tag{9.7}$$

$$- (C_{N_q}^* + C_{N_{\dot{\alpha}}}^*)\tilde{\xi}' + (C_{Y_o}^* + iC_{Z_o}^*) e^{i\phi}$$

$$+ i\,\frac{g\ell}{V^2} + \hat{a}_c\,\frac{V_o}{V}$$

Equation (9.7) can now be integrated.

$$\frac{y_e + iz_e}{\ell} = B_o + B_1 s - C^*_{L_\alpha} I_1 - i\left(\frac{p_o \ell}{V_o}\right) C^*_{N_{p\alpha}} I_2$$

$$- (C^*_{N_q} + C^*_{N_{\dot{\alpha}}}) I_3 + (C^*_{Y_o} + iC^*_{Z_o}) I_4$$

$$+ i\left(\frac{g\ell}{V_o^2}\right)\left[\frac{e^{2C^*_D s} - 2C^*_D s - 1}{(2C^*_D)^2}\right]$$

$$+ \hat{a}_c\left[\frac{e^{C^*_D s} - C^*_D s - 1}{(C^*_D)^2}\right] \qquad (9.8)$$

where

$$I_1 = \int_o^s \int_o^{s_2} \tilde{\xi}\, ds_1\, ds_2$$

$$I_2 = \left(\frac{p_o}{V_o}\right)^{-1} \int_o^s \int_o^{s_2} \left(\frac{p}{V}\right) \tilde{\xi}\, ds_1\, ds_2$$

$$I_3 = \int_o^s \tilde{\xi}\, ds_1$$

$$I_4 = \int_o^s \int_o^{s_2} e^{i\phi}\, ds_1\, ds_2$$

B_o, B_1 are complex constants and

$\frac{s^2}{2}$ is a good approximation for the coefficients of $g\ell V_o^{-2}$ and $\hat{a}_c$.

Note that if the spin to velocity ratio is a constant, I_2 reduces to I_1.

For low spin the integrals provide the same frequencies that are present in $\tilde{\xi}$. Thus the lateral motion of a symmetric missile with epicyclic angular motion is represented by a parabola plus an epicyclic motion. The relative amplitude and phase of the two motions are determined by C_{L_α} and $C_{N_q} + C_{N_{\dot{\alpha}}}$. A slightly asymmetric missile has a tricyclic angular motion and its lateral motion is also a parabola plus a tricyclic motion. The relation between the two three-mode motions is determined by the relative magnitude and phase of the asymmetric force and moment terms as well as the values of C_{L_α} and $C_{N_q} + C_{N_{\dot{\alpha}}}$. For high spin the lateral motion is much simpler. This is due to the fact that the magnitude of an integral of a circular constant frequency motion is the magnitude of the motion divided by its frequency. Thus the integrations in I_1, I_2, and I_3 have the effect of reducing or eliminating the influence of high frequency terms like ϕ_1 and ϕ and retaining only the slow mode ϕ_2. Thus the lateral motion of a missile with high spin is essentially a parabola plus a spiral with the slow mode frequency. The relative magnitude and phase is determined by C_{L_α} and $C_{N_{p\alpha}}$.

6.10 Aerodynamic Jump

The study of the center of mass motion is quite important for ballistic range measurements of aerodynamic force coefficients. An even more important application of this study is present in the requirement that the flight path be sufficiently controlled so that the range instrumentation does not suffer damage. A simple calculation shows that the periodic part of the motion does not have sufficient amplitude to cause difficulty. Indeed this motion is seldom greater in linear extent than a model diameter.

We are, therefore, interested in the average direction of the flight path. The parabolic deflections due to gravity and Coriolis acceleration are easily predicted and, thus, we are primarily concerned with the average effect of the aerodynamic forces.

It should be noted that there are other causes of dispersion of models, i.e., muzzle whip, blast effects. These are usually small with the exception of effect of gun blast on finned missiles. For the short time during which the muzzle gases

are flowing forward over the rear fin surfaces, they can impart a large destabilizing angular momentum to the model and a much smaller linear momentum. This initial angular velocity can generate an angular motion which will give rise to a large displacement. This displacement is precisely the quantity we want to study in general. It is of great importance that the lift of fins in this reverse flow be kept as small as possible.

We will now study in detail this average effect of the aerodynamic force. This effect will, of course, be related to the initial angles and angular velocities present at launch. These initial conditions may be caused by bore clearances, sabot separation, or by blast effects. This average deflection is called aerodynamic jump and may be defined by the equation

$$\text{aero. jump} = \lim_{s\to\infty} -\frac{1}{s}\left\{\left[C^*_{L_\alpha} + i\left(\frac{pd}{V}\right)C^*_{N_{p\alpha}}\right] I_1 + (C^*_{N_q} + C^*_{N_{\dot\alpha}}) I_3 - (C^*_{Y_o} + iC^*_{Z_o}) I_4\right\} \tag{10.1}$$

In order to take the indicated averages of I_1 and I_3 we can solve Equation (8.1) for $\tilde\xi$.

$$\tilde\xi = \frac{\tilde\xi'' + (H - iP)\tilde\xi' - iAe^{i\phi}}{M + iPT} \tag{10.2}$$

$$\therefore\ I_1 = \left[M + iPT\right]^{-1}\left\{\tilde\xi - \tilde\xi_o - \tilde\xi'_o s + \left[H - iP\right]\left[\int_o^s \tilde\xi\, ds_1 - \tilde\xi_o s\right] - iAI_4\right\} \tag{10.3}$$

But for a dynamically stable missile $\tilde\xi$ and its integral are both bounded.

$$\lim_{s\to\infty}\frac{1}{s} I_1 = -\left[M + iPT\right]^{-1}\left\{\left[\tilde\xi'_o + (H - iP)\ \tilde\xi_o\right] + iA \lim_{s\to\infty}\frac{1}{s} I_4\right\} \tag{10.4}$$

No direct measurements of $C_{N_q} + C_{N_{\dot{\alpha}}}$ have been made in ballistic range tests. It is quite reasonable, therefore, to omit this term in our consideration of aerodynamic jump.

$$\therefore \text{ aero. jump} = \left[C^*_{L_\alpha} + i\left(\frac{p\ell}{V}\right) C^*_{N_{p\alpha}}\right]\left[M + iPT\right]^{-1}\left[\gamma'_{\xi_o} + (H - iP)\,\tilde{\xi}_o\right] + J_A\,\Phi \tag{10.5}$$

$$\text{where } J_A = \left[C^*_{Y_o} + iC^*_{Z_o}\right] + i\left[C^*_{L_\alpha} + i\left(\frac{p\ell}{V}\right) C^*_{N_{p\alpha}}\right]\left[M + iPT\right]^{-1} A$$

$$\doteq C^*_{Y_o} + iC^*_{Z_o} + iC^*_{L_\alpha}\left[C_{M_\alpha}\right]^{-1}\left[C_{m_o} + iC_{n_o}\right]$$

$$\Phi = \lim_{s\to 0} \frac{1}{s}\left[I_4\right]$$

Equation (10.5) shows the sensitivity of the aerodynamic jump to initial conditions. Usually $\tilde{\xi}_o$ is small and a good approximation to the symmetric part of the jump is $\left[k_t^2\, C_{L_\alpha}/C_{M_\alpha}\right]\tilde{\xi}'_o$. The asymmetric part depends very much on the roll history. For constant roll,

$$\Phi = \frac{i}{\phi'} \tag{10.6}$$

If the roll is varying in accordance with Equation (5.5.6), Φ can be computed as a function of two parameters[6-9]. One special case of some importance is that where the spin producing moment is large in comparison with the spin damping moment over the one or two periods of the pitching motion and the initial roll rate is zero. Since the aerodynamic jump is an average over this periodic motion, the roll equation for use in Φ assumes the very special form

$$\phi = K_\delta \frac{s^2}{2} \tag{10.7}$$

For this constant roll acceleration,

$$\Phi = \frac{1.25}{\sqrt{K_\delta}} e^{\frac{\pi}{4} i} \qquad K_\delta > 0 \tag{10.8}$$

$$\Phi = \frac{1.25}{\sqrt{-K_\delta}} e^{-\frac{\pi}{4} i} \qquad K_\delta < 0 \ .$$

It is interesting to note that the aerodynamic jump is at right angles to J_A for constant spin and a 45° angle for constant acceleration from zero spin. Note that neither (10.5) or (10.8) show any special effect of a resonant roll rate. This is due to the fact that although the resonance angular motion amplitude can be quite large, its <u>average</u> influence on the trajectory is not exceptionally large. The increased induced drag can, however, affect the gravity drop along the Z_e - axis.

6.11 Spin Lock-in and Catastrophic Yaw

Although spin-pitch resonance can yield large trim angles, the probability of a steady-state spin rate exactly that of the pitching rate is quite small. Moreover, aerodynamic damping usually keeps the trim angle to be a reasonably small multiple of asymmetry angle. By the introduction of roll orientation dependent moments, J. D. Nicolaides [6-11] has demonstrated the possibility of spin pitch lock-in and large multiplying factors for the asymmetry angle. In this section, we will outline the work which has very successfully explained the rather high incidence of resonance and the large trim angles associated with it.

The complex angle of attack in missile fixed coordinates, ξ, can be described by an amplitude, δ, and an orientation, θ. θ is the angle between the plane of the angle of attack and a fixed plane on the missile such as one containing a fin. Nicolaides' model then was that there is both a roll moment and a side moment depending on angle of attack and θ. The revised form of Equation (5.5.2) is

$$\therefore C_{\ell} = \delta_f C_{\ell_\delta} + \left(\frac{p\ell}{V}\right) C_{\ell_p} + \delta C_{\ell_\alpha}(\theta,\delta) \qquad (11.1)$$

If the missile has an angle of rotational symmetry, θ_s, then C_{ℓ_α} is periodic with period θ_s. Now the presence of differential cant, δ_f, excludes the possibility of a plane of mirror symmetry. If the missile with no differential cant ($\delta_f = 0$), has a plane of mirror symmetry, the roll moment due to orientation must be zero when the plane of the angle of attack lies in the plane of symmetry. This is clear from the fact that if we measure θ from a plane of mirror symmetry and transform coordinates by a mirror reflection, the missile maps into itself, roll moments are reversed but otherwise unchanged.

$$\therefore C_{\ell_\alpha}(\theta, \delta) = - C_{\ell_\alpha}(-\theta, \delta) \qquad (11.2)$$

A rotationally symmetric missile with n similar fins has a symmetry angle of $2\pi/n$ and is an odd periodic function of $2\pi/n$. This means that it can usually be represented by a Fourier sine series.

$$C_{\ell_\alpha} = \sum_{k=1}^{\infty} a_k \sin nk\theta \qquad (11.3)$$

$$a_k = a_k(\delta)$$

The simplest form of C_{ℓ_α} for an n fin missile is, therefore,

$$C_{\ell_\alpha} = a_1 \sin n\theta \qquad (11.4)$$

Maple and Synge[6-4] assume that all forces and moments are analytic functions of the transverse velocities in missile fixed coordinates (v,w). This means that these forces and moments must be at worst infinite power series in ξ and $\bar{\xi}$.

But

$$\sin nk\theta = \frac{\xi^{nk} - \bar{\xi}^{nk}}{2i\delta^{nk}} \quad . \qquad (11.5)$$

In order for δC_{ℓ_α} to be analytic in v and w, then, $a_k \delta \sin nk\theta$ must be a polynomial or a convergent infinite series in ξ and $\bar{\xi}$.

$$a_k \delta \sin nk\theta = (a_k \delta^{1 - nk}) \left(\frac{1}{2i}\right) (\xi^{nk} - \bar{\xi}^{nk}) \tag{11.6}$$

The last term in Eq. (11.6) is a polynomial in ξ and $\bar{\xi}$ and, hence, a polynomial in v and w. $a_k \delta^{1 - nk}$ is a function of $\delta = (v^2 + w^2)^{1/2}/V$ and would satisfy the Maple-Synge requirement if it were represented by a power series in δ^2.

$$\therefore a_k \delta^{1 - nk} = \sum_{\ell = 0}^{\infty} b_{k\ell} \delta^{2\ell} \tag{11.7}$$

and

$$a_k(\delta) = \sum_{\ell = 0}^{\infty} b_{k\ell} \delta^{2\ell + nk - 1} \tag{11.8}$$

Thus, the simplest expression for an n fin missile under the Maple-Synge analyticity assumption is

$$C_{\ell_\alpha} = b_{10} \delta^{n - 1} \sin n\theta \tag{11.9}$$

For the general roll moment, (11.1), the roll equation of the last chapter (5.5.6) assumes the form

$$\phi'' + K_p \phi' - K_\delta - K_\alpha (\hat{\theta} - \phi, \delta) = 0 \tag{11.10}$$

where $K_\alpha = \frac{\rho S \ell^3}{2I_x} \delta C_{\ell_\alpha}$

$\hat{\theta} = \theta + \phi$ is orientation of plane of angle of attack with respect to a fixed plane.

During conventional resonance, a missile performs a circular yawing motion at constant frequency $\hat{\theta}'$. For a missile in circular constant frequency motion, Equation (11.10) predicts a constant rolling motion when $\hat{\theta} - \phi = \theta^*$, a constant, and

$$\hat{\theta}' = \phi' = \frac{K_\delta + K_\alpha \ (\theta^*, \delta)}{K_p} \quad . \tag{11.11}$$

When this occurs, the roll motion is "locked" to the circular pitching motion and the missile performs a lunar motion*. This can occur whenever there exists a θ^* which satisfies Equation (11.11) and this equilibrium value of θ^* is a stable value.

$$\frac{1}{K_p} \left(\frac{\partial K_\alpha}{\partial \theta}\right)_{\theta = \theta^*} > 0 \tag{11.12}$$

Thus, for many pitching motions which are near circular, lock-in can occur and a resonance situation can exist. The occurence of lock-in depends on the roll frequency and the pitch frequency being close to each other at some point of the flight since widely different frequencies will make C_{ℓ_α} vary rapidly with a zero average and, hence, it will have no influence on the motion.

If we now consider the possibility of a side moment dependent on orientation, a Magnus like moment could exist for very small roll rate. If this term and an asymmetric moment term are added to Equation (5.22), we have

$$\tilde{C}_m + i\tilde{C}_n = (C_{m_o} + iC_{n_o})e^{i\phi} + \left[C_{SM_\alpha} + \left(\frac{p\ell}{V}\right) C_{M_{p\alpha}} - iC_{M_\alpha}\right] \tilde{\xi} + C_{M_q} \tilde{\mu} - iC_{M_{\dot{\alpha}}} \tilde{\xi}' \tag{11.13}$$

where C_{SM_α} is a function of $\hat{\theta} - \phi$ and δ, and has the same symmetry properties as those of C_{ℓ_α}.

* This motion is so named since it is quite similar to the moon's rotating about the earth in such a way that it presents the same face to our view.

Our differential equation (8.1) becomes

$$\tilde{\xi}'' + (H - iP)\tilde{\xi}' - [M + i(PT + M_s)]\tilde{\xi} = iAe^{i\phi}$$

$$\text{where } M_s = \gamma\left(\frac{\rho S \ell}{2m}\right) k_t^{-2} C_{SM_\alpha} \tag{11.14}$$

For circular motion which is "lock-in" with the rolling motion:

$$(\phi')^2 - P\phi' + M \doteq 0 \tag{11.15}$$

$$\xi = K_3 e^{i\phi_3} \tag{11.16}$$

$$\text{where } \phi_3 = \phi's + \phi_{30}$$

$$K_3 e^{i\phi_{30}} = \frac{A}{\phi' H - PT - M_s(\theta^*, K_3)}$$

If we have an unfortunate value of M_s which makes the denominator of the expression for K_3 quite small, a very large amplification factor is possible giving rise to a situation which is called "catastrophic" yaw by Nicolaides.

TABLE 6-1

NON-MAGNUS COEFFICIENTS

$$\hat{C}_{N_\alpha} = C_{N_\alpha}$$

$$\hat{C}_{N_{\dot{\alpha}}} = C_{N_{\dot{\alpha}}}$$

$$\hat{C}_{N_q} = C_{N_q} + s_{cg} C_{N_\alpha}$$

$$\hat{C}_{N_{\dot{q}}} = C_{N_{\dot{q}}} + s_{cg} C_{N_{\dot{\alpha}}}$$

$$\hat{C}_{M_\alpha} = C_{M_\alpha} - s_{cg} C_{N_\alpha}$$

$$\hat{C}_{M_{\dot{\alpha}}} = C_{M_{\dot{\alpha}}} - s_{cg} C_{N_{\dot{\alpha}}}$$

$$\hat{C}_{M_q} = C_{M_q} - s_{cg} (C_{N_q} - C_{M_\alpha}) - s_{cg}^2 C_{N_\alpha}$$

$$\hat{C}_{M_{\dot{q}}} = C_{M_{\dot{q}}} - s_{cg} (C_{N_{\dot{q}}} - C_{M_{\dot{\alpha}}}) - s_{cg}^2 C_{N_{\dot{\alpha}}}$$

MAGNUS COEFFICIENTS

$$\hat{C}_{N_{p\alpha}} = C_{N_{p\alpha}}$$

$$\hat{C}_{N_{p\dot{\alpha}}} = C_{N_{p\dot{\alpha}}}$$

$$\hat{C}_{N_{pq}} = C_{N_{p\dot{q}}} - s_{cg} C_{N_{p\alpha}}$$

$$\hat{C}_{N_{p\dot{q}}} = C_{N_{p\dot{q}}} - s_{cg} C_{N_{p\dot{\alpha}}}$$

$$\hat{C}_{M_{p\alpha}} = C_{M_{p\alpha}} - s_{cg} C_{N_{p\alpha}}$$

$$\hat{C}_{M_{p\dot{\alpha}}} = C_{M_{p\dot{\alpha}}} - s_{cg} C_{N_{p\dot{\alpha}}}$$

$$\hat{C}_{M_{pq}} = C_{M_{pq}} - s_{cg} (C_{N_{pq}} + C_{M_{p\alpha}}) + s_{cg}^2 C_{N_{p\alpha}}$$

$$\hat{C}_{M_{p\dot{q}}} = C_{M_{p\dot{q}}} - s_{cg} (C_{N_{p\dot{q}}} + C_{M_{p\dot{\alpha}}}) + s_{cg}^2 C_{N_{p\dot{\alpha}}}$$

REFERENCES

6-1. Nicolaides, J. D. Firing Range Method of Obtaining Aerodynamic Data. Dragonfly Summary Report (MX-802), General Electric Company, Schenectady, New York, 1948.

6-2. American Standard Letter Symbols for Aeronautical Sciences, ASA X10.7-1954, American Society of Mechanical Engineers, New York, 1954.

6-3. McShane, E. J., Kelley, J. L. and Reno, F. V. Exterior Ballistics, University of Denver Press, 1953.

6-4. Maple, C. G. and Synge, J. L. Aerodynamic Symmetry of Projectile. Quarterly of Applied Mathematics Vol. IV, pp. 345-366, January 1949.

6-5. Davies, J. M. The Aerodynamics of Golf Balls. Journal of Applied Physics Vol. 20, pp. 821-8, September 1949.

6-6. Sacks, A. H. Aerodynamic Forces, Moments and Stability Derivatives for Slender Bodies of General Cross Section. NACA TN 3283, November 1954.

6-7. Nielsen, K. L. and Synge, J. L. On the Motion of a Spinning Shell. Quarterly of Applied Mathematics, Vol. VI, pp. 345-366, October 1949.

6-8. Nicolaides, J. D. On the Free Flight Motion of Missiles with Slight Configurational Asymmetries. BRL Report No. 858, June 1953.

6-9. Murphy, C. H. and Bradley, J. W. Jump Due to Aerodynamic Asymmetry of a Missile with Varying Roll Rate. BRL Report No. 1077, May 1959.

6-10. Durand, W. F. Aerodynamic Theory Vol. V, Durand Reprinting Committee 1943, pp 110-112.

6-11. Nicolaides, J. D., Two Nonlinear Problems in the Flight Dynamics of Modern Ballistic Missiles, IAS Report 59-17, January 1959.

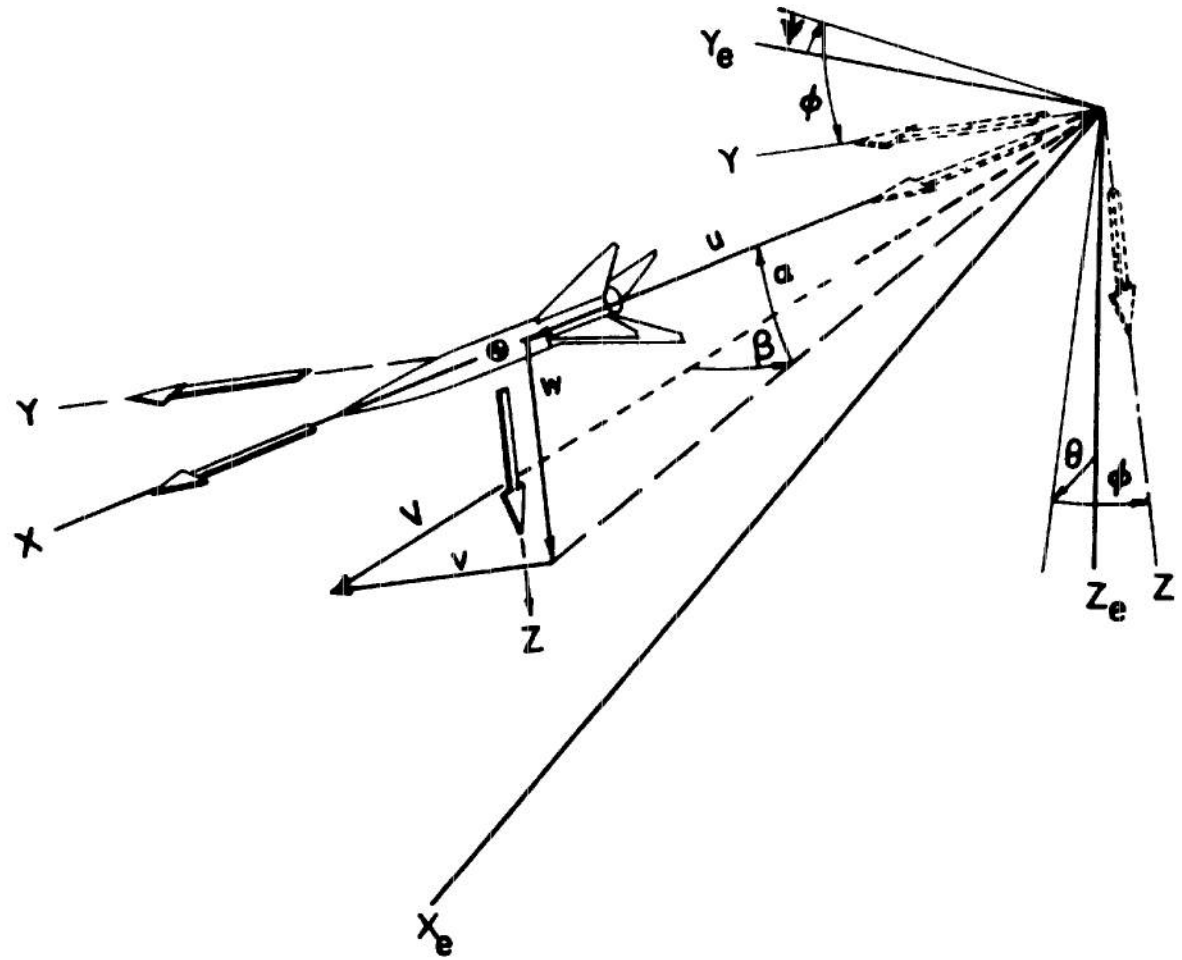

FIG. 6.1 MISSILE FIXED AND EARTH-FIXED COORDINATES

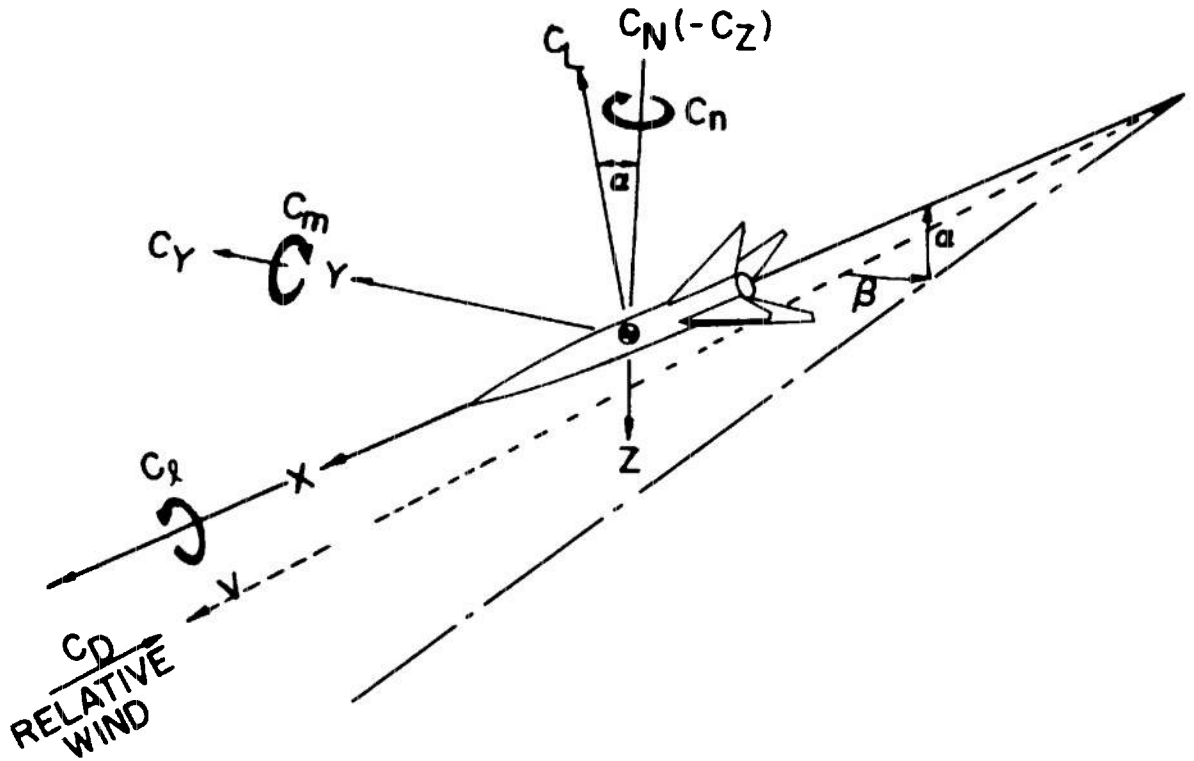

FIG. 6.2 MISSILE AXES SHOWING DIRECTION AND SENSE OF FORCES AND MOMENTS

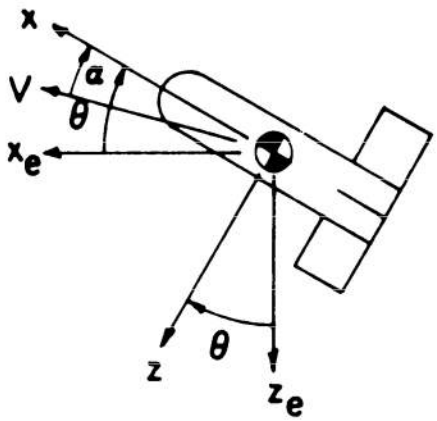

$$\dot{\theta} = q$$

$$\beta = r = 0$$

FIG. 6.3 MISSILE IN PITCHING MOTION

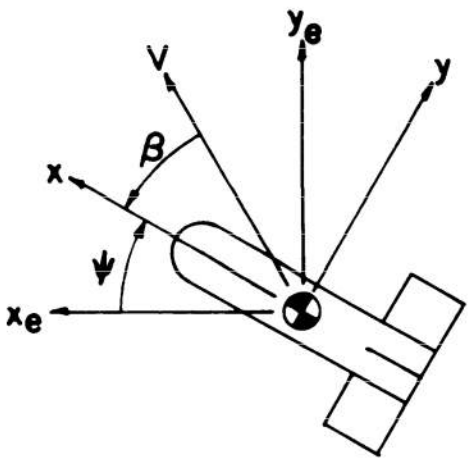

$$\dot{\psi} = r$$

$$\alpha = q = 0$$

FIG. 6.4 MISSILE IN YAWING MOTION

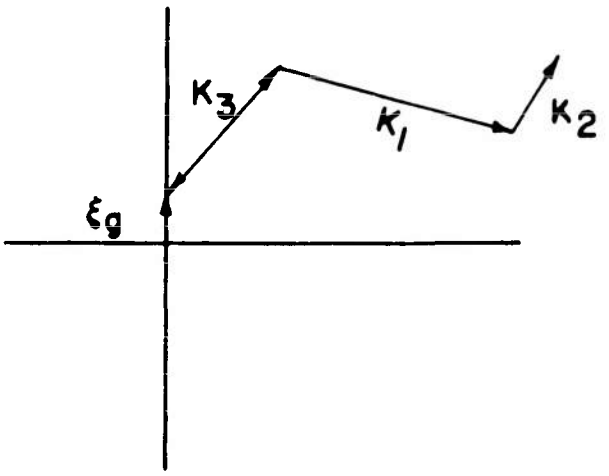

FIG. 6.5 GEOMETRICAL CONSTRUCTION OF PITCHING AND YAWING MOTION

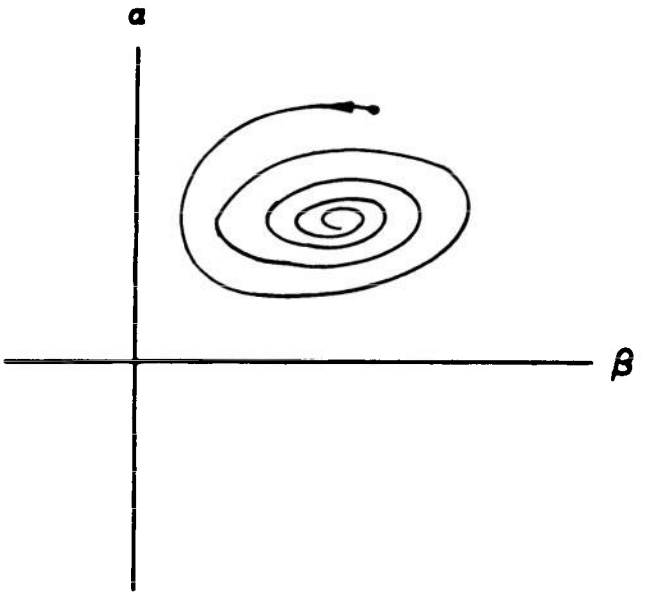

FIG. 6.6 PITCHING AND YAWING MOTION

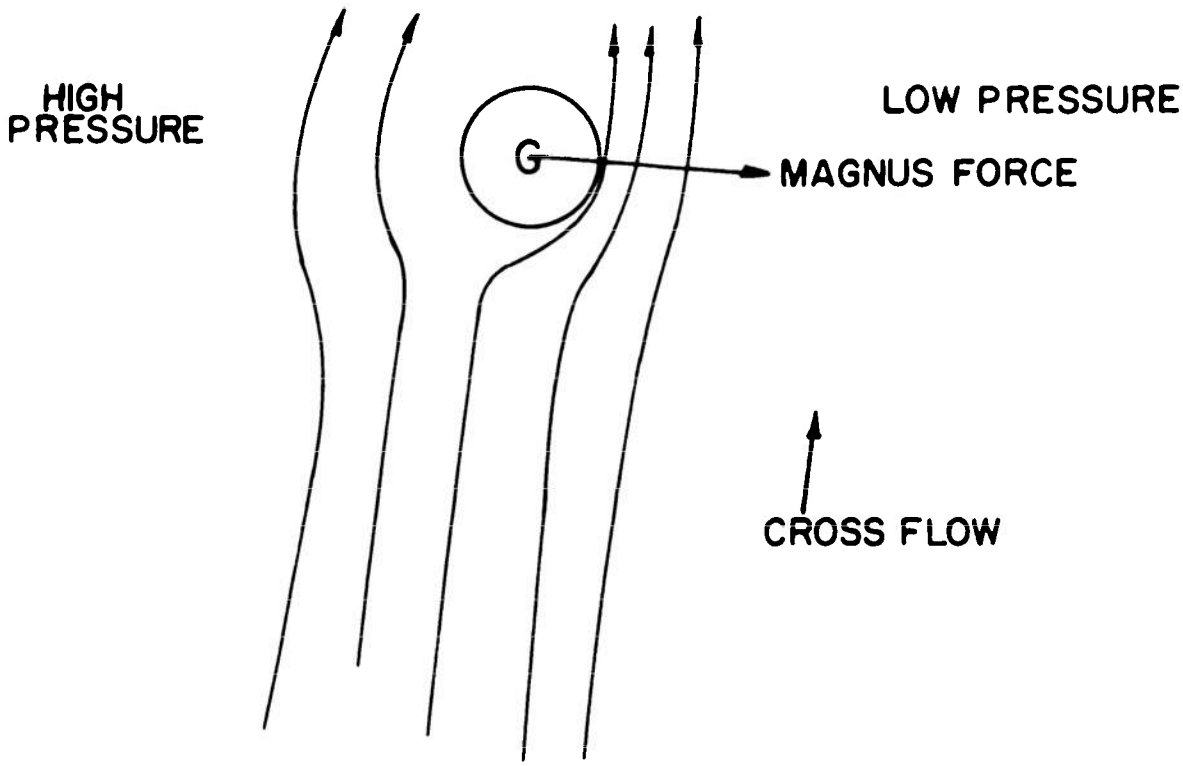

FIG. 6.7 PHYSICAL MODEL OF MAGNUS FORCE

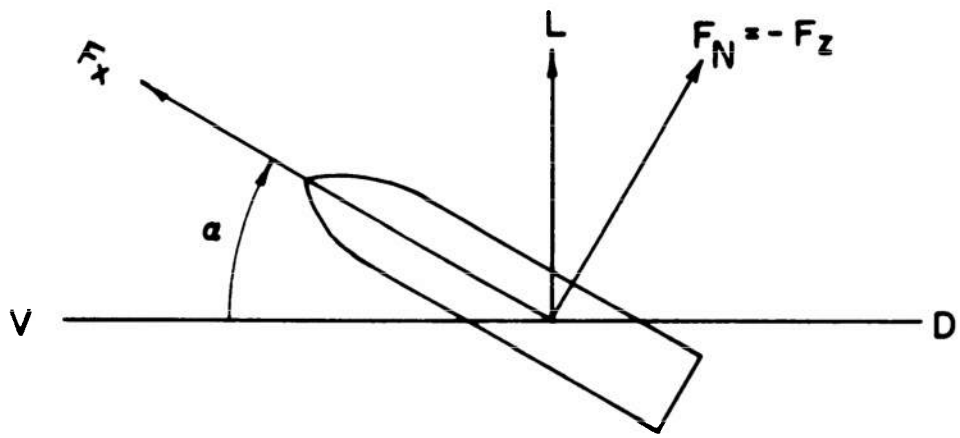

FIG. 6.8 RELATION BETWEEN LIFT AND NORMAL FORCE

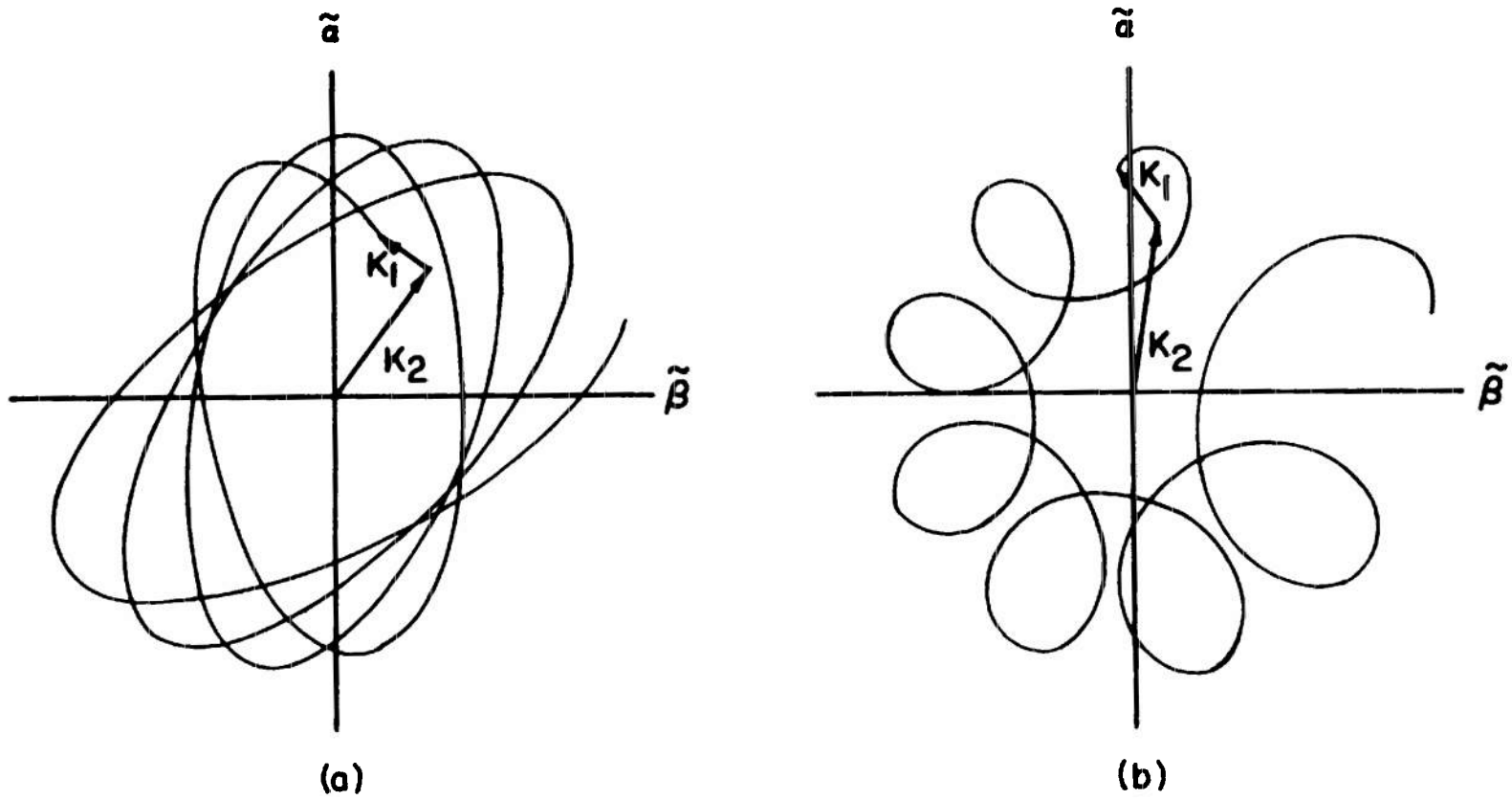

FIG. 6.9 ROLLING STATICALLY STABLE SYMMETRIC MISSILE

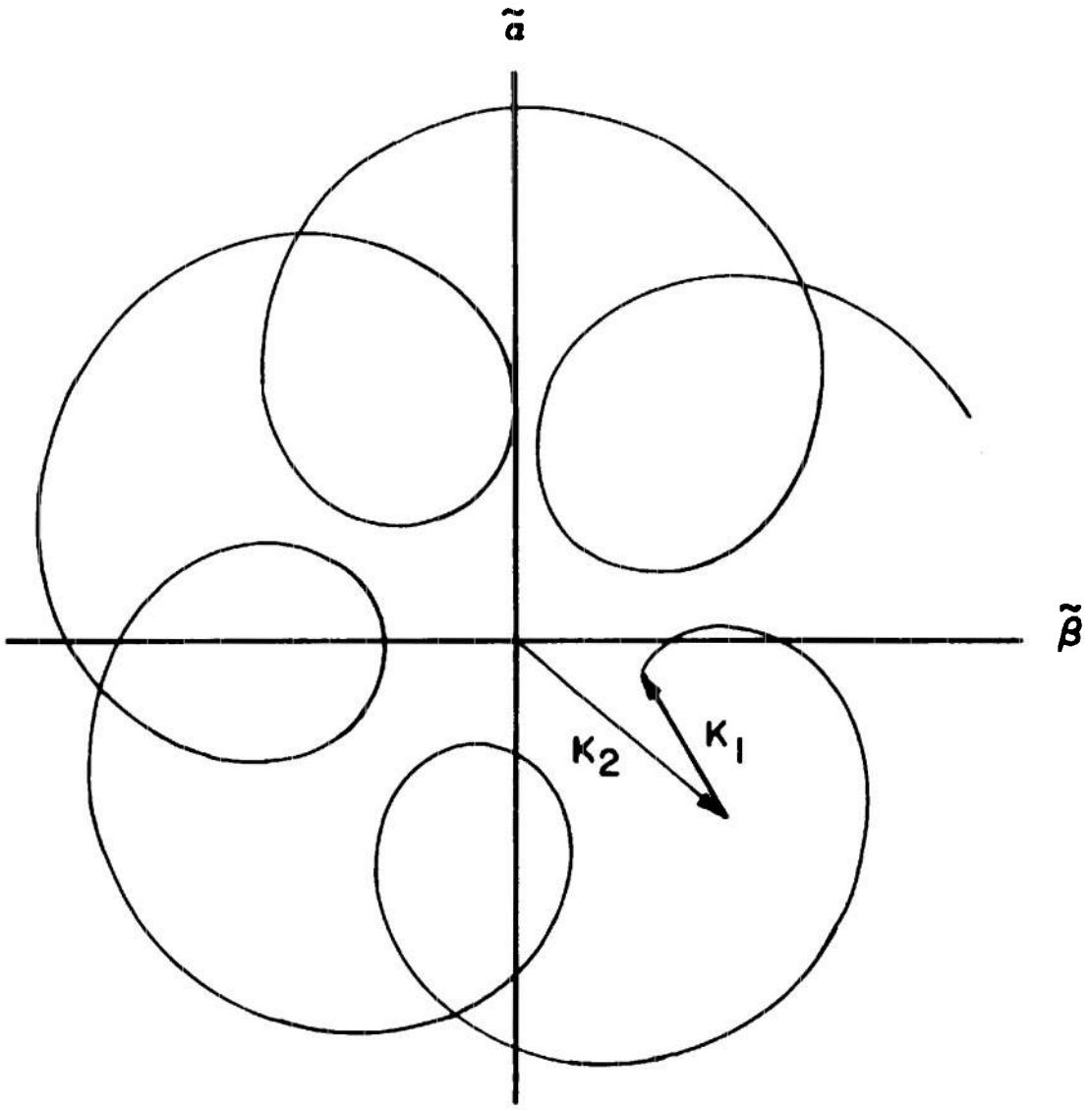

FIG. 6.10 ROLLING STATICALLY UNSTABLE SYMMETRIC MISSILE

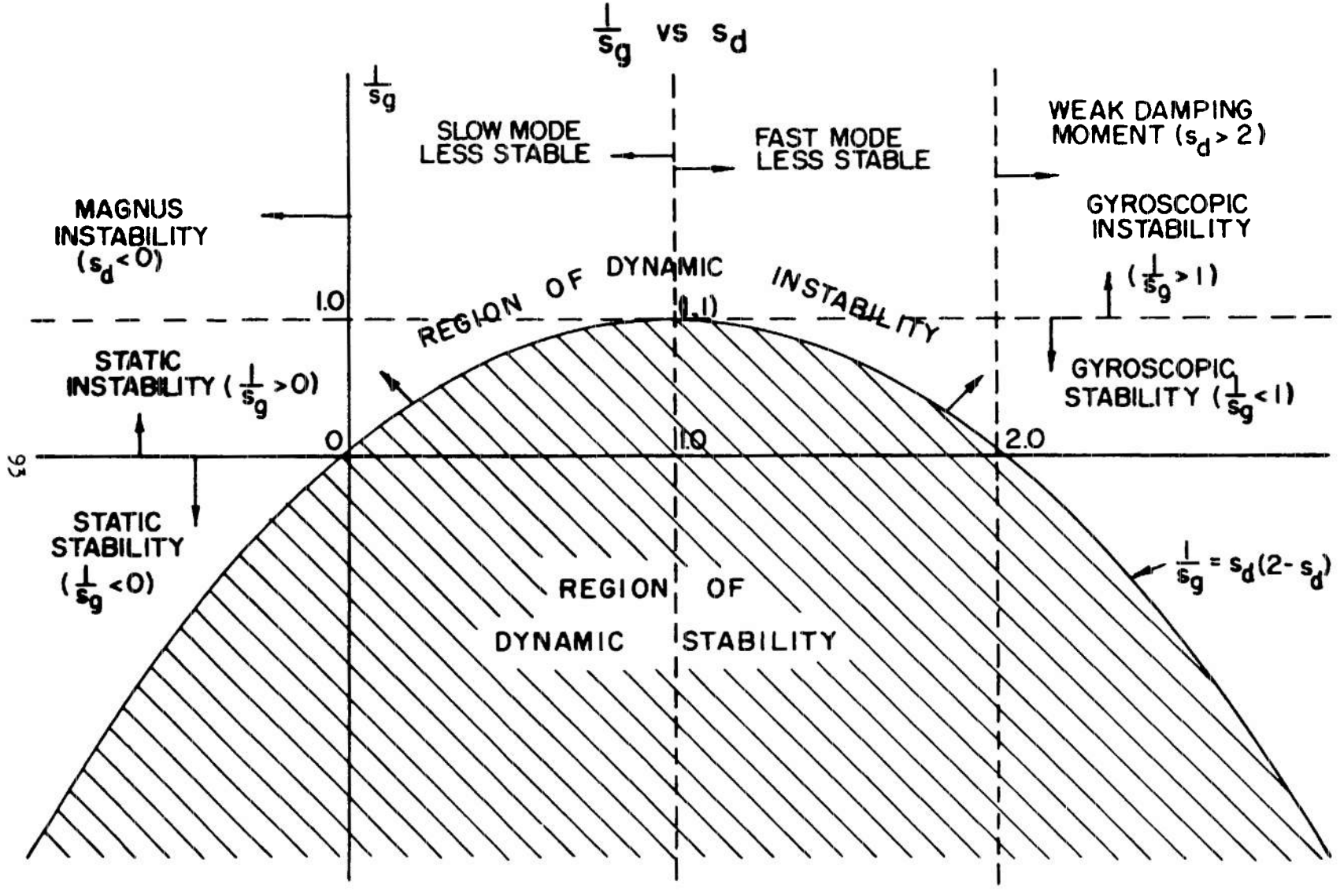
$\frac{1}{s_g}$ vs s_d
$\frac{1}{s_g}$
SLOW MODE LESS STABLE
FAST MODE LESS STABLE
WEAK DAMPING MOMENT ($s_d > 2$)
MAGNUS INSTABILITY ($s_d < 0$)
GYROSCOPIC INSTABILITY ($\frac{1}{s_g} > 1$)
1.0
REGION OF DYNAMIC INSTABILITY
(1,1)
STATIC INSTABILITY ($\frac{1}{s_g} > 0$)
GYROSCOPIC STABILITY ($\frac{1}{s_g} < 1$)
0
1.0
2.0
STATIC STABILITY ($\frac{1}{s_g} < 0$)
$\frac{1}{s_g} = s_d(2 - s_d)$
REGION OF DYNAMIC STABILITY

FIG. 6.11

CHAPTER VII

RANGE MEASUREMENT OF LINEAR COEFFICIENTS

7.1 Geometrical Considerations

The basic information acquired from a ballistic range test is the location of the missile's center of gravity (x_1, x_2, x_3) and the direction cosines of its axis of symmetry. These measurements are taken in the range coordinate system for which the x_1 axis points downrange along the intersection of the horizontal plane and the vertical plane containing the gun, the x_2 axis lies in the horizontal plane pointing to the left and the x_3 axis points up. The theory of the preceding chapter made use of an earth-fixed system, a missile-fixed system rotating with the missile, and a missile-fixed system with zero roll rate. The range system is essentially the same as the earth-fixed system after a rotation of 180° about the x_1 axis

$$\therefore \quad x_e = x_1 \tag{1.1}$$

$$y_e = - x_2 \tag{1.2}$$

$$z_e = - x_3 \tag{1.3}$$

In order to relate the direction cosines to the angles of attack and sideslip in the non-rotating frame of reference yet another coordinate system must be introduced. (y_1, y_2, y_3) This coordinate system is so defined that the y_1 axis is along the missile's axis, the y_2 axis is in the horizontal plane pointing to the right and the y_3 axis points down. Since the y_2 axis is constrained to lie in a plane, these coordinates are called fixed plane coordinates. They are approximately the same as the missile-fixed non-rolling coordinates but are much simpler to use. To verify this statement we will first compute the roll rate of these coordinates.

This can be done through the introduction of unit vectors, $\vec{e}_1$, $\vec{e}_2$, $\vec{e}_3$, along the fixed-plane axes. Since the y_1 axis lies along the missile's axis, its components in the range axis system are precisely the direction cosines of the missile's axis:

$$\vec{e}_1 = (n_1, n_2, n_3) \tag{1.4}$$

The requirement that $\vec{e}_2$ be in the horizontal plane forces its third component to vanish. Since it is a unit vector, perpendicular to $\vec{e}_1$ and points to the right, its remaining components are completely determined.

$$\vec{e}_2 = \left(\frac{n_2}{\sqrt{n_1^2 + n_2^2}} , \frac{- n_1}{\sqrt{n_1^2 + n_2^2}} , 0 \right) \tag{1.5}$$

According to the right hand rule,

$$\vec{e}_3 = \vec{e}_1 \times \vec{e}_2$$

$$= \left(\frac{n_1 n_3}{\sqrt{n_1^2 + n_2^2}} , \frac{n_2 n_3}{\sqrt{n_1^2 + n_2^2}} , - \sqrt{n_1^2 + n_2^2} \right) \tag{1.6}$$

The angular velocity vector $(\omega_1, \omega_2, \omega_3)$ for the fixed plane axes is defined by the relations

$$\omega_1 = \dot{\vec{e}}_2 \cdot \vec{e}_3 = - \vec{e}_2 \cdot \dot{\vec{e}}_3 \tag{1.7}$$

$$\omega_2 = \dot{\vec{e}}_3 \cdot \vec{e}_1 = - \vec{e}_3 \cdot \dot{\vec{e}}_1 \tag{1.8}$$

$$\omega_3 = \dot{\vec{e}}_1 \cdot \vec{e}_2 = - \vec{e}_1 \cdot \dot{\vec{e}}_2 \tag{1.9}$$

Equation (1.7) can be reduced to the following relation

$$\frac{\omega_1 \ell}{V} = \frac{n_3 (n_1 n_2' - n_2 n_1')}{1 - n_3^2} \tag{1.10}$$

Thus the fixed plane coordinates do have a non-zero roll rate. For small pitch and yaw angles and small pitch and yaw angular velocities, n_2, n_3, n_1', n_2', n_3' are first order quantities and n_1 is essentially unity. Therefore, $\omega_1 \ell / V$ is a second order quantity and for small amplitude motion the fixed plane coordinates are equivalent to the missile fixed non-rolling system.

The components of the velocity vector in the non-rolling system may be computed by the relations

$$u = u_1 = \vec{e}_1 \cdot \vec{V} \tag{1.11}$$

$$\tilde{v} \doteq u_2 = \vec{e}_2 \cdot \vec{V} \tag{1.12}$$

$$\tilde{w} \doteq u_3 = \vec{e}_3 \cdot \vec{V} \tag{1.13}$$

where u_1, u_2, u_3 are the components of $\vec{V}$ in the fixed plane system and $\vec{V}$ is the velocity vector for the missile's center of gravity.

If (x_1, x_2, x_3) are the coordinates of the missile's center of gravity, its velocity vector in range coordinates is $(\dot{x}_1, \dot{x}_2, \dot{x}_3)$

$$\therefore \frac{u_2}{V} = \frac{n_2\dot{x}_1 - n_1\dot{x}_2}{\sqrt{n_1^2 + n_2^2}\ \sqrt{(\dot{x}_1)^2 + (\dot{x}_2)^2 + (\dot{x}_3)^2}} \tag{1.14}$$

$$\frac{u_3}{V} = \frac{n_1n_3\dot{x}_1 + n_2n_3\dot{x}_2 - (n_1^2 + n_2^2)\,\dot{x}_3}{\sqrt{n_1^2 + n_2^2}\ \sqrt{\dot{x}_1^2 + \dot{x}_2^2 + \dot{x}_3^2}} \tag{1.15}$$

For small amplitude motion $V \doteq \dot{x}_1$, $n_1 \doteq 1$, and n_2n_3 can be neglected

$$\tilde{\xi} = \frac{\tilde{v} + i\tilde{w}}{V}$$

$$\therefore \doteq n_2 + in_3 - \left(\frac{dx_2}{dx_1} + i\,\frac{dx_3}{dx_1}\right) \tag{1.16}$$

The slope of the trajectory in the x_1x_2 and x_1x_3 plane can be easily computed from measurements and $\tilde{\xi}$ obtained by use of Equation (1.16). For large amplitude the exact Equations (1.14-15) must be used.

Equation (1.16) may seem obvious to the reader as a small angle approximation and he may wonder about the introduction of the fixed plane coordinates and the lengthy vector analysis. In answer we can only say that a careful engineer should always be suspicious of an "obvious" result. As we shall see in the next chapter although this "obvious" result is correct, a similar intuitive feeling that the fixed plane coordinate oscillates about the non-rolling coordinates (i.e., $(\omega_1)_{av} = 0$) is not true.

7.2 Analysis of Motion of Symmetric Missiles

According to the theory of Chapter VI, the pitching and yawing motion of a symmetric missile acted on by linear coefficients is described by the equation:

$$\tilde{\xi} = \tilde{\xi}_g + K_1 e^{i\phi_1} + K_2 e^{i\phi_2} \tag{2.1}$$

where $\tilde{\xi}_g \doteq -(P/M) g \ell V_o^{-2}$

$$K_j = K_{jo} e^{\lambda_j s}$$

$$\phi_j = \phi_{jo} + \phi_j' s$$

$\tilde{\xi}_g$ is measurable for missiles with high spin rates and low velocities. Gravity-induced curvature of the trajectory usually places a lower bound of 500 ft/sec on range tests although special tests have been made at lower velocities over a fraction of the total range length. With this velocity bound, a statically stable missile would have to have an unusually high spin rate so that $\tilde{\xi}_g$ could be measured in a ballistic range test. These spin rates are, however, required for stabilization of bullets and shell. Since P/M may be expressed as $4s_g/P$, we need only consider this ratio to determine the effect of model shape, mass distribution, and spin on $\tilde{\xi}_g$. For most spin stabilized projectiles[7-1]

$$1.1 < s_g < 4$$

$$1/30 < \frac{I_x}{I_y} < 1/10 \tag{2.2}$$

$$.25 < \frac{p\ell}{V} < .65$$

where ℓ is maximum missile diameter.

High values of the stability factor occur with high values of the moment of inertia ratio and spin rate and conversely. Thus the best maximum estimate of P/M may be found by combining the low values of the above inequalities.

$$\therefore \ |\tilde{\xi}_g| < 500 \ (g\ell V_o^{-2}) \tag{2.3}$$

According to Inequality (2.3) a spinning missile with a diameter 10^{-1} ft and a velocity of 500 ft/sec could have a $\tilde{\xi}_g$ of six milliradians. This angle of a third of a degree can be measured but decreases very rapidly with increased velocity. A transonic test of the same missile would produce one-fourth this value of $\tilde{\xi}_g$. A larger missile would, of course, have a proportionately larger $\tilde{\xi}_g$. In any event $\tilde{\xi}_g$ is quite small and can be neglected in the analysis of the angular motion of supersonic missiles. If it is necessary to consider $\tilde{\xi}_g$, it can be estimated and subtracted from the measured $\tilde{\xi}$'s so that the motion to be fitted is a simple epicycle

$$\tilde{\xi} - \tilde{\xi}_g = K_1 e^{i\phi_1} + K_2 e^{i\phi_2} \tag{2.4}$$

After the frequencies of the epicycle have been determined, a better value of $\tilde{\xi}_g$ may be computed by use of Equations (6.6.2.3,25)

$$\tilde{\xi}_g = \frac{-(\phi_1' + \phi_2')(g\ell V^{-2})}{\phi_1' \cdot \phi_2'} \tag{2.5}$$

If the estimate was quite poor, the better value of $\tilde{\xi}_g$ may be subtracted from the measurements and the epicycle fit repeated. At most, one such iteration would be necessary.

Turning now to consider the epicycle of Equation (2.4) we see that there are in general eight unknown parameters. Four of these are the initial amplitudes and orientations of the modal vectors and four are the modal frequencies and damping exponents which are related to the aerodynamic coefficient through Equations (6.6.23-26). If the spin is zero, the modal frequencies and damping exponents are essentially the same and there are only

six unknowns. For this case the angles of attack and sideslip are uncoupled and each are described by damped sine waves which differ only in amplitude and phase. The analysis of this special motion is quite simple and will not be discussed here. The more general eight unknown data reduction will, of course, handle this case and presence of zero spin only introduces two consistency checks on the derived frequencies and damping exponents.

The data reduction is a combined graphical-analytic method which can be divided into two parts:

(1) No damping reduction of short sections of the observed trajectory. Initial determination of frequencies and damping exponents from plots of phase and amplitude at these sections versus position of the section.

(2) Refinement of these initial estimates by an iterative least squares technique which can be done by a digital computer.

Over a short flight path, the damping may be neglected and the frequencies determined from estimates of the spin and static moment coefficient. The approximate slow rate may then be used to reduce the epicyclic motion to a much simpler circular motion by the transformation

$$(\tilde{\xi} - \tilde{\xi}_g)\, e^{-i\phi'_{2a}(s - s_o)} = K_1 e^{i\hat{\phi}_1} + K_2 e^{i\hat{\phi}_2} \qquad (2.6)$$

where $\hat{\phi}_j = \phi_{jo} + \phi'_{2a} s_o + (\phi'_j - \phi'_{2a})\, s$ and

s_o is the coordinate of the center of the interval under analysis.

If the approximate ϕ'_{2a} is close to ϕ'_2, $\hat{\phi}_2$ is a constant and the motion is confined to a circle with radius K_1 and center at $K_2 e^{i\hat{\phi}_{20}}$ (Figure 7.1). Since this transformation is the rotation of each measured complex angle of attack through the angle $-\phi'_2(s - s_o)$, it can be easily done by use of a compass and better values of $\hat{\phi}'_2$ determined by trial and error. Note that ϕ_{10} can be found from the angular location on the circle of the complex angle for $s = s_o$ and ϕ'_1 from the angular location of the other transformed angles. The frequencies

are, however, much better determined from a comparison of phases at consecutive trajectory sections which are some distance apart. Finally, the modal amplitudes at the midpoint of each section are plotted versus position on semi log paper and the slopes used to determine the λ_j's.

If these graphical values are felt to be too inaccurate, they may be improved by a least squares technique. A direct least squares is not possible due to the fact that Equation (2.4) is nonlinear in the ϕ_j' and λ_j's. The relations of the differentials of these quantities is, of course, linear

$$d\tilde{\xi} = \left[e^{\lambda_1 s} \, dK_{10} + sK_1 d\lambda_1 + iK_1 (d\phi_{10} + s d\phi_1') \right] e^{i\phi_1}$$

$$+ \left[e^{\lambda_2 s} \, dK_{20} + sK_2 d\lambda_2 + iK_2 (d\phi_{20} + s d\phi_2') \right] e^{i\phi_2} \qquad (2.7)$$

The differentials of $\tilde{\xi}$ are selected to be the residuals of the fit of Equation (2.4) to the experimental data

$$d\tilde{\xi} = \tilde{\xi}_{\text{observed}} - \tilde{\xi}_{\text{computed}} \qquad (2.8)$$

Thus we have n equations of the form of Equation (2.7) for the differentials of the unknown parameters where n is the number of observations. This set of n linear equations in eight unknowns can then be solved by the usual least squares process and the resulting differentials adding to their corresponding first estimates. If the new residuals for the improved set of parameters are smaller the process has converged and may be repeated until the residuals reach a minimum. Usually no more than two or three iterations are required.

For some tests, the frequencies are observed to vary between successive sections of flight path. This change in frequency is usually due to varying P for a spin-stabilized missile although a strong Mach number variation of the static moment coefficient sometimes is the culprit. The frequencies do vary in at worst a linear fashion so that this phenomena may be handled by the introduction of quadratic expressions for the phase angle

$$\phi_j = \phi_{j_o} + \phi_{j_o}' s + (1/2) \, \phi_j'' \, s^2 \qquad (2.9)$$

and the use of a ten unknowns least squares routine.

When it is necessary to use Equation (2.9), the relations between the frequencies, damping exponents and aerodynamic coefficients must be revised in accordance with the results of Section 6.7. According to that section, the frequency relations are unchanged and apply for the local values of P and M. Experimentally, the frequencies are best determined at the midrange point (s = 0) and hence values of P and M and their derivatives can be obtained for flight conditions at this point.

$$P = \phi'_{10} + \phi'_{20} \tag{2.10}$$

$$M = \phi'_{10}\phi'_{20} - \lambda_1\lambda_2 \tag{2.11}$$

$$P' = \phi''_1 + \phi''_2 \tag{2.12}$$

$$M' = \phi'_1\phi''_2 + \phi''_1\phi'_2 \tag{2.13}$$

The expressions for the damping exponents, however, are changed. According to Equation (6.7.13)

$$\lambda_j = \lambda^*_j - \frac{\phi''_j}{2\phi'_j - P} \tag{2.14}$$

$$\text{where } \lambda^*_j = -\frac{H\phi'_j - PT}{2\phi'_j - P}$$

The λ^*_j at the midrange point can easily be computed from the range measurements of frequencies and damping exponents and H and T obtained from the λ^*_j's by the usual relations.

$$H = -(\lambda^*_1 + \lambda^*_2) \tag{2.15}$$

$$T = \frac{-(\phi'_{20}\lambda_1 + \phi'_{10}\lambda_2)}{\phi'_{10} + \phi'_{20}} \tag{2.16}$$

Frequently, the ϕ''_j's are poorly determined. If it is felt that variations in P and/or M are large enough to affect the damping exponents, their derivatives often can be independently measured or estimated and used in Equations (2.12-13) to obtain sufficiently accurate ϕ''_j's for use in Equation (2.14). This approach naturally depends on the judgement of the program engineer.

Although the angular motion can be analyzed to obtain directly the static moment coefficient, it does not yield values of the damping and Magnus moments but only combinations of these coefficients with the drag and lift coefficients, i.e., H and T. The drag and lift coefficients must, then, be measured or estimated so that the damping and Magnus moments may be obtained. The drag coefficient may be easily obtained while the lift coefficient may be measured in two ways: (1) indirectly from the static moment coefficients of two models at the same Mach number but with different centers of gravity (Table 6-1 and Equation (6.6.7)); and (2) directly from the swerving motion (Equation (6.9.8)).

The analysis of the swerving motion of a symmetric missile is quite simple because Equation (6.9.8) is linear in its two complex unknowns, B_o and B_1, and its three real unknowns, C_{L_α}, $C_{N_{p\alpha}}$, and $C_{N_q} + C_{N_{\dot{\alpha}}}$. Since the coefficient of $C_{N_q} + C_{N_{\dot{\alpha}}}$ is a single integral and the coefficients of C_{L_α} and $C_{N_{p\alpha}}$ are double integrals, $C_{N_q} + C_{N_{\dot{\alpha}}}$ has a much smaller effect on the swerving motion which has not as yet been observed. Thus the swerving motion of a spinning missile is linear in essentially six unknowns and the measured values of y_e and z_e may be fitted by a direct use of the least squares method. If the missile has small or zero spin, the Magnus force has no measurable effect and the problem reduces to five unknowns.

For a nonspinning missile the components of the swerving motion are essentially damped sine waves about a line. The amplitude of the wave is proportional to the lift coefficient and could be obtained graphically. If spin is non-zero, the integrals and least squares solution are much more suitable for calculation by digital machine than by an individual engineer.

7.3 Analysis of Motion of Slightly Asymmetric Missiles

For a rolling motion with a constant or "nearly" constant roll rate, the angular motion of a slightly asymmetric missile is described by the equation:

$$\tilde{\xi} = K_1 e^{i\phi_1} + K_2 e^{i\phi_2} + K_3 e^{i\phi_3} \qquad (3.1)$$

where K_3 is constant and

$$\phi_3 = \phi_{30} + \int_0^s \left(\frac{p\ell}{V}\right) ds_1 .$$

When K_3 is large enough to affect the measured angular motion, Equation (3.1) must be fitted.

Figure 7.2 shows a tricyclic angular motion for which K_3 is 20 milliradians. Analysis of this quite complex motion is almost impossible without knowledge of the roll orientation. In some range tests K_3 is intentionally induced through control surface deflections in order to measure control effectiveness but in most tests it appears through the presence of slight manufacturing errors. Thus it is good policy to determine the rolling motion of all finned missiles undergoing ballistic range tests so that the effect of manufacturing error may be eliminated and the desired static and damping moment coefficient may be obtained.

The roll history can, then, be used to transform the motion to missile fixed coordinates by rotation of each angle through its corresponding roll orientation. (Figure 7.3)

$$\tilde{\xi} e^{-i\phi} = K_1 e^{i(\phi_1 - \phi)} + K_2 e^{i(\phi_2 - \phi)} + K_3 e^{i\phi_{30}} \qquad (3.2)$$

The result should be an epicyclic motion about the point $K_3 e^{i\phi_{30}}$. K_3 and ϕ_{30} are easy to determine since they are the polar coordinates of the center of this epicyclic motion. The origin may be moved to this point and the epicyclic graphical reduction described in Section 7.2 performed. The point could be rotated back through the angle ϕ about the new origin and a somewhat simpler epicycle obtained (Figure 7.4).

The least squares iteration may be performed for the differentials of the unknowns.

$$d\xi = \left[e^{\lambda_1 s} dK_{10} + sK_1 d\lambda_1 + iK_1(d\phi_{10} + sd\phi_1')\right] e^{i\phi_1}$$

$$+ \left[e^{\lambda_2 s} dK_{20} + sK_2 d\lambda_2 + iK_2(d\phi_{20} + sd\phi_2')\right] e^{i\phi_2}$$

$$+ (dK_3 + iK_3 d\phi_{30})\, e^{i\phi_3} \qquad (3.3)$$

Equation (3.3) can be simplified by the fact that the trim amplitude decays rapidly with increased spin rate and at low spin rates the sum of the frequencies is almost zero. For moderate Magnus moment coefficients, the difference of the damping exponents is also quite small for low spin. If the graphical analysis indicates that both of these quantities are small, the differential corrections can be reduced to an eight unknown problem by requiring them to be exactly zero.

$$d\xi = (e^{\lambda_1 s} dK_{10} + iK_1 d\phi_{10})\, e^{i\phi_1}$$

$$+ (e^{\lambda_1 s} dK_{20} + iK_2 d\phi_{20})\, e^{i\phi_2}$$

$$+ (dK_3 + iK_3 d\phi_{30})\, e^{i\phi_3}$$

$$+ s(K_1 e^{i\phi_1} + K_2 e^{i\phi_2})\, d\lambda_1$$

$$+ is(K_1 e^{i\phi_1} - K_2 e^{i\phi_2})\, d\phi_1' \qquad (3.4)$$

The assumption of constant or "almost" constant spin rate is a grave limitation to all of the tricyclic reductions discussed up to this point. In 1954 an entirely new approach to the reduction process was investigated[7-2]. In this approach the actual differential equation for $\tilde{\xi}$ (Equation 6.8.1) with T = 0 was programmed for an analog computer. The four initial conditions and four real parameters contained in H, M and A could be varied by changing potentiometer settings. Experimental values of $\tilde{\alpha}$ and $\tilde{\beta}$ were plotted versus

s and a series of solution curves for different values of the eight parameters calculated. A trial and error process could then be developed to obtain quite good fits of the data (Figure 7.5). An experienced operator could obtain good results in three or four hours.

After our only experienced operator was lost due to the intervention of the stork, the possibility of a completely mechanized reduction was re-examined. In Section 6.8, a closed form solution was derived under the minor approximation that the variation of P in the $\tilde{\xi}'$ of Equation (6.8.1) could be neglected.

$$\tilde{\xi} = K_1 e^{i\phi_1} + K_2 e^{i\phi_2} + \tilde{\xi}_A \tag{3.5}$$

$$\text{where } \tilde{\xi}_A = B \left[e^{(\lambda_1 + i\phi_1')s} \int_0^s e^{-(\lambda_1 + i\phi_1')s_1 + i\phi(s_1)} \, ds_1 \right.$$

$$\left. - e^{(\lambda_2 + i\phi_2')s} \int_0^s e^{-(\lambda_2 + i\phi_2')s_1 + i\phi(s_1)} \, ds_1 \right]$$

$$B = iA \left[\lambda_1 - \lambda_2 + i(\phi_1' - \phi_2') \right]^{-1}$$

The corresponding equation for the differential corrections is

$$\begin{aligned} d\xi = {} & (e^{\lambda_1 s} dK_{10} + iK_1 d\phi_{10}) e^{i\phi_1} \\ & + (e^{\lambda_2 s} dK_{20} + iK_2 d\phi_{20}) e^{i\phi_2} \\ & + (\xi_A / B) dB \\ & + \left(sK_1 e^{i\phi_1} + \frac{\partial \xi_A}{\partial \lambda_1}\right) d\lambda_1 \\ & + \left(sK_2 e^{i\phi_2} + \frac{\partial \xi_A}{\partial \lambda_2}\right) d\lambda_2 \\ & + \left(isK_1 e^{i\phi_1} + \frac{\partial \xi_A}{\partial \phi_1'}\right) d\phi_1' \\ & + \left(isK_2 e^{i\phi_2} + \frac{\partial \xi_A}{\partial \phi_2'}\right) d\phi_2' \end{aligned} \tag{3.6}$$

The initial values of the K_{jo} and ϕ_{jo}'s may be obtained from estimates of initial angles and angular velocities by use of Equations (6.6.21-22). The damping exponents can be initially taken to be zero and the frequencies calculated from the spin and estimated static moment coefficient. For each guessed value of B a sequence of iterations may be, then, computed by a digital computer, and convergence sought. Usually not more than three guesses of the complex number B are necessary to obtain successful convergence. A comparison of these two methods showed better fits (one milliradian standard error instead of two milliradians) but essentially the same values of M, H and A. The differential corrections method has the principal advantage of eliminating the need for a highly trained machine operator.

The swerving motion can be handled in a fashion quite similar to that for a symmetric missile. Two more unknowns must be considered in Equation (6.9.8), C_{Y_o} and C_{Z_o} and the integrals I_j computed. Either Equation (3.2) or Equation (3.5) may be used for $\tilde{\xi}$ and indicated integrations taken. These integrations and the least squares solution are extremely laborious for hand computation but can easily be programmed for a digital computing machine.

7.4 Criteria for Quality of Results

The various aerodynamic parameters, M, H, and T, are related to the frequencies and damping exponents of the angular motion. These in turn may be assigned statistical weights through the least squares differential corrections process. If A_{ij}'s are elements of the inverse matrix obtained from the least squares normal equation, the error in a function of two variables $z = f(x_i, x_j)$ may be computed by the statistical formula

$$\epsilon_z^2 = \left[\left(\frac{\partial f}{\partial x_i} \right)^2 A_{ii} + 2 \frac{\partial f}{\partial x_i} \frac{\partial f}{\partial x_j} A_{ij} + \left(\frac{\partial f}{\partial x_j} \right)^2 A_{jj} \right] \epsilon^2$$

$$\text{where } \epsilon^2 = \frac{\sum \left| \Delta \xi \right|^2}{n - k} \qquad (4.1)$$

k is the number of unknowns in the reduction.

Although Equation (4.1) has the attractive feature of giving a precise standard error for the aerodynamic parameters, it is a relatively blind calculation based on statistical assumptions which are hard to verify. In the drag analysis an alternate approach was used which considered the size of measurable effect of the drag force in comparison with the experimental accuracy. A similar but much more approximate criteria may be derived for the angular and swerving motion.

Since the static moment coefficient may be obtained from the frequency of one modal vector when the spin rate is known, essentially circular motion with amplitude at least three times the measurement error is sufficient. When the spin rate is not known both modal amplitudes must exceed three times the measurement error. These criteria assume that at least two revolutions of the given modal vector are observed and at least ten individual angles have been measured. Good values of the static moment coefficient may need less data but the amplitude requirements must be made larger. These amplitude requirements must be upped for reasonable determination of the damping exponents. With the amount of data specified above, both modal amplitudes should exceed five times the experimental accuracy in $\tilde{\xi}$ for good measurements of the damping rates.

The swerving motion of a symmetric missile is usually a spiral motion with amplitude determined by C_{L_α} and phase by $\frac{p\ell}{V} C_{N_{p\alpha}}$. The asymmetric lift term adds another spiral with amplitude proportional to $\left|C_{Y_o} + iC_{Z_o}\right|$. The average amplitude of these terms may be defined by the equations

$$R_L = C^*_{L_\alpha} \left|I_1\right|_{\text{average}} \tag{4.2}$$

$$R_{MF} = \left(\frac{p\ell}{V}\right)_o C^*_{N_{p\alpha}} \left|I_2\right|_{\text{average}} \tag{4.3}$$

$$R_A = \left|C^*_{Y_o} + iC^*_{Z_o}\right| \left|I_4\right|_{\text{average}} \tag{4.4}$$

If the average radius exceeds three times the distance error, the corresponding force coefficient should be reasonably well determined.

7.5 Experimental Results

Since the 1947 firings of the G. E. Dragonfly, a wide variety of configurations have been tested. These extend from simple geometrical shapes of spheres, cones and cone cylinders to precision scaled models of missiles such as the Nike Zeus, from 20mm bullets to models of the Jupiter and Atlas nose cones and from the Bolz-Nicolaides finned cone-cylinders to five inch models of a delta wing jet fighter. From this wealth of experimental work we will select four programs which not only illustrate the capabilities of ballistic range stability measurements but also contain results of intrinsic aerodynamic importance.

(1) Static Stability of Ring Airfoils.

Since the static moment and normal force are usually easily measured by wind tunnel tests, few ballistic range programs are initiated with the static stability as the primary objective. Of course, when the Reynolds number and/or the Mach number can be better simulated by a ballistic range test, exceptions to this rule are made. In addition to this, some shapes are difficult to mount properly in a wind tunnel and, therefore, may require range tests. A recent test of a series of ring airfoils was made for this reason.

These airfoils had a simple double wedge cross section and the wedge angle was varied from 20° to 35° (Figure 7.6). For all models the center of gravity was located at the midchord point and the maximum diameter, d, was 4.75 in. The other dimensions were

θ deg.	c in.	t/c
20	1.17	0.18
25	1.81	0.23
35	1.70	0.35

These models were tested at supersonic Mach numbers up to 3.7 and were found to be statically stable for Mach numbers in excess of 1.7. Below this Mach number, the internal flow choked and the rings tumbled.

The linearized supersonic theory for thin ring airfoils is quite similar to that for thin two-dimensional airfoils and was developed by H. Mirels[7-4] in 1948. According to this theory, the center of pressure is located at the midchord point and the lift coefficient, C_{L_α}, is $2/\beta$ where $\beta = \sqrt{M^2 - 1}$ and the reference area is one half the wetted area. Thus the theory predicts that the models actually tested should be neutrally stable.

This discrepancy from the thin airfoil theory may be due to the finite thickness of the models. The static moment coefficient is, therefore, plotted versus thickness ratio for M = 3.1. As can be seen from Figure 7.7, the moment coefficient is a linear function of t/c. These values of C_{M_α} actually imply a very large static margin. If C_{L_α} is estimated to be 50 percent greater than its thin airfoil value, the 35° wedge would possess a static margin of almost 30 percent. (Reference length was the chord of the airfoil.)

(2) Dynamic Stability of Cone Cylinders.

With the current emphasis on the glamorous hypersonic speeds, the appearance of severe subsonic or transonic problems is especially unpleasant for the aerodynamic engineer. Unfortunately, a manned re-entry vehicle must fly at these pedestrian velocities and the blunt ICBM nose cones have subsonic impact velocities. Ballistic range tests of a variety of low fineness ratio bodies of revolution similar to shapes used for re-entry have revealed an important subsonic dynamic stability problem. The linear damping moment coefficients have been positive at high subsonic velocities for certain center of gravity locations.

This interesting result was first obtained for cone cylinders with fineness ratio of five[7-5]. (Figure 7.8) The actual dependence of the damping moment coefficients on c.g. location was given in Table 6-1.

$$\hat{C}_{M_q} + \hat{C}_{M_{\dot{\alpha}}} = C_{M_q} + C_{M_{\dot{\alpha}}} - s_{cg}\left[(C_{N_q} + C_{N_{\dot{\alpha}}}) - C_{M_\alpha}\right] - s_{cg}^2 C_{N_\alpha} \qquad (5.1)$$

$$\hat{C}_{N_q} + \hat{C}_{N_{\dot{\alpha}}} = C_{N_q} + C_{N_{\dot{\alpha}}} + s_{cg} C_{N_\alpha} \qquad (5.2)$$

According to Equation (5.1), the sum of the damping moment coefficients is a quadratic function of c.g. location. This equation may be simplified for ballistic range use by the introduction of a modified damping moment coefficient

$$\left[\hat{C}_{M_q} + \hat{C}_{M_{\dot{\alpha}}}\right] = \hat{C}_{M_q} + \hat{C}_{M_{\dot{\alpha}}} - s_{cg}\,\hat{C}_{M_\alpha} \tag{5.3}$$

This quantity is directly computable from the directly measured quantities $C_{M_q} + C_{M_{\dot{\alpha}}}$ and C_{M_α} and the distance to the c.g. from some reference c.g. location. For this modified damping coefficient sum the c.g. dependence is linear and the damping force coefficient sum at the reference point is the slope of a line fitting experimental points in a $\left[\hat{C}_{M_q} + \hat{C}_{M_{\dot{\alpha}}}\right]$ versus s_{cg} plot.

$$\left[\hat{C}_{M_q} + \hat{C}_{M_{\dot{\alpha}}}\right] = C_{M_q} + C_{M_{\dot{\alpha}}} - s_{cg}\,(C_{N_q} + C_{N_{\dot{\alpha}}}) \tag{5.4}$$

Three c.g. locations were used in the tests of the cone cylinder model. These were the centroid, 0.40 caliber forward of the centroid and 0.45 caliber rear of the centroid. The centroid was taken as the reference point and modified damping moment coefficients were plotted against c.g. location for two Mach numbers (Figure 7.9).

At M = 1.26 the scatter of data is rather poor but the subsonic points have very little scatter and are definitely linear with c.g. location. Since the modified damping moment coefficients at the centroid reduce to the unmodified coefficients, we see that $C_{M_q} + C_{M_{\dot{\alpha}}}$ is definitely positive at the centroid for M = .8. Indeed the further information that C_{M_α} at the rear c.g. is 3.7 can be used to show this sum to be positive at the rear c.g. as well.

These values of $C_{M_q} + C_{M_{\dot{\alpha}}}$ are sufficient to make H negative and the missile with the middle or rear c.g. location must, therefore, be dynamically unstable. To add insult to injury, it was found that spinning cone cylinders at M = .8 were dynamically unstable for all c.g. locations. This state of affairs is caused by the Magnus moment. In Figure 7.10, the Magnus moment

coefficient is plotted versus c.g. location. As can be seen from this figure, the center of pressure of the Magnus moment changes radically with Mach number while the Magnus force coefficient which is the slope of the lines in this plot is relatively unaffected. The large negative values of $C_{M_{p\alpha}}$ make T negative and, thus, the dynamic stability factor, s_d, will be negative when H is positive. According to the stability analysis of the preceding chapter, dynamic instability will therefore occur for any spin rate. This simple configuration displays two of the three ways in which a statically unstable missile can not be made dynamically stable by spin. The fourth illustrative program will include the third way ($s_d > 2$).

(3) Magnus Characteristics of Finned Missiles.

A symmetric finned missile with a reasonable stability margin does not require spin for stability and, therefore, a knowledge of its Magnus characteristics is unnecessary. Unfortunately, perfectly symmetric missiles are impossible to manufacture and the aerodynamic asymmetries possible with usual manufacturing tolerances are sufficient to cause undesirable dispersion when the spin rate is zero. Usually this spin rate required to reduce dispersion due to asymmetries is not large enough to encounter Magnus instability although care is required to avoid resonance. It is important to know what are the spin bounds for Magnus instability if any so that too high a spin rate is not induced.

One case where high spin rates may not be avoided is that of a finned rocket with short burning time with respect to the pitching period. In order to avoid dispersion due to rocket jet misalignment, several revolutions during burning should be induced and quite large spin rates are possible. A knowledge of the Magnus characteristics of a proposed rocket shape of this type would be essential to prove the feasibility of its satisfactory design.

A brief examination of the theory of Section 6.7 shows that Magnus instability is impossible if the dynamic stability factor is between zero and two. This bright possibility of no spin upper bound is considerably dimmed by the fact that s_d for every finned missile whose Magnus characteristics have been measured has been found to be outside this interval. Thus, an upper bound on spin for dynamic stability is always present.

A study of the properties of two finned missiles is sufficient to obtain characteristic values of the coefficients and a feeling for the effect of these coefficients on the spin bounds. These missiles -- the Basic Finner[7-6, 7-7] and the 127/60mm Anti-Aircraft Missile[7-8] -- are shown in Figures 7.11 and 7.12 and some of their physical properties are listed below.

TABLE

	$\ell = d$	L/D	c.g.*	k_y	I_x/I_y
Basic Finner	.79"	10	3.90	2.4	.024
127/60mm Missile	2.36"	17	8.25	3.9	.011

The Basic Finner has a ten caliber long cone-cylinder body with 20° total cone angle. Its four simple wedge fins are square in planeform with chord equal to the body diameter, d, and have a thickness ratio of .08. This missile has been tested with various c.g. locations and at various Mach numbers both with and without fins[7-9].

The 127/60mm missile was the longest finned missile tested in a ballistic range.** Its 127mm span fins are mounted at the end of a 39 inch long body whose maximum body diameter is 60mm. This missile is fired from a smoothbore 127mm gun by use of a center ring sabot.

The various aerodynamic coefficients for these missiles are plotted versus Mach number in Figures 7.13-15. Since several c.g. locations were used in the flight tests of the Basic Finner, the normal force coefficient could be measured both directly from the swerving motion as well as indirectly from the static moment coefficient for different c.g. locations. C_{N_α} for the 127/60mm missile could only be obtained from the swerving motion. The normal force is essentially the same for both missiles. The greater effective area of the Basic Finner fins does provide slightly more lift. These fins actually deliver four times the lift of the body as can be seen from the body only curve.

---

* From base in body diameters.

** Recently the 45.5 inch long five inch high altitude gun probe was tested in the Transonic Range and established a new length record.[7-13]

The damping moment and Magnus moment data for the 127/60mm missile are much poorer than those of the Basic Finner. The 127/60mm fins were usually at least slightly damaged by sabot fragments. This damage introduced aerodynamic asymmetry. Since the spin was not measured during this program, a tricycle reduction could not be employed. The epicycle reductions which were used had average to poor fits and corresponding poorer determination of the damping and Magnus coefficients.

The much larger $C_{M_q} + C_{M_{\dot{\alpha}}}$ for the 127/60mm is due to the fact that its fins have twice the lever arm that those of the Basic Finner have and, therefore, the same angular velocity will induce twice as large a cross velocity. This would lead us to expect damping moments four times larger and this expectation is surprisingly well verified by Figure 7.14.

The Magnus moment coefficient behavior for these two missiles is completely unexpected. The moments are even opposite in algebraic sign! A simple physical model can be constructed to explain the positive Magnus moment but not the negative moment.

The 127/60mm missile increases its spin rate throughout its flight through the range. Thus, each fin has a associated force in the direction of rotation. Normally, these forces cancel each other and provide no yaw moment but only a roll moment. The fins, however, are partly in the boundary layer separated flow of the body and it is not unreasonable to expect the lee side fin of a missile at angle of attack to have less effective area and hence less lift force than that of the windward side fin. This unbalanced force will cause the missile's nose to rotate in a direction of the spin and, thereby, generate a positive Magnus moment coefficient.

Since the Basic Finner does not have its fins in a separated flow and has its spin rate at the steady state rate for most of its flight, it is not surprising that its Magnus moment is quite different. An explanation for its negative coefficient is not possible at this time.

These radically different Magnus moments provide essentially different dynamic stability factors. s_d for the Basic Finner is negative while for the 127/60mm it is positive and greater than two. The dynamic stability factors and their associated upper bounds for spin are plotted in Figure 7.16.

(4) Effect of Body Length on $C_{M_{p\alpha}}$ and $C_{M_q} + C_{M_{\dot{\alpha}}}$.

Immediately after World War II, the linearized theory of projectile motion was reasonably well-understood but few actual values of the damping and Magnus coefficients were available. A joint Army-Navy program was initiated to fill this void. Since at that time these measurements could only be made by a ballistic range and the only available range was the BRL Aerodynamics Range, the Army agreed to construct, measure, and launch the models while the Navy provided its data analysis facilities at MIT. The bodies tested were secant ogive cylinders with two caliber heads and three different cylinder lengths. The radius of the secant ogive was twice that of a tangent ogive and was so selected for minimum drag. The total lengths of these models were five, seven, and nine diameters. Three center of gravity locations were used for each body length and tests were made of each configuration at three different supersonic Mach numbers. Thus, twenty-seven sets of linear coefficients were obtained from this ambitious program[7-1]. From this mass of data we will extract several interesting results.

In Figure 7.17 the Magnus moment coefficient for the various total lengths and center of gravity locations is plotted for a Mach number of 1.8. The scatter of the data is clearly small enough to allow a good determination of the Magnus force coefficient and its center of pressure.

A rather simple model for the Magnus force on a cylinder has been obtained by J. C. Martin[7-10]. According to this theory the boundary layer thickness on a cylinder at angle of attack grows as one moves from the windward side to the lee side. If the cylinder is spinning, the spin will cause the plane of symmetry of this boundary layer configurations to rotate to a position out of the plane of the angle of attack. The pressure distribution for the resulting effective shape can, then, be found by the usual slender body approximations and integrated to yield a force component normal to the plane of the angle of attack. For a laminar boundary layer Martin shows that the Magnus force coefficient has the form

$$C_{N_{p\alpha}} = A\hat{L}\delta^* \qquad (5.5)$$

where $\hat{L}$ is the cylinder length in calibers

δ^* is the boundary layer displacement thickness in diameters

and A is a parameter which is independent of length.

The actual boundary layer, however, was partly turbulent and the actual shape was not a cylinder. The displacement for either a laminar or turbulent boundary layer can usually be expressed as a power of the length whose exponent is 1/2 for laminar flow and approximately 1/5 for turbulent flow. If we assume a nth power variation, the c.p. for the Magnus force can be computed.

$$C.P._M = \frac{1}{C_{N_{p\alpha}}} \int_0^{\hat{L}} \hat{L} \frac{dC_{N_{p\alpha}}}{d\hat{L}} \, d\hat{L}$$

$$= \left(\frac{2 - n}{3 - n}\right) \hat{L} \qquad (5.6)$$

where $3/5 < \frac{2 - n}{3 - n} < 9/14$ for $1/2 > n > 1/5$.

The presence of the nose may be incorporated in the theory by replacing the total model length, L, by an effective cylinder length $L - L_n$ where L_n is the same for all models at the same Mach number. Equation (5.6) assumes the form

$$C.P._M = \left(\frac{2 - n}{3 - n}\right) (L - L_n) \qquad (5.7)$$

The possible range of the coefficient in Equation 4.7 is between .600 and .643 and, hence, this $C.P._M$ dependence on type of boundary layer is quite small. The $C.P._M$ is plotted against length in Figure 7.18 and lines fitted with slope .64. The accuracy of this predicted dependence of $C.P._M$ on length is much better than our approximations deserve.

In Figure 7.19, the modified damping coefficients are plotted versus c.g. location. This figure also shows that the force coefficient at the centroid and damping moment coefficient of the centroid are reasonably well determined.

Slender body values of these coefficients have been computed[7-11]. For bodies of revolution whose reference length is base diameter and reference area is the base area then these slender body values reduce to simple expressions

$$C_{N_q} = 2\,\hat{x}_{cg} \tag{5.8}$$

$$C_{N_{\dot{\alpha}}} = \frac{8}{\pi}\,\hat{V} \tag{5.9}$$

$$C_{M_q} = -\,2\,\hat{x}_{cg}^2 + \frac{8}{\pi}\,(\hat{V})(\hat{x}_{cg} - \hat{x}_c) \tag{5.10}$$

$$C_{M_{\dot{\alpha}}} = -\,\frac{8}{\pi}\,(\hat{V})(\hat{x}_{cg} - \hat{x}_c) \tag{5.11}$$

where $\hat{x}_{cg}$ is the distance from the base to the center of gravity in diameters

$\hat{V}$ is body volume in cubed diameters

and $\hat{x}_c$ is distance from the base to the centroid in diameters.

According to these relations $C_{N_q} + C_{N_{\dot{\alpha}}}$ at the centroid is a complicated function of added cylinder length, but $C_{M_q} + C_{M_{\dot{\alpha}}}$ at the centroid has an exceptionally simple form.

$$(C_{M_q} + C_{M_{\dot{\alpha}}})_c = -\,2\,\hat{x}_c^2 \tag{5.12}$$

In Figure (7.20), the ratio of $(C_{M_q} + C_{M_{\dot{\alpha}}})_c$ to $\hat{x}_c^2$ is plotted for the three body lengths and three Mach numbers and compared with the predicted value of -2. The predicted dependence on length is good but the coefficient should be decreased from -2 to -3.5.

A study of the dynamic stability of the nine caliber long models shows that the third possible form of linear instability is actually physically realizable ($s_d > 2$). At a Mach number of 1.8 the forward center of gravity models have a s_d of 2.5. Thus, all three combinations of aerodynamic coefficients for which a body of revolution can not be made dynamically stable by spin ($s_d < 0$, $s_d > 2$, $H > 0$) have been observed.

REFERENCES

7-1* Murphy, C. H. and Schmidt, L. E. The Effect of Length on the Aerodynamic Characteristics of Bodies of Revolution in Supersonic Flight. BRL Report No. 876, August 1953.

7-2 Schmidt, Jo Ann. A Study of the Resonating Yawing Motion of Asymmetrical Missiles by Means of Analog Computer Simulation. BRL Report No. 922, November 1954.

7-3 Murphy, C. H. and Piddington, M. J. Aerodynamic Properties of Ring Airfoils in Supersonic Flight. Journal of Aerospace Sciences, Vol. 27, pp. 954-5, December 1960.

7-4 Mirels, Harold. Theoretical Wave Drag and Lift of Thin Supersonic Ring Airfoils. NACA TN No. 1678, August 1948.

7-5* Schmidt, L. E. The Dynamic Properties of Pure Cones and Cone Cylinders. BRL Memorandum Report No. 759, January 1954.

7-6* Nicolaides, J. D. and MacAllister, L. C. A Review of Aeroballistic Range Research on Winged and/or Finned Missiles. Bureau of Ordnance Ballistic Technical Note No. 5, 1955.

7-7* MacAllister, L. C. The Aerodynamic Properties of a Simple Non-Rolling Finned Cone-Cylinder Configuration Between Mach Numbers 1.0 and 2.5. BRL Report 934, May 1955.

7-8* Nicolaides, J. D. A Transonic Range Study of the Free Flight Performance of the 127/60mm Anti-Aircraft Missile T-144E2. BRL Memorandum Report No. 746, December 1953.

7-9 Boyer, E. D. Free Flight Range Tests of a 10-Caliber Cone Cylinder. BRL Memorandum Report No. 1258, April 1960.

7-10 Martin, J. C. On Magnus Effects Caused by the Boundary-Layer Displacement Thickness on Bodies of Revolution at Small Angles of Attack. Journal of Aeronautical Sciences, Vol. 24, pp. 421-429, June 1957.

7-11 Wood, R. M. and Murphy, C. H. Aerodynamic Derivatives for Both Steady and Nonsteady Motion of Slender Bodies. Journal of the Aeronautical Sciences, Vol. 22, pp. 870-71, December 1955.

---

* The aerodynamic coefficients of these references differ from those of this book in two ways: (1) The force coefficients (C_N's) have the opposite signs; (2) the coefficients of angular velocities ($C_{N_{p\alpha}}$, $C_{N_q} + C_{N_{\dot{\alpha}}}$, $C_{M_{p\alpha}}$, $C_{M_q} + C_{M_{\dot{\alpha}}}$) are twice those of this book due to the use of $\ell/2$ instead of ℓ in reducing the angular velocities to dimensionless quantities.

7-12 Nicolaides, J. D. and Bradey, J. J., "Magnus Moment on Pure Cones in Supersonic Flight", NAVORD Report 6183, January 1959.

7-13 Marks, S. T., Boyer, E. D., "A Second Test of an Upper Atmosphere Gun Probe System", BRL MR 1464, April 1963.

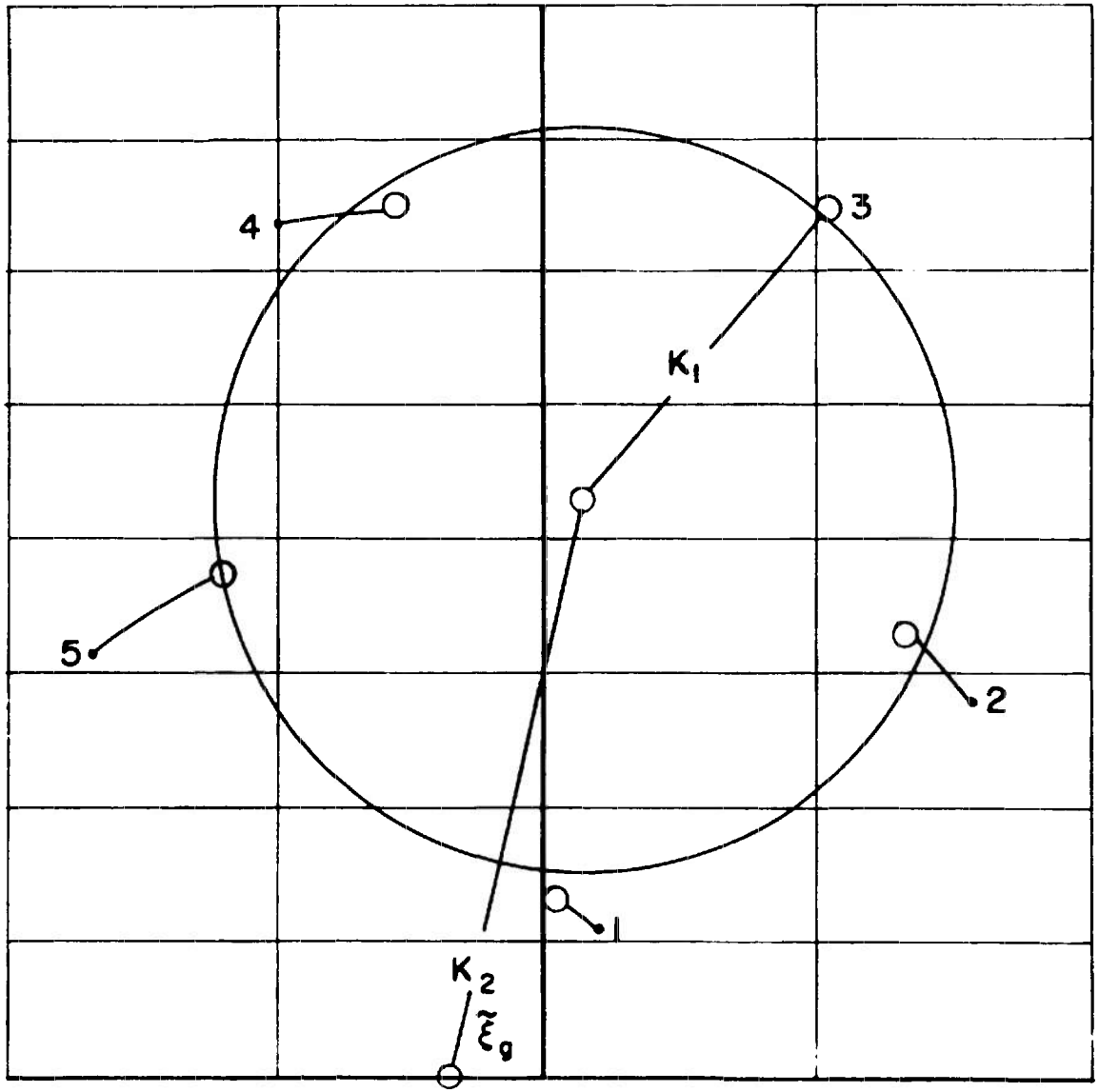

FIG. 7.1

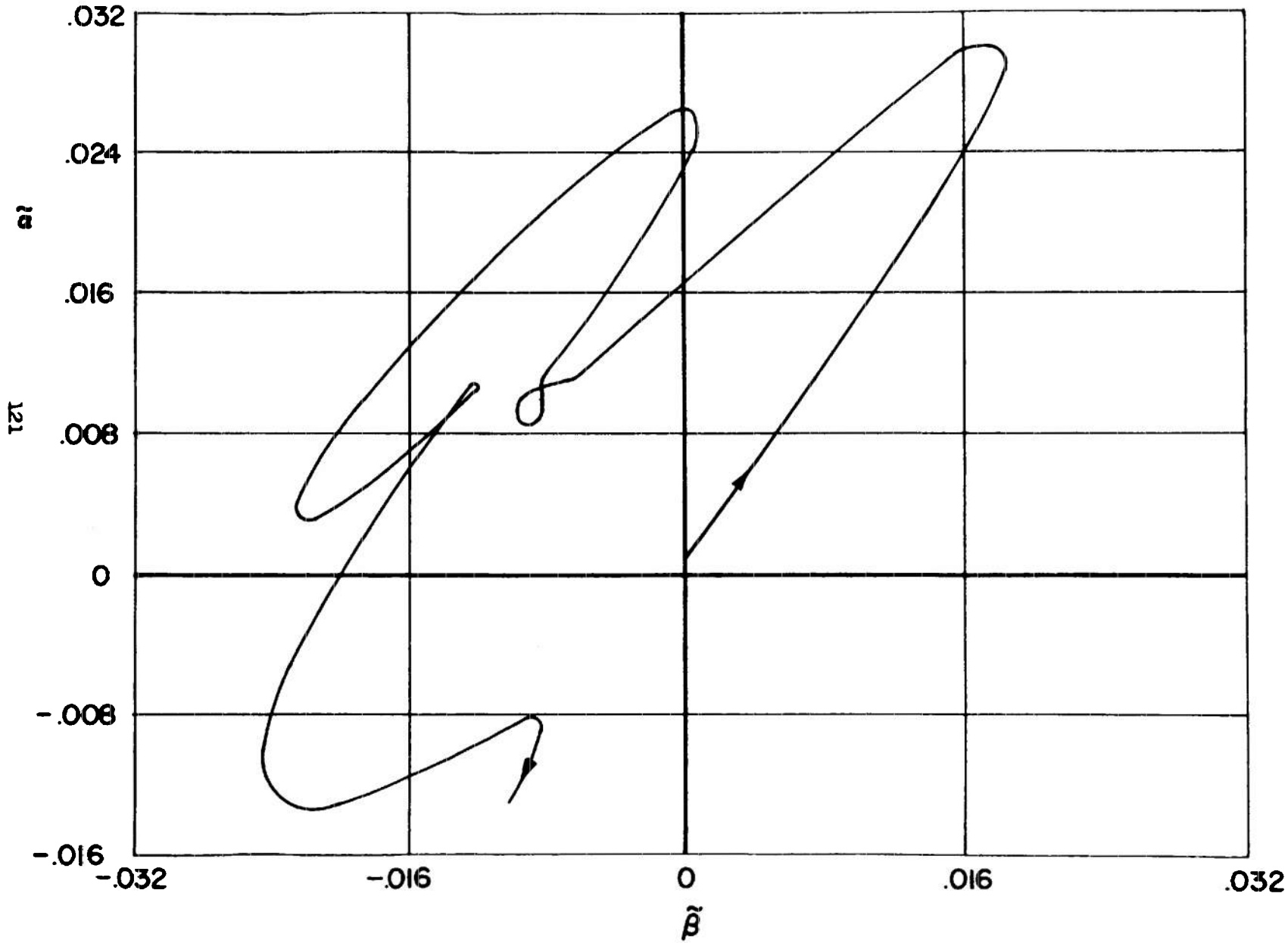

FIG. 7.2

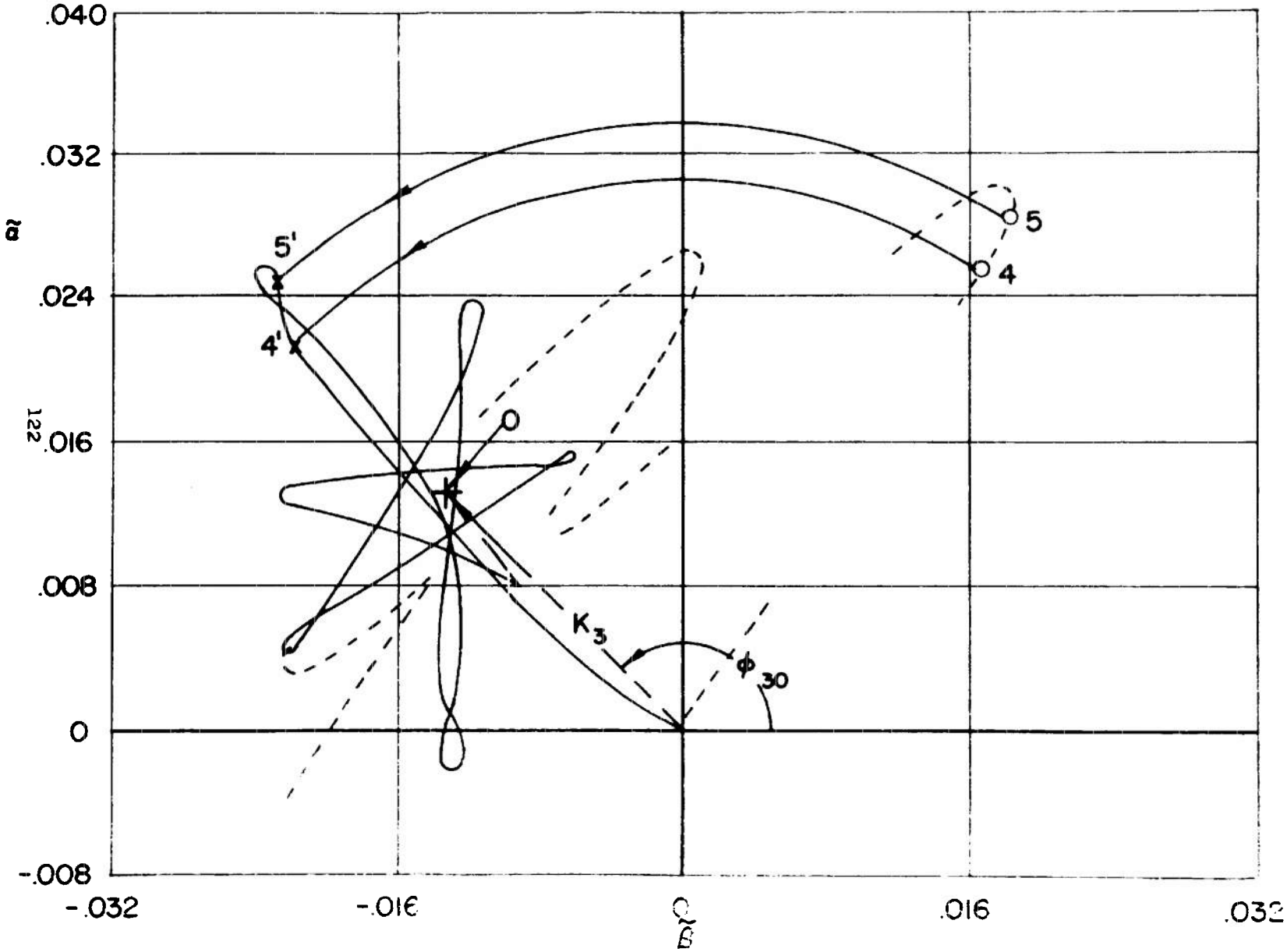
.040
.032
.024
.016
.008
0
-.008
-.032
-.016
.016
.032
$\tilde{\alpha}$
$\tilde{\beta}$
5'
4'
5
4
0
K
K_3
ϕ_{30}

FIG. 7 3

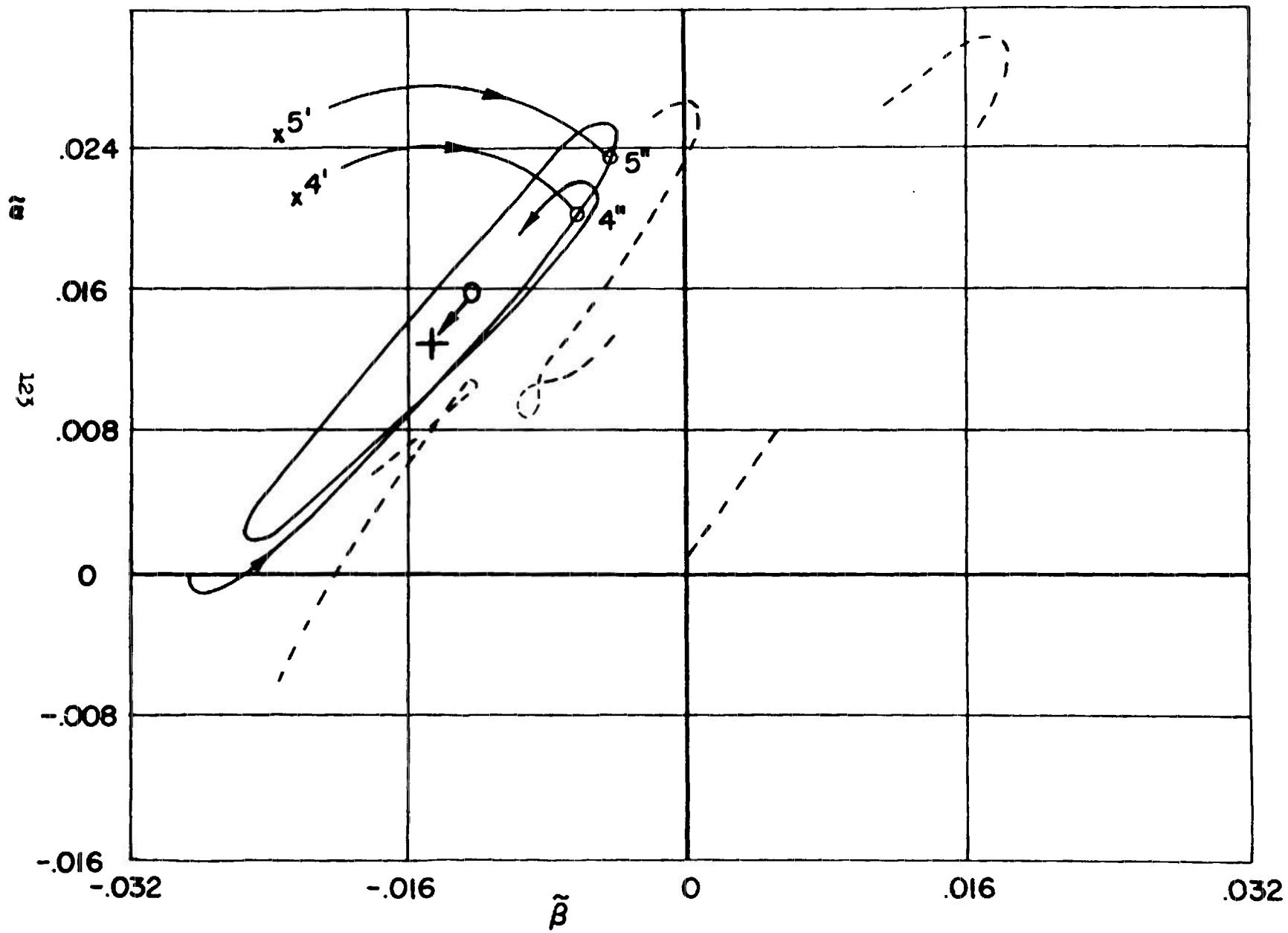
x5'
x4'
5"
4"
0
.024
.016
.008
0
-.008
-.016
-.032
-.016
0
.016
.032
$\tilde{\alpha}$
$\tilde{\beta}$
123

FIG. 7.4

ANGULAR MOTION OF ASYMMETRIC MISSILE WITH VARYING ROLL

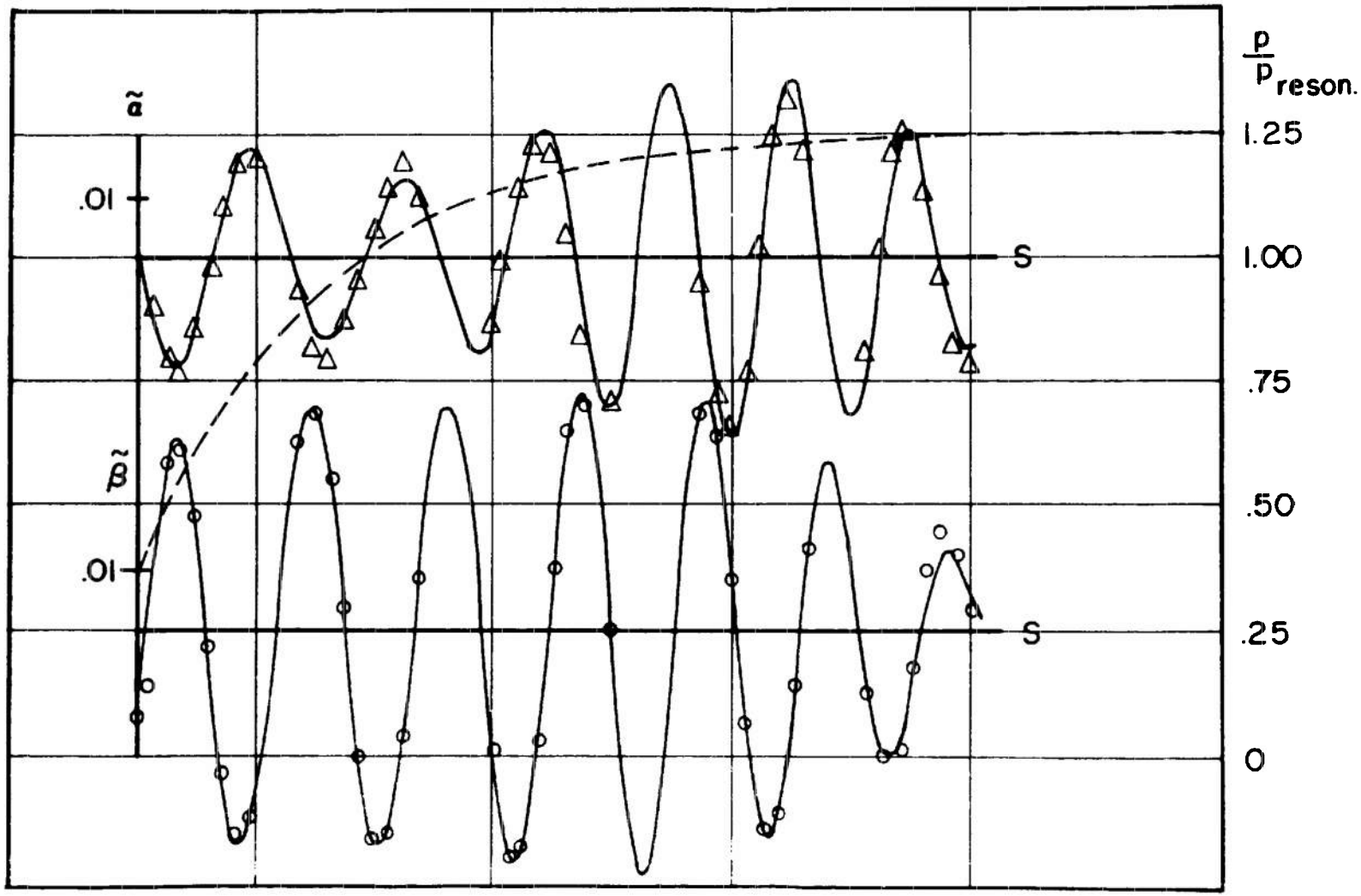

FIG. 7.5

RING AIRFOIL

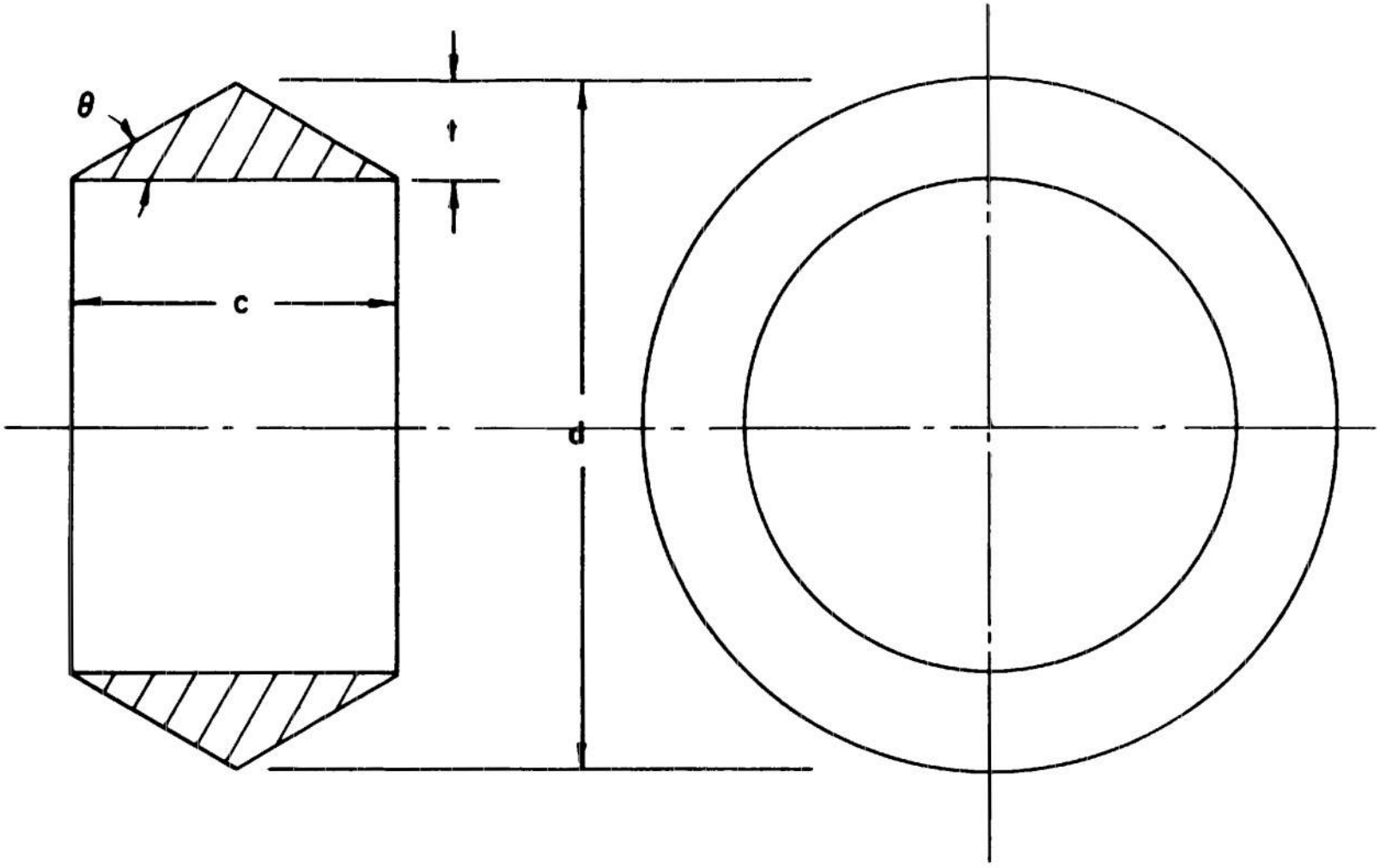

FIG. 7.6

STATIC MOMENT COEFFICIENT
VS
THICKNESS RATIO

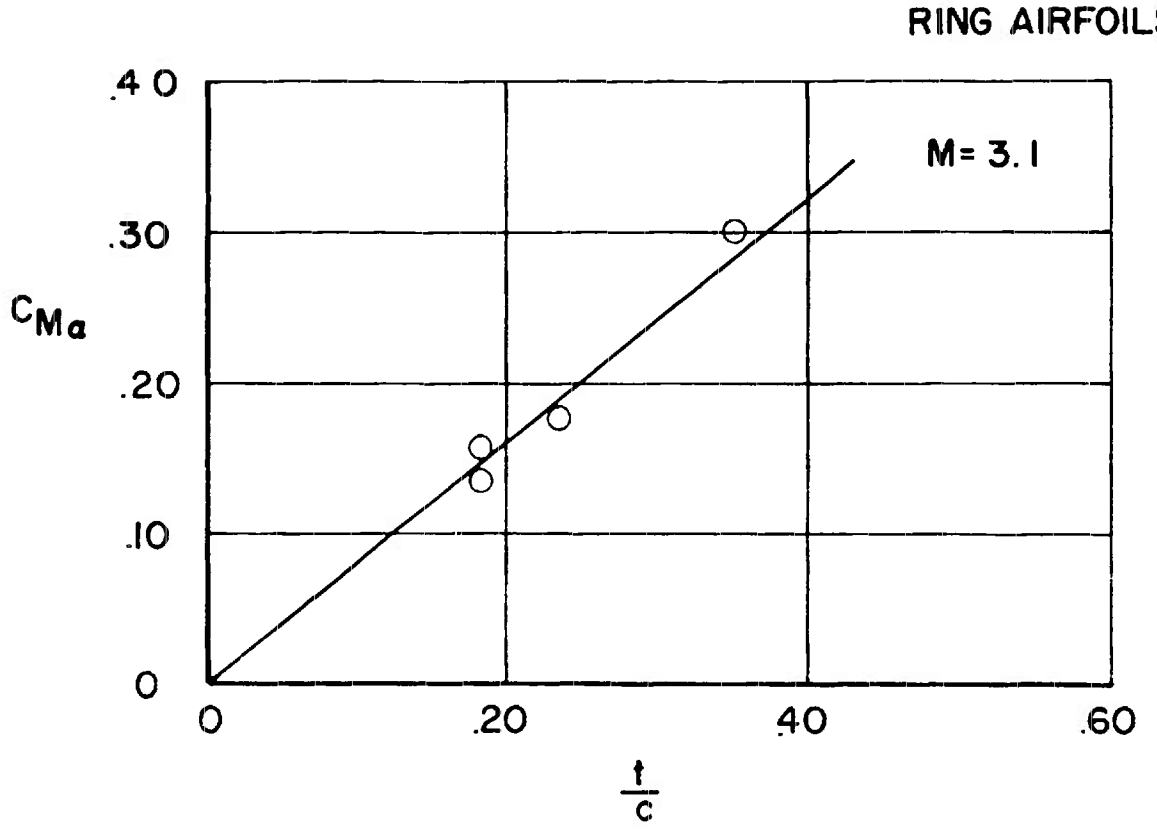

FIG. 7.7

CONE CYLINDER

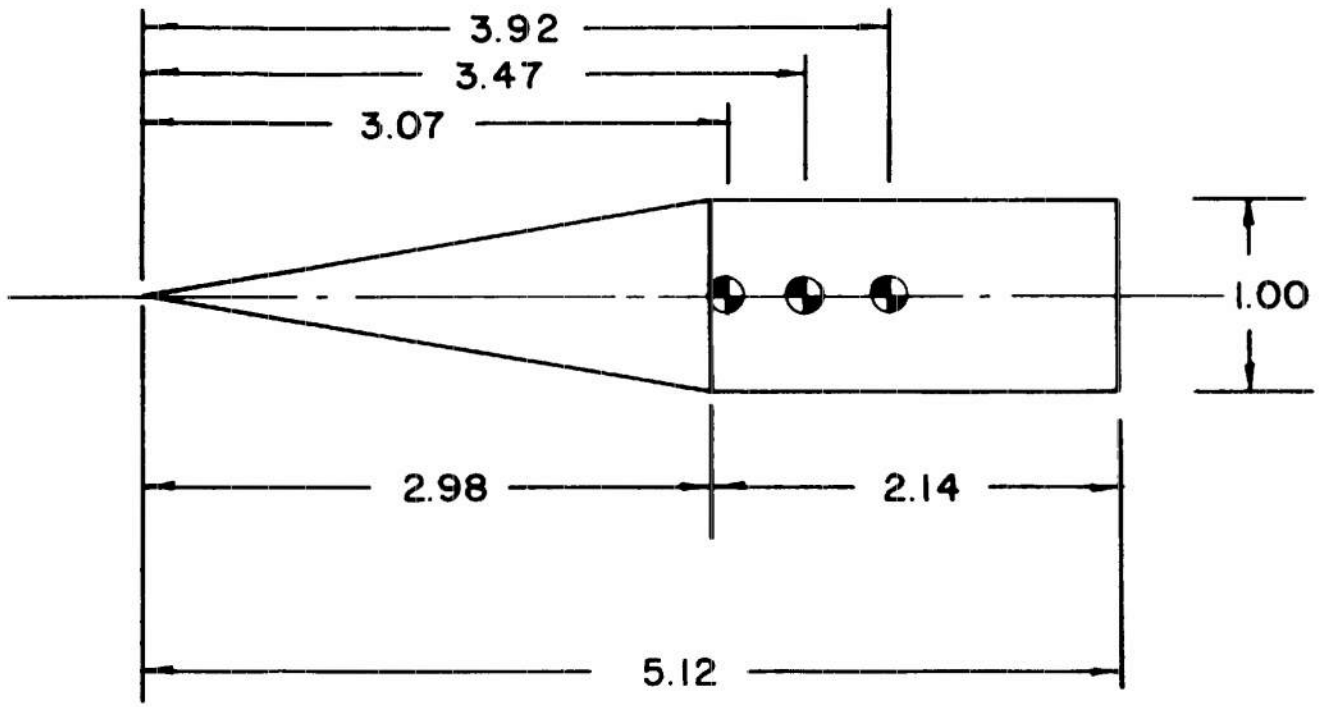

NOTE: ALL DIMENSIONS ARE IN CALIBERS

FIG. 7.8

MODIFIED DAMPING MOMENT COEFFICIENTS VS CENTER OF GRAVITY

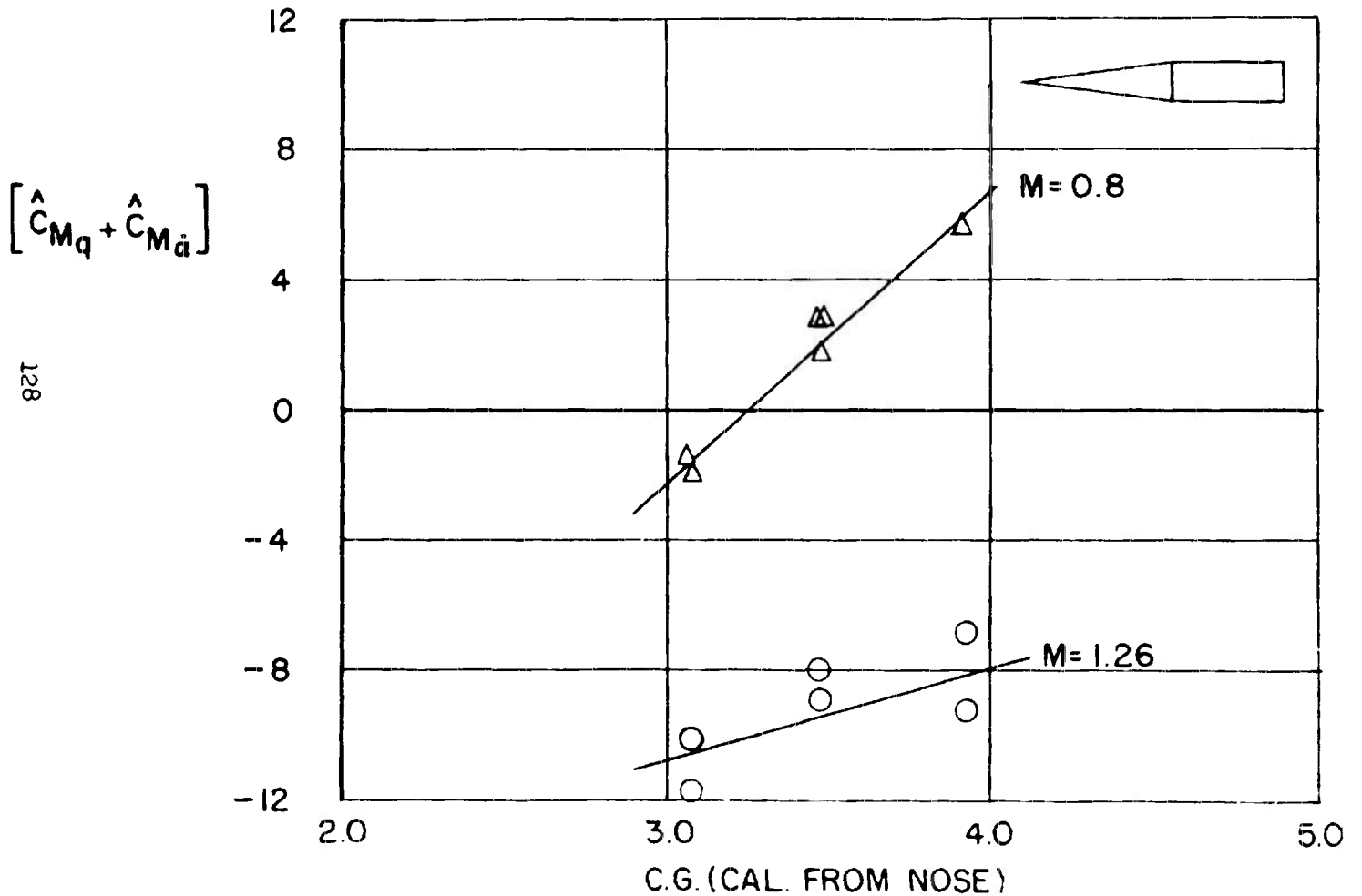

FIG. 7.9

MAGNUS MOMENT COEFFICIENT VS CENTER OF GRAVITY

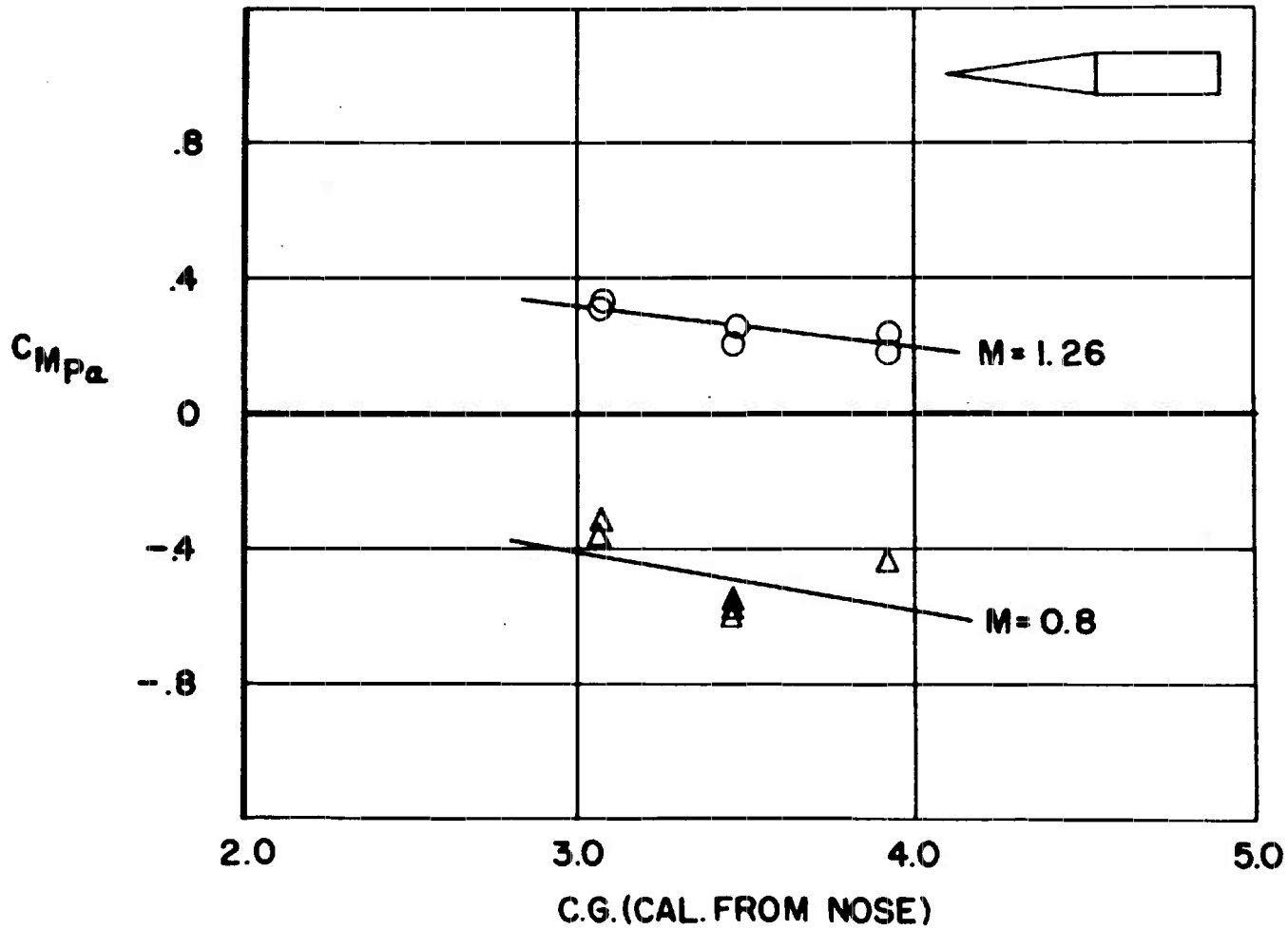

FIG. 7.10

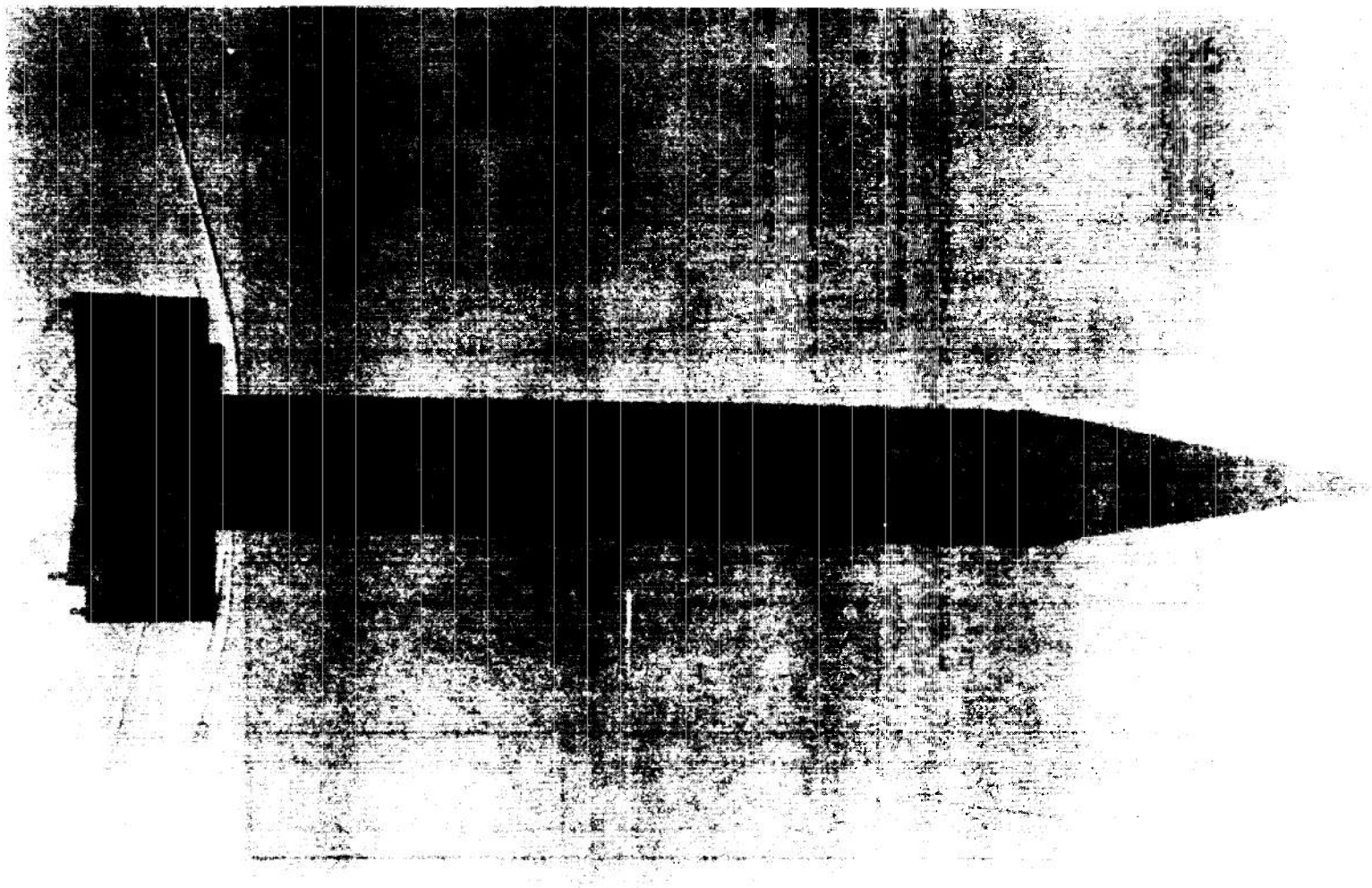

SHADOWGRAPH OF BASIC FINNER

FIG. 7.11

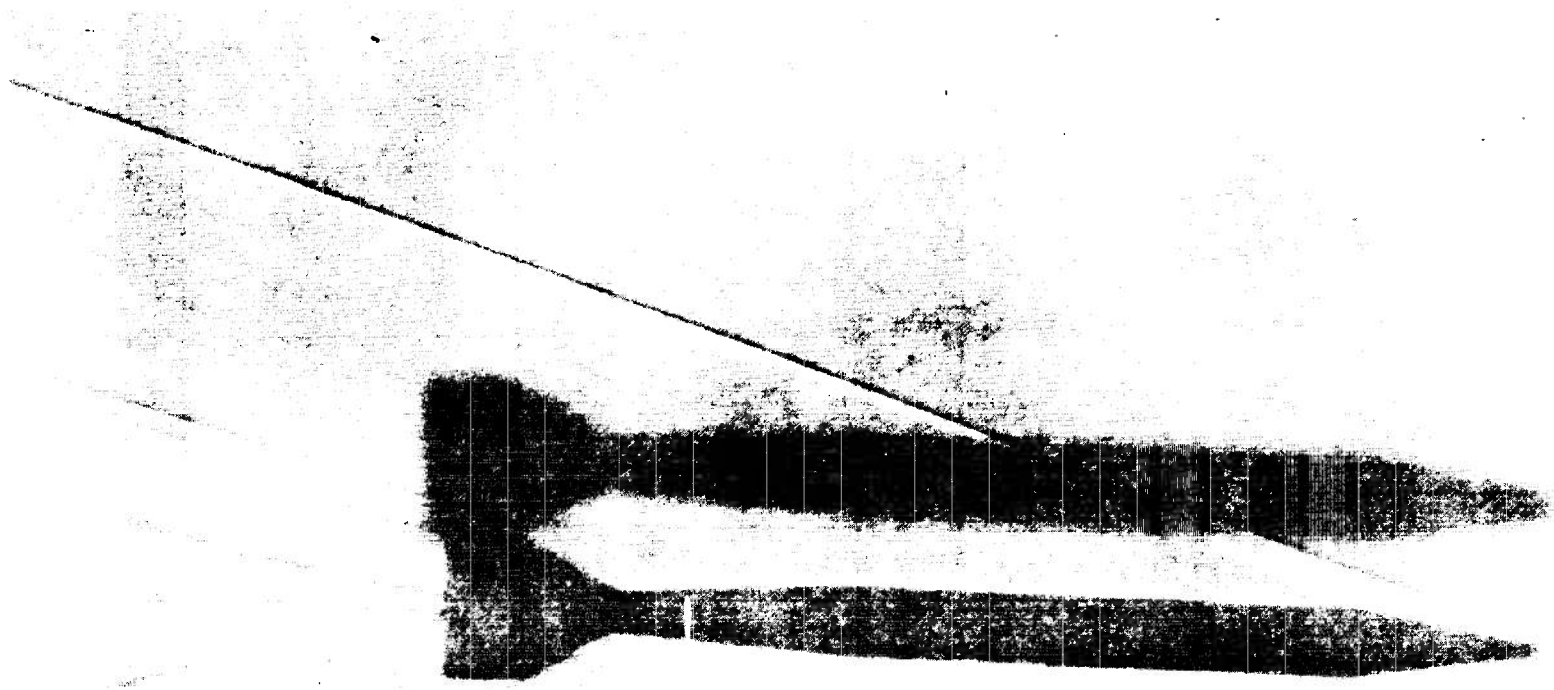

SHADOWGRAPH OF 127/60 mm ANTI-AIRCRAFT MISSILE

FIG. 7.12

NORMAL FORCE COEFFICIENT
VS
MACH NUMBER

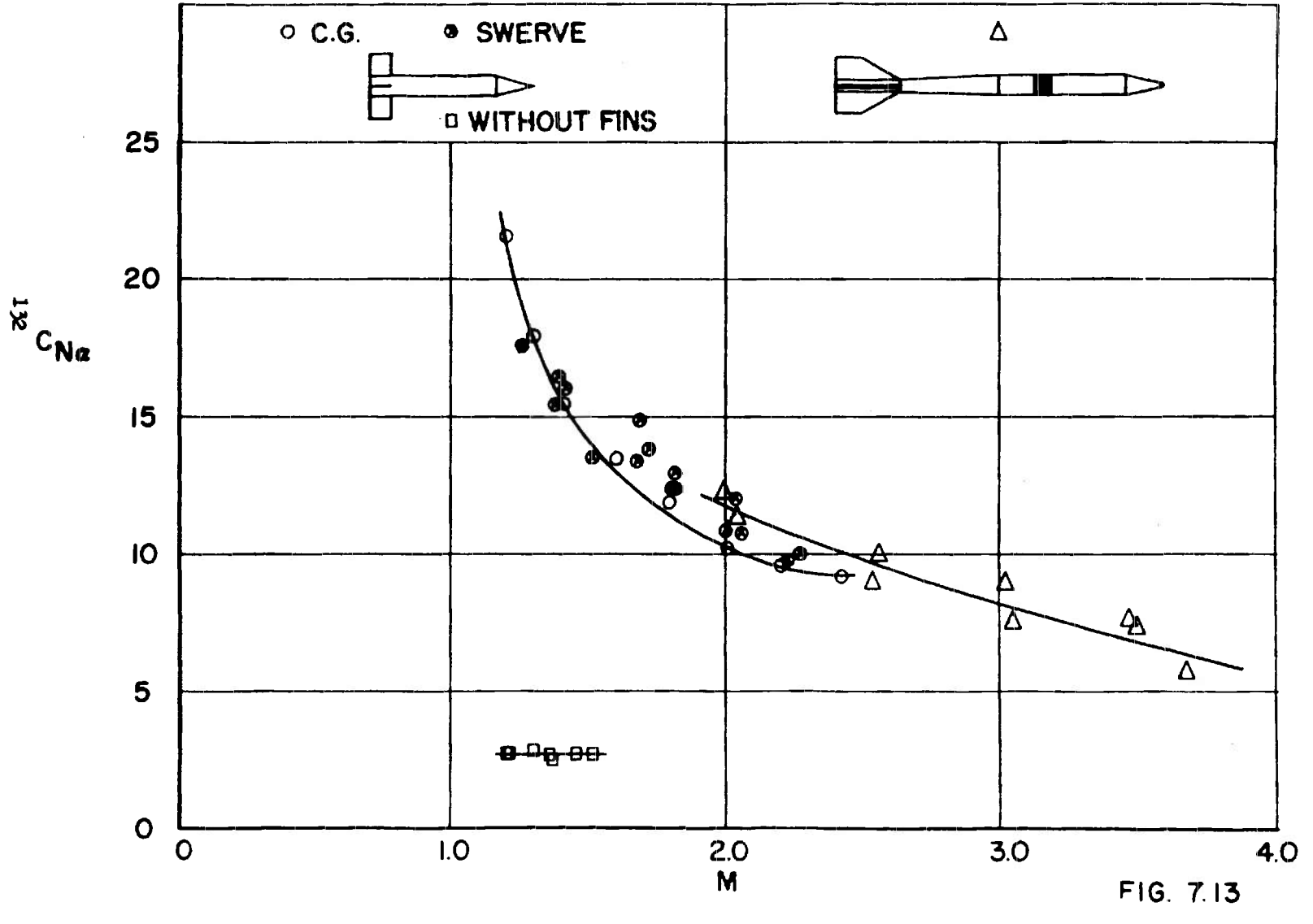

FIG. 7.13

DAMPING MOMENT COEFFICIENTS VS MACH NUMBER

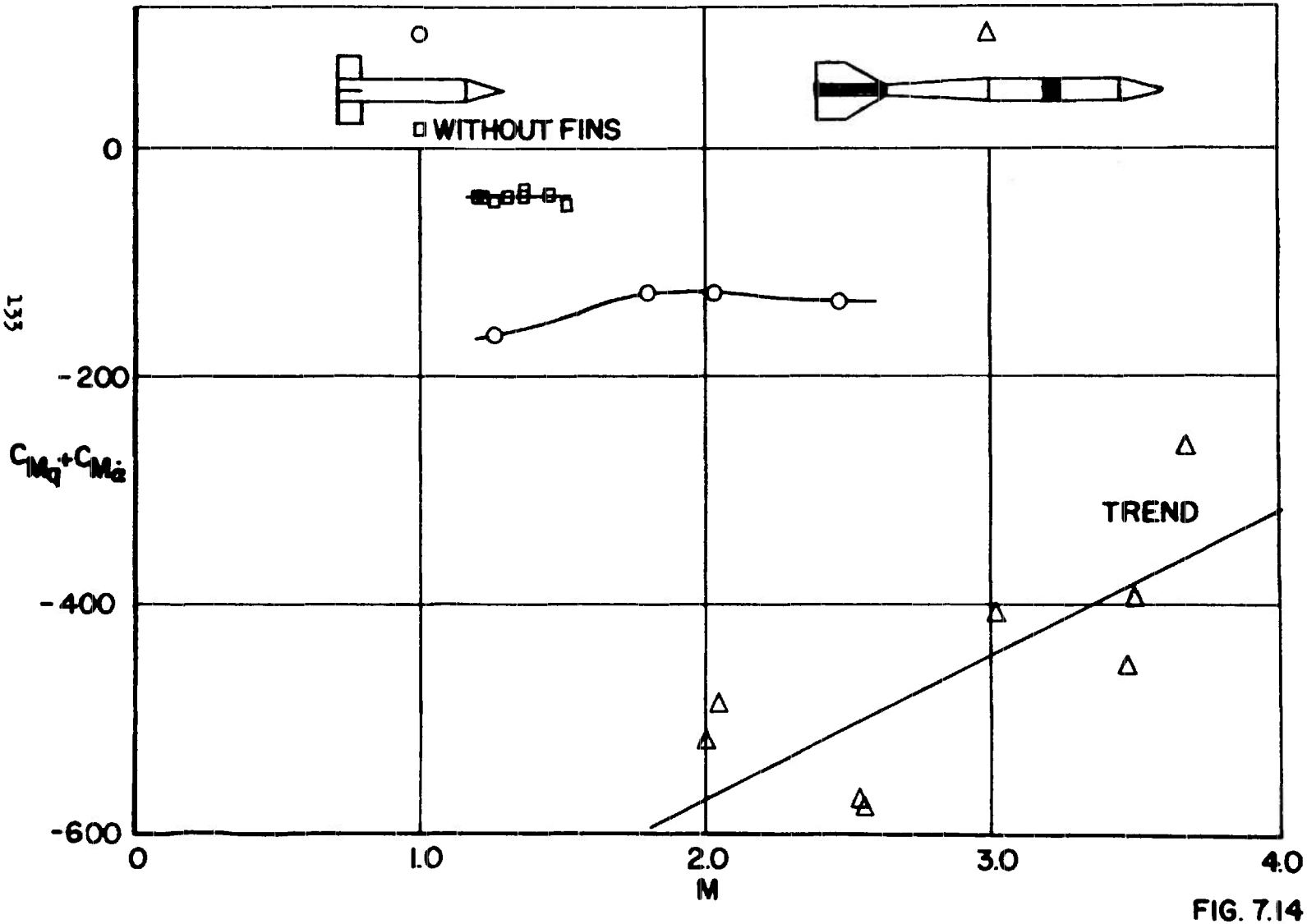

FIG. 7.14

MAGNUS MOMENT COEFFICIENT
VS
MACH NUMBER

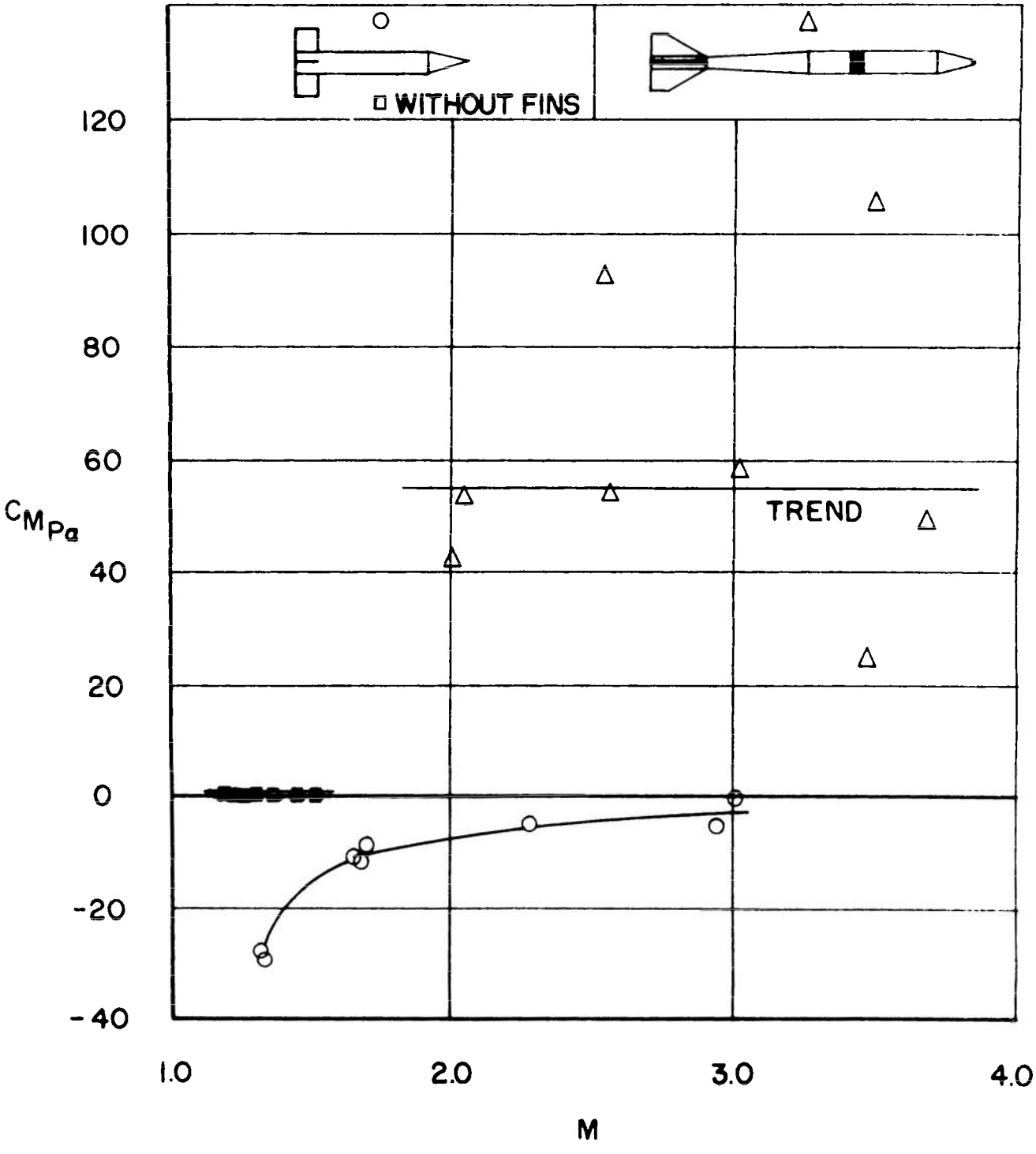

FIG. 7.15

DYNAMIC STABILITY CHARACTERISTICS

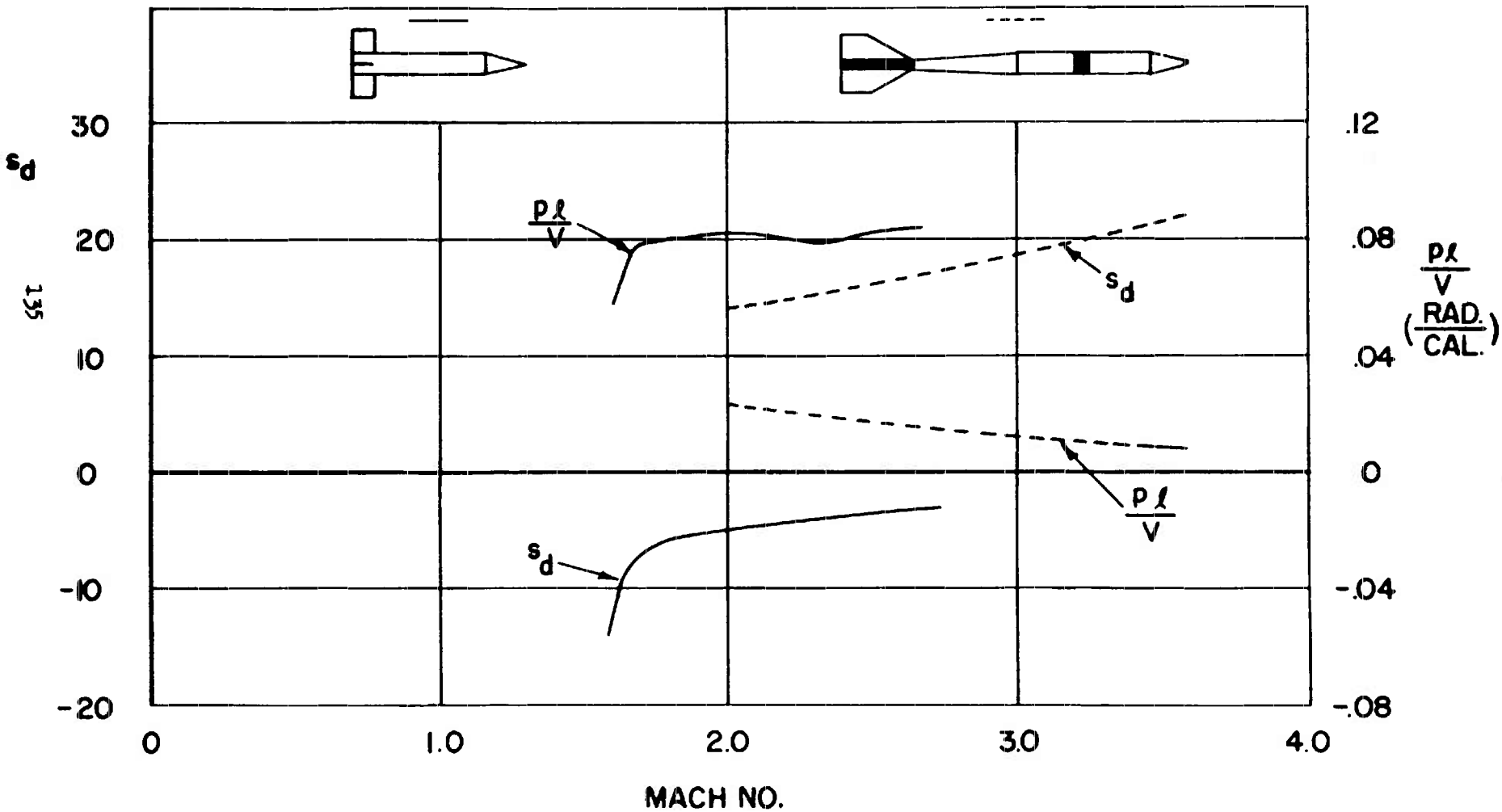

FIG. 7.16

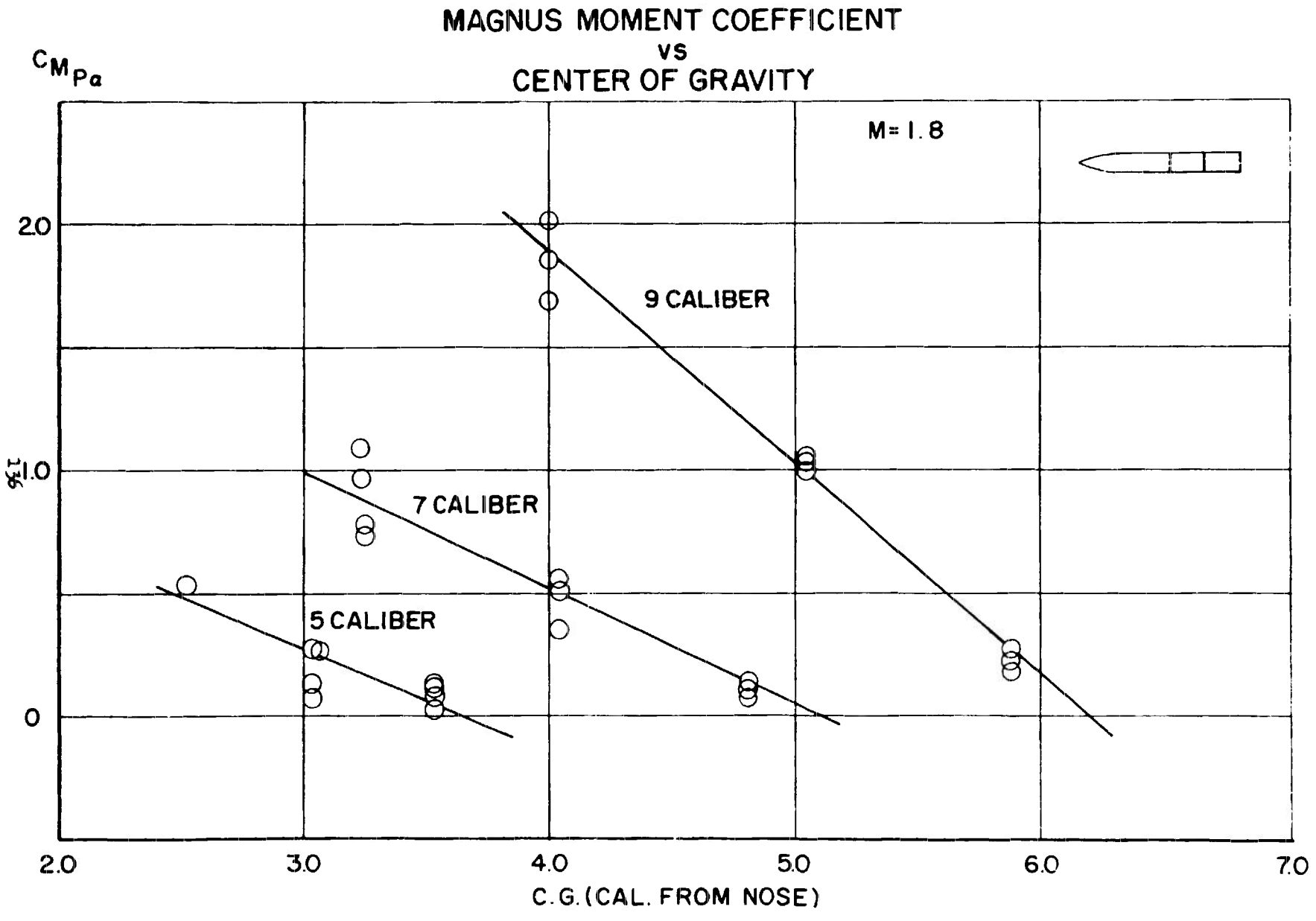
MAGNUS MOMENT COEFFICIENT
VS
CENTER OF GRAVITY
$C_{M_{P\alpha}}$
M= 1.8
9 CALIBER
7 CALIBER
5 CALIBER
2.0
1.0
0
2.0
3.0
4.0
5.0
6.0
7.0
C.G. (CAL. FROM NOSE)

FIG. 7.17

THE CENTERS OF PRESSURE OF THE MAGNUS FORCES VS LENGTH

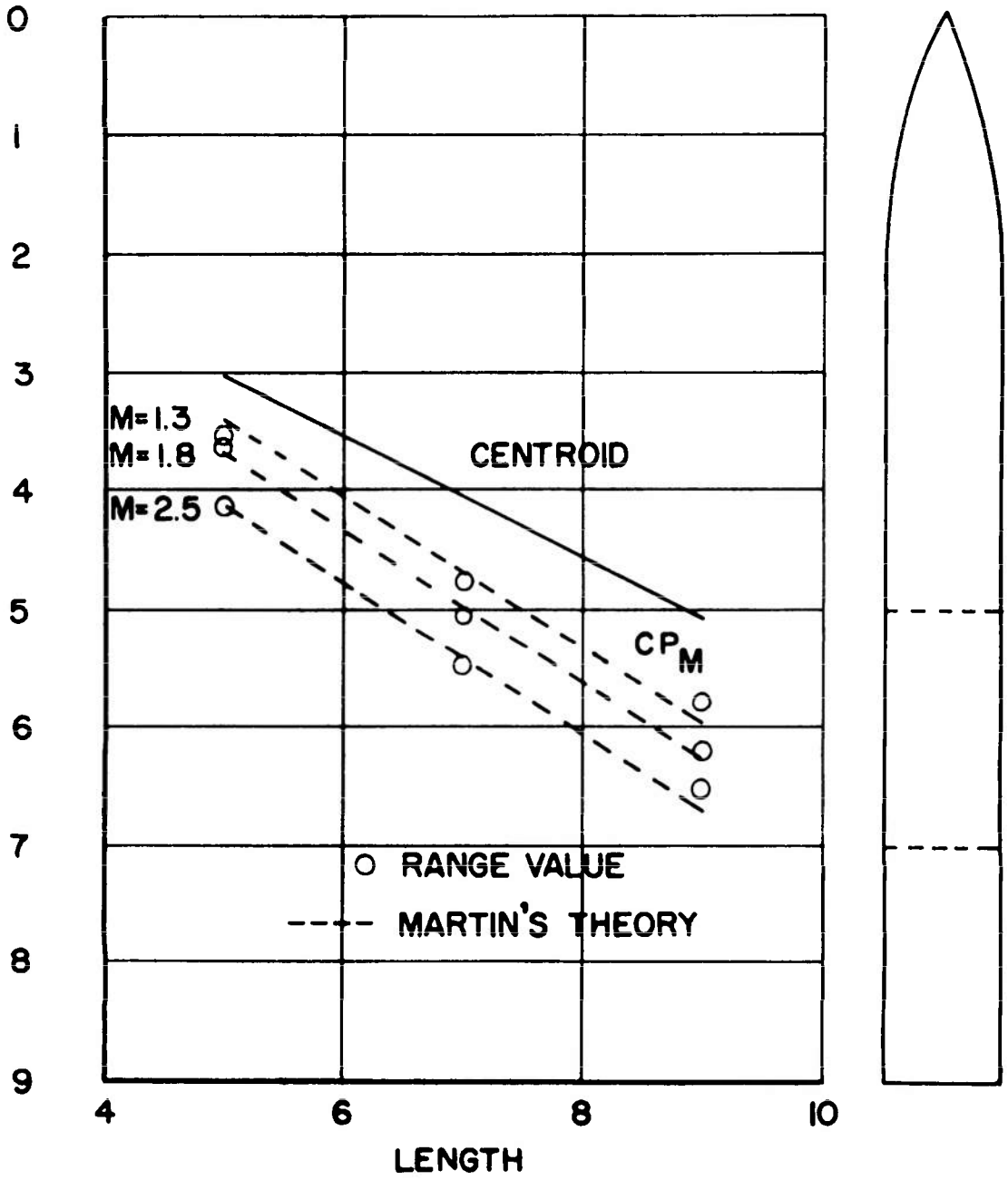

FIG. 7.18

MODIFIED DAMPING MOMENT COEFFICIENTS
VS
CENTER OF GRAVITY

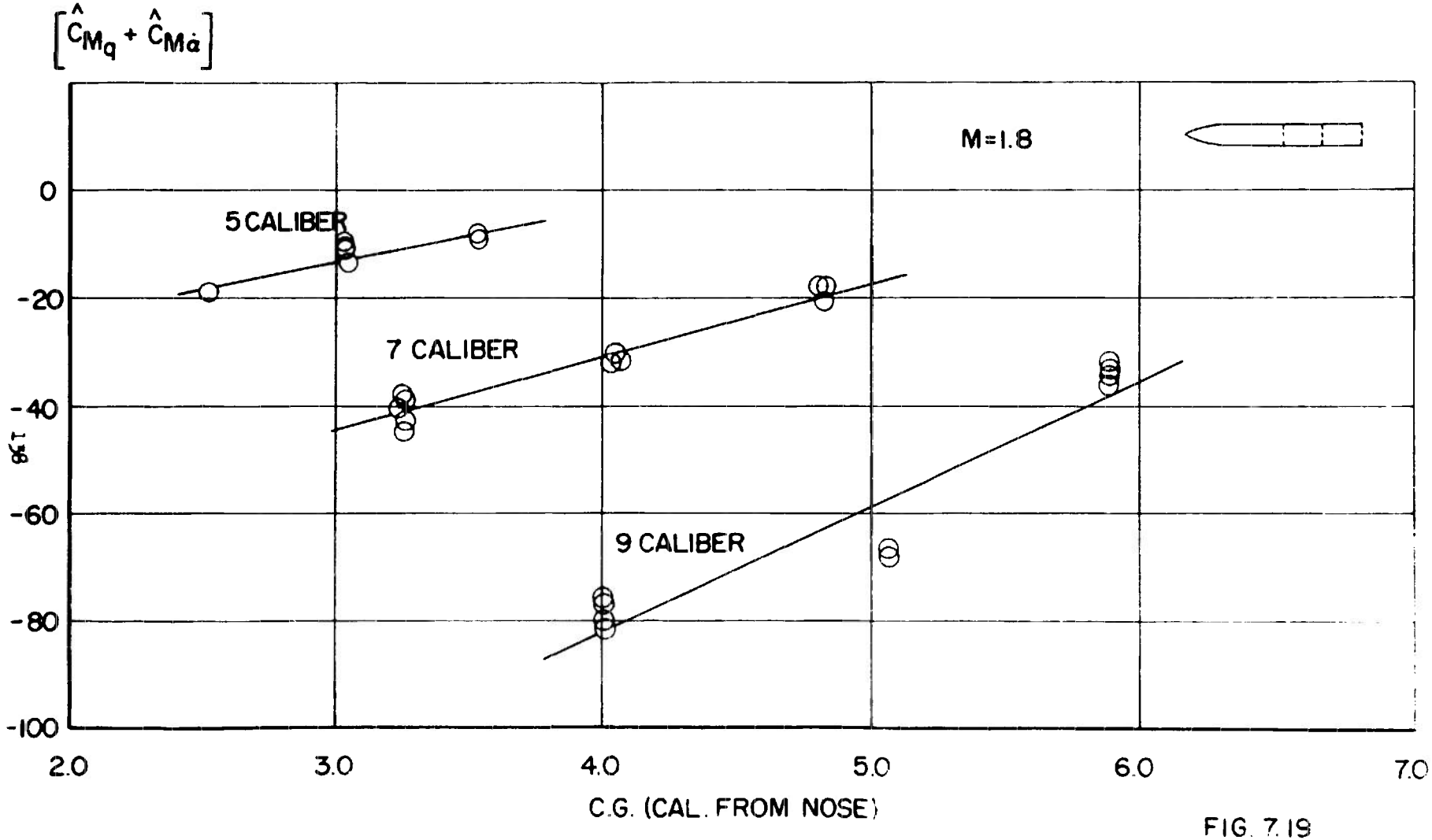

FIG. 7.19

DAMPING MOMENT COEFFICIENT AT CENTROID
VS
LENGTH

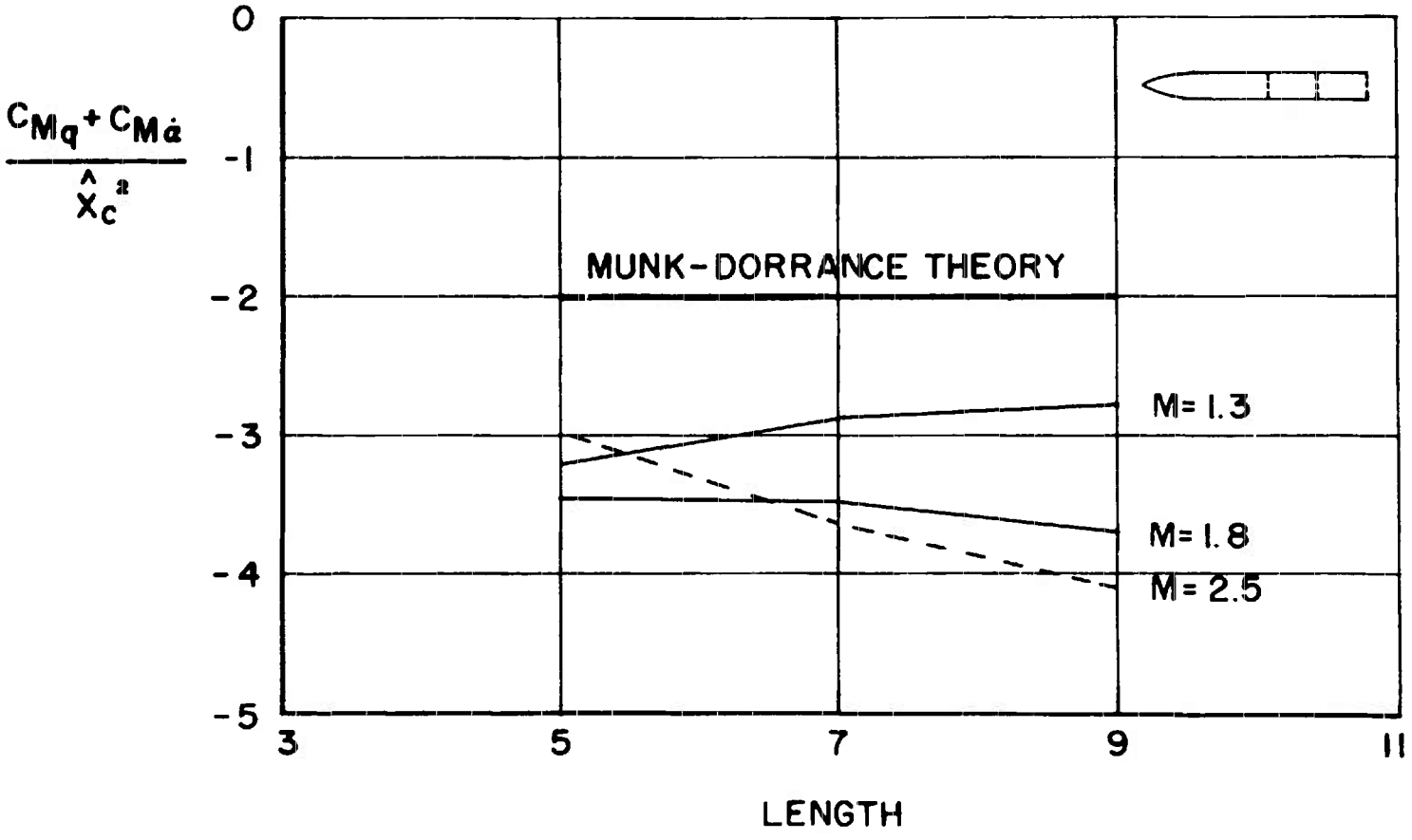

FIG. 7.20

CHAPTER VIII

RANGE MEASUREMENT OF CUBIC COEFFICIENTS

8.1 Introduction

In Section 5.3, we considered the effect of a drag coefficient which was a linear function of the squared angle of attack. In that case, it was found that the usual drag analysis yielded a "range" value of the drag coefficient which corresponded to an "average" δ^2, i.e. $\bar{\delta}^2$.

The analysis of the pitching and swerving motion up to this point has been limited to linear forces and moments. Thus, the corresponding coefficients were assumed to be independent of angle. The large angle of attack program involving the 20mm bullet which was mentioned in Section 5.3 included complete reductions of the pitching and swerving motion. Although angles up to twenty-five degrees were used and these angles were outside the linearity range for the forces and moments, reasonably good fits of the observed motion were obtained. The derived values of the various coefficients did vary with the amplitude of the pitching motion. Thus, it should be possible to correlate these "range" values of the coefficients with the proper effective angles.

In this chapter, the angular motion of missiles acted on by a cubic static moment will be analyzed in detail. This will be done first by neglecting the influence of geometric nonlinearities ($\gamma' = 0$, $\gamma = 1$). Then moderately large geometric angles, a cubic Magnus moment and linear lift force, and damping moments will be inserted and relations between the "range" values and the proper average angles derived. Finally, a similar analysis will be developed for swerving motion with cubic lift and Magnus forces. The utility of these relations will be demonstrated by comparison with certain exact solutions, and application to actual range flight tests.

8.2 Cubic Static Moment: Quasi-Linear Solution

The simplest possible nonlinearity in the aerodynamic moment is a cubic static moment. The usual symmetry consideration requires that it assume the following form

$$C_m + iC_n = -iC_{M_\alpha}\xi$$

$$= -i(c_o + c_2\delta^2)\xi \qquad (2.1)$$

The definition of $C_{M_{(\alpha}}$ in Equation (2.1) is essentially different from that used by most aerodynamicists. $C_{M_{(\alpha}}$ is defined here as the coefficient of the angle of attack in an expansion of the static moment, not the derivative of the static moment. This distinction vanishes for a linear moment but is important otherwise.

The assumption that only a cubic static moment is acting reduces Equation (2.12) to a very simple form

$$\tilde{\xi}'' - iP\tilde{\xi}' - (M_o + M_2\delta^2)\tilde{\xi} = 0 \tag{2.2}$$

where $M_o = \frac{\rho S \ell}{2m} k_t^{-2} c_o$

$$M_2 = \frac{\rho S \ell}{2m} k_t^{-2} c_2$$

If M_2 vanishes, the solution to Equation (2.2) would be

$$\tilde{\xi} = K_1 e^{i\phi_1} + K_2 e^{i\phi_2} \tag{2.3}$$

$$\text{where } \phi_j = \phi_{jo} + \left[\frac{P}{2} \pm \sqrt{\left(\frac{P}{2}\right)^2 - M_o}\right] s$$

Our objective is to find an approximate solution to the nonlinear Equation (2.2) which has a form similar to that of Equation (2.3). This solution would then supply relations between the observed frequencies, the observed damping exponents, the static moment coefficients, c_o, c_2 and the modal amplitudes, K_1, K_2.

The technique used will be an extension of the Kryloff-Bogoliuboff equivalent linearization method[8-1,2]. This method is a generalization of the method used in Section 6-7 for variable coefficients and can be used for nonlinear damping as well. Somewhat more accurate analyses of the cubic static moment motion are possible from a consideration of the exact elliptic integral solutions but these analyses lead to essentially the same relations when applied to ballistic range data[8-3,4]. We will make use of the exact solution to determine the error implicit in our approximations.

We assume that the K_j and ϕ_j's of Equation (2.3) are functions of τ and differentiate that equation twice.

$$\tilde{\xi}' = (K_1' + i\phi_1' K_1)e^{i\phi_1} + (K_2' + i\phi_2' K_2)e^{i\phi_2} \tag{2.4}$$

$$\begin{aligned}\tilde{\xi}'' = &\left[K_1'' - (\phi_1')^2 K_1 + i(2\phi_1' K_1' + \phi_1'' K_1)\right] e^{i\phi_1} \\ &+ \left[K_2'' - (\phi_2')^2 K_2 + i(2\phi_2' K_2' + \phi_2'' K_2)\right] e^{i\phi_2}\end{aligned} \tag{2.5}$$

Equations (2.3-2.5) may now be substituted in Equation (2.2) and the result divided by $K_1 e^{i\phi_1}$.

$$\begin{aligned}&(\phi_1')^2 - P\phi_1' + M_o - \frac{K_1''}{K_1} - i\left[(2\phi_1' - P)\frac{K_1'}{K_1} + \phi_1''\right] \\ &\quad = -M_2\delta^2\left(1 + \frac{K_2}{K_1}e^{-i\hat{\phi}}\right) \\ &\quad\quad - \left\{\left[(\phi_2')^2 - P\phi_2' + M_o\right]K_2 - K_2'' - i\left[(2\phi_2' - P)K_2' + K_2\phi_2''\right]\right\} K_1^{-1}e^{-i\hat{\phi}}\end{aligned} \tag{2.6}$$

$$\begin{aligned}\delta^2 &= \xi\,\bar{\xi} \\ &= K_1^2 + K_2^2 + K_1K_2\left[e^{i\hat{\phi}} + e^{-i\hat{\phi}}\right] \\ &= K_1^2 + K_2^2 + 2K_1K_2\cos\hat{\phi} \\ &\text{where } \hat{\phi} = \phi_1 - \phi_2\end{aligned} \tag{2.7}$$

For a linear static moment, the left and right sides of Equation (2.6) are quite similar in form with the exception of the presence of factor $K_1^{-1}e^{-i\hat{\phi}}$. If ϕ_j' and K_j vary slowly in a period of $\hat{\phi}$, the linearized Equation (2.6) could only be satisfied by requiring that both sides vanish. Another way of saying this would be that the periodic term on the right of the linearized Equation (2.6) has no effect on the almost constant terms on the left side. Indeed, the average of this term over a period of $\hat{\phi}$ is essentially zero. The influence of the fluctuating nonlinear term will, therefore, be obtained by computing its average over a period of $\hat{\phi}$.

$$\left[M_2\delta^2\left(1 + \frac{K_2}{K_1}\, e^{-i\hat{\phi}}\right)\right]_{av.} = \frac{M_2}{2\pi} \int_0^{2\pi} \delta^2\left(1 + \frac{K_2}{K_1}\, e^{-i\hat{\phi}}\right) d\hat{\phi}$$

$$= \frac{M_2}{2\pi} \int_0^{2\pi} \left[K_1^2 + 2K_2^2 + K_1K_2e^{i\hat{\phi}}\right.$$

$$\left. + (2K_1^2 + K_2^2)\, \frac{K_2}{K_1}\, e^{-i\hat{\phi}} + K_2^2e^{-2i\hat{\phi}}\right] d\hat{\phi}$$

$$= M_2(K_1^2 + 2K_2^2) \tag{2.8}$$

Equation (2.6) may now be averaged with the aid of Equation (2.8), the small damping term in the real part may be neglected in comparison with the squared frequency, and a pair of real equations formed from the real and imaginary parts.

$$(\phi_1')^2 - P\phi_1' + M_o + M_2\delta_{e1}^2 = 0 \tag{2.9}$$

$$\frac{K_1'}{K_1} = -\frac{\phi_1''}{2\phi_1' - P} \tag{2.10}$$

where $\delta_{e1}^2 = K_1^2 + 2K_2^2$

Similar relations for the other mode may be obtained by multiplying Equation (2.6) by $(K_1/K_2)e^{i\hat{\phi}}$ and averaging the result.

$$(\phi_2')^2 - P\phi_2' + M_o + M_2\delta_{e2}^2 = 0 \tag{2.11}$$

$$\frac{K_2'}{K_2} = -\frac{\phi_2''}{2\phi_2' - P} \tag{2.12}$$

where $\delta_{e2}^2 = 2K_1^2 + K_2^2$

According to Equations (2.10) and (2.12), damping of the modal amplitudes can be caused by frequency changes. These changes may be caused by Mach number dependence of the coefficient, change in air density such as occurs for an exiting or entering missile or changes in the spin to velocity ratio, P. The relations for these variations are exactly the same as those derived in Section 6.7. The nonlinear frequency equations, Equations (2.9) and (2.11), show a fourth cause of a frequency change. This would be caused by a change in modal amplitude and would entail a coupling between the frequency and damping equations. For constant coefficients and no aerodynamic damping, the modal amplitudes and frequencies are constant and this complication is not present. Whenever linear aerodynamic damping is considered, this coupling effect must be considered.

For the analysis of range data acquired from missiles with cubic static moments, the frequency equations with the average or mid-range values of the proper equivalent squared amplitude, δ_{ej}^2 need only be considered. Modified relations for the sum and products of the frequencies now follow by first eliminating M_o between Equations (2.9) and (2.11) and then eliminating P between these equations.

$$\phi_1' + \phi_2' = P + M_2 \left(\frac{K_1^2 - K_2^2}{\phi_1' - \phi_2'} \right) \tag{2.13}$$

$$\phi_1' \cdot \phi_2' = M_o + M_2 \delta_e^2 \tag{2.14}$$

$$\text{where } \delta_e^2 = \frac{\phi_1' \delta_{e2}^2 - \phi_2' \delta_{e1}^2}{\phi_1' - \phi_2'}$$

$$= K_1^2 + K_2^2 + \frac{\phi_1' K_1^2 - \phi_2' K_2^2}{\phi_1' - \phi_2'}$$

According to Equation (2.14), the product of the measured frequencies should be plotted versus the effective squared angle, δ_e^2 and a line fitted. The intercept of the line is proportional to the linear term in the static moment while its slope is proportional to the cubic term.

8.3 Cubic Static Moment: Exact Solution

In order to obtain the exact solution of Equation (2.2), it is necessary to eliminate the coupling term $iP\tilde{\xi}'$. For the case of no aerodynamic damping and a constant roll to velocity ratio, this can be done by transforming coordinates to a coordinate system which is rolling with roll rate P/2

$$\tilde{\xi} = \hat{\xi} e^{i(1/2)Ps} \tag{3.1}$$

$$\therefore \hat{\xi}'' - \hat{M}_o(1 + m_2\delta^2)\hat{\xi} = 0 \tag{3.2}$$

where $\hat{M}_o = M_o - P^2/4$

$$m_2 = M_2/\hat{M}_o$$

Equation (3.2) has a very nice property of possessing an exact solution. This property is not shared by the other nonlinear equations to be studied in this chapter. Since a comparison of the exact solution with the approximate solution of Section 8.2 will establish confidence in this approximate method, we will now derive this solution.

First we write the conjugate of Equation(3.2)

$$\overline{\hat{\xi}''} - (\hat{M}_o + M_2\delta^2)\overline{\hat{\xi}} = 0 \tag{3.3}$$

Multiplying Equation (3.2) by $\overline{\hat{\xi}}'$, Equation (3.3) by $\hat{\xi}'$, and adding, we have

$$\hat{\xi}''\overline{\hat{\xi}}' + \overline{\hat{\xi}}''\hat{\xi}' - (\hat{M}_o + M_2\delta^2)(\hat{\xi}\,\overline{\hat{\xi}}' + \overline{\hat{\xi}}\,\hat{\xi}') = C_1' = 0 \tag{3.4}$$

where $C_1 = \hat{\xi}'\overline{\hat{\xi}}' - (\hat{M}_o\delta^2 + \frac{M_2\delta^4}{2})$

C_1 is twice the sum of the kinetic and potential energies and is constant for the conservative cubic moment. A second first integral may be obtained by eliminating the static moment between Equations (3.2) and (3.3).

$$\hat{\xi}''\overline{\hat{\xi}} - \overline{\hat{\xi}}''\hat{\xi} = iC_2' = 0 \tag{3.5}$$

where $C_2 = i(\overline{\hat{\xi}}'\hat{\xi} - \hat{\xi}'\overline{\hat{\xi}})$

In order to interpret this constant of the motion polar coordinates are introduced.

$$\hat{\xi} = \delta e^{i\hat{\theta}} \tag{3.6}$$

$$\therefore \quad C_1 = (\delta')^2 + (\delta\hat{\theta}')^2 - (\hat{M}_o\delta^2 + \frac{M_2\delta^4}{2}) \tag{3.7}$$

$$C_2 = 2\delta^2\hat{\theta}' \tag{3.8}$$

Thus C_2 is twice the flight path component of angular momentum. These equations may be combined to yield simple relations for δ and $\hat{\theta}$

$$(\delta^2)' = \pm \sqrt{-C_2^2 + 4C_1\delta^2 + 4\hat{M}_o\delta^4 + 2M_2\delta^6} \tag{3.9}$$

$$\hat{\theta}' = (1/2)\, C_2\delta^{-2} \tag{3.10}$$

The solution to Equation (3.9) is an elliptic function of the first kind[8-5]. Of the four possible combinations of signs for $\hat{M}_o$ and M_2, three correspond to periodic motions. These three are illustrated in Figure 8.1 and may be identified by the following types:

(a) Stable at small angles; more stable at larger angles ($\hat{M}_o < 0$, $M_2 < 0$).

(b) Stable at small angles; less stable at larger angles ($\hat{M}_o < 0$, $M_2 > 0$).

(c) Unstable at small angles; stable at larger angles ($\hat{M}_o > 0$, $M_2 < 0$).

These periodic solutions may be written in terms of the sine amplitude function.

type (a) moment

$$\delta^2 = \delta_2^2 - (\delta_2^2 - \delta_1^2)\, sn^2(\omega s, k) \tag{3.11}$$

type (b) moment

$$\delta^2 = \delta_1^2 + (\delta_2^2 - \delta_1^2)\, sn^2(\tilde{\omega} s, k) \tag{3.12}$$

$$\omega^2 > 0$$

type (c) moment

$$\delta^2 = \delta_2^2 - (\delta_2^2 - \delta_1^2)\, sn^2(\omega s,\ k)$$

$$\hat{M}_o + M_2 \left(\frac{\delta_1^2 + \delta_2^2}{2} \right) \leq 0 \tag{3.13}$$

where δ_1 is minimum value of δ

δ_2 is maximum value of δ

$$\omega^2 = -\hat{M}_o - \frac{M_2}{2}(\delta_1^2 + 2\delta_2^2)$$

$$\tilde{\omega}^2 = -\hat{M}_o - \frac{M_2}{2}(2\delta_1^2 + \delta_2^2)$$

$$k^2 = -\frac{M_2(\delta_2^2 - \delta_1^2)}{2\omega^2} \qquad \text{types (a) and (c)}$$

$$= \frac{M_2(\delta_2^2 - \delta_1^2)}{2\tilde{\omega}^2} \qquad \text{type (b)}$$

The inequalities associated with Equations (3.12-13) are quite important in themselves. Three interesting observations may be made:

1. For type (a) static moment, periodic motion of any amplitude is possible.

2. For type (b) static moment, symmetric planar periodic motions ($P = 0$, $\delta_1 = 0$) are possible for all amplitudes for which the moment does not change sign; circular motion ($\delta_1 = \delta_2$), however, is possible only when the nonlinear part of the moment is not greater than two-thirds of the linear part.

3. For type (c) static moment, possible periodic motions are those for which the median value of δ^2 yields a stable moment. The variables δ_1 and δ_2 may be approximately related to the modal amplitudes K_1 and K_2 by the equations

$$\delta_1^2 = (K_1 - K_2)^2 \tag{3.14}$$

$$\delta_2^2 = (K_1 + K_2)^2 \tag{3.15}$$

The period of the elliptic sine function in Equations (3.11-12) corresponds to half the period of $\hat{\phi}$ in Equation (2. 7) since that equation can be put in the form

$$\delta^2 = \delta_2^2 - (\delta_2^2 - \delta_1^2)\sin^2(\hat{\phi}/2)$$
$$= \delta_1^2 + (\delta_2^2 - \delta_1^2)\sin^2(\hat{\phi} + \pi)/2 \qquad (3.16)$$

$$\therefore \hat{\phi}' = \phi_1' - \phi_2' = \frac{\pi\omega}{K(k)} \qquad \text{types (a) and (c)}$$
$$= \frac{\pi\tilde{\omega}}{K(k)} \qquad \text{type (b)} \qquad (3.17)$$

where K(k) is the complete elliptic integral of the first kind. (The period of $sn(\omega s, k)$ is $4K/\omega$.)

$\hat{\phi}'$ may be computed from the quasi-linear frequencies of Equations (2.9) and (2.11) for two special motions; circular ($\delta_1^2 = \delta_2^2$; $K_1K_2 = 0$) or planar* ($\delta_1^2 = 0$; $K_1 = K_2$).

For circular motion

$$\phi_1' - \phi_2' = \sqrt{-\hat{M}_o(1 + m)} + \sqrt{-\hat{M}_o(1 + 2m)} \qquad (3.18)$$

and for planar motion

$$\phi_1' - \phi_2' = 2\sqrt{-\hat{M}_o(1 + (3/4)m)} \qquad (3.19)$$

where $m = m_2\delta_2^2 = \dfrac{M_2\delta_2^2}{\hat{M}_o}$

m is the ratio of the cubic part of the static moment to the linear part. Equations (3.18) and (3.19) are compared with the corresponding exact equations for different moment types in Figures 8.2 and 8.3. These figures show amazingly good agreement of the approximate curve and the exact one.

---

* This motion is called planar although except for zero spin it is not planar in range coordinates. In other words, planar epicyclic motion is motion which includes zero total angle of attack.

7.4 Effect of Large Angles on Epicyclic Frequencies

When large angles* are considered, two quite different effects become important. First the simple geometric relations of Section 7.1 between the direction cosines and the angles of attack and sideslip must be re-examined and then the derivative of the cosine of the total angle of attack, γ', must be retained in the equations of pitching and yawing motion.

Although Equations (7.1.14-15) must be used to calculate the transverse components of the velocity vector in the fixed plane coordinates, the exact transformation between these coordinates and the non-rolling coordinates seems to be quite formidable. Our geometrical intuition may provide some help. The motion of the 2 and 3 axes of the fixed plane system is directly related to the missile's periodic pitching and yawing motion and, therefore, the average roll rate of the fixed plane system should be zero and frequencies measured in the fixed-plane coordinates the same as those measured in non-rolling coordinates. To verify this conjecture for our cubic analysis we must, therefore, show that at least the second order approximation in average angular velocity of the fixed plane axes is zero.

Since $\omega_1 \ell/V$ as given by Equation (7.1.10) is at most second order we can use the first order approximations for n_2 and n_3 (Equations (7.1.16))

$$n_2 = \frac{\tilde{v}}{V} + \frac{x_2'}{\ell} \tag{4.1}$$

$$n_3 = \frac{\tilde{w}}{V} + \frac{x_3'}{\ell} \tag{4.2}$$

When the higher order terms in Equation (7.1.10) are omitted, it reduces to

$$\frac{\omega_1 \ell}{V} = \frac{n_3(n_1 n_2' - n_2 n_1')}{1 - n_3^2}$$

$$\doteq n_3 n_2' \tag{4.3}$$

---

* Angles are usually thought to be large when the approximations $\theta = \sin\theta = \tan\theta$, $\cos\theta = 1$ are not very well satisfied. A glance at a table of trigometric functions shows that angles in excess of fifteen degrees cause these relations to be in error by more than 3% and could be considered to be large.

Equations (4.1-3) may now be combined.

$$\frac{\omega_1 \ell}{V} = \frac{\tilde{w}\tilde{v}'}{V^2} + \frac{x_3'\tilde{v}' + x_2''\tilde{w}}{V\ell} + \frac{x_3' x_2''}{\ell^2} \tag{4.4}$$

The trajectory terms in Equations (4.1, 2,4) arise from the lift force and are much smaller than the first terms in each of those equations and, therefore, will be neglected. A good approximation for the transverse velocities is our familiar epicycle

$$\frac{\tilde{v}}{V} = K_1 \cos \phi_1 + K_2 \cos \phi_2 \tag{4.5}$$

$$\frac{\tilde{w}}{V} = K_1 \sin \phi_1 + K_2 \sin \phi_2 \tag{4.6}$$

$$\begin{aligned} \frac{\omega_1 \ell}{V} &\doteq -(K_1 \sin \phi_1 + K_2 \sin \phi_2)(K_1 \phi_1' \sin \phi_1 + K_2 \phi_2' \sin \phi_2) \\ &= -\frac{1}{2}\left[K_1^2 \phi_1' + K_2^2 \phi_2'\right] \\ &\quad + \frac{1}{2}\left[K_1^2 \phi_1' \cos 2\phi_1 + K_2^2 \phi_2' \cos 2\phi_2\right] \\ &\quad - (\phi_1' + \phi_2') K_1 K_2 \sin \phi_1 \sin \phi_2 \end{aligned} \tag{4.7}$$

According to Equation (4.7) $\omega_1 \ell/V$ has a non-zero average! This set back to our geometrical intuition may be overcome by the realization that Equation (4.7) allows us to state the relation between frequencies in the range's fixed plane coordinates, ϕ_{jr}', and frequencies in the theory's non-rolling coordinates, ϕ_j'. Since the measured frequencies are actually averages

$$\phi_1' = \phi_{1r}' + \left(\frac{\omega_1 \ell}{V}\right)_{av} \tag{4.8}$$

$$\phi_2' = \phi_{2r}' + \left(\frac{\omega_1 \ell}{V}\right)_{av} \tag{4.9}$$

$$\therefore \quad \phi_1' \doteq \phi_{1r}' - \frac{1}{2}\left[K_1^2 \phi_1' + K_2^2 \phi_2'\right] \tag{4.10}$$

$$\phi_2' \doteq \phi_{2r}' - \frac{1}{2}\left[K_1^2 \phi_1' + K_2^2 \phi_2'\right] \tag{4.11}$$

The differential equation for a cubic static moment and large geometrical angles can be obtained from Equation (6.6.8)

$$\tilde{\xi}'' - \left(\frac{\gamma'}{\gamma} + iP \right) \tilde{\xi}' - M\tilde{\xi} = 0 \tag{4.12}$$

where $M = \gamma \frac{\rho S \ell}{2m} k_t^{-2} C_{M_\alpha}$

$$\doteq M_o + M_2 \delta^2$$

$$M_o = \frac{\rho S \ell}{2m} k_t^{-2} c_o \qquad \text{and}$$

$$M_2 = \frac{\rho S \ell}{2m} k_t^{-2} \left[c_2 - \left(\frac{1}{2} \right) c_o \right] .$$

Note that the definition of M_2 differs from that following Equation (2.2). This difference arises from the retention of the cosine in the definition of M. If the numerical effect of this difference is large, this means that the nonlinearity in M is primarily a geometrical nonlinearity rather than an aerodynamic nonlinearity.

Since $\gamma = (1 - \delta^2)^{1/2}$, the γ' term can be quickly computed

$$\frac{\gamma'}{\gamma} = \frac{1}{2} \frac{(\gamma^2)'}{\gamma^2}$$

$$= - \frac{1}{2} \frac{(\delta^2)'}{1 - \delta^2} \tag{4.13}$$

$$\doteq - \frac{1}{2} (\delta^2)'$$

From Equations (2.7) and (4.13) we see that if damping is neglected in comparison with frequency

$$\frac{\gamma'}{\gamma} = - \frac{i}{2} K_1 K_2 \hat{\phi}' \left[e^{i\hat{\phi}} - e^{-i\hat{\phi}} \right] = K_1 K_2 \hat{\phi}' \sin \hat{\phi} \tag{4.14}$$

These equations may now be substituted in Equation (4.12), solved for the damping and frequency of the first mode, and averaged over a cycle of the difference frequency. The resulting equation for damping is the same as before but the frequency equation for the first mode becomes

$$(\phi_1')^2 - P\phi_1' + M_o + M_2\delta_{e1}^2 + K_2^2(\phi_1' - \phi_2') \frac{\phi_2'}{2} = 0 \qquad (4.15)$$

Similarly, the frequency equation for the second mode becomes

$$(\phi_2')^2 - P\phi_2' + M_o + M_2\delta_{e2}^2 + K_1^2(\phi_2' - \phi_1') \frac{\phi_1'}{2} = 0 \qquad (4.16)$$

Equations (4.15-4.16) differ from Equations (2.9) and (2.11) by the presence of the last terms. Equations similar to Equations (2.13-14) may now be derived by first eliminating M_o between Equations (4.15-16) and then eliminating P.

$$\phi_1' + \phi_2' + \frac{1}{2}\left[K_1^2\phi_1' + K_2^2\phi_2'\right] = P + M_2\left(\frac{K_1^2 - K_2^2}{\phi_1' - \phi_2'}\right) \qquad (4.17)$$

$$\phi_1' \cdot \phi_2' + \frac{1}{2}\left[K_1^2(\phi_1')^2 + K_2^2(\phi_2')^2\right] = M_o + M_2\delta_e^2 \qquad (4.18)$$

Thus the γ'/γ term does have a noticeable effect on the equations for sum and product of the frequencies in the non-rolling coordinates. What is measured, however, are the frequencies in range coordinates. If Equations (4.10-11) are used to eliminate the non-rolling frequencies and fourth powers of K_j's omitted, we have the following

$$\phi_{1r}' + \phi_{2r}' - \frac{1}{2}(K_1^2\phi_{1r}' + K_2^2\phi_{2r}') = P + M_2\left(\frac{K_1^2 - K_2^2}{\phi_{1r}' - \phi_{2r}'}\right) \qquad (4.19)$$

$$\phi_{1r}' \cdot \phi_{2r}' \left(1 - \left(\frac{1}{2}\right)(K_1^2 + K_2^2)\right) = M_o + M_2\delta_e^2 \qquad (4.20)$$

The second term in Equation (4.18) comes from the cosine of the total angle of attack and could be quite large in comparison with $\phi_1' \cdot \phi_2'$ since it involves the square of the higher frequency and this frequency could be much larger than the lower frequency. The modification of Equation (2.14) due to range frequencies and the cosine terms is Equation (4.20) and it can be seen that this modification is quite small. The two effects mentioned at the beginning of this section, therefore, almost cancel each other and should be either both retained or both omitted from the relation for the product of the frequencies.

The left side of Equation (4.20) contains an additional effect of the cosine of the total angle of attack through the definition of M_2.

$$M_o + M_2\delta_e^2 = \frac{\rho S \ell^3}{2I_y}\left[c_o(1 - (1/2)\,\delta_e^2) + c_2\delta_e^2\right] \tag{4.21}$$

If Equation (4.20) is multiplied by $\left[\frac{\rho S \ell^3}{2I_y}\right]^{-1}(1 + (1/2)\,\delta_e^2)$ and fourth powers of the modal amplitudes neglected, the following very convenient form results.

$$\left[C_{M_\alpha}\right]_r = \left(\frac{\rho S \ell^3}{2I_y}\right)^{-1} \phi'_{1r} \cdot \phi'_{2r} \left[1 + (1/2)\left(\frac{\phi'_{1r}K_1^2 - \phi'_{2r}K_2^2}{\phi'_{1r} - \phi'_{2r}}\right)\right]$$

$$= c_o + c_2\delta_e^2 \tag{4.22}$$

Thus the range value of the static moment coefficient, $\left[C_{M_\alpha}\right]_r$, is essentially the product of the range measured frequencies and a set of $\left[C_{M_\alpha}\right]_r$'s for the same Mach number and a cubic static moment should yield a straight line where plotted versus δ_e^2. The intercept is c_o, the zero amplitude static moment derivative, and the slope is c_2, the cubic coefficient in an expansion of the static moment.

8.5 Cubic Magnus Moment

As could be seen in Section 8.4, the effect of large geometric angles is rather small and will be neglected in the remainder of this chapter. Equation (4.20) is quite simple to apply and will be used in the data analysis. It now remains to include the aerodynamic damping terms. The only damping nonlinearity which has been measured in a ballistic range has been a cubic Magnus moment and we will restrict our study to this nonlinearity. It is a simple exercise for the reader to incorporate any other type of nonlinearity he may prefer. The exact expressions for arbitrary nonlinearities will be derived in the next chapter.

For cubic static and Magnus moments Equation (6.6.12) assumes the form

$$\tilde{\xi}'' + (H - iP)\tilde{\xi}' - \left[M_o + M_2\delta^2 + iP(T_o + T_2\delta^2)\right]\tilde{\xi} = 0 \qquad (5.1)$$

where $C_{M_{p\alpha}} = \hat{c}_o + \hat{c}_2\delta^2$

$$T_o = \frac{\rho S \ell}{2m}\left[C_{L_\alpha} + k_a^{-2}\hat{c}_o\right]$$

$$T_2 = \frac{\rho S \ell}{2m} k_a^{-2}\hat{c}_2$$

The quasi-linear analysis of previous section results in the same frequency equations [Equations (2.9-11)] but different damping equations

$$\phi_1' = \frac{P + \sqrt{P^2 - 4(M_o + M_2\delta_{e1}^2)}}{2} \qquad (5.2)$$

$$\phi_2' = \frac{P - \sqrt{P^2 - 4(M_o + M_2\delta_{e2}^2)}}{2} \qquad (5.3)$$

$$\frac{K_1'}{K_1} = \lambda_1 = \frac{-\phi_1'' - \left[\phi_1' H - P(T_o + T_2\delta_{e1}^2)\right]}{2\phi_1' - P} \qquad (5.4)$$

$$\frac{K_2'}{K_2} = \lambda_2 = \frac{-\phi_2'' - \left[\phi_2' H - P(T_o + T_2\delta_{e2}^2)\right]}{2\phi_2' - P} \qquad (5.5)$$

One unfortunate feature of Equations (5.2-5) is the way they are coupled. The damping equations are affected by the derivatives of the frequencies but these derivatives in turn involve the damping. If Equation (5.2) is differentiated,

$$\phi_1'' = \frac{-2M_2(K_1^2\lambda_1 + 2K_2^2\lambda_2)}{\sqrt{P^2 - 4(M_o + M_2\delta_{e1}^2)}}$$

$$= \frac{-2M_2(K_1^2\lambda_1 + 2K_2^2\lambda_2)}{(2\phi_1' - P)} \qquad (5.6)$$

Equation (5.6) and a similar equation for ϕ_2'' may be used to eliminate the derivatives of the frequencies from Equations (5.4-5)

$$\lambda_1 - 2M_2 \left[\frac{K_1^2\lambda_1 + 2K_2^2\lambda_2}{(2\phi_1' - P)^2} \right] = \lambda_{10} + \lambda_{12}\delta_{e1}^2 \tag{5.7}$$

$$\lambda_2 - 2M_2 \left[\frac{2K_1^2\lambda_1 + K_2^2\lambda_2}{(2\phi_2' - P)^2} \right] = \lambda_{20} + \lambda_{22}\delta_{e2}^2 \tag{5.8}$$

where $\lambda_{10} = - \dfrac{\phi_1' H - PT_o}{2\phi_1' - P}$

$$\lambda_{20} = - \frac{\phi_2' H - PT_o}{2\phi_2' - P}$$

$$\lambda_{12} = \frac{PT_2}{2\phi_1' - P}$$

$$\lambda_{22} = \frac{PT_2}{2\phi_2' - P}$$

M_2 can be obtained from the measured frequencies and the left sides of above equation can then be computed for each test. In most cases, however, the M_2 term is quite small and will, therefore, be omitted in the remainder of this discussion. Equations (5.7-8) show that for a series of tests of the same configuration at the same Mach number the measured damping exponents should be plotted versus δ_{ei}^2 . If the points fall on lines whose slopes are negatives of each other, the Magnus moment is cubic with cubic coefficient determined by the slope.

In most range tests, this plot is not made but the linear formulas (Equations 6.6.23-26) are used to compute range values of the damping in pitch and Magnus moment coefficients. If these formulas are applied to Equations (5.7-8), and the static moment is assumed to be linear, the following relations result

$$\left[C_{M_{p\alpha}}\right]_r = \hat{c}_o + \hat{c}_2\delta_e^2 \tag{5.9}$$

$$\left[C_{M_q} + C_{M_{\dot{\alpha}}}\right]_r = C_{M_q} + C_{M_{\dot{\alpha}}} + \hat{c}_2\Delta \tag{5.10}$$

$$\text{where } \Delta = -\frac{I_y}{I_x}\left(\frac{\phi_1' + \phi_2'}{\phi_1' - \phi_2'}\right)(K_1^2 - K_2^2)$$

It is interesting to note the reappearance of δ_e^2. This should not be too surprising since the Magnus moment is the imaginary coefficient of $\tilde{\xi}$ while the static moment is the real part of the same coefficient. Equation (5.9) contains a warning that a dependence of the range-measured damping moments coefficient on amplitude of motion does not necessarily imply a nonlinear damping moment. A nonlinear Magnus moment can have this effect.

8.6 Cubic Lift and Magnus Forces

The swerving motion for linear aerodynamic forces has been discussed in some detail in Section 6.9. For simplicity, we will neglect damping force, the asymmetry force, gravity and Coriolis acceleration. These quantities may be easily incorporated in the nonlinear analysis as additive terms. In range coordinates then, Equation (6.9.7) reduces to

$$\frac{x_2'' + ix_3''}{\ell} = f\,\tilde{\xi} \tag{6.1}$$

$$\text{where } f = C_{L_\alpha}^* + i\frac{p\ell}{V}C_{N_{p\alpha}}^*$$

If the lift and Magnus forces are cubic in δ, f has the form $f_o + f_2\delta^2$. Integrating 6.1 with the excellent approximation $s = \frac{x_1}{\ell}$, we have*

$$\frac{x_2 + ix_3}{\ell} = B_o + B_1 s + \int_o^s \int_o^{s_1} (f_o + f_2\delta^2)\,\tilde{\xi}\, ds_2 ds_1 \tag{6.2}$$

* Note that B_i' of this equation are the negatives of B_i of Equation (6.9.8).

If f were linear, this reduces to the form

$$\frac{x_2 + ix_3}{\ell} = B_{o\ell} + B_{1\ell}s + f_o I_1 \tag{6.3}$$

$$\text{where } I_1 = \int_o^s \int_o^{s_1} \tilde{\xi}\, ds_2 ds_1$$

Now motion caused by nonlinear forces has been well fitted by Equation (6.3) and provided a range value of f.

$$f_r = f_o + f_2 \delta_{es}^2 \tag{6.4}$$

where δ_{es}^2 is an effective value of δ^2 for the swerving motion.

It remains to determine this effective value of δ^2. To do this we will assume that ξ is well approximated by an epicycle without damping.

$$\therefore I_1 = C_{o\ell} + C_{1\ell}s + I_\ell \tag{6.5}$$

$$\text{where } I_\ell = -\left[\frac{K_1 e^{i\phi_1}}{(\phi_1')^2} + \frac{K_2 e^{i\phi_2}}{(\phi_2')^2} \right]$$

and

$$\frac{x_2 + ix_3}{\ell} = \hat{B}_{o\ell} + \hat{B}_{1\ell}s + f_o I_\ell \tag{6.6}$$

$$\text{where } \hat{B}_{i\ell} = B_{i\ell} + f_o C_{i\ell}$$

But

$$\int_o^s \int_o^{s_1} \delta^2 \tilde{\xi}\, ds_2 ds_1 = C_o + C_1 s + I_c \tag{6.7}$$

where

$$I_c = -\left[\frac{K_1 \delta_{e1}^2 e^{i\phi_1}}{(\phi_1')^2} + \frac{K_2 \delta_{e2}^2 e^{i\phi_2}}{(\phi_2')^2} + \frac{K_1^2 K_2 e^{i(2\phi_1 - \phi_2)}}{(2\phi_1' - \phi_2')^2} + \frac{K_1 K_2^2 e^{i(2\phi_2 - \phi_1)}}{(2\phi_2' - \phi_1')^2} \right]$$

Therefore the equation for the cubic forces becomes

$$\frac{x_2 + ix_3}{\ell} = \hat{B}_o + \hat{B}_1 s + f_o I_\ell + f_2 I_c \tag{6.8}$$

where $\hat{B}_i = B_i + f_o C_{i\ell} + f_2 C_i$

In order to reduce Equation (6.8) to the form of (6.6), the effective δ^2 would have to satisfy the equation

$$\delta^2_{es} I_\ell - I_c = 0 \tag{6.9}$$

Except for certain special cases, I_c is not proportional to I_ℓ and, hence, a constant δ^2_{es} will not satisfy Equation (6.9). Our experience in data analysis implies that it should be possible to select a constant value of δ^2_{es}. The key to the solution lies in the fact that the data analysis is based on a least squares technique. We will, therefore, define δ^2_{es} to be that number which makes the integral over the observed trajectory of the squared magnitude of the left side of Equation (6.9) a minimum. This approach is quite similar to that used for a quadratic drag coefficient in Section 5.3.

δ^2_{es} is, therefore, defined by the requirement that

$$\int_{-L/2}^{L/2} (\delta^2_{es} I_\ell - I_c)(\delta^2_{es} \bar{I}_\ell - \bar{I}_c)\, ds \text{ is a minimum}$$

We differentiate the above, set the result equal to zero and solve for δ^2_{es}.

$$\delta^2_{es} = \frac{1/L \int_{-L/2}^{L/2} (I_c \bar{I}_\ell + \bar{I}_c I_\ell) ds}{2/L \int_{-L/2}^{L/2} I_\ell \bar{I}_\ell \, ds} \tag{6.10}$$

For large L the numerator is the average value of $I_c\bar{I}_\ell + \bar{I}_c I_\ell$ and the denominator is twice the average of $I_\ell\bar{I}_\ell$. δ_{es}^2 can be quickly computed and reduced to the form

$$\therefore \delta_{es}^2 = \frac{(\phi_2')^4 K_1^2 \delta_{e1}^2 + (\phi_1')^4 K_2^2 \delta_{e2}^2}{(\phi_2')^4 K_1^2 + (\phi_1')^4 K_2^2} \tag{6.11}$$

For the special case of a spin stabilized missile $\phi_2' << \phi_1'$ and the effective δ^2 reduces to the simple form

$$\delta_{es}^2 = \delta_{e2}^2 \tag{6.12}$$

This is one of the special cases which directly satisfies Equation (6.9). A second important case is that of a nonspinning missile ($\phi_1' = -\phi_2'$). For this condition

$$\delta_{es}^2 = \frac{K_1^4 + 4K_1^2K_2^2 + K_2^4}{K_1^2 + K_2^2} \tag{6.13}$$

In any event the range values of C_{L_α} and $C_{N_{p\alpha}}$ should be plotted versus δ_{es}^2 and the existence of a cubic force dependence on δ determined.

8.7 Experimental Results

As can be seen from the preceding analysis, the cubic coefficients can only be obtained from a set of tests of the same configuration at the same Mach number but flying at different effective angles of attack. These considerations lead to a need for at least three and preferably five tests in each set. Although the analysis has been applied to the data obtained from finned missiles these programs were not large enough to allow cross checks of the results and no good wind tunnel data was available.

The ogive-cylinder program[8-6] of Section 7-4 (4) included tests of identical models with three different center of gravity locations at the same Mach number. This redundancy of data can and will be used to determine the validity of the cubic analysis. In a second program[8-7] the large angle behavior of a 20mm shell was specifically studied. Some of the results of this program can be used to increase further our confidence in the cubic analysis.

Wind tunnel measurements of the Magnus force and moment for the seven caliber ogive cylinder[8-8] and static force and moment for the 20mm shell[8-9] are available and will be compared with the results of the nonlinear reduction at the same Mach numbers with different center of gravity locations. In Figure 8.4, the range value of C_{M_α} is plotted versus the effective squared angle of attack for the nine caliber long models at Mach number of 1.8. As can be seen from this figure, the points for each center of gravity location fall on lines with well determined slopes.

Of the twenty-seven possible combinations of length, Mach numbers, and center of gravity location, the data was sufficiently good to determine sixteen values of the cubic coefficient, c_2. (Table 8-1) For some of the Mach numbers and length, wind tunnel measurements of the static moment were available. These were fitted by cubics and the cubic coefficients are listed in Table 8-1. At all seven points of comparison the agreement is good.

Since models with three different center of mass locations were tested, a second check is possible. If the normal force is expanded as a cubic section of δ, the usual center of gravity relation (Table 6-1) provided that

$$c_o(s_{cg}) = c_o - s_{cg}a_o \tag{7.1}$$

$$c_2(s_{cg}) = c_2 - s_{cg}a_2 \tag{7.2}$$

where $C_{N_\alpha} = a_o + a_2\delta^2$ and $c_i(s_{cg})$

are the moment coefficients for a center of mass located s_{cg} calibers forward of that for the c_i's.

This means that the c_i's for different center of mass locations are linear functions of location. In Figure 8.5, the slopes and intercepts of Figure 8.4 are plotted versus center of gravity location. The fact that the cubic coefficients as well as the linear coefficients fall on a straight line is another point in the favor of the cubic analysis. The slopes of these lines are a_2 and a_o respectively. The c.g. intercept of the c_o line is the location

of the center of pressure and the c.g. intercept of the a_2 line is the c.g. location for which the cubic coefficient is zero and the moment is exactly linear. This point is rear of the rear center of gravity tested.

For a total of seven of the nine combinations of length and Mach number it was possible to determine a_2 from the variation of c_2 with c.g. location. The wind tunnel measurements of normal force may be analyzed to yield cubic coefficients as well as linear coefficients. These are tabulated in Table 8-2 and the agreement with the range values is seen to be reasonably good.

If the lift force is cubic in angle of attack, it can be written in the form

$$C_{L_\alpha} = a_{L0} + a_{L2}\delta^2 \tag{7.3}$$

From the relation connecting the lift, drag, and normal forces (Equation (6.6.7)), the coefficients of the normal and lift forces satisfy the following equations.

$$a_o = a_{L0} + C_{D_o} \tag{7.4}$$

$$a_2 = a_{L2} - (1/2)\, a_{L0} + C_{D_\delta 2} \tag{7.5}$$

In Section 8.6, it is shown that the range value of the lift coefficient of a spinning missile should be plotted versus δ_{e2}^2 and the cubic coefficient can be obtained from the slope of a line through the data. This technique is illustrated in Figure 8.6. Values of a_o and a_2 could be computed for eight combinations of length and Mach number and these are compared with values obtained from $\left[C_{M_\alpha}\right]_r$ and wind tunnels in Table 8.2.

Finally, in the 20mm shell program it was possible to study the influence of quite large angles. In Figure 8.7, the range static moment coefficient is plotted versus effective squared angle of attack and we see that the data is essentially bilinear. Each line corresponds to a cubic segment in the moment plane. If the parameters of each cubic are calculated from the slope and intercept of its corresponding line in Figure 8.7, they can be pieced together

to form a smooth moment plot. (Figure 8.8). An examination of the spark shadowgraphs reveals that flow separation occurs at about 21° and this explains the sudden change in the moment curve at this point. In Figure 8.9, $\left[C_{L_\alpha}\right]_r$ is plotted versus δ_{e2}^2 and the corresponding lift force is shown in Figure 8.10.

Since wind tunnel measurements were available, a further verification is possible. The data were divided into that for angles less than 21° and that for angles greater than 21° and pairs of cubics fitted. The resulting coefficients are given in Table 8.3. The agreement for such different experimental conditions is quite good*.

In view of this success with cubic static moments, our interest turns quite naturally to cubic Magnus moments. According to Equations (5.9-10) the range values of damping in pitch and Magnus moment coefficients are both affected by the presence of a cubic Magnus moment. Thus values of this cubic coefficient may be computed from a plot of $\left[C_{M_{p\alpha}}\right]_r$ and $\left[C_{M_q} + C_{M_{\dot{\alpha}}}\right]_r$ versus δ_e^2 and Δ respectively. (See Figures 8.11-12) Eight cubic Magnus coefficients were determined for the ogive cylinder and these results appear in Table 8-4. In four cases Δ had a wide enough range to determine $\hat{c}_2$ from $\left[C_{M_q} + C_{M_{\dot{\alpha}}}\right]_r$ and the pairs of values of $\hat{c}_2$ are all within their combined probable errors. Unfortunately, with the exception of the one value for the nine caliber long models these probable errors are quite large. Thus, the measurements of cubic Magnus moments are quite delicate.

The swerving motions of the ogive cylinder were examined to determine any influence of a cubic Magnus force. In only two out of the six combinations of length and Mach number was this effect large enough to measure and these two cases are shown in Figure 8.13. The cubic Magnus moment coefficients given in Table 8-4 for different center of gravity locations could be analyzed to yield four indirect values of the cubic Magnus coefficient, $\hat{a}_2$. The agreement of these coefficients is reasonably good.

---

* Additional examples of the analysis of cubic static moments are supplied by References 8-10 and 8-11.

TABLE 8-1

CUBIC STATIC MOMENT COEFFICIENT, c_2, FOR OGIVE CYLINDERS

$S = \pi d^2/4$; $\ell = d$

Mach Number	Forward c.g.		Middle c.g.		Rear c.g.	
	Range	Wind Tunnel	Range	Wind Tunnel	Range	Wind Tunnel
			L/d = 5			
1.3		- 5	- 8 ± 2	0	2.5 ± 5	8
1.8		- 36		- 18	8 ± 2	0
			L/d = 7			
1.3	-53 ± 3		-13 ± 3		18 ± 5	13
1.8	-31 ± 3	- 28		- 8	0 ± 8	8
2.5	-71 ± 3	- 66		- 28		
			L/d = 9			
1.3	-89 ± 3				0.3 ± .03	
1.8	-76 ± 10		-41 ± 3		-9.5 ± .8	
2.5			-76 ± 5		-2.5 ± 1.5	

TABLE 8-2

LINEAR AND CUBIC NORMAL FORCE COEFFICIENTS FOR OGIVE CYLINDERS

Mach Number	a_o			a_2		
	c.g.	Swerve	Wind Tunnel	c.g.	Swerve	Wind Tunnel
			L/d = 5			
1.3	2.50	2.52	2.34	17	13 ± 0.5	12
1.8	2.88	2.88	2.80	-	25 ± 5	17
			L/d = 7			
1.3	2.60	2.50	-	51	25 ± 3	-
1.8	2.88	2.88	2.74	31	23 ± 10	25
2.5	3.08	3.06	3.08	46	69 ± 10	46
			L/d = 9			
1.3	2.70	2.72		43	43 ± 3	
1.8	2.90	3.13		36 ± 1	38 ± 5	
2.5	3.33	3.06		87	76 ± 5	

TABLE 8-3

BI-CUBIC STATIC MOMENT AND LIFT COEFFICIENT FOR 20mm SHELL

	c_o	c_2	a_{L0}	a_{L2}	
Wind Tunnel	2.10	-2.8	2.57	10.2	before separation
Range	2.11	-2.5	2.52	9.2	$\delta = \sin 21^\circ$
Wind Tunnel	1.86	0.0	3.69	0.0	after separation
Range	1.83*	0.3	3.64*	1.0	$\delta = \sin 21^\circ$

* Evaluated at separation angle of 21°. The 20mm shell flying at an angle of 25° with separated flow is shown in Figure 8.14.

TABLE 8-4

CUBIC MAGNUS FORCE AND MOMENT COEFFICIENT FOR OGIVE CYLINDERS

L/d = 7

Mach No.		$\hat{c}_2$ f.c.g.	$\hat{c}_2$ m.c.g.	$\hat{c}_2$ r.c.g.	$\hat{a}_2$ c.g.	$\hat{a}_2$ swerve
1.3	$\left[C_{M_{p\alpha}}\right]_r$	40 ± 13	13 ± 3	--	- 36	$- 42 \pm 3$
	$\left[C_{M_q} + C_{M_{\dot{\alpha}}}\right]_r$	50 ± 36	--	--		
1.8	$\left[C_{M_{p\alpha}}\right]_r$	90 ± 40	--	0 ± 3	- 56	--
	$\left[C_{M_q} + C_{M_{\dot{\alpha}}}\right]_r$	65 ± 36	--	--		
2.5	$\left[C_{M_{p\alpha}}\right]_r$	90 ± 13	--	15 ± 8	- 48	--
	$\left[C_{M_q} + C_{M_{\dot{\alpha}}}\right]_r$	70 ± 10	--	--		

L/d = 9

1.8	$\left[C_{M_{p\alpha}}\right]_r$	74 ± 5	--	$13 \pm .5$	- 31	--*
	$\left[C_{M_q} + C_{M_{\dot{\alpha}}}\right]_r$	66 ± 8	--			

* a_2 for Mach number 1.3 was given in Figure 8.13 as $- 19 \pm 2$.

REFERENCES

8-1 Kryloff, N. and Bogoliuboff, N. B. Introduction to Nonlinear Mechanics. (translated by S. Lefschetz), Princeton University Press, 1947.

8-2 Murphy, C. H. Effect of Varying Air Density on the Nonlinear Pitching and Yawing Motion of a Symmetric Missile. BRL Report No. 1162, February 1962.

8-3 Rasmussen, M. L. Determination of Nonlinear Pitching-Moment Characteristics of Axially Symmetric Models from Free-Flight Data. NASA TN D-144, February 1960.

8-4 Kirk, Donn B. A Method for Obtaining the Nonlinear Aerodynamic Stability Characteristics of Bodies of Revolution from Free-Flight Tests. NASA TN D-780, March 1961.

8-5 Byrd, P. F. and Friedman, M. D. Handbook of Elliptic Integrals for Engineers and Physicists. Springer-Verlag, Berlin, 1954.

8-6 Murphy, C. H. and Schmidt, L. E. The Effect of Length on the Aerodynamic Characteristics of Bodies of Revolution in Supersonic Flight. BRL Report No. 876, August 1953.

8-7 Roecker, E. T. Large Yaw Firings of the 20mm, HEI, T282E1 Shell with Fuze T196 at Mach Number 2.3. BRL Memorandum Report No. 888, April 1955.

8-8 Luchuk, W. and Sparks, W. Wind-tunnel Magnus Characteristics of the 7-Caliber Army-Navy Spinner Rocket. NAVORD 3813, September 1954.

8-9 Buford, W. E. Aerodynamic Characteristics of 20mm Shell T-282E1, HEI. BRL Memorandum Report 834, October 1954.

8-10 Intrieri, P. F. Free Flight Measurements of the Static and Dynamic Stability and Drag of a 10° Blunted Cone at Mach Numbers 3.5 and 8.5. NASA TN D-1299, May 1962.

8-11 Kirk, D. B. and Miller, R. J. Free Flight Tests of Fifth Stage Scout Entry Vehicle at Mach Numbers of 5 and 17. NASA TN D-1425, October 1962.

PLANAR MOTION
TYPE(a) MOMENT

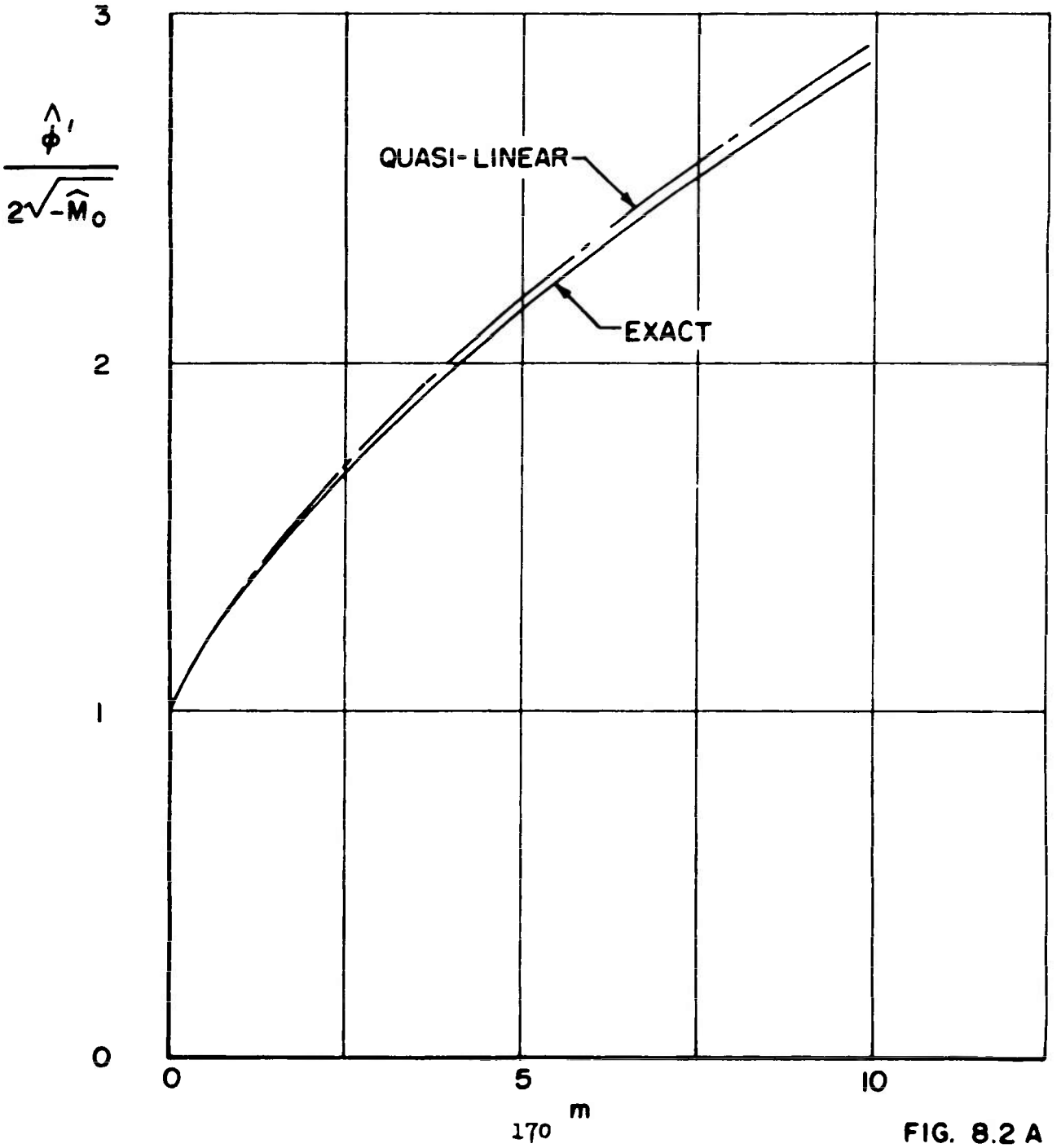

FIG. 8.2 A

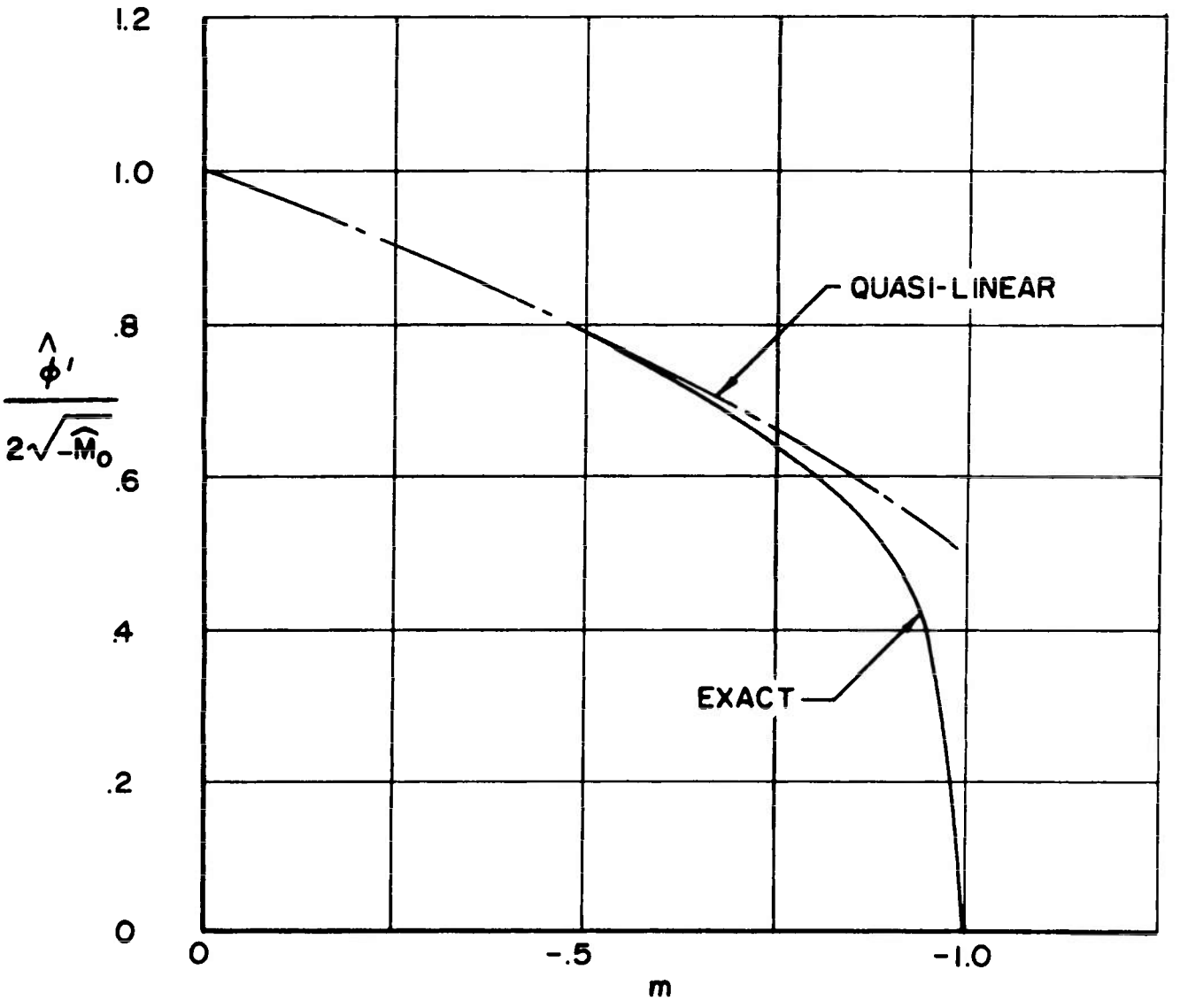
PLANAR MOTION
TYPE (b) MOMENT
1.2
1.0
.8
.6
.4
.2
0
$\frac{\hat{\phi}'}{2\sqrt{-\hat{M}_0}}$
QUASI-LINEAR
EXACT
0
-.5
-1.0
m

FIG. 8.2B

PLANAR MOTION
TYPE (c) MOMENT

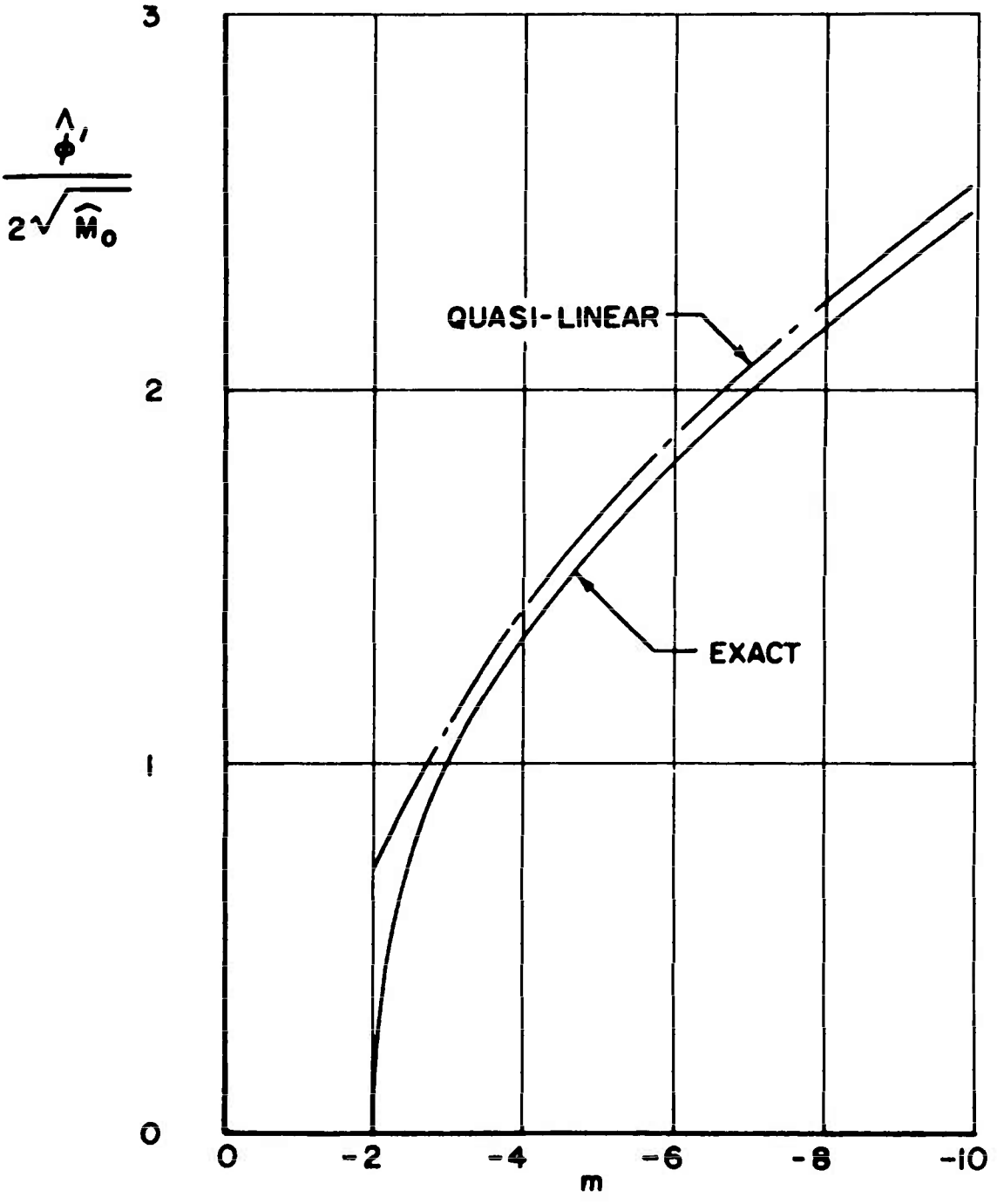

FIG. 8.2 C

CIRCULAR MOTION
TYPE (a) MOMENT

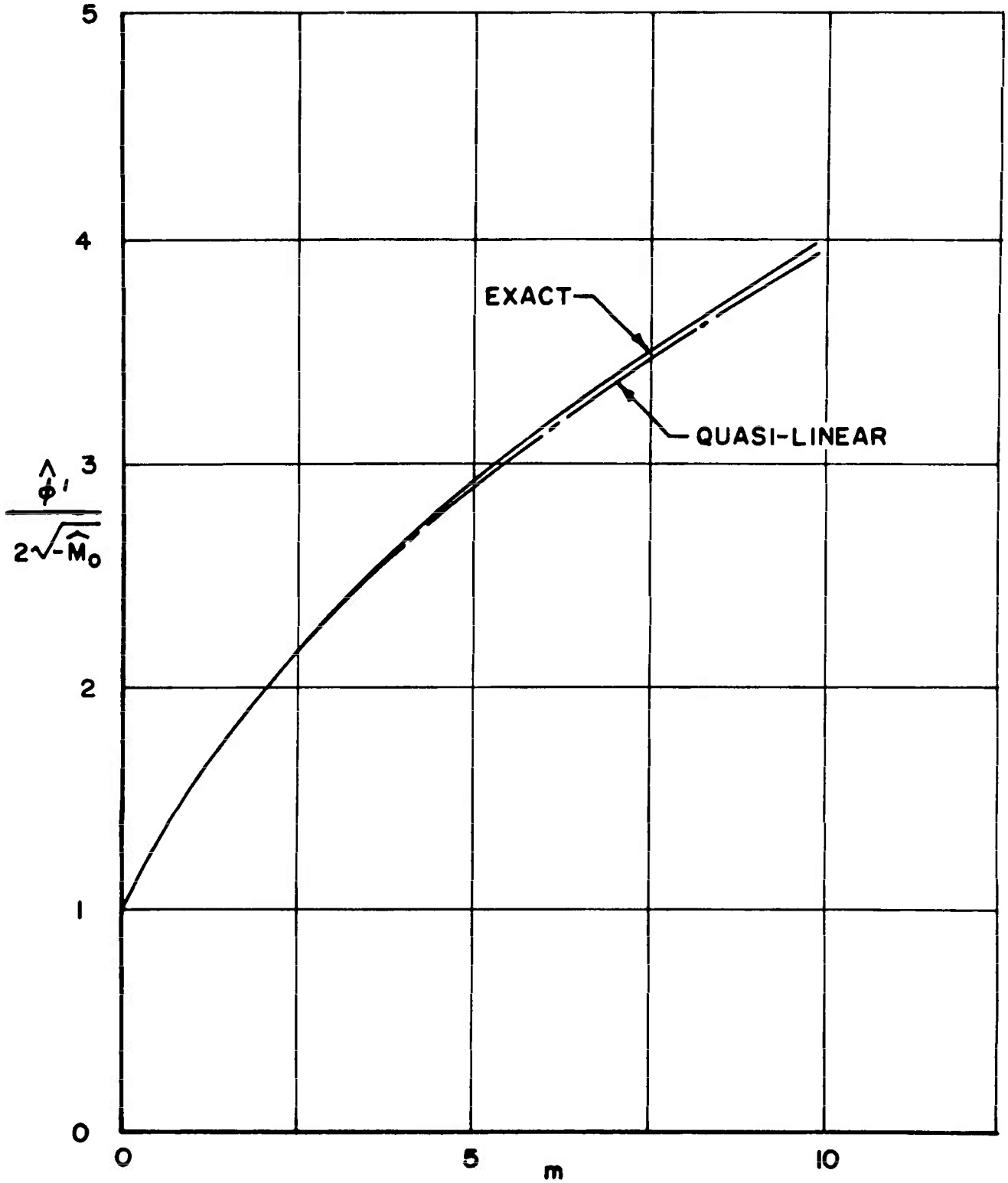

FIG. 8.3 A

CIRCULAR MOTION
TYPE (b) MOMENT

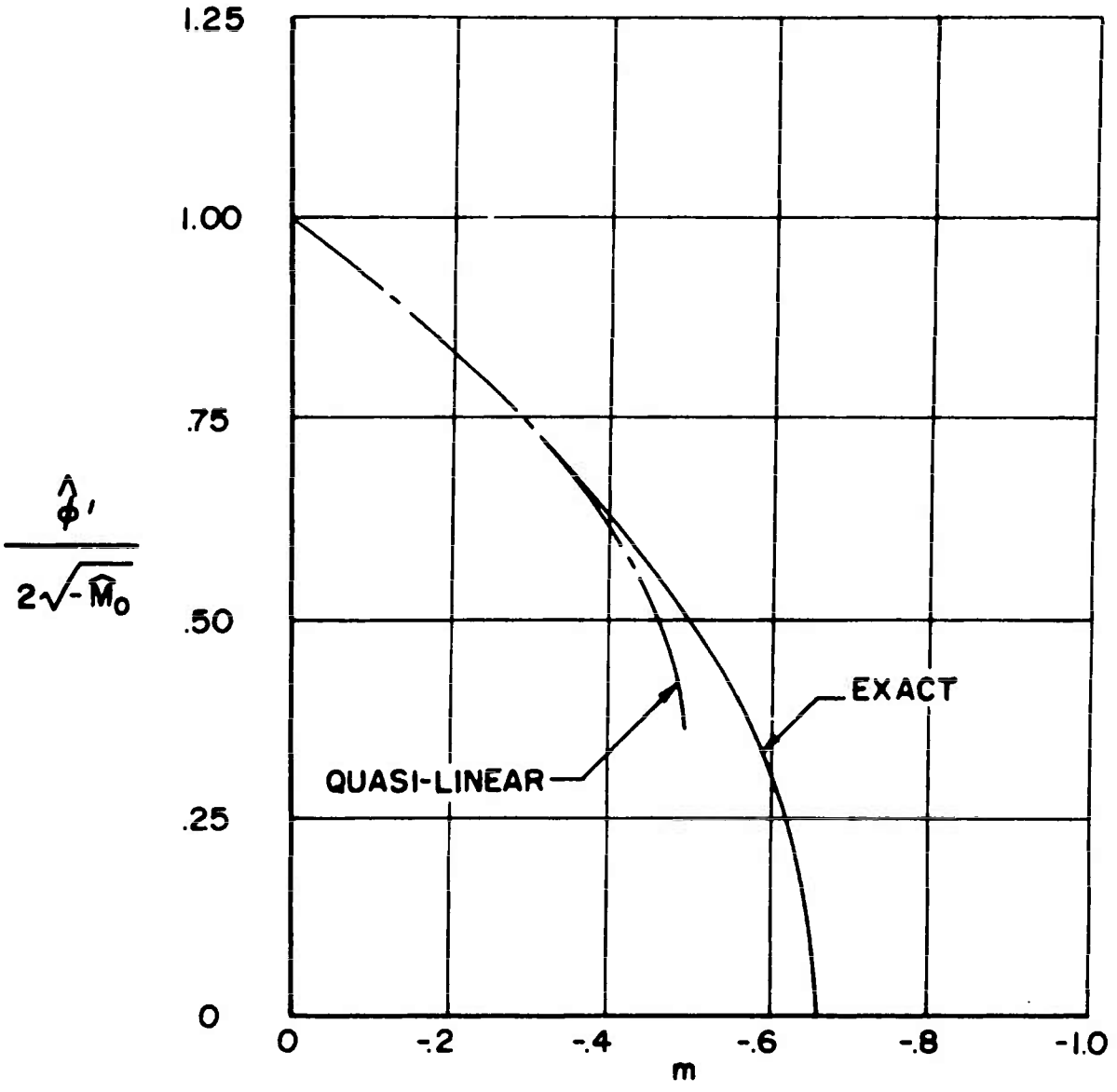

FIG. 8.3 B

CIRCULAR MOTION
TYPE (c) MOMENT

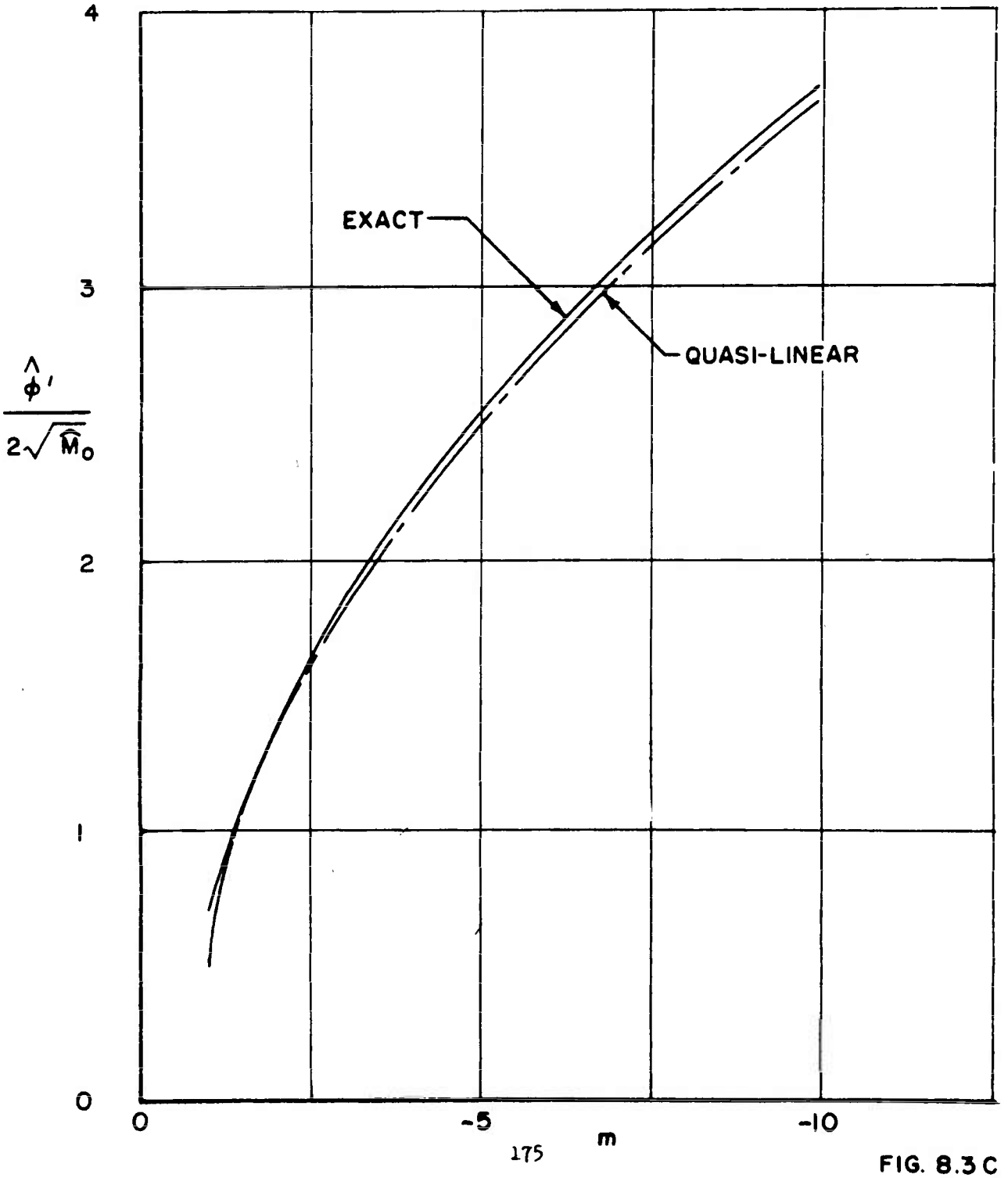

FIG. 8.3 C

$[C_{M_\alpha}]_r$ vs $10^2\,\delta_e^2$

M = 1.8
9 CAL. MODEL

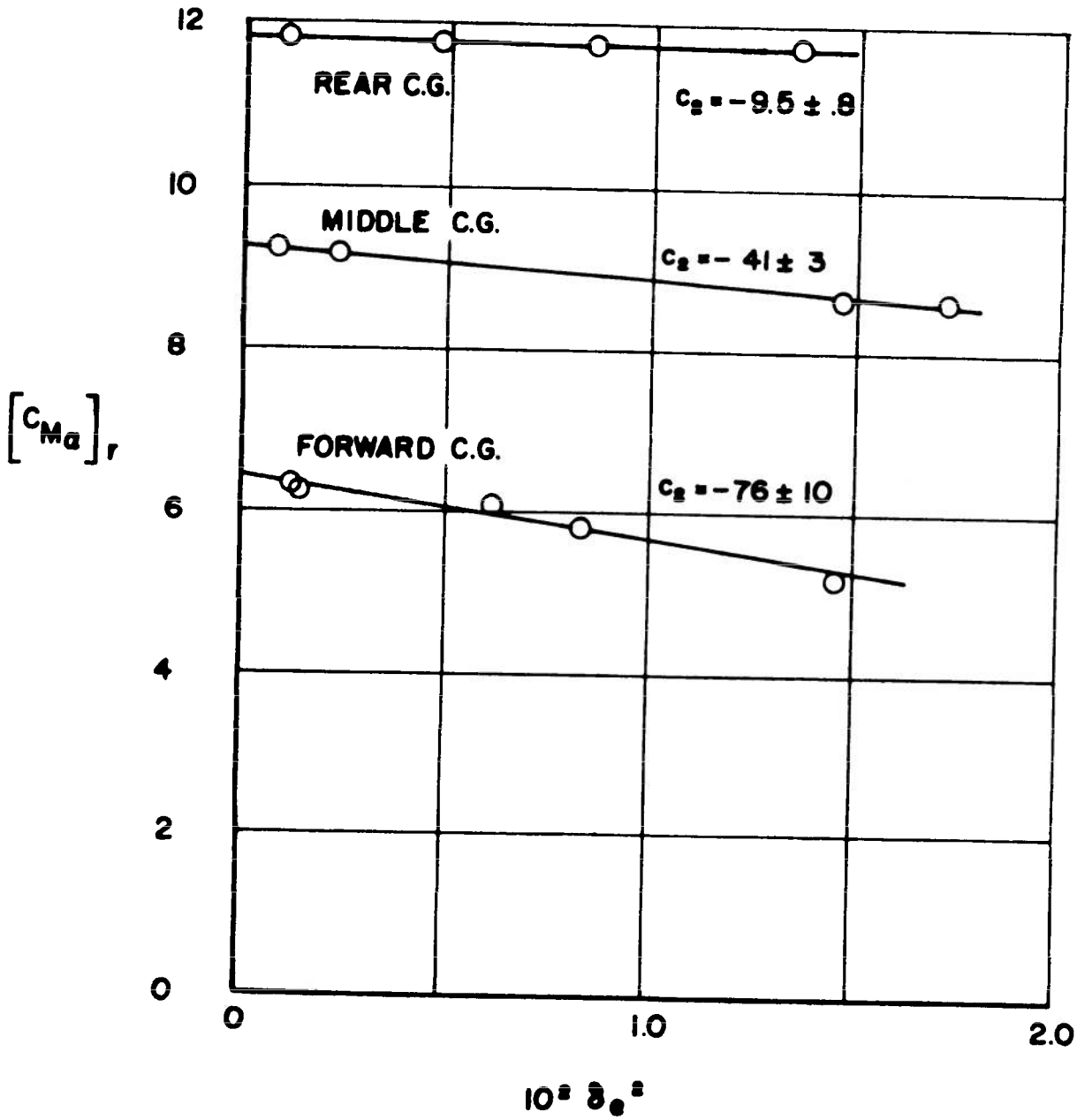

FIG. 8.4

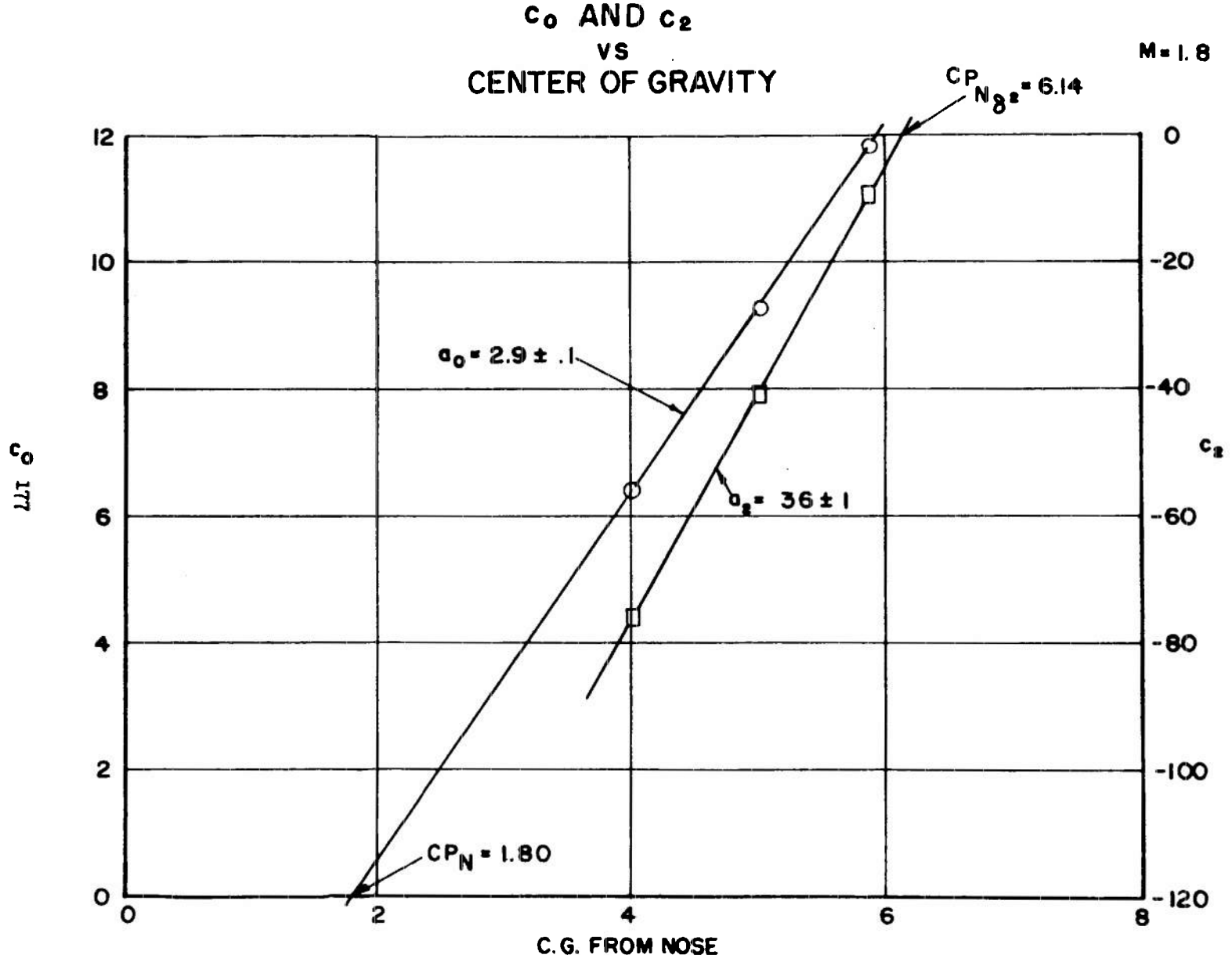
c_0 AND c_2
VS
CENTER OF GRAVITY
M = 1.8
$CP_{N_{\delta^2}} = 6.14$
$a_0 = 2.9 \pm .1$
$a_2 = 36 \pm 1$
$CP_N = 1.80$
c_0
c_2
C.G. FROM NOSE
0
2
4
6
8
10
12
-20
-40
-60
-80
-100
-120

FIG. 8.5

$[C_{L_\alpha}]_r$ vs $10^2 \delta_{e_2}^2$

M = 1.8

9 CAL. MODEL

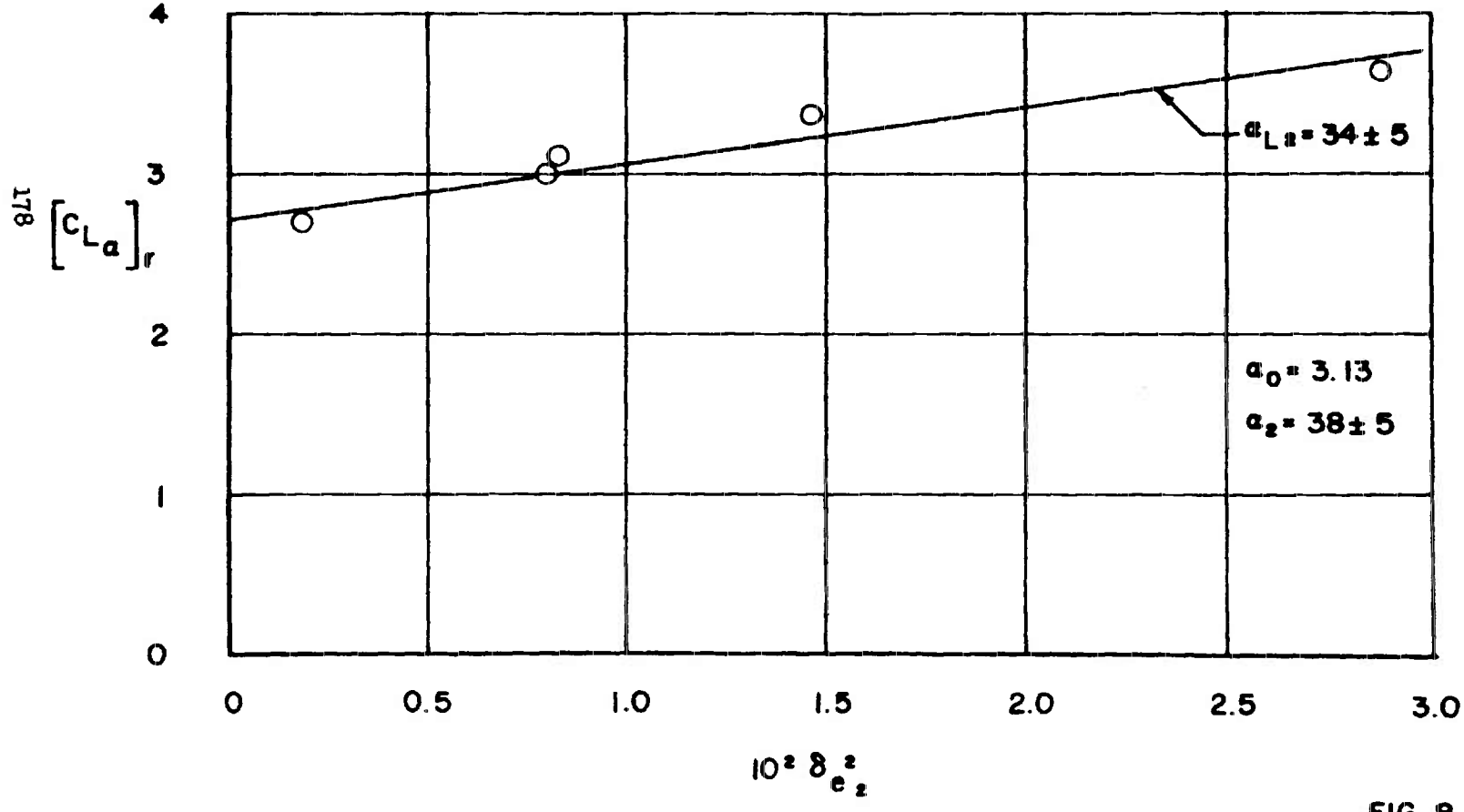

FIG. 8.6

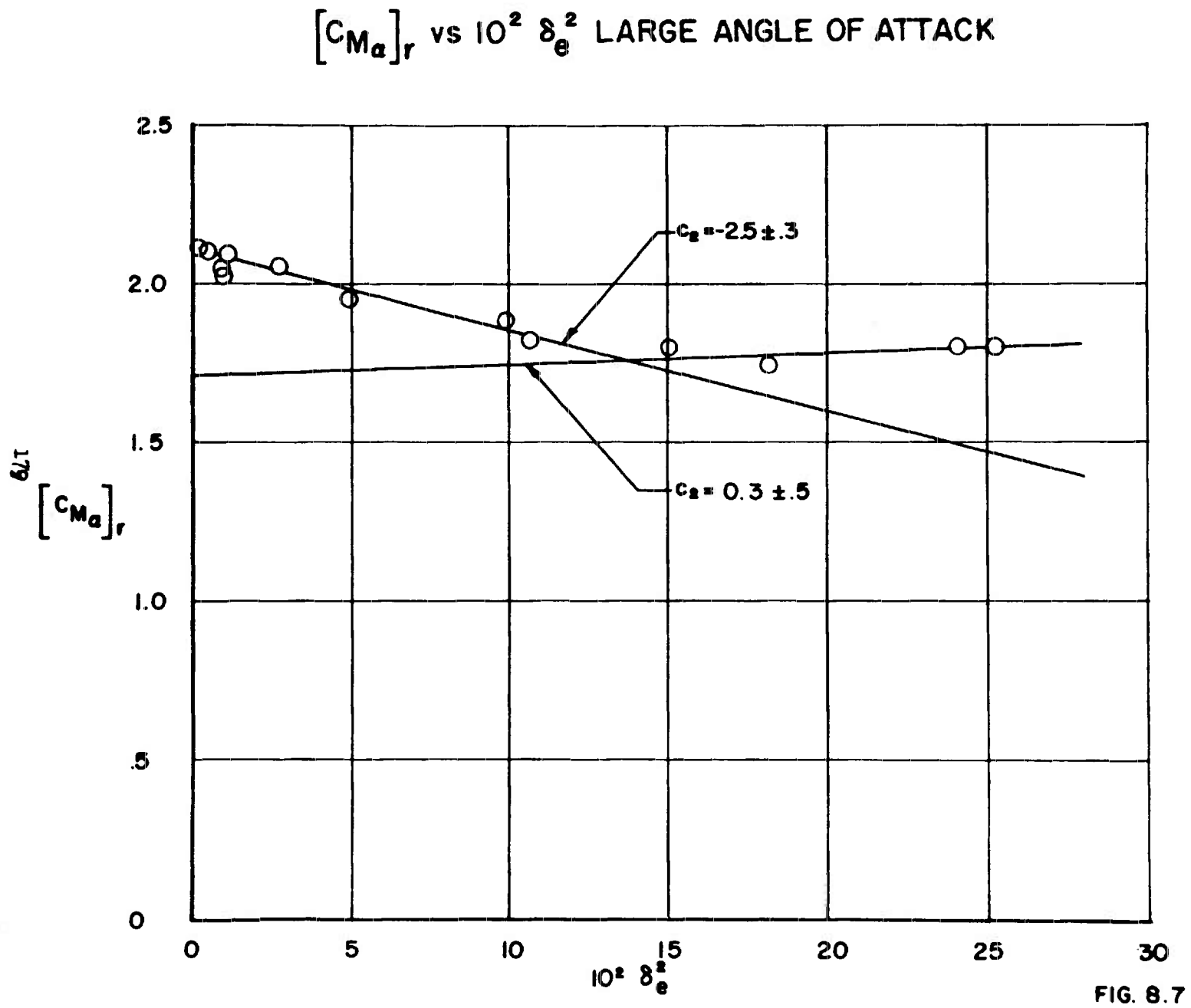
$[C_{M_\alpha}]_r$ vs $10^2\ \delta_e^2$ LARGE ANGLE OF ATTACK
2.5
2.0
1.5
1.0
.5
0
δ_{LT}
$[C_{M_\alpha}]_r$
$c_2 = -2.5 \pm .3$
$c_2 = 0.3 \pm .5$
0
5
10
15
20
25
30
$10^2\ \delta_e^2$

FIG. 8.7

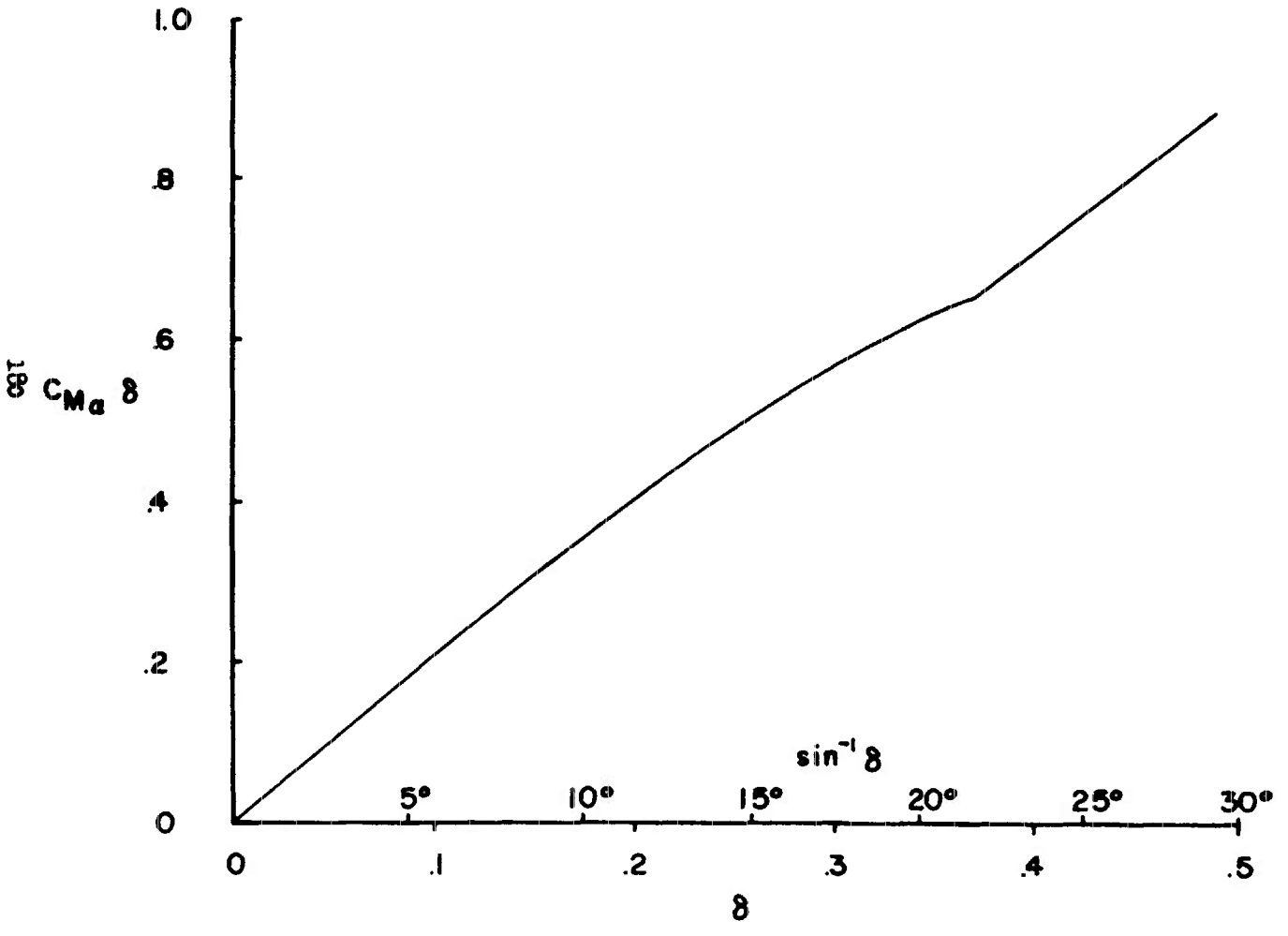
STATIC MOMENT
vs
RESULTANT ANGLE OF ATTACK
1.0
.8
.6
.4
.2
0
$C_{M_\alpha}\,\delta$
$\sin^{-1}\delta$
5°
10°
15°
20°
25°
30°
0
.1
.2
.3
.4
.5
δ

FIG. 8.8

$[C_{L_\alpha}]_r$ vs $10^2 \delta^2_{e2}$ LARGE ANGLE OF ATTACK

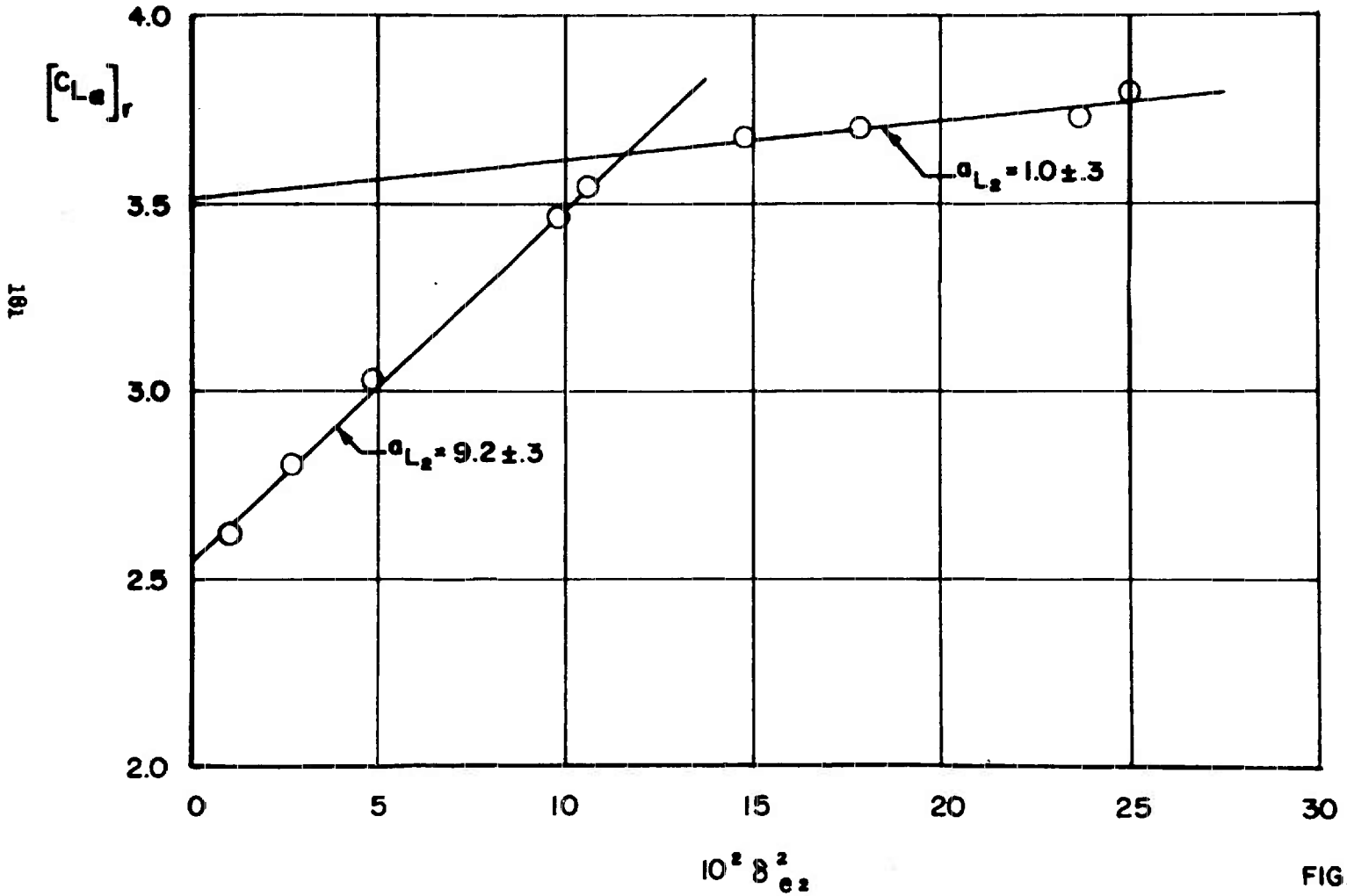

FIG. 8.9

LIFT FORCE
VS
RESULTANT ANGLE OF ATTACK

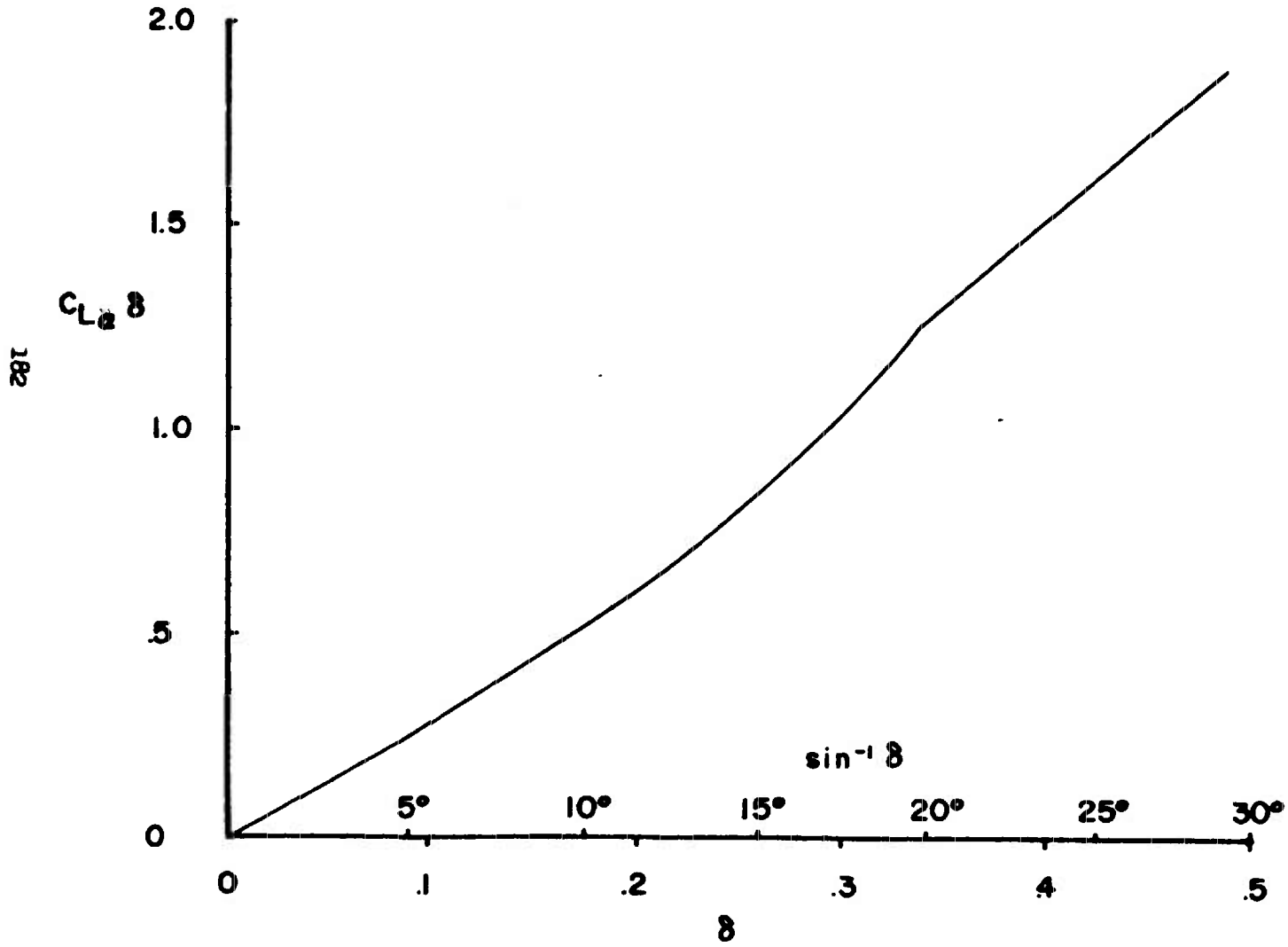

FIG. 8.10

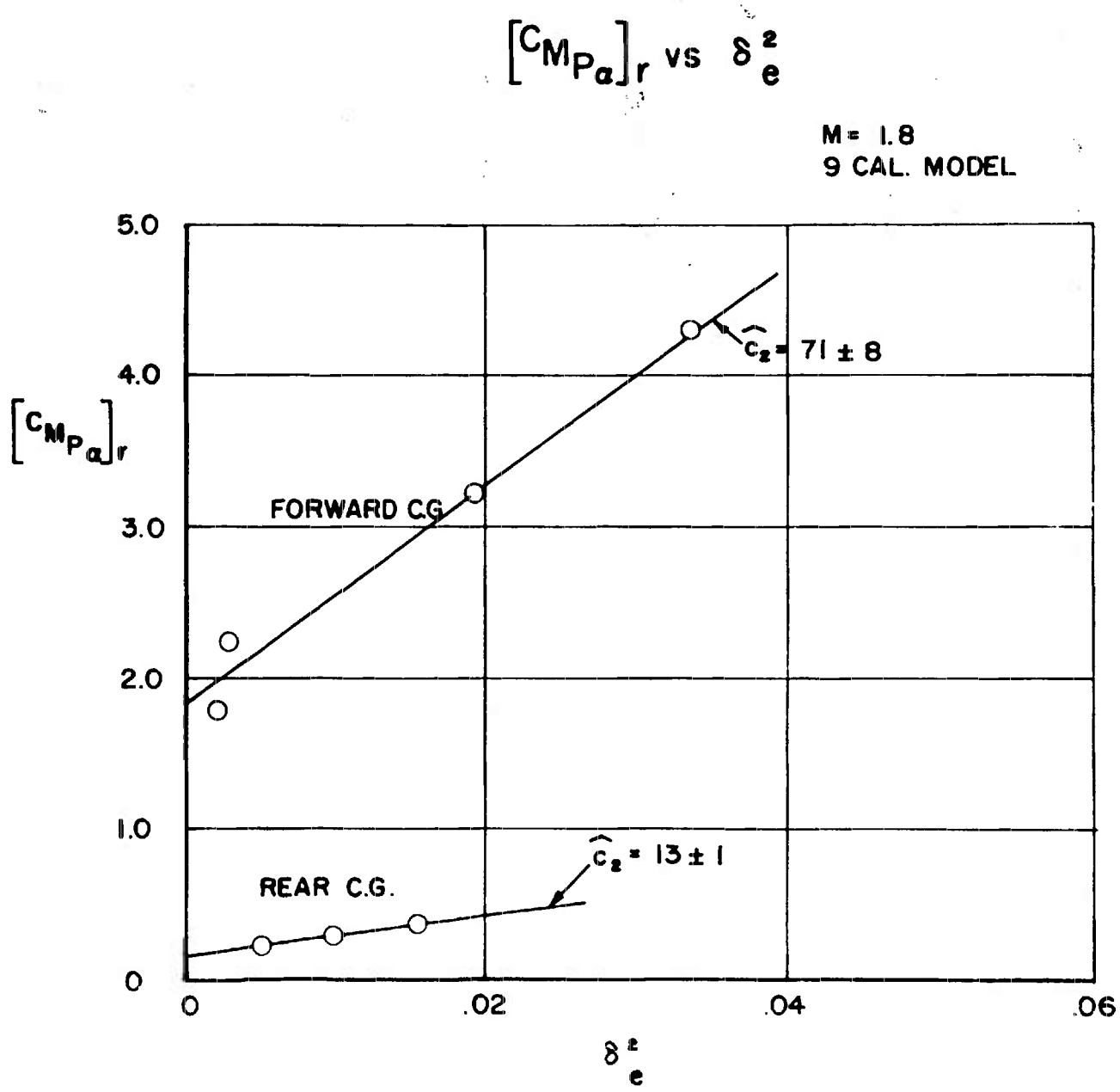
$[C_{M_{P_\alpha}}]_r$ vs δ_e^2
M = 1.8
9 CAL. MODEL
5.0
4.0
3.0
2.0
1.0
0
$[C_{M_{P_\alpha}}]_r$
FORWARD C.G.
$\hat{c}_2$ = 71 ± 8
REAR C.G.
$\hat{c}_2$ = 13 ± 1
0
.02
.04
.06
δ_e^2

FIG. 8.11

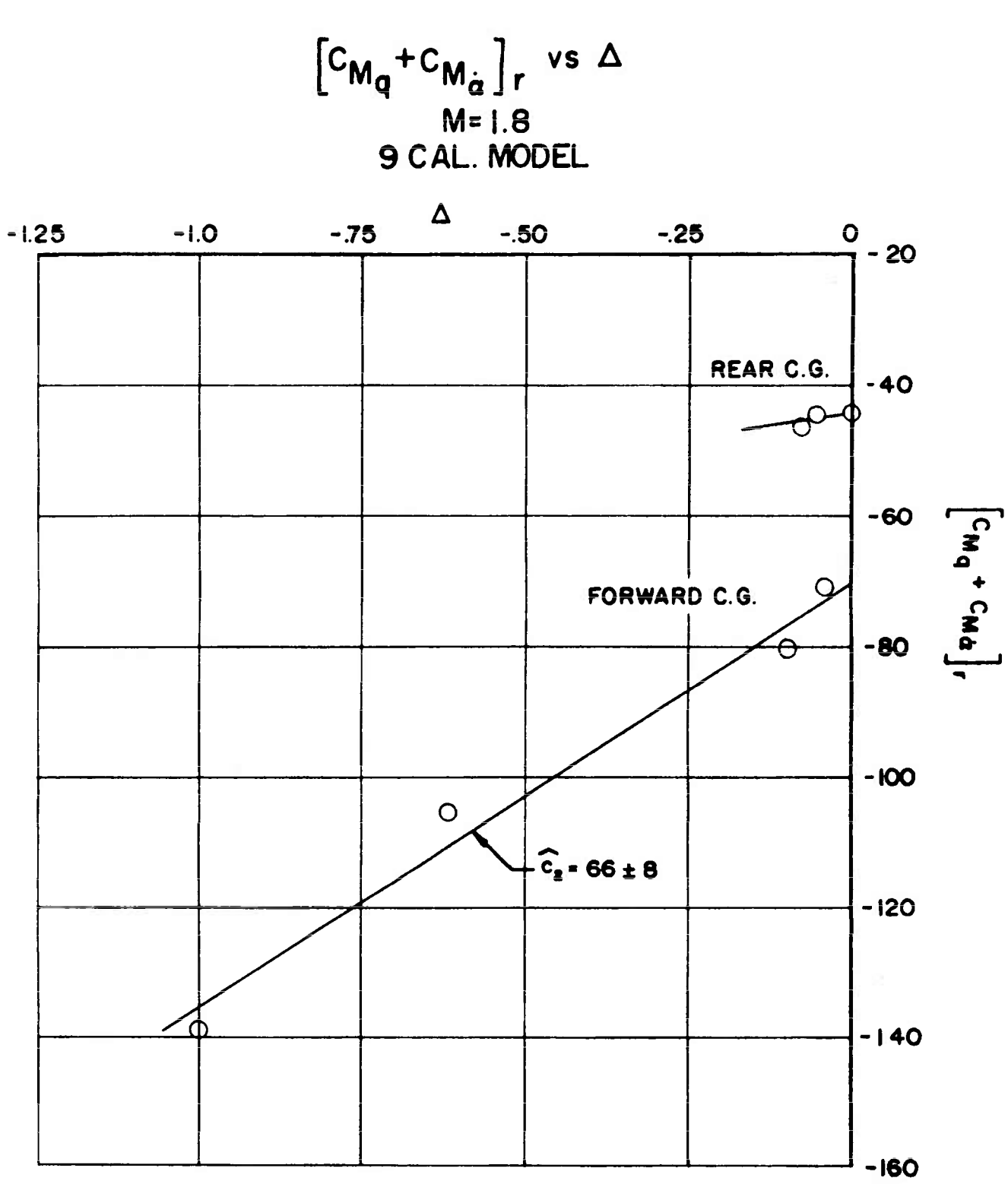
$[C_{M_q}+C_{M_{\dot{\alpha}}}]_r$ vs Δ
M=1.8
9 CAL. MODEL
Δ
-1.25
-1.0
-.75
-.50
-.25
0
-20
-40
-60
-80
-100
-120
-140
-160
REAR C.G.
FORWARD C.G.
$\hat{c}_2 = 66 \pm 8$
$[C_{M_q} + C_{M_{\dot{\alpha}}}]_r$

FIG. 8.12

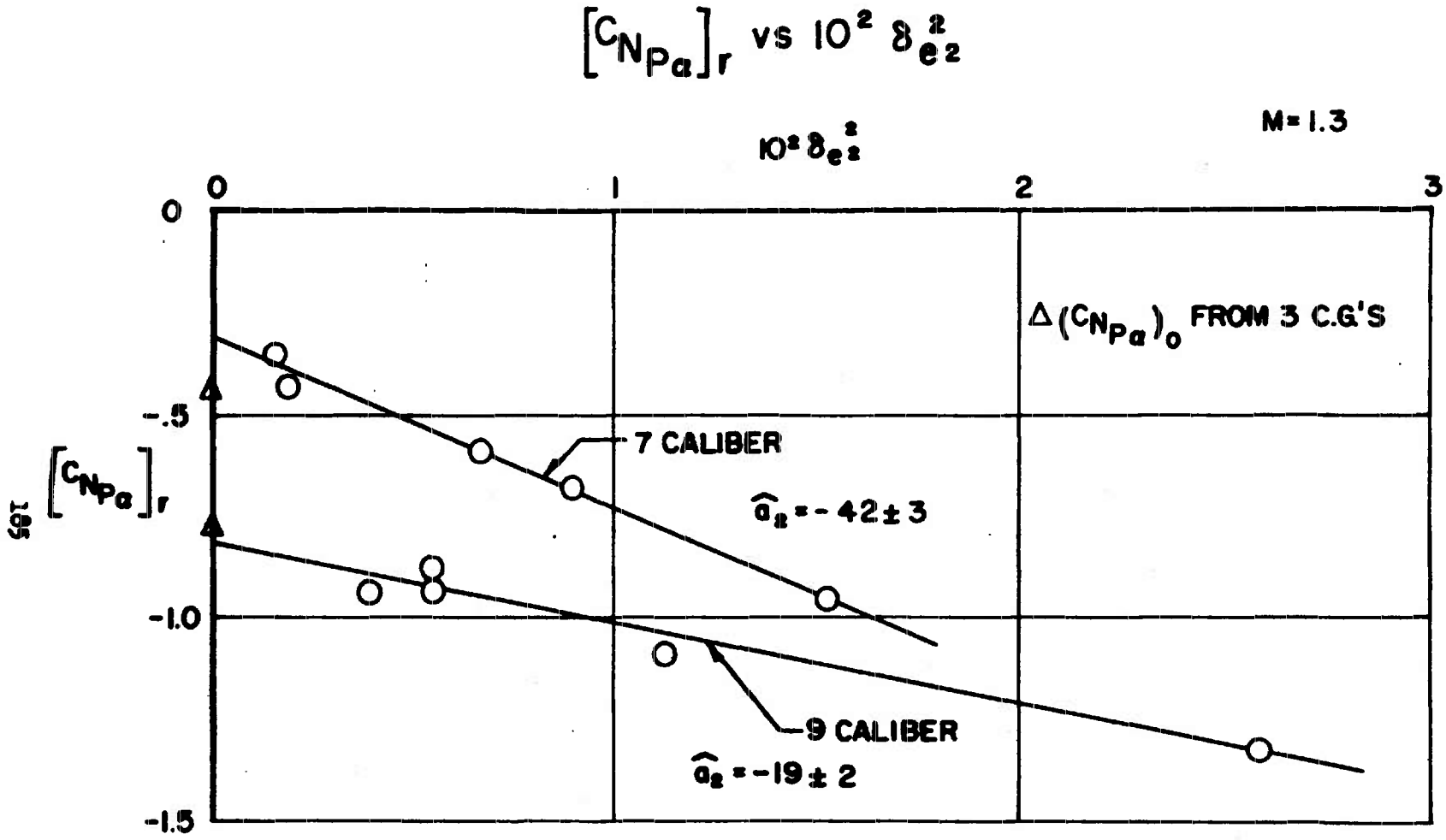
$[C_{N_{P\alpha}}]_r$ vs $10^2\,\delta_{e2}^2$
M = 1.3
$10^2\,\delta_{e2}^2$
0
1
2
3
0
-.5
-1.0
-1.5
$[C_{N_{P\alpha}}]_r$
$\Delta(C_{N_{P\alpha}})_0$ FROM 3 C.G.'S
7 CALIBER
$\hat{a}_2 = -42 \pm 3$
9 CALIBER
$\hat{a}_2 = -19 \pm 2$

FIG. 8.13

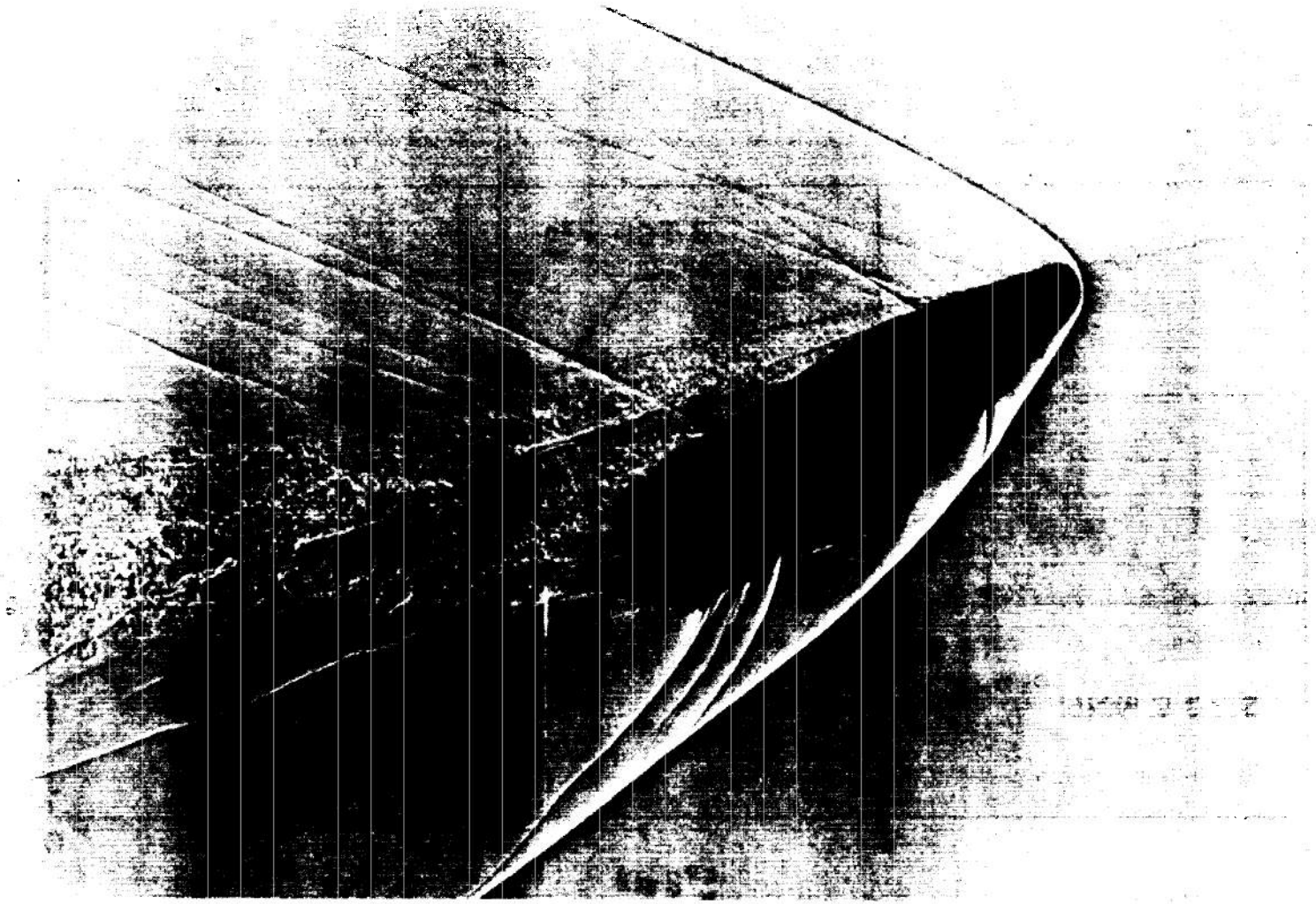

SHADOWGRAPH OF 20-mm SHELL AT LARGE YAW

FIG. 8.14

CHAPTER IX

PREDICTION OF NONLINEAR MOTION

9.1 Introduction

In the last chapter, we considered the measurement of certain nonlinear forces and moments by analyzing the motion induced by these quantities and observed on a ballistic range. In this chapter, we consider the inverse problem of predicting the motion caused by known nonlinear forces and moments. The actual expression for this force and moment may be either measured experimentally in a ballistic range or wind tunnel or computed from a theoretical model.

The problem will first be attacked by a generalization of the quasi-linear method of Section 8.2. This method provides effective values of frequencies and damping exponents in terms of "averages" of the linear and nonlinear aerodynamic terms but is limited by the assumption that the motion for at least a number of nutations is epicyclic. The behavior for a large number of cycles is determined by the consideration of the modal amplitudes alone and the use of an "amplitude plane". Finally, the limitation to epicyclic motion is removed for the special case of a strongly nonlinear cubic static moment. In this case, the trigonometric functions of the epicycle are replaced by elliptic functions and use is made of "quasi-constants" of the motion.

9.2 The Quasi-Linear Analysis

Quasi-linear analyses such as that of Kryloff and Bogoliuboff usually become extremely complex when applied to general real fourth order differential systems. We have already seen that the linearized motion of a rotationally symmetric missile can be described by a very simple fourth order system -- one that can be written in the form of a second order equation in one complex variable.

The nonlinear analysis will, therefore, be limited so that this symmetry is preserved. This is the reason symmetric direction cosines (u/V, v/V, w/V) and not nonsymmetric Eulerian angles were used to locate the velocity vector with respect to the missile axis system. In this chapter, the aerodynamic

coefficients are assumed to be functions of the complex ξ, and its derivative, ξ', which are independent of roll orientation. Clearly, the magnitude of these two two-dimensional vectors and the orientation angle between them possess this property. Now the angular velocity can be resolved into a radial component along the complex angle of attack and circumferential one perpendicular to the complex angle of attack, and one of these plus the magnitude of the angular velocity is sufficient to determine this orientation angle. With these remarks in mind, we will introduce the rotationally invarient quantities

$$\delta^2 = |\xi|^2 = \xi\bar{\xi}, \quad |\xi'|^2 = \xi'\bar{\xi}', \text{ and}$$

$$(\delta^2)' = 2\delta\delta' = (\xi\bar{\xi}' + \xi'\bar{\xi}).$$

and assume that aerodynamic coefficients are at most functions of these quantities.

The actual quasi-linear analysis initially parallels that of Section 6.7 for varying coefficients. (Equation (6.7.8-10)). As in that section we assume that the solution can be written in the form of an epicycle whose frequencies are not necessarily constants and whose amplitudes are not necessarily exponentially varying.

$$\tilde{\xi} = K_1 e^{i\phi_1} + K_2 e^{i\phi_2} \tag{2.1}$$

Differentiating Equation (2.1) twice we have

$$\tilde{\xi}' = (\lambda_1 + i\phi_1')K_1 e^{i\phi_1} + (\lambda_2 + i\phi_2')K_2 e^{i\phi_2} \tag{2.2}$$

$$\tilde{\xi}'' = \left[\lambda_1' + \lambda_1^2 - (\phi_1')^2 + i(\phi_1'' + 2\lambda_1\phi_1')\right] K_1 e^{i\phi_1}$$

$$+ \left[\lambda_2' + \lambda_2^2 - (\phi_2')^2 + i(\phi_2'' + 2\lambda_2\phi_2')\right] K_2 e^{i\phi_2} \tag{2.3}$$

where $\lambda_j = \dfrac{K_j'}{K_j}$

Since Equation (2.1) is the solution to the homogeneous linearized equation of pitching and yawing motion, we will apply this quasi-linear method to the homogeneous exact equation:

$$\tilde{\xi}'' + \left(H - \frac{\gamma'}{\gamma} - iP\right)\tilde{\xi}' - (M + iPT)\,\tilde{\xi} = 0 \tag{2.4}$$

where H, M, and T may be functions of

$$\delta^2,\ |\xi'|^2,\ \text{and}\ (\delta^2)'\ .$$

Inclusion of the small inhomogeneous gravity term, G, in Equation (2.4) imposes great difficulties on the nonlinear analysis and, hence, will not be done.

Equations (2.1-3) are now substituted in Equation (2.4) and the result rearranged.

$$\begin{aligned}
&(\phi_1')^2 - P\phi_1' + M_o - \lambda_1(\lambda_1 + H_o) - \lambda_1' \\
&\quad - i\left[(2\phi_1' - P)\lambda_1 + \phi_1'' + H_o\phi_1' - PT_o\right] \\
&= \left[H - H_o - \frac{\gamma'}{\gamma}\right]\left[(\lambda_1 + i\phi_1') + (\lambda_2 + i\phi_2')\frac{K_2}{K_1}e^{-i\hat{\phi}}\right] \\
&\quad - \left[(M - M_o) + iP(T - T_o)\right]\left[1 + \frac{K_2}{K_1}e^{-i\hat{\phi}}\right] \\
&\quad - \left\{\left[(\phi_2')^2 - P\phi_2' + M_o - \lambda_2(\lambda_2 + H_o) - \lambda_2'\right]\right. \\
&\quad \left. - i\left[(2\phi_2' - P)\lambda_2 + H_o\phi_2' - PT_o + \phi_2''\right]\right\}\frac{K_2}{K_1}e^{-i\hat{\phi}}
\end{aligned} \tag{2.5}$$

where $\hat{\phi} = \phi_1 - \phi_2$

For the linear equation, the right side of equation (2.5) is fluctuating with an average very close to zero and the left side is at most slowly varying. In Section 6.7, the frequency and damping exponent for the one-mode were

obtained by setting the left side of Equation (2.5) equal to zero. In Section 8.2, the quasi-linear solution for no damping, small geometrical angles and cubic static moment was derived by averaging the right side of Equation (2.5) with $T = H = \gamma' = T_o = H_o = 0$. In order to incorporate these previously excluded terms, we will take the average of all the terms on the right under the quasi-linear assumption that these averages are good approximations of the effect of "small" nonlinearities. The small terms involving λ_j in the real part of Equation (2.5) will be omitted in comparison with M_o.

$$
\begin{aligned}
&(\phi_1')^2 - P\phi_1' + M_o - i\left[(2\phi_1' - P)\,\lambda_1 + H_o\phi_1' - PT_o + \phi_1''\right] \\
&\quad = \frac{i}{2\pi}\int_o^{2\pi} (H - H_o - \frac{\gamma'}{\gamma})\left[\phi_1' + \phi_2'\left(\frac{K_2}{K_1}\right) e^{-i\hat{\phi}}\right] d\hat{\phi} \\
&\quad - \frac{1}{2\pi}\int_o^{2\pi} \left[(M - M_o) + iP(T - T_o)\right]\left[1 + \frac{K_2}{K_1}\, e^{-i\hat{\phi}}\right] d\hat{\phi}
\end{aligned}
\tag{2.6}
$$

It was shown in Section 8.4 that γ'/γ is well approximated by an odd function of $\hat{\phi}$ and, hence, only affects the frequency. With this in mind, we separate Equation (2.6) into real and imaginary parts.

$$
\begin{aligned}
&(\phi_1')^2 - P\phi_1' - \frac{1}{2\pi}\int_o^{2\pi} \left\{\left[(H - \frac{\gamma'}{\gamma})\,\phi_2' - PT\right]\left(\frac{K_2}{K_1}\right) \sin\hat{\phi}\right. \\
&\qquad \left. - M\left[1 + \frac{K_2}{K_1}\cos\hat{\phi}\right]\right\} d\hat{\phi} = 0
\end{aligned}
\tag{2.7}
$$

$$
\lambda_1 = \lambda_1^* - \frac{\phi_1''}{2\phi_1' - P} \tag{2.8}
$$

$$\text{where } \lambda_1^* = \frac{-1}{2\pi(2\phi_1' - P)} \int_0^{2\pi} \left\{ H\left[\phi_1' + \phi_2' \frac{K_2}{K_1} \cos\hat{\phi}\right] \right.$$

$$\left. - PT\left[1 + \frac{K_2}{K_1}\cos\hat{\phi}\right] + M \frac{K_2}{K_1}\sin\hat{\phi} \right\} d\hat{\phi}$$

Similar expressions apply for the other mode except the algebraic sign in front of the sine $\hat{\phi}$ term in λ_2^* is reversed due to the oddness of the sine function.

Equation (2.7) can be solved for ϕ_1' and differentiated to obtain ϕ_1''. Since ϕ_1' depends on amplitude when nonlinearities are present ϕ_1'' will contain λ_j's. Thus, Equation (2.8) is not solved for λ_1 since ϕ_1'' also has λ_1 as well as λ_2 in it. An important simple relation for frequency is that derived in Section 8.2 for cubic static moment, small geometrical angles, and no aerodynamic damping. The same relation may be obtained from Equation (2.7) if the no aerodynamic damping condition were replaced by the requirement that the average of (H - PT) sin $\hat{\phi}$ is zero. This would occur, for example, if H and T were only functions of δ^2. Under these conditions then

$$\phi_1' = \frac{P}{2} + \sqrt{-\hat{M}_o\left[1 + m_2(K_1^2 + 2K_2^2)\right]} \tag{2.9}$$

$$\phi_2' = \frac{P}{2} - \sqrt{-\hat{M}_o\left[1 + m_2(2K_1^2 + K_2^2)\right]} \tag{2.10}$$

Equation (2.9) can be differentiated and substituted in Equation (2.8).

$$\lambda_1\left[1 + \frac{m_2K_1^2}{2\left[1 + m_2(K_1^2 + 2K_2^2)\right]}\right] + \lambda_2\left[\frac{2m_2K_2^2}{2\left[1 + m_2(K_1^2 + 2K_2^2\right]}\right]$$

$$= \lambda_1^* - \left[\frac{M_o' - P'\phi_1'}{4\hat{M}_o} + \frac{M_2'm_2(K_1^2 + 2K_2^2)}{4M_2}\right]\left[1 + m_2(K_1^2 + 2K_2^2)\right]^{-1} \tag{2.11}$$

A similar equation can be derived for the other mode.

$$\lambda_1 \left[\frac{2m_2K_1^2}{2\left[1 + m_2(2K_1^2 + K_2^2)\right]} \right] + \lambda_2 \left[1 + \frac{m_2K_2^2}{2\left[1 + m_2(2K_1^2 + K_2^2)\right]} \right]$$

$$= \lambda_2^* - \left[\frac{M_o' - P'\phi_2'}{4\hat{M}_o} + \frac{M_2'm_2(2K_1^2 + K_2^2)}{4M_2} \right] \left[1 + m_2(2K_1^2 + K_2^2)\right]^{-1} \tag{2.12}$$

Equations (2.11-12) may be solved simultaneously for λ_1 and λ_2 .

$$\lambda_j = a_{j1}\left[\lambda_1^* - \frac{M_o'}{4\hat{M}_o}\right] + a_{j2}\left[\lambda_2^* - \frac{M_o'}{4\hat{M}_o}\right] + a_{j3}\left[\frac{M_o'}{\hat{M}_o} - \frac{M_2'}{M_2}\right]$$

$$+ a_{j4}\left[\frac{P'\phi_j'}{\hat{M}_o}\right] \tag{2.13}$$

where the a_{jk}'s are defined in Table 9.1.

One important occasion for which M_o and M_2 are variable is that of a missile entering or leaving the earth's atmosphere. (See Section 6.7). If this missile's static moment coefficients are constants,

$$\frac{M_o'}{M_o} = \frac{M_2'}{M_2} = \frac{\rho'}{\rho} = \tilde{\sigma} \tag{2.14}$$

and

$$\frac{M_o'}{\hat{M}_o} = \frac{M_o'/M_o}{1 - s_g} = \frac{\tilde{\sigma}}{1 - s_g} \tag{2.15}$$

where $\tilde{\sigma} = \ell\sigma \cos \Psi$, $\sigma = \frac{1}{22{,}000 \text{ ft.}}$ and

Ψ is the angle the trajectory makes with a downward pointing vertical.

$$\therefore \quad \lambda_j = a_{j1}\left[\lambda_1^* - \frac{\tilde{\sigma}}{4(1 - s_g)}\right] + a_{j2}\left[\lambda_2^* - \frac{\tilde{\sigma}}{4(1 - s_g)}\right]$$

$$+ a_{j3}\left[\frac{s_g\tilde{\sigma}}{1 - s_g}\right] + a_{j4}\left(\frac{P'\phi_j'}{\hat{M}_o}\right) \qquad (2.16)$$

TABLE 9.1

$$a_{11} = \left(\frac{2}{d}\right)\left[1 + m_2(K_1^2 + 2K_2^2)\right]\left[2 + m_2(4K_1^2 + 3K_2^2)\right]$$

$$a_{12} = -\left(\frac{4}{d}\right)\left[m_2K_2^2\right]\left[1 + m_2(2K_1^2 + K_2^2)\right]$$

$$a_{13} = \left(\frac{1}{2d}\right)\left[2m_2(K_1^2 + 2K_2^2) + m_2^2(4K_1^4 + 7K_1^2K_2^2 + 4K_2^4)\right]$$

$$a_{14} = \left(\frac{1}{2d}\right)\left[2 + m_2(4K_1^2 + 3K_2^2) - 2\left(\frac{\phi_2'}{\phi_1'}\right)(m_2K_2^2)\right]$$

$$a_{21} = -\left(\frac{4}{d}\right)\left[m_2K_1^2\right]\left[1 + m_2(K_1^2 + 2K_2^2)\right]$$

$$a_{22} = \left(\frac{2}{d}\right)\left[1 + m_2(2K_1^2 + K_2^2)\right]\left[2 + m_2(3K_1^2 + 4K_2^2)\right]$$

$$a_{23} = \left(\frac{1}{2d}\right)\left[2m_2(2K_1^2 + K_2^2) + m_2^2(4K_1^4 + 7K_1^2K_2^2 + 4K_2^4)\right]$$

$$a_{24} = \left(\frac{1}{2d}\right)\left[2 + m_2(3K_1^2 + 4K_2^2) - 2\left(\frac{\phi_1'}{\phi_2'}\right)(m_2K_1^2)\right]$$

$$d = 4 + 14m_2(K_1^2 + K_2^2) + m_2^2(12K_1^4 + 21K_1^2K_2^2 + 12K_2^4)$$

9.3 The Amplitude Plane

Two distinctive properties of a nonlinear homogeneous system are the dependence of the type of motion on initial conditions and the existence of limit motions. A linear second order complex system, for example, will have essentially the same motion for any initial condition since any solution is a linear combination of two linearly independent solutions and the only possible limit motion is the trivial one of the zero amplitude motion for dynamically stable systems.

For a second order system with coefficients which are independent of the independent variable, the phase plane is the best method for studying these properties. In a phase plane, the dependent variable is plotted versus its derivative and solutions appear as trajectories through each point. With the exception of singular points, every point has only one curve through it. The initial values of the variable and its derivative locate the particular trajectory which is the solution for those initial values. Thus, a look at the phase plane immediately reveals the relationship between initial conditions and the various possible motions and yields boundaries on these conditions for particular motions. The existence, size, and shape of limit motions are also revealed by this two dimensional phase space.

A fourth order system has, in general, a four dimensional phase space. One selection of these four coordinates would be the magnitudes and orientation angles of the initial complex angle of attack and initial complex angular velocity. Since rotationally symmetric missiles should have a rotationally symmetric phase space, their phase space is essentially three dimensional. Its coordinates could be the magnitudes of the initial angle of attack and the initial angular velocity and the angular orientation of one with respect to the other.

A three dimensional phase space is, however, quite difficult to use. The quasi-linear damping equations

$$\frac{K_j'}{K_j} = \lambda_j \; ; \; j = 1,2 \qquad (3.1)$$

indicate a possible two dimensional space which might be used. This simplicity in dimensionality is paid for by the assumption that the actual nonlinear motion can be described by epicycles whose frequencies and amplitudes vary throughout the missile's flight. Since the general behavior of the motion and the existence of limit motions are revealed by Equations (3.1), the frequency equations may be neglected and only the two equations for the modal amplitudes considered.*

As was previously noted, phase planes are used for equations which do not contain functions of the independent variable other than the dependent variable appearing in the phase plane. For this reason, we require that the λ_j's be functions on only the modal amplitudes themselves, i.e., $M_o' = M_2' = P^{'j} = 0$, etc. From basic symmetry, we see that the squares of amplitudes should appear in the λ_j's. We, therefore, rewrite Equation (3.1) in the form

$$(K_1^2)' = 2K_1^2\lambda_1 \ (K_1^2, K_2^2) \tag{3.2}$$

$$(K_2^2)' = 2K_2^2\lambda_2 \ (K_1^2, K_2^2) \tag{3.3}$$

The independent variable, s, may now be eliminated by dividing Equation (3.3) by Equation (3.2)

$$\frac{dK_2^2}{dK_1^2} = \frac{K_2^2\lambda_2 \ (K_1^2, K_2^2)}{K_1^2\lambda_1 \ (K_1^2, K_2^2)} \tag{3.4}$$

Equation (3.4) describes the angular motion by means of a point moving in the K_1^2 - K_2^2 plane which we will call the amplitude plane. For any point in this plane, the quasi-linear frequencies and damping exponents may be computed from Equations (2.7-8) for the one-mode and similar equations for the two-mode and except for the phase angles, ϕ_{jo}, the motion is completely determined.

Although Equation (3.4) is a nonlinear equation, it is first order and, therefore, much simpler than the fourth order Equation (2.4). The amplitude plane could be generated by numerically integrating Equation (3.4) for a variety of initial modal amplitudes. Equations of this form, however, have

* A rigorous justification for the quasi-linear treatment of limit motions is given in Reference 9-13.

been extensively studied by H. Poincare[9-2] who showed that the basic behavior of the amplitude plane trajectories is fixed by the location and type of Equation (3.4) singularities. (Singularities are points for which both the numerator and denominator of the right side of Equation (3.4) vanish.) A consideration of Equations (3.4) indicates the existence of three categories of possible singularities:

(1) the origin ($K_1^2 = K_2^2 = 0$)

(2) the K_1^2 intercepts of the one-mode zero damping curve ($K_2^2 = 0$, $\lambda_1 = 0$)

(3) the K_2^2 intercepts of the two-mode zero damping curves ($K_1^2 = 0$, $\lambda_2 = 0$)

(4) the intersection of the zero damping curves ($\lambda_1 = 0$, $\lambda_2 = 0$) .

According to Poincare's classification, there are four possible types of first order singularities: nodes, saddles, spirals, and centers. In Figure 9-2, a node and a saddle are shown while a spiral appears in Figure 9-3c and a center in Figure 9-3d. The particular curve along which the actual motion moves is determined by the initial modal amplitudes as specified by initial conditions. If the coordinates are translated so that the singularity is at the origin, Equation (3.4) has the form

$$\frac{dy}{dx} = \frac{ax + by + P(x,y)}{cx + dy + Q(x,y)} \tag{3.5}$$

where* $ad - bc \neq 0$ and P and Q vanish to at least the second order at the origin. The criteria for the type of singularity may now be stated in terms of the coefficients a, b, c, d and their discriminant $D = (b - c)^2 + 4ad$. (See page 44 of reference 9-3.):

(1) The singularity is a node if (a) $D > 0$ and $ad - bc < 0$ or (b) $D = 0$. (Note that if $ad = 0$, it is a node if $bc > 0$.)

(2) The singularity is a saddle if $D > 0$ and $ad - bc > 0$.

(3) The singularity is a spiral if $D < 0$ and $b + c \neq 0$.

---

* If $ad - bc = 0$ and the origin is a singularity, $a = b = c = d = 0$ and the singularity is at least second order.

(4) The singularity may be a center if $D < 0$ and $b + c = 0$; otherwise, it is a spiral*.

For the linear case, the λ_j' are constants and the origin is the only singular point. If the spin is zero, $\lambda_1 = \lambda_2$, and all the trajectories go either toward or away from the origin which is a node. (See Figure 9-1a) The particular curve which describes a given motion is specified by initial values of K_j and the direction of motion along the curve by the sign of the λ_j's. For positive λ_j's, the motion undamps away from the origin. When spin is not zero, the damping exponents are not necessarily equal and may even differ in sign. The origin can, therefore, be either a node (Figure 9-2a) or a saddle (Figure 9-2b). All these figures display an important characteristic of linear systems -- i.e., the type of motion is independent of initial conditions.

Amplitude planes will now be constructed for two simple nonlinearities and one fairly general nonlinearity. In the first example, the effect of quadratic dependence in δ of $C_{M_q} + C_{M_{\dot\alpha}}$ on the motion of a nonspinning missile will be considered while in the second the effect of a cubic Magnus moment on the motion of a spinning missile will be described. In both of these examples, small geometrical angles ($\gamma \doteq 1$, $\gamma' = 0$) and a linear static moment will be assumed. In the third example, the effect of a cubic static moment and a very general nonlinear aerodynamic damping moment on a nonspinning missile will be studied in detail.

9.3a <u>Zero Spin</u> - Quadratic $C_{M_q} + C_{M_{\dot\alpha}}$ 9-11

For this case, the damping in pitch coefficients have the form

$$C_{M_q} + C_{M_{\dot\alpha}} = d_o + d_2\delta^2 \tag{3.6}$$

and

$$\xi'' + (H_o + H_2\delta^2)\xi' - M\xi = 0 \tag{3.7}$$

---

* If $P = Q = 0$, the singularity is a center. In reference 9-4, the conditions for a center are given when P and Q are quadratic functions of x and y. Since equalities seldom occur in practice -- only inequalities, the distinction between a center and a very slow spiral is purely academic.

$$\text{where } H_o = \frac{\rho S \ell}{2m} \left[C_{L_\alpha} - C_D - k_t^{-2} d_o \right]$$

$$H_2 = - \frac{\rho S \ell}{2m} k_t^{-2} d_2$$

From Equation (2.8) and the corresponding equation for the two-mode,

$$\lambda_1 = - \left(\frac{1}{2}\right) \left[H_o + H_2 K_1^2 \right] \tag{3.8}$$

$$\lambda_2 = - \left(\frac{1}{2}\right) \left[H_o + H_2 K_2^2 \right] \tag{3.9}$$

The amplitude plane for the interesting case where the damping changes sign ($H_o H_2 < 0$) is shown in Figure 9-1b. The zero damping curves are vertical and horizontal straight lines with intercepts $(-H_o/H_2, 0)$ and $(0, -H_o/H_2)$. The tests of this section show that both of these singularities are saddle points. These lines intercept at a planar singularity point $(-H_o/H_2, -H_o/H_2)$ which is a node.

If H_o is positive, the origin is a stable node and Figure 9-1b shows a characteristic nonlinear dependence of the type of motion on initial conditions. For initial modal amplitudes which are inside the square formed by the axes and the zero damping lines, the motion will damp to zero amplitude; for modal amplitudes outside this square, the motion will grow into an undamped spiral motion.

If H_o is negative, the origin becomes an unstable node and the planar node becomes a stable node. For any initial conditions, the motion will become a planar motion with maximum amplitude $K_1 + K_2 = 2|H_o/H_2|^{1/2}$. This limit motion is another property of nonlinear systems. It is interesting to note that had we restricted ourselves to planar motion $\xi = \delta e^{i\theta}$, the corresponding differential equations would be that for the van der Pol oscillator.

$$\delta'' + (H_o + H_2 \delta^2) \delta' + M\delta = 0 \tag{3.10}$$

This planar singularity is precisely the limit cycle predicted by the one-degree-of-freedom theory. This example is, therefore, a generalized van der Pol equation.

9.3b Cubic Magnus Moment.[9-11]

For this example, spin is constant but non-zero, damping in pitch and static moments are linear, and the Magnus moment is cubic in δ.

$$C_{M_{p\alpha}} = \hat{c}_o + \hat{c}_2\delta^2 \tag{3.11}$$

$$\tilde{\xi}'' + (H - iP)\tilde{\xi}' - \left[M + iP(T_o + T_2\delta^2)\right]\tilde{\xi} = 0 \tag{3.12}$$

Equation (3.11) is precisely Equation (8.5.1) with $M_2 = 0$. The quasi-linear expressions for the damping exponents are those given in Section (8.5).

$$\lambda_1 = \lambda_{10} + \lambda_{12}(K_1^2 + 2K_2^2) \tag{3.13}$$

$$\lambda_2 = \lambda_{20} + \lambda_{22}(2K_1^2 + K_2^2) \tag{3.14}$$

where $\lambda_{jo} = -\dfrac{\phi_j' H - PT_o}{2\phi_j' - P}$

$$\lambda_{j2} = \frac{PT_2}{2\phi_j' - P} \qquad (\therefore \lambda_{12} = -\lambda_{22})$$

The zero damping curves in the amplitude plane are, therefore, straight lines with slopes - 1/2, - 2.

When spin is not zero, the origin is either a node ($\lambda_{10}\lambda_{20} > 0$) or a saddle ($\lambda_{10}\lambda_{20} < 0$). These two possibilities are shown in Figures 9-2a and 9-2b for a linear Magnus moment. For a cubic Magnus moment, the intercepts and intersection of the zero damping lines must be studied.

$$\lambda_{10} + \lambda_{12}(K_1^2 + 2K_2^2) = 0 \tag{3.15}$$

$$\lambda_{20} - \lambda_{12}(2K_1^2 + K_2^2) = 0 \tag{3.16}$$

Singularities exist at the intercepts, $(-\lambda_{10}/\lambda_{12}, 0)$ and $(0, \lambda_{20}/\lambda_{12})$, and at the point of intersection $\left(\frac{\lambda_{10} + 2\lambda_{20}}{3\lambda_{12}} , \frac{2\lambda_{10} + \lambda_{20}}{-3\lambda_{12}} \right)$. The type of singularity at the intercept $(-\lambda_{10}/\lambda_{12}, 0)$ can now be found by substituting Equations (3.13-14) in Equation (3.4) and translating the origin to this circular singularity.

$$\frac{dy}{dx} = \frac{y\left[2\lambda_{10} + \lambda_{20} - \lambda_{12}(2x + y)\right]}{(\lambda_{12}x - \lambda_{10})(x + 2y)} \tag{3.17}$$

where $x = K_1^2 + \frac{\lambda_{10}}{\lambda_{12}}$

$y = K_2^2$

$$D = (b - c)^2 + 4ad$$

$$= (3\lambda_{10} + \lambda_{20})^2 \geq 0 \tag{3.18}$$

$$ad - bc = \lambda_{10}(2\lambda_{10} + \lambda_{20}) \tag{3.19}$$

For these relations and the conditions given after Equation (3.5), we see that we will have a 1 - mode circular singularity in the first quadrant if $\lambda_{10}\lambda_{12} < 0$. This singularity is a saddle if $\lambda_{10}(2\lambda_{10} + \lambda_{20}) > 0$ and is a node otherwise. Similarly, a 2 - mode circular singularity exists if $\lambda_{20}\lambda_{22} = -\lambda_{20}\lambda_{12} < 0$. This singularity is a saddle if $\lambda_{20}(\lambda_{10} + 2\lambda_{20}) > 0$ and is a node otherwise.

The character of singularity at the point of intersection (a mixed mode singularity) can be found by transferring the origin to that point.

$$\frac{dy}{dx} = \frac{(2\lambda_{10} + \lambda_{20})(2x + y) - 3\lambda_{12}(2x + y)y}{(\lambda_{10} + 2\lambda_{20})(x + 2y) + 3\lambda_{12}(x + 2y)x} \tag{3.20}$$

$$\therefore D = 33\lambda_{10}^2 + 78\lambda_{10}\lambda_{20} + 33\lambda_{20}^2$$

$$= \frac{33}{\lambda_{20}^2}\left[\frac{\lambda_{10}}{\lambda_{20}} + 1.812\right]\left[\frac{\lambda_{10}}{\lambda_{20}} + .552\right] \tag{3.21}$$

$$ad - bc = 3(\lambda_{10} + 2\lambda_{20})(2\lambda_{10} + \lambda_{20}) \tag{3.22}$$

$$b + c = 3(\lambda_{10} + \lambda_{20}) \tag{3.23}$$

The existence and type of singularity can now be determined in the usual way with the following results:

(1) A mixed mode singularity exists if λ_{12} has the opposite sign to λ_{10} and $-2 < \frac{\lambda_{10}}{\lambda_{20}} < -.5$.

(2) This singularity is a node if

$$-2 < \frac{\lambda_{10}}{\lambda_{20}} \leqq -1.812 \quad \text{or} \quad -.552 \leqq \frac{\lambda_{10}}{\lambda_{20}} < -.5$$

(3) This singularity is a spiral singularity if

$$-1.812 < \frac{\lambda_{10}}{\lambda_{20}} < -1 \text{ or } -1 < \frac{\lambda_{10}}{\lambda_{20}} < -.552$$

(4) This singularity is a center* if

$$\frac{\lambda_{10}}{\lambda_{20}} = -1.$$

---

* To prove that it must be a center, the relations of Reference 9-4 are required.

Most of the possible amplitude planes are shown in Figure 9-3a-d. In Figure 9-3a, the curve terminating at the singular point is called the separatrix and for a missile with stable small amplitude motion it divides all initial conditions into two families: those which yield a motion tending to zero amplitudes and those which yield motion which grows without bound. Figures 9-3b and 9-3c demonstrate the existence of circular limit motion and epicyclic limit motion respectively while Figure 9-3d shows the very special case of epicyclic motion with periodic variation of the amplitudes. The predictions of the separatrix, the limit circular motion and the limit epicyclic motion have been tested by numerical integration of the exact differential equations with great success[9-5]. This success reinforces our confidence in the quasi-linear theory.

9-3c Cubic Static Moment - Nonlinear Damping - Zero Spin.[9-12]

For this case, we will study a very general form of the aerodynamic moment with the approximation $\mu = -i\xi'$

$$C_m + iC_n = -i\left[(c_o + c_2\delta^2 + c^*)\xi + d\xi'\right] \tag{3.24}$$

where $d = d(\delta^2)$ is a function of δ^2 and

$c^* = c^*((\delta^2)')$ is a function of $(\delta^2)'$

To define c_o uniquely, we will require that $c^*(o) = 0$. The presence of $(\delta^2)'$ in c^* indicates that this term probably affects the damping as well as the more conventional amplitude dependent damping term $d\xi'$.

The simplest nonlinear form of d and c^* can be obtained by assuming them to be linear in δ^2 and $(\delta^2)'$ respectively.

$$\therefore C_m + iC_n = -i\left\{\left[c_o + c_2\delta^2 + c_2^*(\delta^2)'\right]\xi + \left[d_o + d_2\delta^2\right]\right\} \tag{3.25}$$

These two nonlinear damping terms have different directions and so depend on the eccentricity of the quasi-linear elliptic motion. For circular motion, $\xi = \delta_o e^{i\theta}$ and ξ' is perpendicular to ξ.

$$C_m + iC_n = -i\delta_o e^{i\theta}\left[c_o + c_2\delta_o^2 + i\theta'(d_o + d_2\delta_o^2)\right] \tag{3.26}$$

For planar motion, however, $\xi = \delta e^{i\theta_o}$ and ξ' has the same direction as ξ

$$C_m + iC_n = -ie^{i\theta_o}\left[(c_o + c_2\delta^2)\delta + [d_o + (d_2 + 2c_2^*)\delta^2]\delta'\right] \qquad (3.27)$$

Thus the damping moment depends on the shape of the motion. This result casts some doubt on the standard wind tunnel method of measuring aerodynamic damping by forcing planar oscillation and determining the net energy required to maintain the oscillation. If the actual damping moment has the form of Equation (3.25), these wind tunnel measurements could lead to quite erroneous predictions of actual flight behavior.

Returning now to the more general Equation (3.24), we derive the corresponding equation of pitching and yawing motion for small geometrical angles

$$\xi'' + H(\delta^2)\xi' - M^*((\delta^2)')\xi - (M_o + M_2\delta^2)\xi = 0 \qquad (3.28)$$

$$\text{where } H(\delta^2) = \frac{\rho S \ell}{2m}\left[C_{L_\alpha} - C_D - k_t^{-2}\, d\right]$$

$$M^* = \frac{\rho S \ell}{2m} k_t^{-2}\, c^* \quad .$$

For Equation (3.28), the quasi-linear damping exponents can be obtained from Equation (2.13).

$$\lambda_1 = \frac{2}{d}\left\{\left[1 + m_2(K_1^2 + 2K_2^2)\right]\left[2 + m_2(4K_1^2 + 3K_2^2)\right]\lambda_1^* - 2m_2K_2^2\left[1 + m_2(2K_1^2 + K_2^2)\right]\lambda_2^*\right\} \qquad (3.29)$$

$$\lambda_2 = \frac{2}{d}\left\{-2m_2K_1^2\left[1 + m_2(K_1^2 + 2K_2^2)\right]\lambda_1^* + \left[1 + m_2(2K_1^2 + K_2^2)\right]\left[2 + m_2(3K_1^2 + 4K_2^2)\right]\lambda_2^*\right\} \qquad (3.30)$$

where

$$d = 4 + 14m_2(K_1^2 + K_2^2) + m_2^2(12K_1^4 + 21K_1^2K_2^2 + 12K_2^4)$$

$$\lambda_1^* = -\frac{1}{4\pi}\int_0^{2\pi}\left\{H\left[1 + \frac{\phi_2' K_2}{\phi_1' K_1}\cos\hat{\phi}\right] + M^*\frac{K_2}{\phi_1' K_1}\sin\hat{\phi}\right\}d\hat{\phi}$$

$$\lambda_2^* = -\frac{1}{4\pi}\int_0^{2\pi}\left\{H\left[1 + \frac{\phi_1' K_1}{\phi_2' K_2}\cos\hat{\phi}\right] - M^*\frac{K_1}{\phi_2' K_2}\sin\hat{\phi}\right\}d\hat{\phi}$$

$$\delta^2 = K_1^2 + K_2^2 + 2K_1K_2\cos\hat{\phi}$$

$$(\delta^2)' = -2K_1K_2\hat{\phi}'\sin\hat{\phi}$$

$$\hat{\phi}' = \phi_1' - \phi_2'$$

$$= \sqrt{-M_o\left[(1 + m_2(K_1^2 + 2K_2^2)\right]} + \sqrt{-M_o\left[(1 + m_2(2K_1^2 + K_2^2)\right]}$$

Equations (3.29-30) are symmetric in the modal amplitudes and, hence, only half of the amplitude plane need be studied because the line $K_1^2 = K_2^2$ is a line of mirror symmetry. We will, therefore, consider only the lower pie shape part of the amplitude plane bounded by the K_1^2 - axis and the line $K_1^2 = K_2^2$ and obtain the upper half by symmetry.

It is important to note that singularities on the boundaries of this region represent simple types of motion: circular and planar. We will, therefore, study the implications of Equation (3.29-30) in the vicinity of these boundaries, i.e., for almost circular motion and for almost planar motion. Throughout this work we will assume H and M^* to be differentiable functions.

With this in mind, H and M^* will be expanded about a circular motion $\delta = \delta_c = K_1$, $\delta' = 0$.

$$H = H_c + \left[\frac{dH}{d\delta^2}\right]_c (\delta^2 - \delta_c^2) \tag{3.31}$$

$$M^* = \left[\frac{dM^*}{d(\delta^2)'}\right]_o (\delta^2)' \tag{3.32}$$

where $H_c = H(\delta_c^2)$

$$\left[\frac{dH}{d\delta^2}\right]_c = \left[\frac{dH}{d\delta^2}\right]_{\delta^2 = \delta_c^2} \quad \text{and}$$

$$\left[\frac{dM^*}{d(\delta^2)'}\right]_o = \left[\frac{dM^*}{d(\delta^2)'}\right]_{(\delta^2)' = 0}$$

Equations (3.31-32) may now be substituted into Equations (3.29-30) and the results simplified for almost circular motion ($K_2 << K_1$).

$$\lambda_1 = -\frac{(1 + m_c)}{2 + 3m_c} \left\{H_c + \left[\frac{dH}{d\delta^2}\right]_c (K_1^2 - \delta_c^2)\right\} \tag{3.33}$$

$$\lambda_2 = \frac{2 + 5m_c + 4m_c^2}{2(1 + m_c)(1 + 2m_c)} \lambda_1$$

$$+ \frac{1}{2}\left\{\sqrt{\frac{1 + m_c}{1 + 2m_c}} \left[\frac{dH}{d\delta^2}\right]_c + \left[1 + \sqrt{\frac{1 + m_c}{1 + 2m_c}}\right]\left[\frac{dM^*}{d(\delta^2)'}\right]_o\right\} K_1^2 \tag{3.34}$$

where

$$m_c = m_2\delta_c^2 = \frac{M_2\delta_c^2}{M_o}$$

A singular point exists on the K_1^2 axis at $K_1 = \delta_c$ when

$$H_c = 0 \tag{3.35}$$

Smaller circular motions ($K_1 < \delta_c$) grow toward $K_1 = \delta_c$ and larger circular motions decay when

$$\left[\frac{dH}{d\delta^2}\right]_c > 0 \tag{3.36}$$

This singularity represents a true limit cycle if almost circular motion tends to become more circular near the singularity. ($\lambda_2 < 0$)

$$\left[\frac{dH}{d\delta^2}\right]_c + \left[1 + \sqrt{\frac{1 + 2m_c}{1 + m_c}}\right]\left[\frac{dM^*}{d(\delta^2)'}\right]_o < 0 \text{ for } K_2 << K_1 = \delta_c \tag{3.37}$$

Inequalities (3.36-37) are precisely the conditions that the circular singularity be a stable node. A somewhat more convenient form of these inequalities is

$$\left[\frac{dH}{d\delta^2}\right]_c > 0 \tag{3.36}$$

$$\left[\frac{dM^*}{d(\delta^2)'}\right]_o \Big/ \left[\frac{dH}{d\delta^2}\right]_c < \frac{-1}{1 + \sqrt{\frac{1 + 2m_c}{1 + m_c}}} \; ; \tag{3.38}$$

A positive λ_2 would make the singularity a saddle. If we define an unstable saddle as one for which trajectories on the origin side of the saddle are directed away from the origin, we see that the singularity is an unstable saddle if Inequality (3.36) and not Inequality (3.38) are satisfied. Finally, a negative $\left[\frac{dH}{d\delta^2}\right]_c$ has the effect of reversing the stability of the singularity. These conditions are summarized in Figure 9-4.

The prediction of a circular limit motion when conditions (3.35-36, 38) are satisfied can be verified by direct numerical integration of the actual differential equations of pitching and yawing motion. This has been done for M^* and H linear in $(\delta^2)'$ and δ^2 respectively and motions like that of Figure 9-5 have been obtained.

One very interesting result can be obtained from the Figure and the various Inequalities. If the damping moments are only functions of $\delta^2 (M^* = 0)$, every circular singularity must be a saddle! This was shown in our first examples to be the case when H was quadratic in δ and we now see that this is true whenever H is a differentiable function of δ^2 and the aerodynamic moment is a function of only δ. Under these conditions, a circular limit motion is impossible. Since circular limit motions have been observed in ballistic range tests, a more complicated moment such as one containing terms like $c^* \xi$ must be present.

Turning now to the question of almost planar motion ($K_1 \doteq K_2$) we will consider motion in vicinity of the planar motion $K_1 = K_2 = K_p$.

$$\therefore \delta_p^2 = 2K_p^2(1 + \cos \hat{\phi}) \tag{3.39}$$

$$(\delta^2)_p' \doteq - 2K_p^2 \hat{\phi}_p' \sin \hat{\phi} \tag{3.40}$$

where

$$\hat{\phi}_p' = \sqrt{-M_o(4 + 3m_p)}$$

$$m_p = \frac{4M_2K_p^2}{M_o}$$

The nature of the almost planar motion near this planar motion can be conveniently studied by use of the variables ϵ_1 and ϵ_2 which are defined by the equations:

$$K_j = K_p(1 + \epsilon_j) \qquad j = 1,2 \tag{3.41}$$

Since only motions near this planar motion are of interest, the ϵ_j's will be assumed to be small in comparison with unity and, hence, higher powers of the ϵ_j's will be neglected in comparison with their linear powers or unity.

Therefore, the variations of δ^2, $\hat{\phi}'$ and $(\delta^2)'$ can be computed as a small perturbation of the corresponding variations in δ_p^2, $\hat{\phi}_p'$ and $(\delta^2)_p'$.

$$\delta^2 = \delta_p^2 + 2K_p^2(1 + \cos\hat{\phi})(\epsilon_1 + \epsilon_2) \tag{3.42}$$

$$\hat{\phi}' = \phi_1' - \phi_2'$$

$$= \frac{1}{2}\left[\sqrt{-M_o\left[4 + m_p(3 + 2\epsilon_1 + 4\epsilon_2)\right]}\right.$$

$$\left. + \sqrt{-M_o\left[4 + m_p(3 + 4\epsilon_1 + 2\epsilon_2)\right]}\right]$$

$$= \hat{\phi}_p'\left[1 + \frac{3m_p(\epsilon_1 + \epsilon_2)}{8 + 6m_p}\right] \tag{3.43}$$

$$(\delta^2)' = (\delta^2)_p' - K_p^2\hat{\phi}_p' \sin\hat{\phi}\left(\frac{8 + 9m_p}{4 + 3m_p}\right)(\epsilon_1 + \epsilon_2) \tag{3.44}$$

H and M can now be expanded about the planar motion.

$$H = H_p + \left[\frac{dH}{d\delta^2}\right]_p\left[\delta^2 - \delta_p^2\right] \tag{3.45}$$

$$M^* = M_p^* + \left[\frac{dM^*}{d(\delta^2)'}\right]_p\left[(\delta^2)' - (\delta^2)_p'\right] \tag{3.46}$$

where the p subscript on a function of δ^2 or $(\delta^2)'$ denotes that function evaluated for $\delta^2 = \delta_p^2$ or $(\delta^2)' = (\delta^2)_p'$. Relations (3.42-46) together with the proper expansion of $\phi_2' K_2/\phi' K_1$ and $K_2/\phi_1' K_1$ may be placed in the definition of λ_1^* with the result

$$\lambda_1^* = \lambda_p^* - \frac{1}{4\pi} \int_0^{2\pi} \left\{ H_p \left(\frac{4 + 2m_p}{4 + 3m_p} \right) \quad (\epsilon_1 - \epsilon_2) \cos \hat{\phi} \right.$$

$$+ 2 \left[\frac{dH}{d\delta^2} \right]_p \quad K_p^2 (\epsilon_1 + \epsilon_2) \sin^2 \hat{\phi}$$

$$- \frac{2M_p^* \left[4(1 + m_p)\epsilon_1 - (4 + m_p)\epsilon_2 \right] \sin \hat{\phi}}{\hat{\phi}_p' (4 + 3m_p)}$$

$$\left. - 2 \left[\frac{dM^*}{d(\delta^2)'} \right]_p \quad K_p^2 \left(\frac{8 + 9m_p}{4 + 3m_p} \right) (\epsilon_1 + \epsilon_2) \sin^2 \hat{\phi} \right\} d\hat{\phi} \tag{3.47}$$

where $\lambda_p^* = - \frac{1}{4\pi} \int_0^{2\pi} \left[(H_p)(1 - \cos \hat{\phi}) + (M_p^*) \left(\frac{2 \sin \hat{\phi}}{\hat{\phi}_p'} \right) \right] d\hat{\phi}.$

The terms involving $\left[\frac{dH}{d\delta^2} \right]_p$ and M_p^* may be integrated by parts and the results combined with the other terms.

$$\lambda_1^* = \lambda_p^* - \frac{[H]_1}{4(4 + 3m_p)} \left\{ \left[(8 + 5m_p)\epsilon_1 + m_p \epsilon_2 \right] \right.$$

$$- \left[m_p \epsilon_1 + (16 + 11m_p)\epsilon_2 \right] r_o$$

$$\left. + \left[(16 + 17m_p)\epsilon_1 + 7m_p \epsilon_2 \right] r_2 \right\} \tag{3.48}$$

where $$r_j = \frac{\left[\frac{dM^*}{d(\delta^2)'}\right]_j K_p^2}{[H]_1} \qquad j = 0,2$$

$$\left[\frac{dM^*}{d(\delta^2)'}\right]_j = \frac{1}{\pi}\int_0^{2\pi}\left[\frac{dM^*}{d(\delta^2)'}\right]_p \cos j\hat{\phi}\ d\hat{\phi} \qquad j = 0,2$$

$$[H]_1 = \frac{1}{\pi}\int_0^{2\pi} H_p \cos\hat{\phi}\ d\hat{\phi}\ .$$

A similar relation for λ_2^* may be obtained by interchanging ϵ_1 and ϵ_2 in Equation (3.48).

The numerical subscript on the outside of the bracketed expressions in λ_1 identifies that term as a particular Fourier cosine coefficient. It is quite surprising that the influence of H on λ_1 is completely determined by its first order Fourier cosine coefficient. The influence of M^*, however, is specified by the zeroth and second order Fourier cosine coefficients of its first derivative. These coefficients are computed for fixed modal amplitudes, K_j, and are thus functions of these amplitudes.

For a planar singularity λ_p^* vanishes and the λ_j are linear in the ϵ_j. Thus, only planar value of the coefficients of Equations (3.29-30) are needed to calculate the λ_j's.

$$\lambda_j = a_{j_1}\lambda_1^* + a_{j_2}\lambda_2^* \tag{3.49}$$

where $$a_{11} = a_{22} = \frac{2(4 + 3m_p)(8 + 7m_p)}{(8 + 9m_p)(8 + 5m_p)}$$

$$a_{12} = a_{21} = \frac{-4m_p(4 + 3m_p)}{(8 + 9m_p)(8 + 5m_p)}$$

$$\therefore \lambda_1 = -\frac{[H]_1\left[b\epsilon_1 + a\epsilon_2\right]}{2(8 + 5m_p)(8 + 9m_p)} \tag{3.50}$$

$$\lambda_2 = -\frac{[H]_1\left[a\epsilon_1 + b\epsilon_2\right]}{2(8 + 5m_p)(8 + 9m_p)} \tag{3.51}$$

$$\text{where } a = -m_p(8 + 3m_p) + (128 + 200m_p + 75m_p^2)\, r_o$$

$$+ 3m_p(8 + 5m_p)\, r_2$$

$$b = 64 + 96m_p + 33m_p^2 + 3m_p(8 + 5m_p)\, r_o$$

$$+ (128 + 248m_p + 105m_p^2)\, r_2$$

The differential equation for solution curves in the vicinity of a planar singularity in the amplitude plane is

$$\frac{d\epsilon_2}{d\epsilon_1} \doteq \frac{\lambda_2}{\lambda_1} = \frac{a\epsilon_1 + b\epsilon_2}{b\epsilon_1 + a\epsilon_2} \tag{3.52}$$

According to the usual criteria, the singularity must be either a saddle or a node. It is a node if $a^2 - b^2$ is negative and a saddle if $a^2 - b^2$ is positive.

$$a^2 - b^2 = (a + b)(a - b) \tag{3.53}$$

$$= -4(8 + 5m_p)(8 + 9m_p)$$

$$\times \left[2(2 + m_p) + (r_o + r_2)(8 + 5m_p)\right]$$

$$\times \left[(4 + 3m_p)(1 - 2r_o) + 4(2 + 3m_p)r_2\right]$$

Note that if r_o and r_2 both vanish and m_p is outside the interval $(-2, -8/9)$, $a^2 - b^2$ is negative. Thus, if the aerodynamic moment coefficients are functions of δ^2 alone and not functions of $(\delta^2)'$, all planar singularities are nodes and almost planar motions near a planar singular motion will tend to that planar singular motion if neighboring planar motions tend to the planar singular motion.

Another interesting special case is that for which H and M^* are linear in δ^2 and $(\delta^2)'$ respectively.

$$H = H_o + H_2\delta^2 \tag{3.54}$$

$$M^* = M_2^*(\delta^2)' \tag{3.55}$$

A simple calculation shows that

$$[H]_1 = 2H_2K_p^2 \tag{3.56}$$

$$r_o = \frac{M_2^*}{H_2} \tag{3.57}$$

$$r_2 = 0 \tag{3.58}$$

The amplitude of the planar singular motion is fixed by the condition $\lambda_p^* = 0$ to be

$$K_p^2 = - H_o(H_2 - 2M_2^*)^{-1} = - H_oH_2^{-1}(1 - 2r_o)^{-1} > 0 \tag{3.59}$$

For $r_2 = 0$, $a^2 - b^2$ reduces to a simple form. A planar singularity, therefore, will be a node if

$$(8 + 5m_p)(8 + 9m_p)(4 + 3m_p)(1 - 2r_o)$$

$$x \left[4 + 2m_p + r_o(8 + 5m_p)\right] > 0 \tag{3.60}$$

When m_p is excluded from the interval $(-2, -8/9)$ and r_o is replaced by its actual value, this Inequality can be written in a very concise form.

$$- \left[\frac{4 + 2m_p}{8 + 5m_p}\right] < \frac{M_2^*}{H_2} < \frac{1}{2} \tag{3.61}$$

According to Inequalities (3.61), $(1 - 2r_o)$ has to be positive and, hence, Equation (3.59) shows us that H_o and H_2 must have opposite algebraic signs. A negative H_o causes small amplitude motion to grow and, hence, the planar node will be a stable node if

$$H_o < 0, \quad H_2 > 0 \tag{3.62}$$

The various possibilities are summarized in Figure 9-6.

9.4 The Perturbation Method

The work of this chapter has assumed that epicyclic motion which is essentially a linear combination of trigonometric functions is a good approximation of the actual motion. The value of this approximation should diminish as the static moment becomes strongly nonlinear. In Section 8.3, the exact solution for a cubic static moment was derived in terms of elliptic functions. In this section, we will use this solution rather than the epicyclic solution as our basic solution and consider the effects of both linear and nonlinear damping to be perturbation of this elliptic function solution*. The discussion will not contain all the necessary details but will be more in the nature of an outline.

For simplicity, we will neglect the geometrical terms γ'/γ, assume all coefficients to be independent of arclength**, and require constant spin. The approach will be to manipulate Equation (2.4) to obtain differential equations for the energy and angular momentum. First, we transform Equation (2.4) by the relation

$$\tilde{\xi} = \hat{\xi}^{i(1/2)Ps} \tag{4.1}$$

$$\therefore \hat{\xi}'' - \left[\hat{M}_o + M_2\delta^2\right]\hat{\xi} = -H\hat{\xi}' + \left[M^* + iP(T - \frac{H}{2})\right]\hat{\xi} \tag{4.2}$$

where $\hat{M}_o = M_o - \frac{P^2}{4}$

$$M^* = M - M_o - M_2\delta^2$$

The conjugate of Equation (4.2) is

$$\bar{\hat{\xi}}'' - \left[\hat{M}_o + M_2\delta^2\right]\bar{\hat{\xi}} = -H\bar{\hat{\xi}}' + \left[M^* - iP(T - \frac{H}{2})\right]\bar{\hat{\xi}} \tag{4.3}$$

---

* This perturbation method is an extension and modification of the work of Reference 9-6 and 9-7.

** The effect of varying coefficients is considered in Reference 9-8.

Multiplying Equation (4.2) by $\bar{\hat{\xi}}'$, Equation (4.3) by $\hat{\xi}'$, and adding, we have an equation for the change of total energy.

$$C_1' = - H\left[2C_1 + 2\hat{M}_o\delta^2 + M_2\delta^4\right] + (M^*)\ (\delta^2)'$$

$$+ P(T - \frac{H}{2})\ C_2 \qquad (4.4)$$

where $C_1 = |\hat{\xi}'|^2 - \hat{M}_o\delta^2 - M_2\ \frac{\delta^4}{2}$ total energy

$C_2 = i(\bar{\hat{\xi}}'\hat{\xi} - \hat{\xi}'\bar{\hat{\xi}})$ angular momentum

The equation for the variation of angular momentum may be obtained by eliminating $\hat{M}_o + M_2\delta^2$ from Equations (4.2-3).

$$C_2' = - HC_2 + 2P(T - \frac{H}{2})\ \delta^2 \qquad (4.5)$$

When damping is zero ($H = T = M^* = 0$), the amplitude variation is given by Equation (8.3.9) which is repeated here

$$(\delta^2)' = \pm\sqrt{- C_2^2 + 4C_1\delta^2 + 4\hat{M}_o\delta^4 + 2M_2\delta^6} \qquad (4.6)$$

The actual solutions in terms of the sine amplitude function are given in Section 8.3. The requirement of rotational symmetry once again leads us to the restriction that the aerodynamic coefficients are functions of δ^2, $(\delta^2)'$, and $|\xi'|^2$. But $(\delta^2)'$ and $|\xi'|^2$ are functions of C_1, C_2 and δ^2 through Equation (4.6) and the definition of C_1 respectively. Thus Equations (4.4-5) have the form

$$C_j' = f_j(C_1, C_2, \delta^2) \qquad j = 1,2 \qquad (4.7)$$

For a conservative system $f_j = 0$, and Equation (4.6) applies. We assume that the damping functions, f_j, represent small damping and, hence, C_1 and C_2 vary very little over a period of the nutation. If this is the case, it is reasonable to use the no damping solution for δ^2 in f_j and to assume that only the average effect of the δ^2 is important.

$$C_j' = \left[f_j\right]_a \tag{4.8}$$

where $\left[f_j\right]_a = \frac{1}{P^*} \int_0^{P^*} f_j \, ds$ and

P^* is a period of δ^2.

Since the solutions for δ^2 are usually given in terms of the extreme values δ_1^2 and δ_2^2, this average function will contain δ_1^2 and δ_2^2 as well as C_1 and C_2. These two sets of variables are related by Equation (4.6) and the fact that $(\delta^2)'$ vanishes for extremum values of δ^2.

$$4C_1\delta_j^2 + 4\hat{M}_o\delta_j^4 + 2M_2\delta_j^6 = C_2^2 \qquad j = 1,2 \tag{4.9}$$

Thus, either set could be eliminated in favor of the other. In view of our previous work with the amplitude plane, a third set is much more convenient. These variables are generalized squared modal amplitudes and will be defined so that the sum of their square roots is the maximum amplitude, δ^2, and the difference is the minimum amplitude. Instead of using the previous symbols K_j^2, as was done in Equations (8.3.14-15), we will use new symbols, x_j, so that any possible confusion with the epicylic modal amplitudes can be eliminated.

$$\therefore \delta_1^2 = (\sqrt{x_1} - \sqrt{x_2})^2 \tag{4.10}$$

$$\delta_2^2 = (\sqrt{x_1} + \sqrt{x_2})^2 \tag{4.11}$$

According to Equations (4.10-11), the x_j axes correspond to constant amplitude circular motion in the same way as the K_j^2 axes did in the quasi-linear method.

Equations (4.9-11) may now be combined to relate the x_j's and C_j's.

$$C_1 = -\left[2\hat{M}_o(x_1 + x_2) + \frac{M_2}{2}(3x_1^2 + 10x_1x_2 + 3x_2^2)\right] \tag{4.12}$$

$$C_2 = 2(x_1 - x_2)\sqrt{-\hat{M}_o - M_2(x_1 + x_2)} \tag{4.13}$$

According to Equation (4.13), the angular momentum is zero when $x_1 = x_2$ and, hence, this line retains the locus of planar motion*. Equation (4.13) indicates a second possibility for planar motion, i.e.,

$$\hat{M}_o + M_2(x_1 + x_2) = 0 \tag{4.14}$$

An inspection of the various solutions of Section 8.3 shows that this can occur for the type (c) moments and represents oscillations about the trim equilibrium angle of $\sqrt{-\hat{M}_o/M_2}$. For the type (c), the line given by Equation (4.14) is also the locus of planar motions.

If Equations (4.12-13) are differentiated and solved for x_j', the final equations for the generalized amplitude plane follow.

$$x_1' = \frac{\left[2\hat{M}_o + M_2(x_1 + 3x_2)\right] C_1' + \left[2\hat{M}_o + M_2(5x_1 + 3x_2)\right] \sqrt{-\hat{M}_o - M_2(x_1 + x_2)}\, C_2'}{-8\omega^2\tilde{\omega}^2} \tag{4.15}$$

$$x_2' = \frac{\left[2\hat{M}_o + M_2(3x_1 + x_2)\right] C_1' - \left[2\hat{M}_o + M_2(3x_1 + 5x_2)\right] \sqrt{-\hat{M}_o - M_2(x_1 + x_2)}\, C_2'}{-8\omega^2\tilde{\omega}^2} \tag{4.16}$$

where $\omega^2 = -\hat{M}_o - M_2\left[\dfrac{3x_1 + 2\sqrt{x_1x_2} + 3x_2}{2}\right]$

$\tilde{\omega}^2 = -\hat{M}_o - M_2\left[\dfrac{3x_1 - 2\sqrt{x_1x_2} + 3x_2}{2}\right]$ and

C_j''s are given by Equation (4.8).

As an example of this perturbation method, we will consider the special case of Section 9.3c.

---

* This motion is planar in the roofed coordinates specified by Equation (4.1). Only when spin is zero will the motion be planar in the eyes of a nonspinning observer.

$$H = H_o + H_2\delta^2 \tag{4.17}$$

$$M^* = M_2^*(\delta^2)' \tag{4.18}$$

$$P = 0 . \tag{4.19}$$

Equations (4.8) reduce to

$$C_1' = -\left\{\left[H_o + (H_2 - 2M_2^*)\delta^2\right]\left[2C_1 + 2\hat{M}_o\delta^2 + M_2\delta^4\right]\right\}_a - M_2^*C_2^2 \tag{4.20}$$

$$C_2' = -\left[H_o + H_2\delta_a^2\right]C_2 \tag{4.21}$$

Before using these equations in Equations (4.15-16), we must compute the average value of δ^{2n} for n = 1, 2, 3. In general, this is quite tedious since it involves the calculation of integrals of $sn^{2n}\omega s$. This can be done numerically, however, and Equations (4.15-16) may then be integrated to construct a generalized amplitude plane for particular values of the coefficients. To derive general conditions on the coefficients for the various limit motions, it is necessary to locate singular points and calculate the δ_a^{2n}'s in their vicinities. For two special cases - circular singularities and planar singularities - the necessary algebra is not excessive. From this partial information about the complete generalized amplitude planes, it is then possible to infer the general form of these planes and select interesting sets of values of the coefficients for numerical construction of specific generalized amplitude planes. For almost circular motion ($x_1 >> x_2$), it can be shown that [9-9]

$$\delta_a^{2n} \doteq x_1^n + nx_1^{n-1}x_2\left(n - \frac{m_c}{2 + 3m_c}\right) \tag{4.22}$$

Equations (4.20-22) may now be placed in Equations (4.15-16).

$$\frac{x_1'}{x_1} \doteq -\frac{2(1 + m_c)}{(2 + 3m_c)}\left[H_o + H_2x_1\right] \tag{4.23}$$

$$\frac{x_2'}{x_2} \doteq -(2 + 3m_c)^{-2}\left\{(4 + 9m_c + 6m_c^2)H_o - \left[m_cH_2 + 2(2 + 3m_c)^2 M_2^*\right]x_1\right\} \tag{4.24}$$

Equation (4.23) is exactly the same as Equation (3.33) which was derived from the quasi-linear method. The symbols of that equation may be easily related to those of Equation (4.23) by a consideration of the coefficients defined by Equations (3.31) and (4.17) respectively

$$H_o = H_c - \left[\frac{dH}{d\delta^2}\right]_c \delta_c^2 \tag{4.25}$$

$$H_2 = \left[\frac{dH}{d\delta^2}\right]_c \tag{4.26}$$

Equation (4.24) and the corresponding quasi-linear Equation (3.34) do differ markedly. The importance of this difference can be most conveniently evaluated by comparing the two sets of conditions for a circular singularity which is a node. The quasi-linear conditions may be written in the form

$$\delta_c^2 = - H_o/H_2 > 0 \tag{4.27}$$

$$H_2 > 0 \tag{4.28}$$

$$\frac{M_2^*}{H_2} < \frac{-1}{1 + \sqrt{1 + 2m_c}\,\sqrt{1 + m_c}} \tag{4.29}$$

Relations (4.27-28) are the same as those derived from the perturbation method. The perturbation method form of Inequality (4.29) can be derived by setting $x_1' = 0$ and $x_2' < 0$, and eliminating H_o between Equations (4.23) and (4.24).

$$\frac{M_2^*}{H_2} < \frac{-(1 + m_c)}{2 + 3m_c} \tag{4.30}$$

For a linear static moment ($m_c = 0$), Inequalities (4.29-30) are the same. Their asymptotic values - $(1 + \sqrt{2})^{-1}$ and (-1/3), however, differ by 35%. For a type (b) moment, the quasi-linear expression limits m_c to the interval (- 1/2, 0) while the perturbation expression is valid for the complete range

in m_c for which almost circular motions are possible ($-2/3 < m_c < 0$). These differences and others may be seen in Figure 9-4 where both upper bounds are plotted as functions of m_c.

The algebra for almost planar motion* is more lengthy and will only be outlined here. If the common value of x_j for planar motion is identified by x_p, the maximum amplitude of the motion is $2\sqrt{x_p}$. Our generalized definition of m_p is

$$m_p = \frac{4M_2 x_p}{M_o} \tag{4.31}$$

and our generalized ϵ_j's of Equations (3.41) are defined by**

$$x_j = x_p(1 + 2\epsilon_j) \qquad j = 1,2 \tag{4.32}$$

For these variables, the average values of δ^{2n} can be determined

$$\delta_a^{2n} = \left[A_{2n} + 2B_{2n}(\epsilon_1 + \epsilon_2)\right](4x_p)^n \tag{4.33}$$

where A_{2n} and B_{2n} are combinations of complete elliptic integrals of the first and second kind which in turn are functions of m_p. These quantities are explicitly derived and defined in Reference 9-10.

The amplitude of the planar singular motion $2\sqrt{x_p}$ is fixed by the condition $x_j' = 0$ to be

$$x_p = \frac{-H_o\Delta}{H_2 - 2M_2^*} \tag{4.34}$$

where

$$\Delta = \Delta(m_p) = \frac{2 + m_p - 2A_2 - m_p A_4}{4\left[(2 + m_p)A_2 - 2A_4 - m_p A_6\right]}$$

---

* Only the symmetric planar motion for which $x_1 = x_2$ will be considered here. Planar motion about trim is studied in Reference 9-10.

** The 2 appears in Equation (4.32) because x_j corresponds to K_j^2 and $1 + 2\epsilon_j$ is the first order approximation of $(1 + \epsilon_j)^2$.

The corresponding equation for the quasi-linear method is Equation (3.59) which differs from the above by the absence of Δ. One interesting characteristic of Equation (4.34) is that for certain values of H_2/H_o, M_2^*/H_2, and M_2/M_o and a type (c) moment, it has two roots. The m_p's for the members of such a pair lie in the intervals (- 2.535, - 2.164), and (- 2.164, - 2) respectively. If we omit consideration of the second member of these pairs ($m_p < - 2.164$, $m_p > - 1$), the conditions for a stable node may be quickly stated.

$$H_o < 0, \quad H_2 > 0 \tag{4.35}$$

$$\frac{1 - 4A_2\Delta}{2} < \frac{M_2^*}{H_2} < \frac{1}{2} \tag{4.36}$$

The lower bound in Inequality (4.36) differs from that of Inequality (3.61). The two lower bounds are compared in Figure 9-6.

Now that we have considered the implications of singularities on the coordinate axes and the line $x_1 = x_2$, we want to show how information about the remainder of the generalized amplitude plane can be inferred. First, it is necessary to combine the various boundaries for M_2^*/H_2 in one plot. To do this, we must compute m_c in terms of m_p.

From Equations (4.27, 31, 34),

$$m_c = \left(\frac{M_2}{M_o}\right) \delta_c^2 = - \frac{M_2 H_o}{M_o H_2} \tag{4.37}$$

$$m_p = 4\left(\frac{M_2}{M_o}\right) x_p = - \frac{4M_2 H_o \Delta}{M_o(H_2 - 2M_2^*)} \tag{4.38}$$

$$\therefore \frac{m_c}{m_p} = \left[1 - \left(\frac{2M_2^*}{H_2}\right)\right] \left(\frac{1}{4\Delta}\right) \tag{4.39}$$

By means of Equation (4.39), Figure 9-6 can be replotted in terms of m_c and superimposed on Figure 9-4. The result is Figure 9-7.

This figure has a number of interesting features. For a Type (b) moment, it can be seen that as M_2^*/H_2 is increased a circular node and planar saddle change to a circular saddle and a planar saddle which in turn change to a circular saddle and a planar node! This disappearance of the node from the x_1 - axis and later appearance on the line $x_1 = x_2$ implies its motion through the generalized amplitude plane and the possible existence of a limit motion varying between two nonzero modal amplitudes. This conjecture was checked by the numerical calculation of the generalized amplitude plane for $m_c = -.55$ and $M_2^*/H_2 = -1$. (Figure 9-8). This figure demonstrates the existence of the stable node. The differential equations of pitching and yawing motion for these parametric values were then calculated on an analogue computer and it was found that the motion quickly went to a limit motion with constant maximum and minimum amplitudes. (Figure 9.9a) These maximum and minimum amplitudes are those assigned by the location of the node in the generalized amplitude plane.

Finally, we note that the dotted region of Figure 9-7 appears to be quite interesting due to the presence of two stable limit motions. A sample generalized amplitude plane is shown in Figure 9-10 and a plot of the angular motion approaching the planar motion is given in Figure 9-9b. The ability of the perturbation method to predict fairly unexpected motions is very impressive.

Charles H. Murphy
CHARLES H. MURPHY

REFERENCES

9-1 Kryloff, N. and Bogoliuboff, N. B. Introduction to Nonlinear Mechanics. Translated by S. Lefschetz, Princeton University Press, 1947.

9-2 Poincaré, H. Sur les Courbes Definies par une Equation Differentielle. Oeuvres,(Gauthier-Villars), Paris, Vol. I, (1892)

9-3 Stoker, J. J. Nonlinear Vibrations in Mechanical and Electrical Systems. Interscience Publishers, New York, 1950.

9-4 Frommer, M. Uber das Auftreten von Wirbeln und Strudeln (geschlossener und spiraliger Integralkurven) in der Umgebung rationaler Unbestimmtheitsstellen. Math. Ann. 109 (1934) 395-424.

9-5 Cohen, C. J. and Hubbard, E. C. Unpublished NORC Computations, Naval Proving Ground. May 1956. (See BRL Report 995)

9-6 Thomas, L. H. The Theory of Spinning Shell. BRL Report 839, November 1952.

9-7 Reed, H. L., Jr. The Dynamics of Shell. BRL Report 1030, October 1957.

9-8 Murphy, C. H. Effect of Varying Air Density on the Nonlinear Pitching and Yawing Motion of a Symmetric Missile. BRL Report 1162, February 1962.

9-9 Murphy, C. H. The Effect of Strongly Nonlinear Static Moment on the Combined Pitching and Yawing Motion of a Symmetric Missile. BRL Report No. 1114, August 1960.

9-10 Murphy, C. H. and Hodes, B. A. Planar Limit Motion of Nonspinning Symmetric Missiles Acted on by Cubic Aerodynamic Moments. BRL Memorandum Report No. 1358, June 1961.

9-11 Murphy C. H. The Prediction of Nonlinear Pitching and Yawing Motion of Symmetric Missiles. Journal of the Aeronautical Sciences, Vol. 24, pp. 473-479, July 1957.

9-12 Murphy, C. H. Quasi-Linear Analysis of the Nonlinear Motion of a Nonspinning Symmetric Missile. Journal of Applied Mathematics and Physics (ZAMP), Vol. 14, pp. 630-643, 1963.

9-13 Haseltine, W. R., Existence Theorems for Nonlinear Ballistics, J. Soc. Indust. Appl. Math. Vol 11, pp 553-563, Sept. 1963.

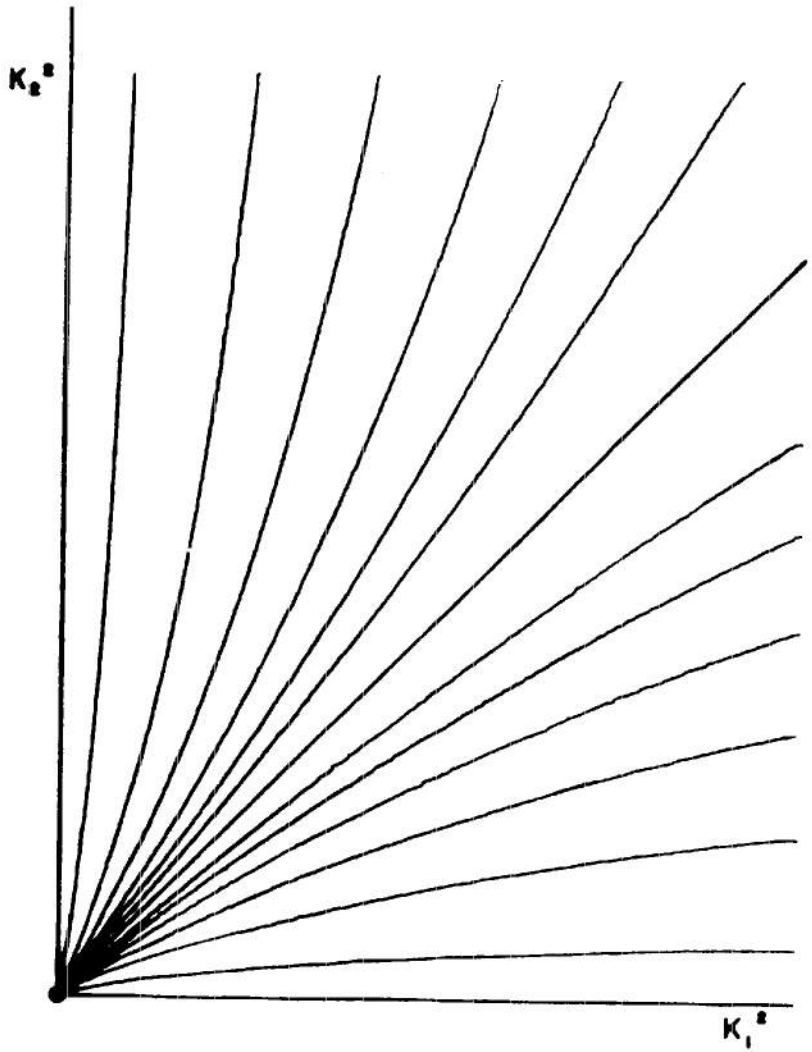

CONSTANT H

FIG. 9-1a

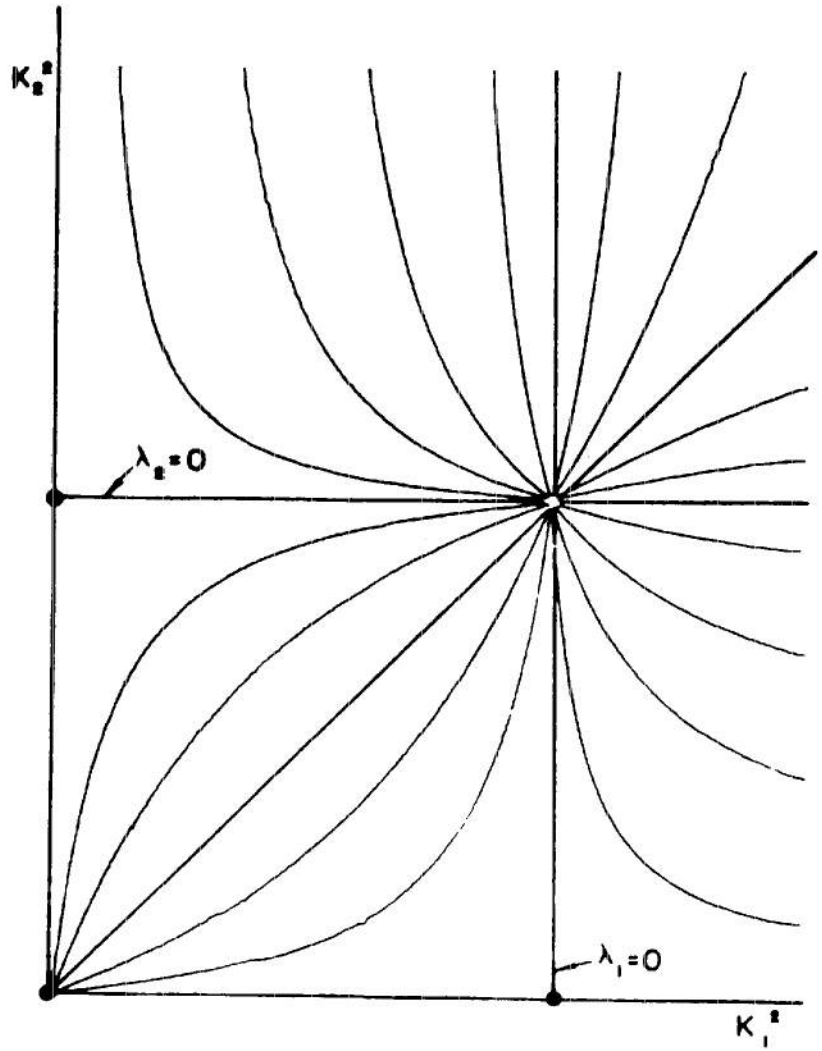

QUADRATIC $H_1 (H_0 H_2 < 0)$

FIG. 9-1b

AMPLITUDE PLANE FOR LINEAR EQUATION

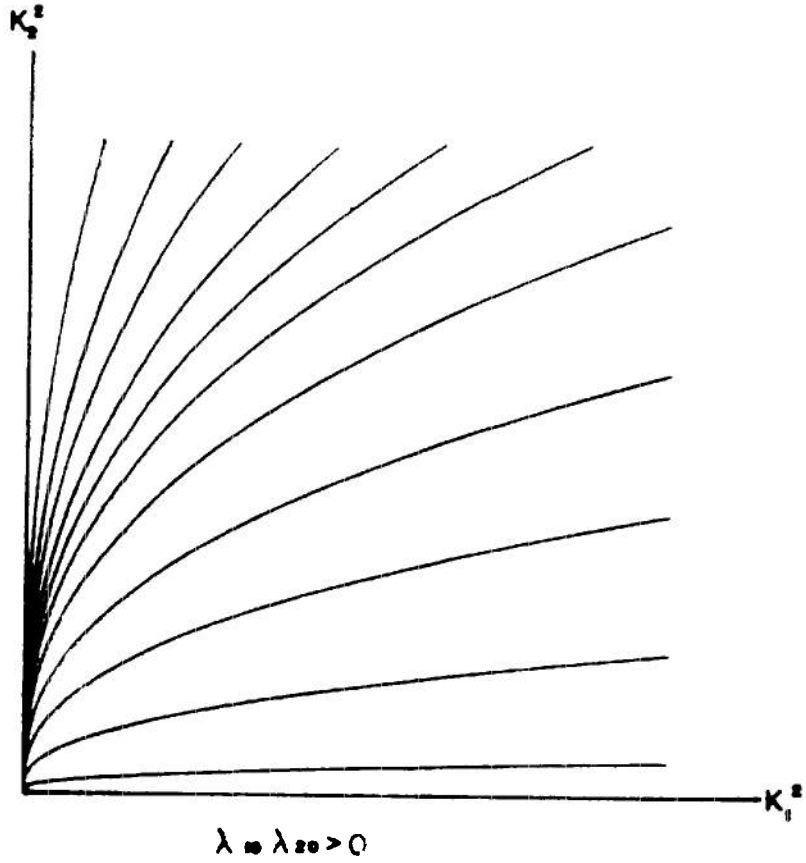

FIG 9-2a

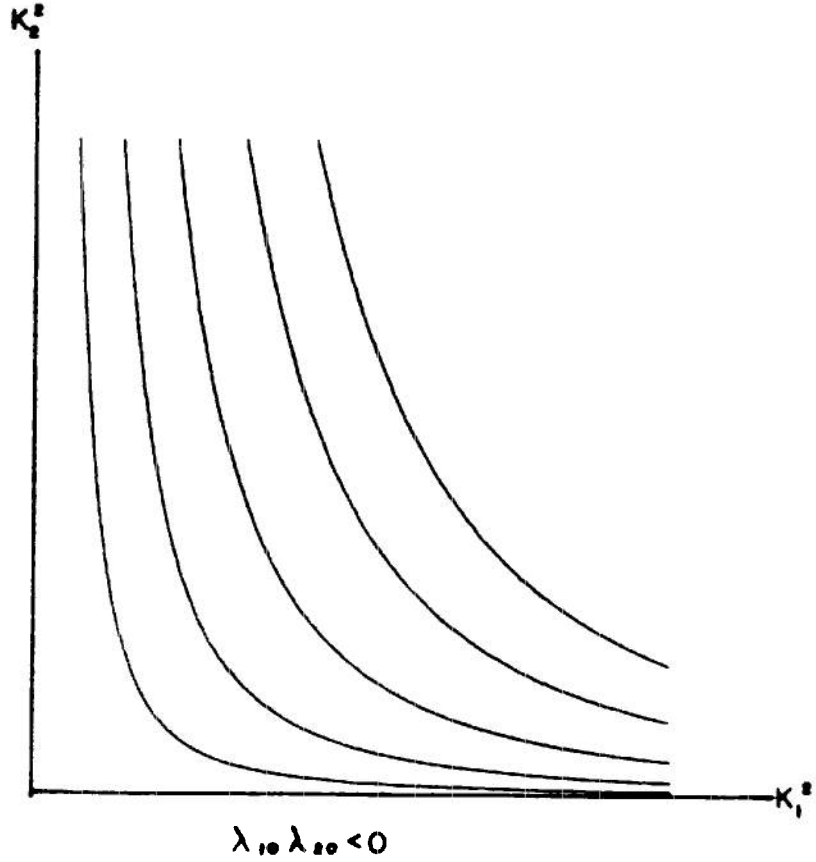

FIG. 9-2b

AMPLITUDE PLANE FOR CUBIC MAGNUS MOMENT ($\lambda_{10}\lambda_{20}>0$)

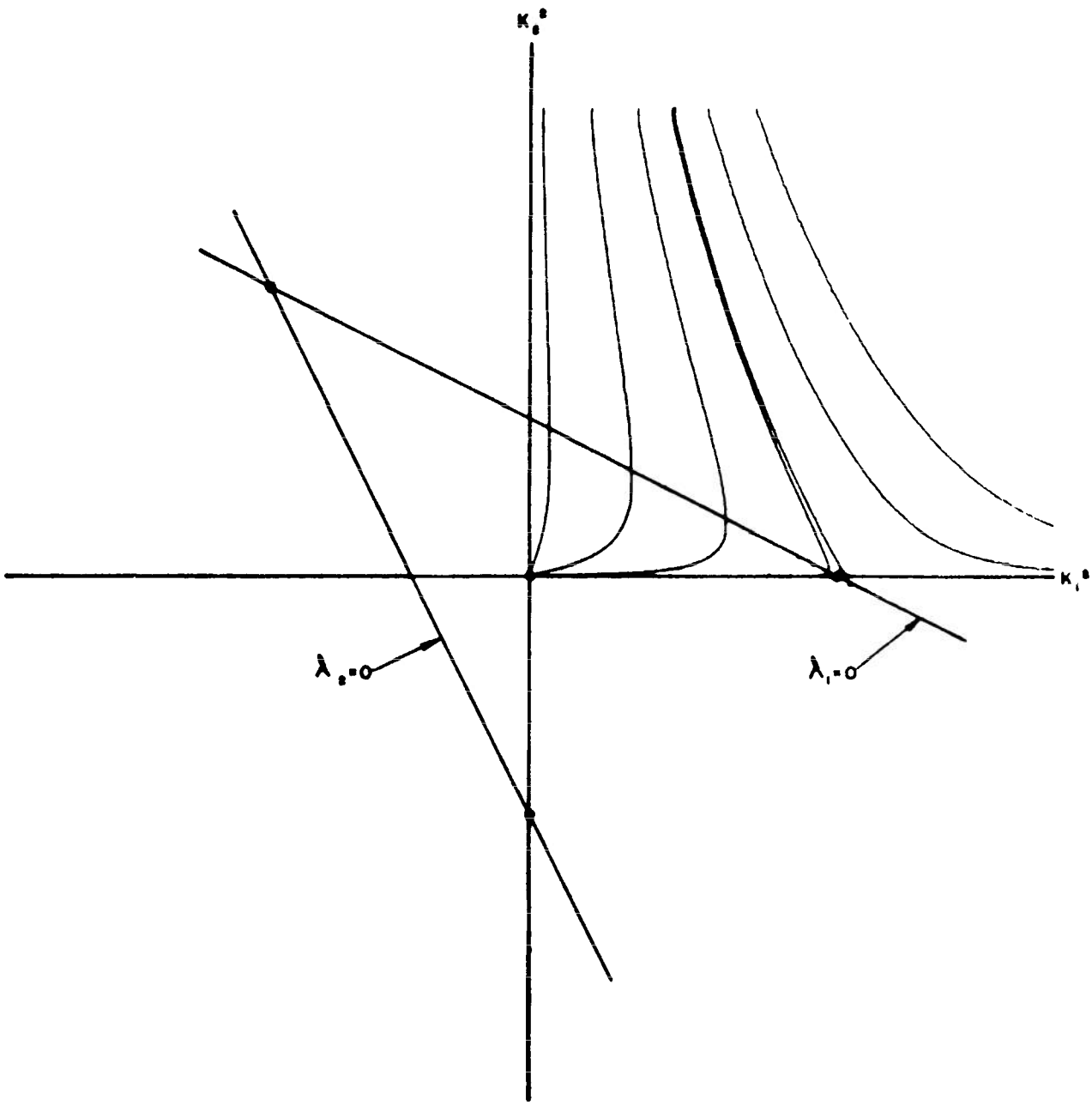

FIG. 9-3a

AMPLITUDE PLANE FOR CUBIC MAGNUS MOMENT ($\lambda_{10}\,\lambda_{20} < 0$)

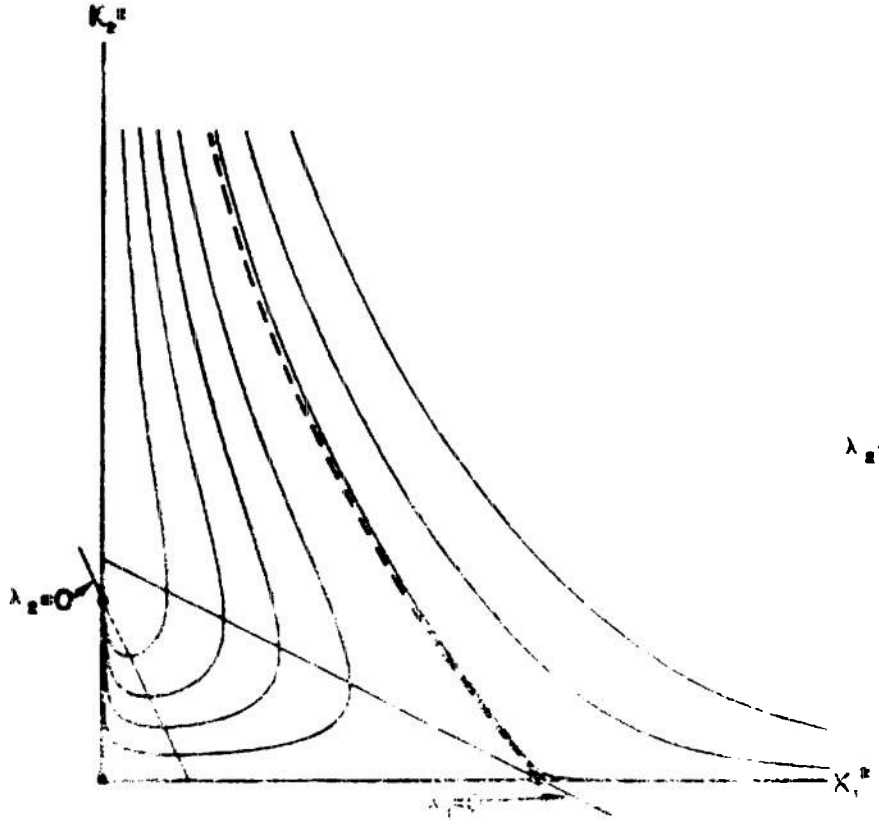

FIG. 9- 3b

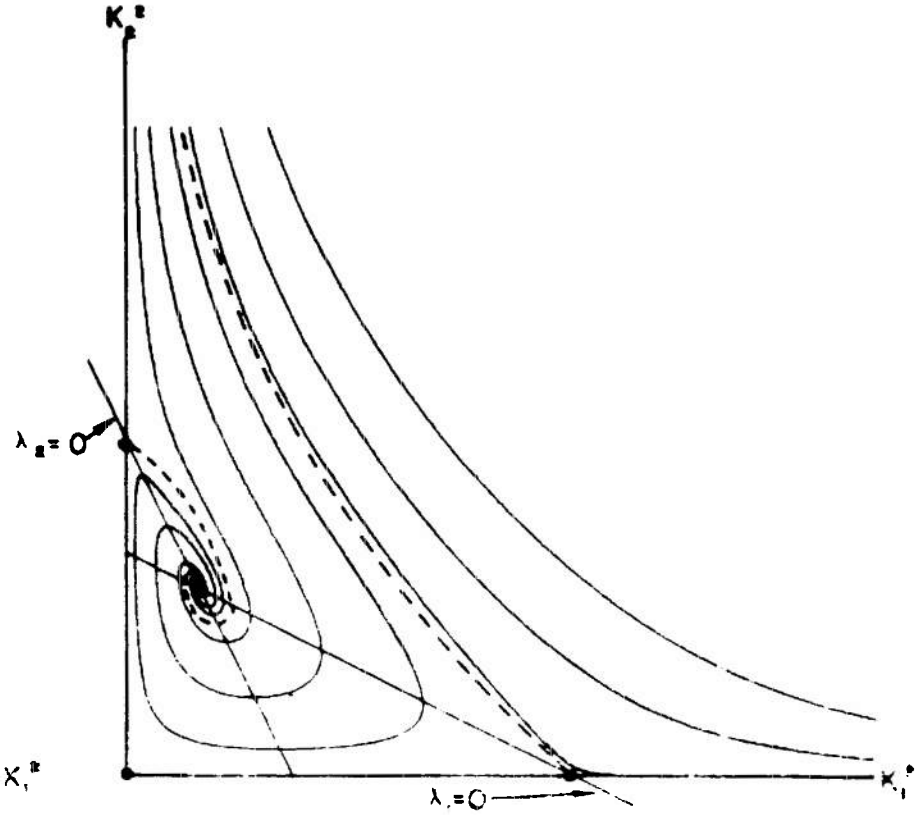

FIG. 9- 3a

AMPLITUDE PLANE FOR CUBIC MAGNUS MOMENT ($\lambda_{10} = -\lambda_{20}$)

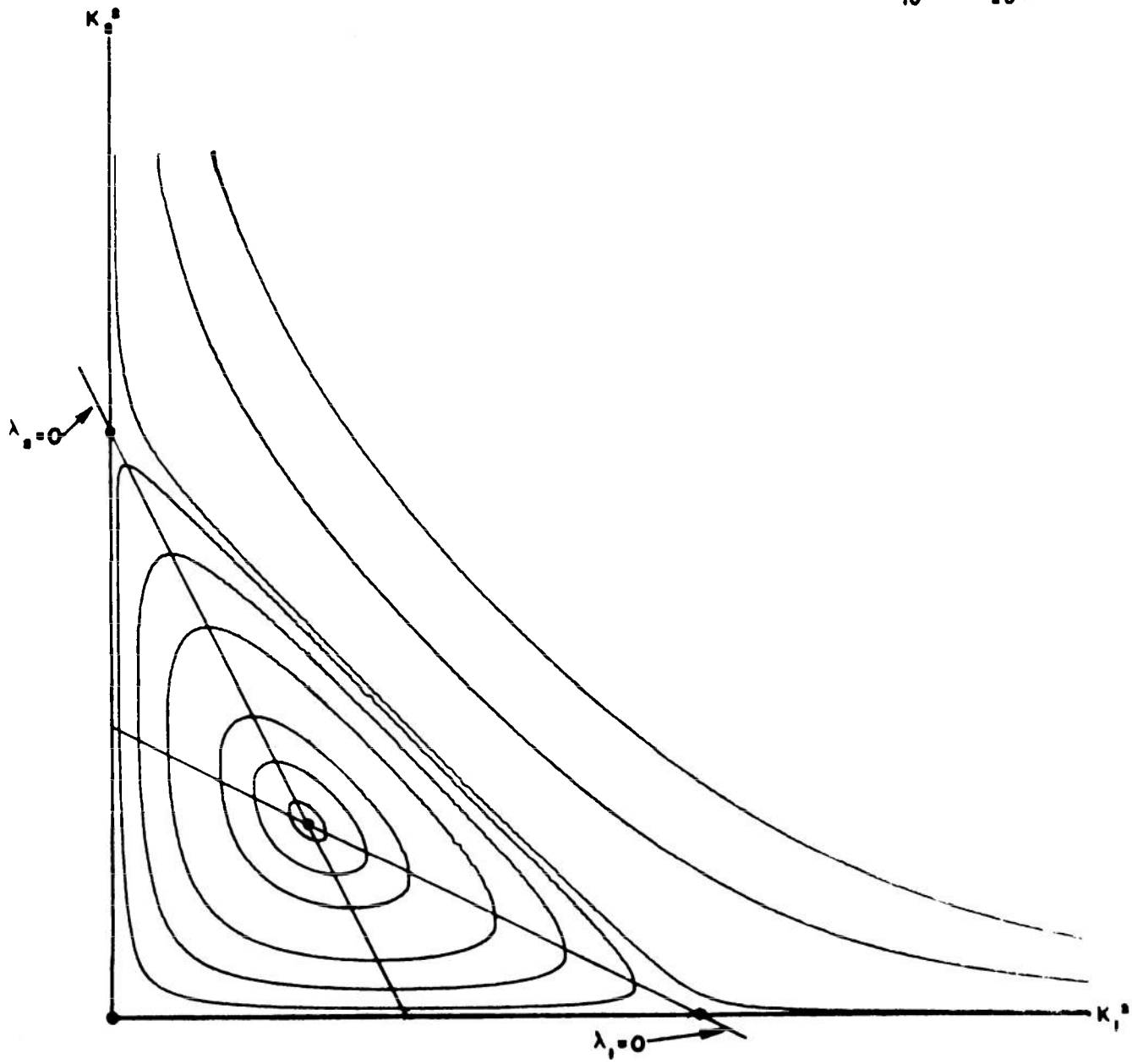

FIG. 9-3 d

CIRCULAR SINGULARITIES
FOR
NONLINEAR DAMPING MOMENTS

$$\left[\frac{dH}{d\delta^2}\right]_c > 0$$

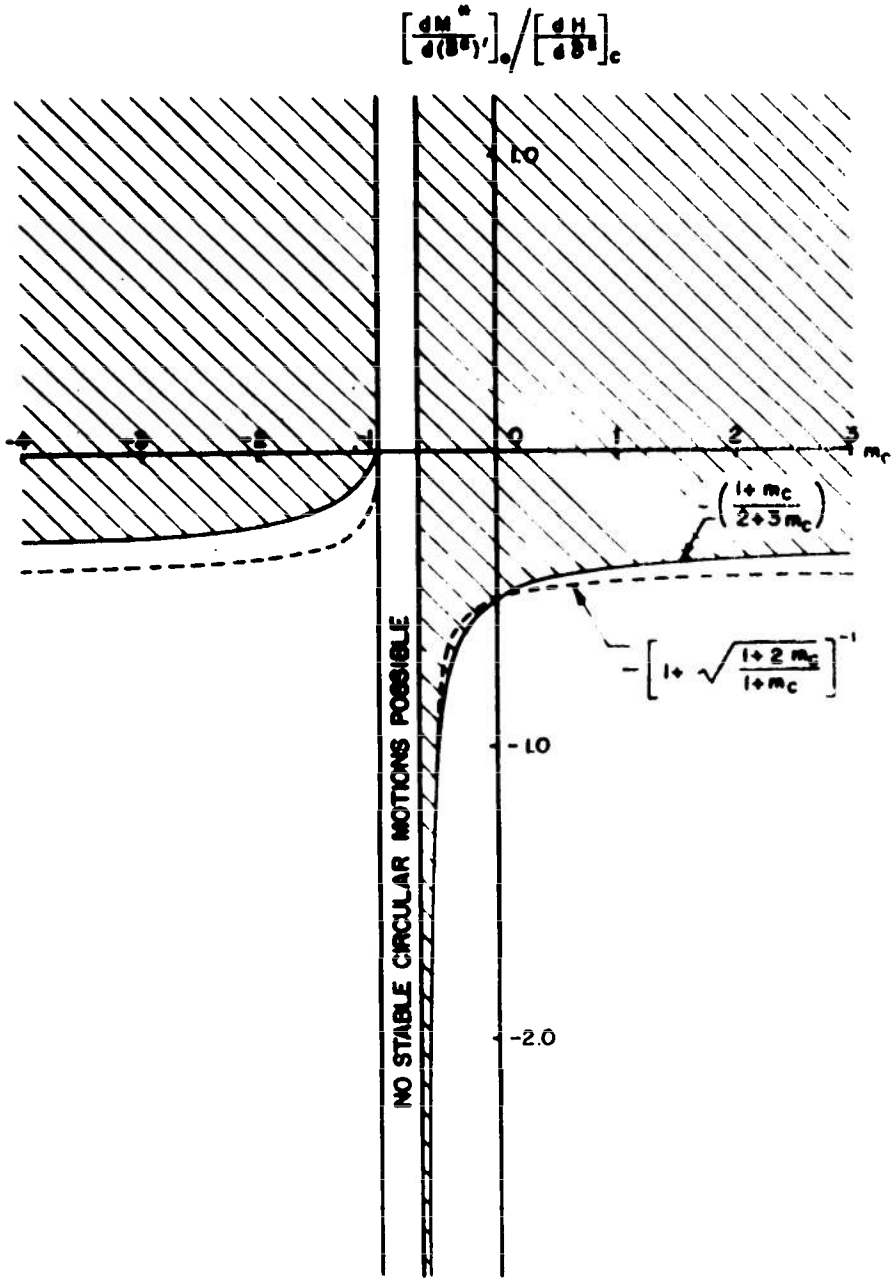

FIG. 9.4

CIRCULAR LIMIT MOTION;

$$\left[\frac{dM^*}{d(\delta^2)'}\right]_o \Big/ \left[\frac{dH}{d\delta^2}\right]_c = -1$$

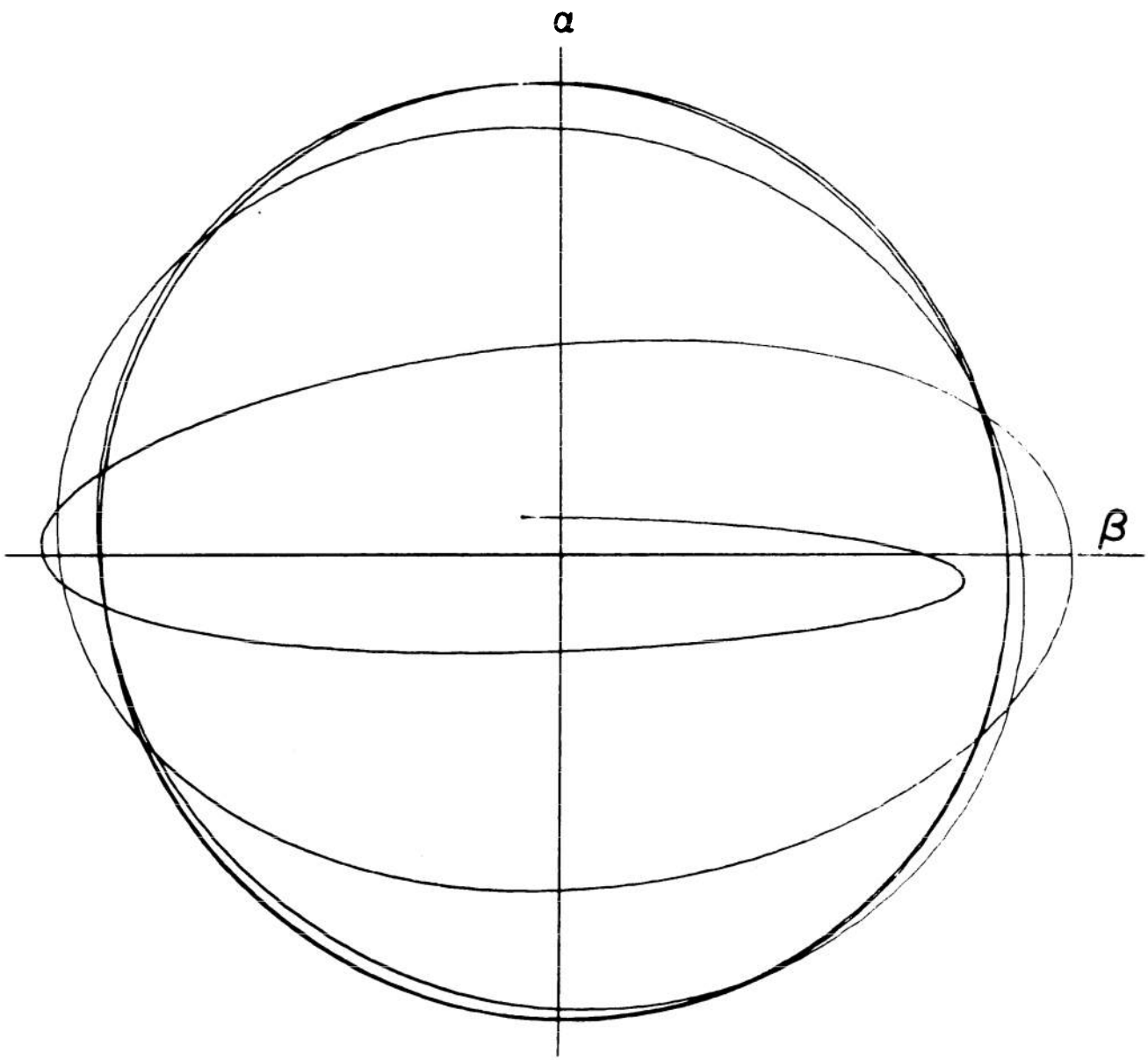

FIG. 9-5

PLANAR SINGULARITIES
$H_e < 0$
REVERSE SIGNS OF H_e AND H_s TO REVERSE STABILITY

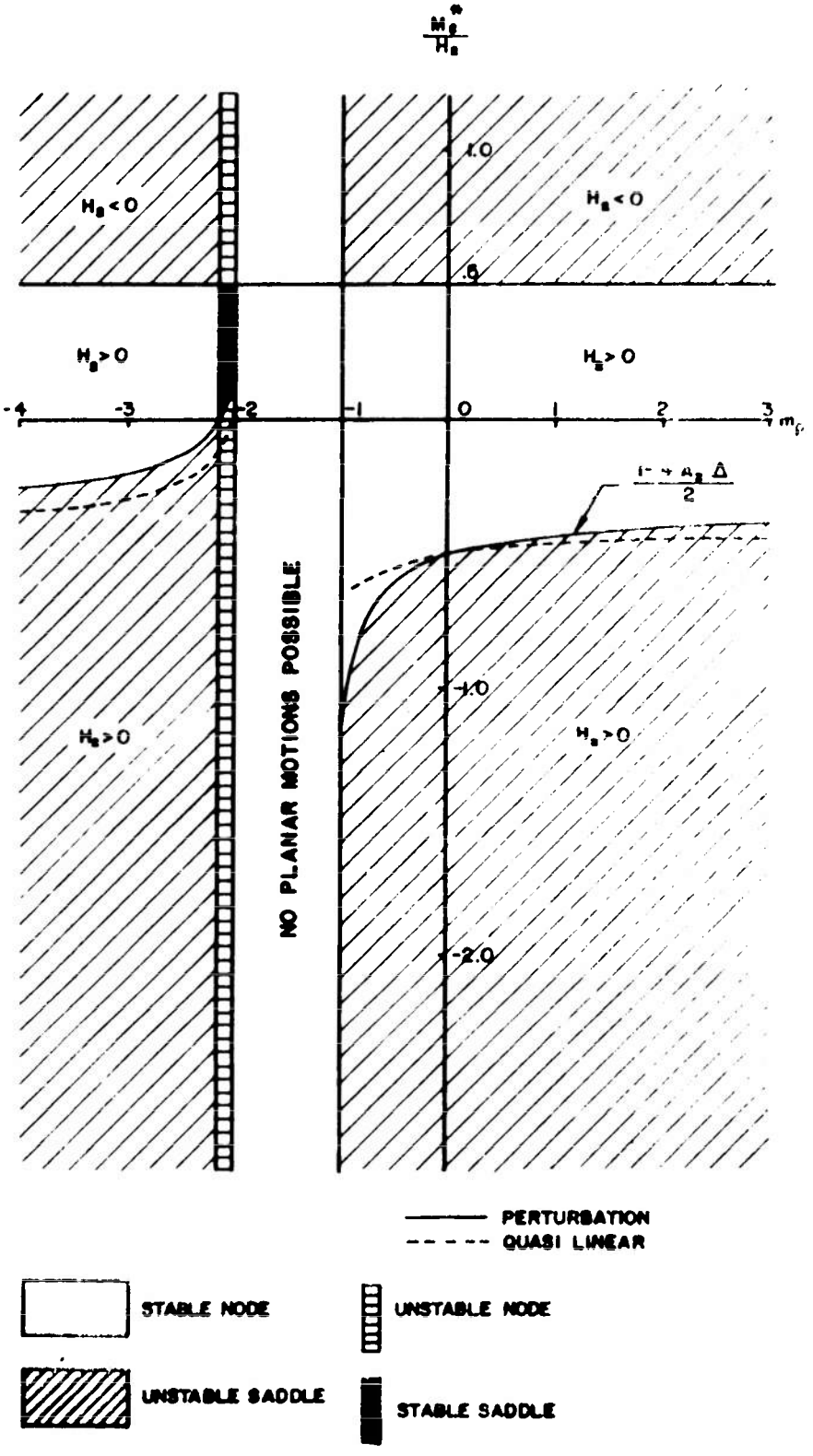

FIG. 9-6

PLANAR AND CIRCULAR SINGULARITIES

$H_0 < 0$, $H_2 > 0$

REVERSE SIGNS OF H_0 AND H_2 TO REVERSE STABILITY

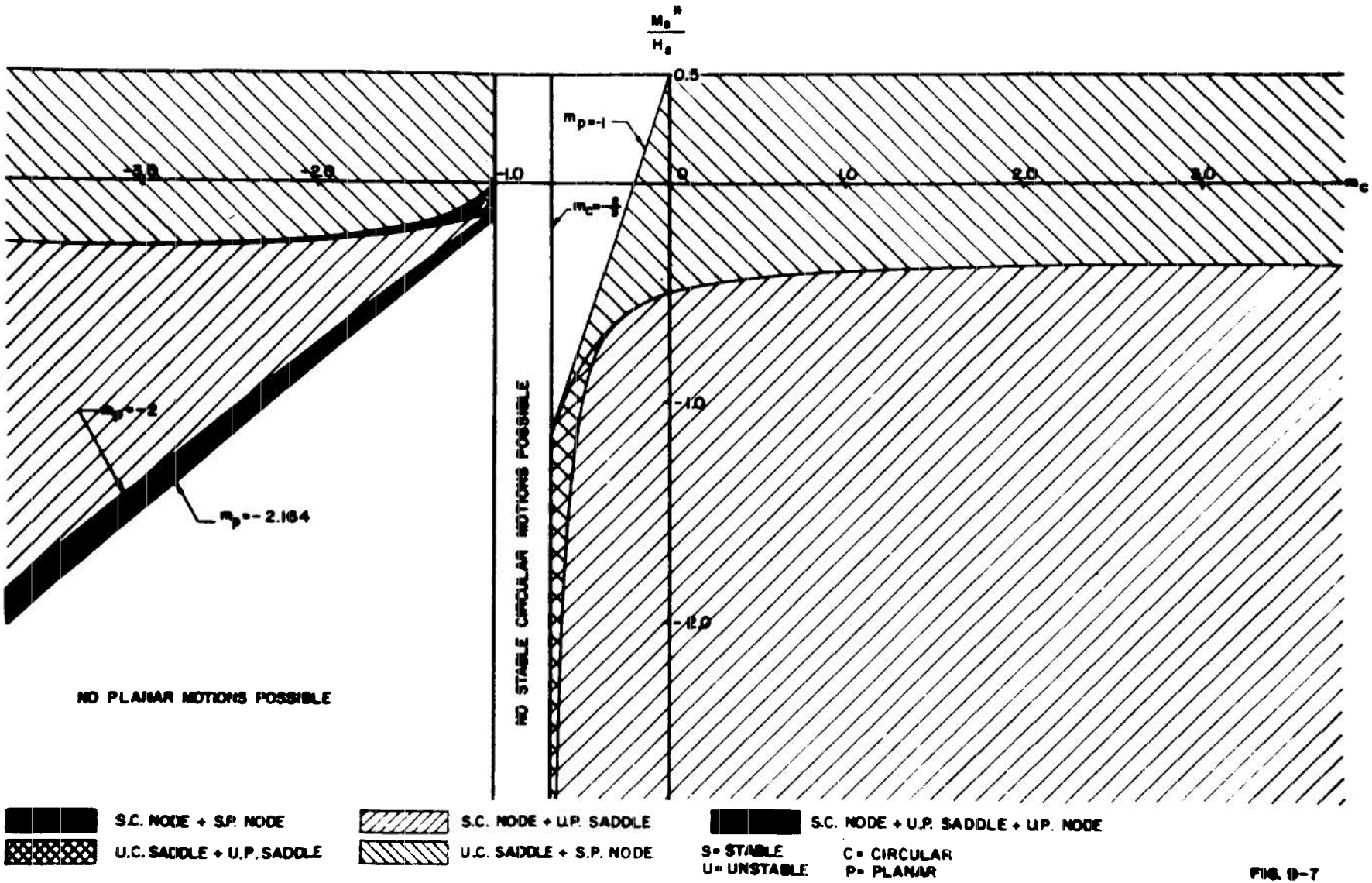

FIG. 9-7

AMPLITUDE PLANE (TYPE b MOMENT)

$(m_c=.55,\ \frac{M_2^*}{H_2}=-1)$

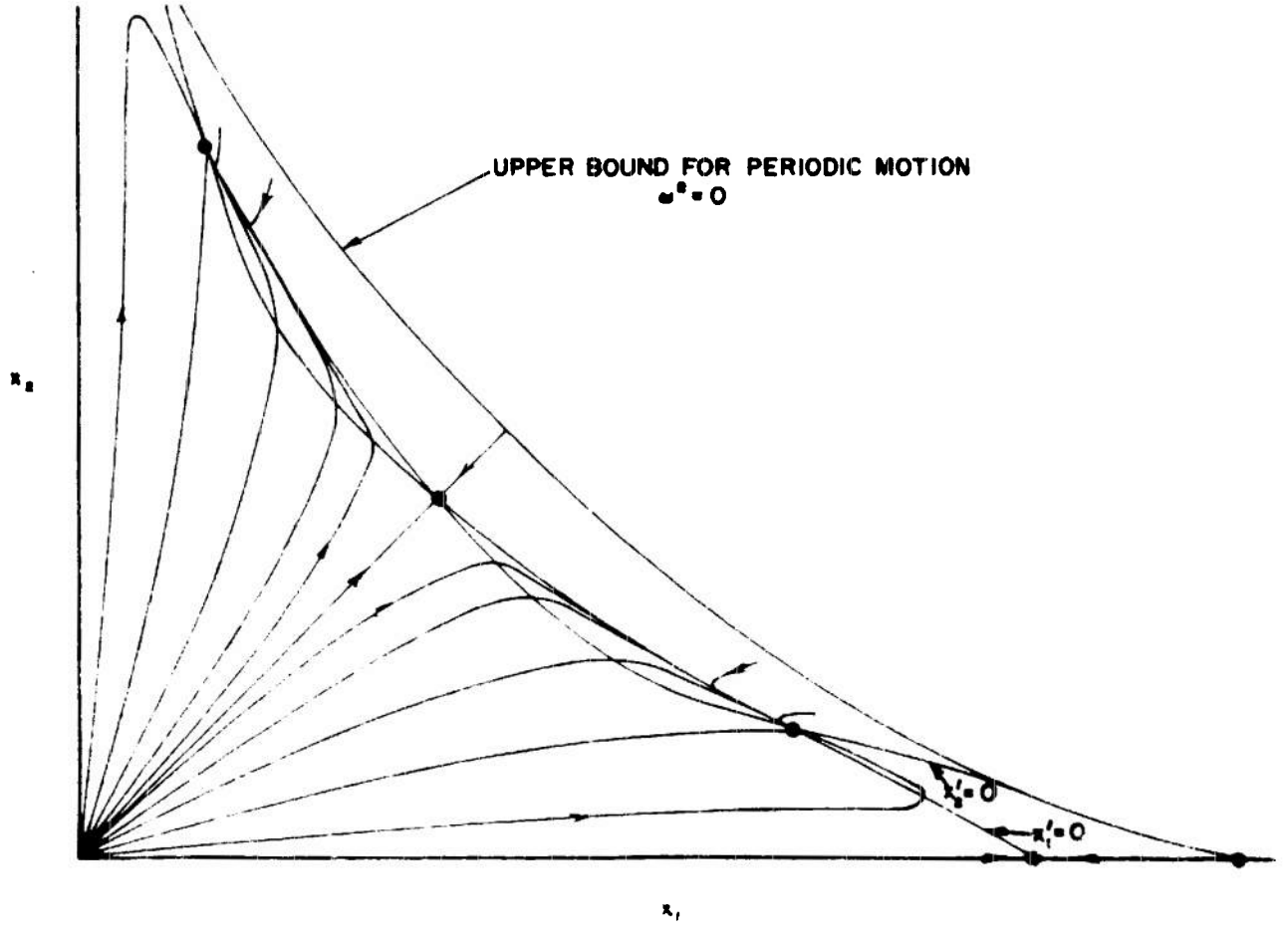

FIG. 5-5

PITCHING AND YAWING LIMIT MOTION

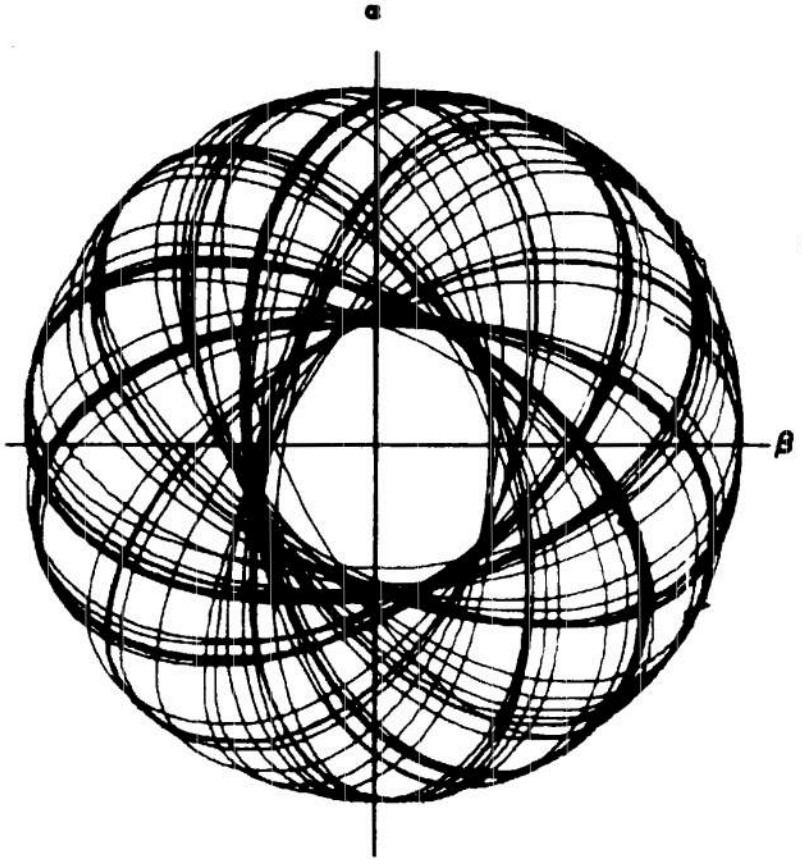

"OVAL" LIMIT MOTION
TYPE b MOMENT (FIG. 9-8)

FIG. 9-9a

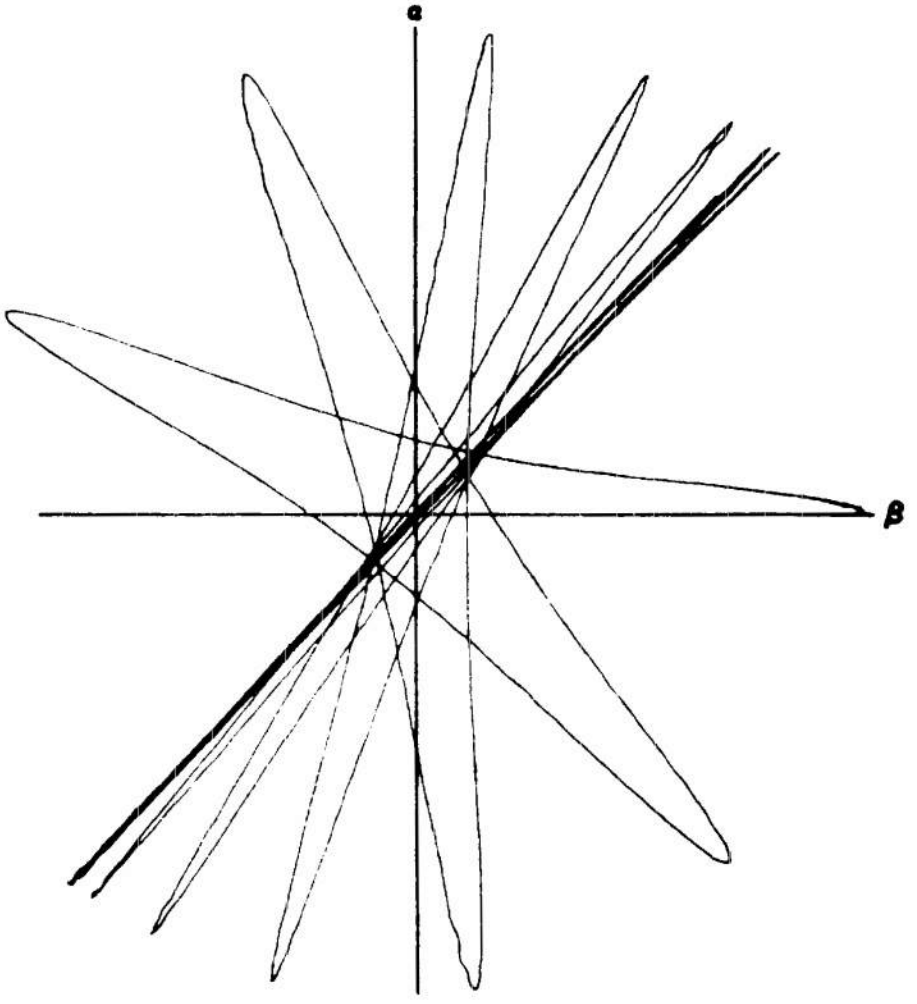

PLANAR LIMIT MOTION
TYPE c MOMENT (FIG. 9-10)

FIG. 9-9b

AMPLITUDE PLANE (TYPE c MOMENT)

$(m_c = -1.1,\ \frac{M_s^*}{H_s} = -\frac{1}{9})$

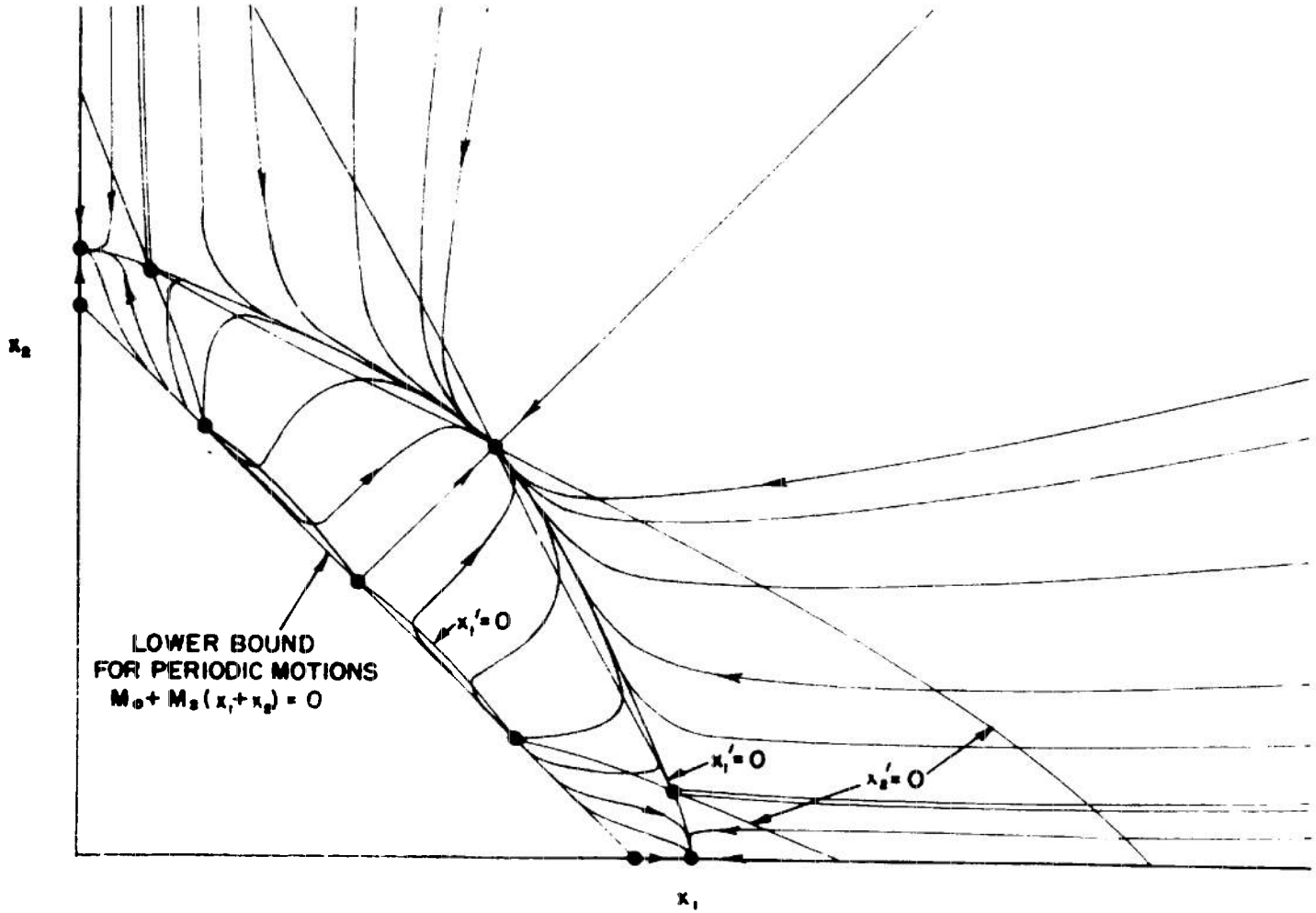

FIG 5-10

DISTRIBUTION LIST

No. of Copies	Organization
20	Commander Defense Documentation Center ATTN: TIPCR Cameron Station Alexandria, Virginia, 22314
1	Commanding General U. S. Army Materiel Command ATTN: AMCRD-RP-Bal Research and Development Directorate Washington, D. C., 20315
5	Commanding Officer Picatinny Arsenal ATTN: Feltman Research and Engineering Laboratories Dover, New Jersey
1	Commanding Officer Harry Diamond Laboratories ATTN: Technical Information Office Branch 012 Washington 25, D. C.
1	Commanding General U. S. Army Missile Command ATTN: Deputy Commanding General for Ballistic Missiles Redstone Arsenal, Alabama, 35809
1	Commanding General U. S. Army Missile Command ATTN: Deputy Commanding General for Guided Missiles, Mr. A. Jenkins Redstone Arsenal, Alabama, 35809
1	Redstone Scientific Information Center ATTN: Chief, Document Section U. S. Army Missile Command Redstone Arsenal, Alabama, 35809
1	Research Analysis Corporation ATTN: Document Control Office 6935 Arlington Road Bethesda, Maryland Washington 14, D. C., 20014
1	Army Research Office 3045 Columbia Pike Arlington, Virginia
2	Commanding Officer Army Research Office (Durham) ATTN: ORDOR 10, Cases 940-942 Box CM, Duke Station Durham, North Carolina
1	Chief of Research and Development ATTN: Director/Special Weapons Missiles and Space Division Washington, D. C., 20310
4	Chief, Bureau of Naval Weapons ATTN: DIS-33 Director, Special Projects Office (Sp-43) Department of the Navy Washington 25, D. C.
1	Commanding Officer and Director David W. Taylor Model Basin ATTN: Aerodynamics Laboratory Washington, D. C., 20007
2	Commander Naval Ordnance Laboratory White Oak Silver Spring 19, Maryland
2	Commander Naval Missile Center Point Mugu, California

DISTRIBUTION LIST

No. of Copies	Organization
1	Commanding Officer U. S. Naval Air Development Center Johnsville, Pennsylvania
3	Commander U. S. Naval Ordnance Test Station ATTN: Technical Library Aeroballistics Laboratory Code 5034 Dr. W. Haseltine China Lake, California, 93557
2	Superintendent U. S. Naval Postgraduate School ATTN: Dr. Head Monterey, California
2	Commander U. S. Naval Weapons Laboratory ATTN: Dr. C. Cohen Dahlgren, Virginia
4	AFSC (SCT) Andrews Air Force Base Washington 25, D. C.
1	AEDC ATTN: Deputy Chief of Staff Research and Development Arnold Air Force Station Tullahoma, Tennessee
1	APGC (PGAPI) Eglin Air Force Base, Florida, 32542
1	Air Force Plant Representative Republic Aviation Corporation Farmingdale, Long Island, New York
1	AFFDL (FDC) Wright Patterson Air Force Base Ohio

No. of Copies	Organization
3	Director National Aeronautics and Space Administration ATTN: Mr. A. Sieff Mr. H. Allen Mr. M. Tobak Ames Research Center Moffett Field, California
1	Director National Aeronautics and Space Administration 1520 H Street Washington 25, D. C.
1	Director National Aeronautics and Space Administration Langley Research Center Langley Field, Virginia
1	Director National Aeronautics and Space Administration Lewis Research Center Cleveland Airport Cleveland, Ohio
1	Scientific and Technical Information Facility ATTN: NASA Representative (S-AK/RKT) P.O. Box 5700 Bethesda, Maryland, 20014
1	Director Marshall Space Flight Center Redstone Arsenal, Alabama, 35809
2	Illinois Institute of Technology ATTN: Mr. W. Casier Mr. V. Volpe Chicago 16, Illinois

DISTRIBUTION LIST

No. of Copies	Organization
1	AVCO-Everett Research Laboratory ATTN: Arnold Goldberg 2385 Revere Beach Parkway Everett 49, Massachusetts, 02149
1	Alpha Research, Inc. ATTN: Technical Library 1266 Coast Village Road Santa Barbara, California, 93103
1	CONVAIR, A Division of General Dynamics Corporation Ordnance Aerophysics Laboratory ATTN: Mr. J. Arnold Daingerfield, Texas
1	CONVAIR, A Division of General Dynamics Corporation ATTN: Wallace W. Short P.O. Box 1950 San Diego 12, California
1	Cornell Aeronautical Laboratory, Inc. ATTN: Mr. J. Desmond, Librarian Buffalo, New York
1	Douglas Aircraft Company ATTN: J. Hindes, A260 300 Ocean Park Boulevard Santa Monica, California
1	General Electric Company ATTN: Mr. Smith - MSVD Library 5198 Chestnut Street Philadelphia, Pennsylvania
1	General Motors Corporation Defense Systems Division, Box T ATTN: Dr. A. Charters Santa Barbara, California

No. of Copies	Organization
1	Goodyear Aircraft Corporation ATTN: Jay McKee, Librarian Akron 15, Ohio
1	Institute of Aerospace Sciences ATTN: Librarian 2 East 64th Street New York 21, New York
1	Institute for Defense Analyses ATTN: Dr. J. Martin 1825 Connecticut Avenue, N. W. Washington 9, D. C.
1	ITT Federal Laboratories ATTN: Dr. H. Zuekerberg 500 Washington Avenue Nutley 10, New Jersey
1	Lockheed Aircraft Corporation Missiles and Space Vehicles Division ATTN: Mr. R. Nelson Sunnyvale, California
1	McDonnall Aircraft Corporation W. Box 516 St. Louis 66, Missouri
1	University of California Engineering Extension Department of Engineering ATTN: Dr. S. Houston Los Angeles 24, California
1	United Aircraft Corporation Research Department ATTN: Mr. C. King East Hartford 8, Connecticut
1	Wright Aeronautical Division Curtis-Wright Corporation ATTN: Sales Department (Government) Wood-Ridge, New Jersey

DISTRIBUTION LIST

No. of Copies	Organization
2	Applied Physics Laboratory The Johns Hopkins University ATTN: Mr. G. Seielstad 8621 Georgia Avenue Silver Spring, Maryland
1	Jet Propulsion Laboratory ATTN: I. Newlan, Chief Reports Group 4800 Oak Grove Drive Pasadena, California, 91103
1	University of Michigan Willow Run Laboratories ATTN: Mr. M. Corey P.O. Box 2008 Ann Arbor, Michigan
1	University of Southern California Engineering Center ATTN: Dr. H. Saffell, Director Los Angeles 7, California
1	Stanford University Department of Aeronautical Engineering ATTN: Mr. C. Sabin Stanford, California
1	Professor George F. Carrier Harvard University Division of Engineering and Applied Physics Cambridge 38, Massachusetts
1	Professor Francis H. Clauser, Jr. Chairman, Department of Aeronautics The Johns Hopkins University Baltimore 18, Maryland
2	Professor E. V. Laitone University of California Berkeley, California
1	Professor Lester Lees California Institute of Technology Guggenheim Aeronautical Laboratory Pasadena 4, California
1	Professor Clark B. Millikan California Institute of Technology Director, Guggenheim Aeronautical Laboratory Pasadena 4, California
1	Professor M. W. Oliphant Georgetown University Department of Mathematics Washington 7, D. C.
1	Professor A. Ormsbee University of Illinois Department of Aeronautical Engineering Urbana, Illinois
1	Professor R. Probstein Brown University Providence, Rhode Island
1	Dr. M. V. Morkovin The Martin Company Baltimore 3, Maryland
1	Dr. A. E. Puckett Hughes Aircraft Company Systems Development Laboratories Florence Avenue at Teal Street Culver City, California
1	Dr. Samuel Houston University of California, Los Angeles Los Angeles, California
1	Mr. Lawrence E. Schmidt 108 Spruce Road Paoli, Pennsylvania

DISTRIBUTION LIST

No. of Copies	Organization
4	Australian Group c/o Military Attache Australian Embassy 2001 Connecticut Avenue, N. W. Washington, D. C.
10	The Scientific Information Officer Defence Research Staff British Embassy 3100 Massachusetts Avenue, N. W. Washington 8, D. C.
	Of Interest to: The Royal College of Science and Technology ATTN: Mr. J. Little Department of Natural Philosophy Glasgow, C. 1
4	Defence Research Member Canadian Joint Staff 2450 Massachusetts Avenue, N. W. Washington 8, D. C.

AD Accession No. ____________ UNCLASSIFIED

Ballistic Research Laboratories, APG
FREE FLIGHT MOTION OF SYMMETRIC MISSILES
C.H.Murphy

BRL Report No. 1216 July 1963

RDT & E Project No. 1M010501A005
UNCLASSIFIED Report

Symmetric missiles - Motion
Drag and rolling motion
Linear coefficients
Cubic coefficients
Measurements of coefficients

The linearized angular motion of a symmetric missile is developed in some detail with some consideration of the rolling motion, drag, aerodynamic jump and the effect of varying coefficients. The tricyclic motion of a missile with misaligned control surfaces is briefly considered. This linear theory is, then, applied to the analysis of ballistic range data.

Next, simple cubic nonlinearities in static moment and Magnus moment are treated by a quasi-linear analysis and these cubic coefficients obtained from ballistic range flight data. More generalized relations for arbitrary symmetric nonlinear terms are derived and their use in the construction of "amplitude" planes indicated. These amplitude planes have proven to be quite useful for the prediction of missile flight performance. Finally, the influence of strongly nonlinear static moments is determined by a perturbation method which makes use of two quasi-constants of the motion -- total energy and angular momentum.

AD Accession No. ____________ UNCLASSIFIED

Ballistic Research Laboratories, APG
FREE FLIGHT MOTION OF SYMMETRIC MISSILES
C.H.Murphy

BRL Report No. 1216 July 1963

RDT & E Project No. 1M010501A005
UNCLASSIFIED Report

Symmetric missiles - Motion
Drag and rolling motion
Linear coefficients
Cubic coefficients
Measurements of coefficients

The linearized angular motion of a symmetric missile is developed in some detail with some consideration of the rolling motion, drag, aerodynamic jump and the effect of varying coefficients. The tricyclic motion of a missile with misaligned control surfaces is briefly considered. This linear theory is, then, applied to the analysis of ballistic range data.

Next, simple cubic nonlinearities in static moment and Magnus moment are treated by a quasi-linear analysis and these cubic coefficients obtained from ballistic range flight data. More generalized relations for arbitrary symmetric nonlinear terms are derived and their use in the construction of "amplitude" planes indicated. These amplitude planes have proven to be quite useful for the prediction of missile flight performance. Finally, the influence of strongly nonlinear static moments is determined by a perturbation method which makes use of two quasi-constants of the motion -- total energy and angular momentum.

AD Accession No. ____________ UNCLASSIFIED

Ballistic Research Laboratories, APG
FREE FLIGHT MOTION OF SYMMETRIC MISSILES
C.H.Murphy

BRL Report No. 1216 July 1963

RDT & E Project No. 1M010501A005
UNCLASSIFIED Report

Symmetric missiles - Motion
Drag and rolling motion
Linear coefficients
Cubic coefficients
Measurements of coefficients

The linearized angular motion of a symmetric missile is developed in some detail with some consideration of the rolling motion, drag, aerodynamic jump and the effect of varying coefficients. The tricyclic motion of a missile with misaligned control surfaces is briefly considered. This linear theory is, then, applied to the analysis of ballistic range data.

Next, simple cubic nonlinearities in static moment and Magnus moment are treated by a quasi-linear analysis and these cubic coefficients obtained from ballistic range flight data. More generalized relations for arbitrary symmetric nonlinear terms are derived and their use in the construction of "amplitude" planes indicated. These amplitude planes have proven to be quite useful for the prediction of missile flight performance. Finally, the influence of strongly nonlinear static moments is determined by a perturbation method which makes use of two quasi-constants of the motion -- total energy and angular momentum.

AD Accession No. ____________ UNCLASSIFIED

Ballistic Research Laboratories, APG
FREE FLIGHT MOTION OF SYMMETRIC MISSILES
C.H.Murphy

BRL Report No. 1216 July 1963

RDT & E Project No. 1M010501A005
UNCLASSIFIED Report

Symmetric missiles - Motion
Drag and rolling motion
Linear coefficients
Cubic coefficients
Measurements of coefficients

The linearized angular motion of a symmetric missile is developed in some detail with some consideration of the rolling motion, drag, aerodynamic jump and the effect of varying coefficients. The tricyclic motion of a missile with misaligned control surfaces is briefly considered. This linear theory is, then, applied to the analysis of ballistic range data.

Next, simple cubic nonlinearities in static moment and Magnus moment are treated by a quasi-linear analysis and these cubic coefficients obtained from ballistic range flight data. More generalized relations for arbitrary symmetric nonlinear terms are derived and their use in the construction of "amplitude" planes indicated. These amplitude planes have proven to be quite useful for the prediction of missile flight performance. Finally, the influence of strongly nonlinear static moments is determined by a perturbation method which makes use of two quasi-constants of the motion -- total energy and angular momentum.

AD ______ Accession No. ______ UNCLASSIFIED

Ballistic Research Laboratories, APG
FREE FLIGHT MOTION OF SYMMETRIC MISSILES
C.H. Murphy

BRL Report No. 1216 July 1963

RDT & E Project No. 1M010501A005
UNCLASSIFIED Report

Symmetric missiles - Motion
Drag and rolling motion
Linear coefficients
Cubic coefficients
Measurements of coefficients

The linearized angular motion of a symmetric missile is developed in some detail with some consideration of the rolling motion, drag, aerodynamic jump and the effect of varying coefficients. The tricyclic motion of a missile with misaligned control surfaces is briefly considered. This linear theory is, then, applied to the analysis of ballistic range data.

Next, simple cubic nonlinearities in static moment and Magnus moment are treated by a quasi-linear analysis and these cubic coefficients obtained from ballistic range flight data. More generalized relations for arbitrary symmetric nonlinear terms are derived and their use in the construction of "amplitude" planes indicated. These amplitude planes have proven to be quite useful for the prediction of missile flight performance. Finally, the influence of strongly nonlinear static moments is determined by a perturbation method which makes use of two quasi-constants of the motion -- total energy and angular momentum.

AD ______ Accession No. ______ UNCLASSIFIED

Ballistic Research Laboratories, APG
FREE FLIGHT MOTION OF SYMMETRIC MISSILES
C.H. Murphy

BRL Report No. 1216 July 1963

RDT & E Project No. 1M010501A005
UNCLASSIFIED Report

Symmetric missiles - Motion
Drag and rolling motion
Linear coefficients
Cubic coefficients
Measurements of coefficients

The linearized angular motion of a symmetric missile is developed in some detail with some consideration of the rolling motion, drag, aerodynamic jump and the effect of varying coefficients. The tricyclic motion of a missile with misaligned control surfaces is briefly considered. This linear theory is, then, applied to the analysis of ballistic range data.

Next, simple cubic nonlinearities in static moment and Magnus moment are treated by a quasi-linear analysis and these cubic coefficients obtained from ballistic range flight data. More generalized relations for arbitrary symmetric nonlinear terms are derived and their use in the construction of "amplitude" planes indicated. These amplitude planes have proven to be quite useful for the prediction of missile flight performance. Finally, the influence of strongly nonlinear static moments is determined by a perturbation method which makes use of two quasi-constants of the motion -- total energy and angular momentum.

AD ______ Accession No. ______ UNCLASSIFIED

Ballistic Research Laboratories, APG
FREE FLIGHT MOTION OF SYMMETRIC MISSILES
C.H. Murphy

BRL Report No. 1216 July 1963

RDT & E Project No. 1M010501A005
UNCLASSIFIED Report

Symmetric missiles - Motion
Drag and rolling motion
Linear coefficients
Cubic coefficients
Measurements of coefficients

The linearized angular motion of a symmetric missile is developed in some detail with some consideration of the rolling motion, drag, aerodynamic jump and the effect of varying coefficients. The tricyclic motion of a missile with misaligned control surfaces is briefly considered. This linear theory is, then, applied to the analysis of ballistic range data.

Next, simple cubic nonlinearities in static moment and Magnus moment are treated by a quasi-linear analysis and these cubic coefficients obtained from ballistic range flight data. More generalized relations for arbitrary symmetric nonlinear terms are derived and their use in the construction of "amplitude" planes indicated. These amplitude planes have proven to be quite useful for the prediction of missile flight performance. Finally, the influence of strongly nonlinear static moments is determined by a perturbation method which makes use of two quasi-constants of the motion -- total energy and angular momentum.

AD ______ Accession No. ______ UNCLASSIFIED

Ballistic Research Laboratories, APG
FREE FLIGHT MOTION OF SYMMETRIC MISSILES
C.H. Murphy

BRL Report No. 1216 July 1963

RDT & E Project No. 1M010501A005
UNCLASSIFIED Report

Symmetric missiles - Motion
Drag and rolling motion
Linear coefficients
Cubic coefficients
Measurements of coefficients

The linearized angular motion of a symmetric missile is developed in some detail with some consideration of the rolling motion, drag, aerodynamic jump and the effect of varying coefficients. The tricyclic motion of a missile with misaligned control surfaces is briefly considered. This linear theory is, then, applied to the analysis of ballistic range data.

Next, simple cubic nonlinearities in static moment and Magnus moment are treated by a quasi-linear analysis and these cubic coefficients obtained from ballistic range flight data. More generalized relations for arbitrary symmetric nonlinear terms are derived and their use in the construction of "amplitude" planes indicated. These amplitude planes have proven to be quite useful for the prediction of missile flight performance. Finally, the influence of strongly nonlinear static moments is determined by a perturbation method which makes use of two quasi-constants of the motion -- total energy and angular momentum.